

2017

Fabrication of 3-Dimensional Polymeric Drug Delivery Systems

Yu Chen
University of Wollongong

Follow this and additional works at: <https://ro.uow.edu.au/theses1>

University of Wollongong

Copyright Warning

You may print or download ONE copy of this document for the purpose of your own research or study. The University does not authorise you to copy, communicate or otherwise make available electronically to any other person any copyright material contained on this site.

You are reminded of the following: This work is copyright. Apart from any use permitted under the Copyright Act 1968, no part of this work may be reproduced by any process, nor may any other exclusive right be exercised, without the permission of the author. Copyright owners are entitled to take legal action against persons who infringe their copyright. A reproduction of material that is protected by copyright may be a copyright infringement. A court may impose penalties and award damages in relation to offences and infringements relating to copyright material.

Higher penalties may apply, and higher damages may be awarded, for offences and infringements involving the conversion of material into digital or electronic form.

Unless otherwise indicated, the views expressed in this thesis are those of the author and do not necessarily represent the views of the University of Wollongong.

Recommended Citation

Chen, Yu, Fabrication of 3-Dimensional Polymeric Drug Delivery Systems, Doctor of Philosophy thesis, Australian Research Council Centre of Excellence for Electromaterials Science,, University of Wollongong, 2017. <https://ro.uow.edu.au/theses1/75>

Research Online is the open access institutional repository for the University of Wollongong. For further information contact the UOW Library: research-pubs@uow.edu.au



UNIVERSITY
OF WOLLONGONG
AUSTRALIA

Australian Research Council Centre of Excellence for Electromaterials Science,
Intelligent Polymer Research Institute, Australian Institute for Innovative
Materials

Fabrication of 3-Dimensional Polymeric Drug Delivery Systems

Yu Chen

This thesis is presented as part of the requirement for the Award of the Degree
of **Doctor of Philosophy** from the University of Wollongong

2017

Dedication

This work is dedicated to my family for their love and support.

Declaration

I, Yu Chen, declare that this thesis, submitted in fulfilment of the requirements for the award of Doctor of Philosophy, in the school of Mechanical, Materials, and Mechatronic Engineering, University of Wollongong, is wholly my own work unless otherwise referenced or acknowledged. The document has not been submitted for qualifications at any other academic institution.

Yu Chen

March 2017

Acknowledgements

Firstly, I would like to thank my supervisors Professor Gordon G. Wallace, Professor Simon E. Moulton, and Doctor Zhilian Yue for their kind supervision. Your patient guidance and valuable advice supported me to focus on my study and fulfil this investigation. I appreciate your great help with my publication and thesis writing. I am also willing to express my great thanks to Professor Mark Cook for his profound knowledge in epilepsy which provided valuable information for my research.

Then, I would like to thank those who directly assisted with my experiment and publication writing. I would like to thank Dr. Qi Gu for his help with cell culture. I also would like to thank Dr. Patricia Hayes, Dr. Sina Naficy, Dr. Javad Foroughi, Mr. Tony Romeo, Dr. Mitchell Nancarrow, Associate Professor Jun Chen, Dr. Chen Zhao, and Dr. Binbin Zhang for equipment training and related discussion. I am also grateful to Dr. Stephen Beirne, Dr. Syed Ashraf, Dr. Sanjeev Gambhir for help with 3D electrodes, pyrrole monomer, and graphene oxide preparation. I am also grateful to Associate Professor Michael Higgins, Associate Professor Peter Innis, and Dr. Pawel Wagner for their discussion, advice and as a panel on my research proposal.

I also want to express my thanks to Professor Jeremy Crook, Dr. Caiyun Wang, Dr. Xiao Liu, Dr. Toni Camphell, Professor Geoffrey Spinks, Dr. Simone Ciampi, Dr. Kerry Gilmore, Dr. Rouhollah Jalili, Mr.Phil Smugreski, Ms. Natalie Foxon, and Ms. Karla House for their routine help and discussion on my study.

I would like to greatly thank all friends in IPRI and AIIM not listed here for their support to my work and life.

I would like to acknowledge all the financial support including the scholarships (IPTA and UPA) from University of Wollongong, Australian government research training program scholarship.

At last, but not least, most sincere thanks to my family my parents, my younger brother, my lovely wife and daughter for their endless love, support, and encouragement.

Publications

Yu Chen, Zhilian Yue, Simon E. Moulton, Patricia Hayes, Mark J. Cook, Gordon G. Wallace. A simple and versatile method for microencapsulation of anti-epileptic drugs for focal therapy of epilepsy, *Journal of Materials Chemistry B*, **2015**, 3, 7255-7261.

Contribution: Yu Chen carried out all experimental work, analysed the data and wrote the manuscript.

Jonathan L. Jiang, Zhilian Yue, Sebastien H. Bauquier, Alan Lai, Yu Chen, Karen J. McLean, Amy J. Halliday, Yi Sui, Simon Moulton, Gordon G. Wallace, Mark J. Cook. Injectable phenytoin loaded polymeric microspheres for the control of temporal lobe epilepsy in rats, *Restorative Neurology and Neuroscience*, **2015**, 33, 823-834.

Contribution: Yu Chen carried out the microsphere sample preparation and characterization and analysed the data.

Qi Gu, Eva Tomaskovic-Crook, Rodrigo Lozano, Yu Chen, Robert M. Kapsa, Qi Zhou, Gordon G. Wallace, and Jeremy M. Crook. Functional 3D neural mini-tissues from printed gel-based bioink and human neural stem cells, *Advanced Healthcare Materials*, **2016**, 5, 1429-1438.

Contribution: Yu Chen carried out the SEM sample preparation, observation and assisted in writing the manuscript.

Sebastien H. Bauquier, Jonathan L. Jiang, Zhilian Yue, Alan Lai, Yu Chen, Simon E. Moulton, Karen J. McLean, Sara Vogrin, Amy J. Halliday, Gordon Wallace, and Mark J.

Cook. Antiepileptic effects of lacosamide loaded polymers implanted subdurally in GAERS, *International Journal of Polymer Science*, **2016**, In Press.

Contribution: Yu Chen carried out the lacosamide loaded polymer fibre fabrication and assisted in writing the manuscript.

Yu Chen, Qi Gu, Zhilian Yue, Jeremy M. Crook, Simon E. Moulton, Mark J. Cook, Gordon G. Wallace. Development of drug-loaded polymer microcapsules for treatment of epilepsy, *Biomaterials Science*, **2017**, submitted.

Contribution: Yu Chen carried out all experimental work, analysed the data and wrote the manuscript.

Yu Chen, Zhilian Yue, Simon E. Moulton, Mark Cook, Gordon G. Wallace. Biodegradable composite mats: controlled dual drug delivery system for combined therapy. *11th Annual International Electromaterials Symposium*, 8-10 February **2017**.

Yu Chen, Simon E. Moulton, Zhilian Yue, Sara Ahmadi, Mark Cook, Gordon G. Wallace. Novel 3D printing electrodes for controllable delivery of anti-epilepsy drug by electrical stimulation, *10th Annual International Electromaterials Symposium*, 11-13 February **2015**.

Yu Chen, Simon E. Moulton, Zhilian Yue, Mark Cook, Gordon G. Wallace. A simple and versatile method for the fabrication of microencapsulation contain anti-epilepsy drug: from injection to implantation, *9th Annual International Electromaterials Symposium*, P85, 12-14 February **2014**.

Simon Moulton, Adrian Gestos, Javad Foroughi, Yu Chen, Zhilian Yue, Gordon Wallace. Advanced Polymeric Nano-Yarn 3D Structures for Drug Delivery, *MRS Fall Meeting*, H6.02, 1-6 December **2013**.

Yu Chen, Simon E. Moulton, Mark Cook, Gordon G. Wallace. Control of drug release via microencapsulation of Anti-epilepsy drug into tunable bio-degradable polymer, *4th Asia-Pacific Symposium on Nanobionics*, 14-15 November **2013**.

Yu Chen, Simon E. Moulton, Mark Cook, Gordon G. Wallace. Electrospun bio-degradable polymer fibers for anti-epilepsy brain drug delivery, *8th Annual International Electromaterials Symposium*, P56, 13-15 February **2013**.

Abstract

Development of new polymer structures for local drug delivery to the brain is an exciting research area. The main aim of this study is to develop biocompatible controlled drug delivery systems, using biodegradable or conducting polymers, for the treatment of central nervous system disorders such as epilepsy.

Epilepsy affects 1% of the global population and is drug-resistant in more than 30% of cases. The reasons for this are still not well understood. However, there is a significant body of evidence pointing to the blood-brain barrier. Resective surgery can provide an alternative method of epilepsy control; however, this treatment option is not suitable for most epilepsy sufferers. To improve the therapeutic efficacy of epilepsy medication, a promising approach is to deliver anti-epilepsy drugs directly to affected brain areas using appropriately designed implantable local drug delivery systems, therefore avoiding the blood-brain barrier. The drug delivery systems must meet some criteria, including high drug encapsulation efficiency, biodegradability, neuro-cytocompatibility and predictability of drug release profiles. Here, Chapter 3 investigates the development of fibre- and sphere-based microcapsules that exhibit controllable and uniform morphologies and drug release profiles as predicted by mathematical modelling. Importantly, both forms of fabricated microcapsules are compatible with human brain-derived neural stem cells and their differentiation to neurons and supporting neuroglia, indicating clinical compliance for neural transplantation and therapeutic drug delivery.

After that, to develop effective local delivery systems with longer release periods and more diverse release profiles, preparation of a variety of core-shell microcapsules via novel core-shell electrojetting, where a more hydrophobic polymer shell acts as a physical barrier to control the rate of drug release from the drug-loaded polymeric core, was considered in Chapter 4. The resulting microcapsules demonstrated high drug encapsulation efficiency, narrow size distribution and uniform morphology. Moreover, the release rate of drugs can be modulated by controlling the morphologies of the core-shell microcapsules.

Combination therapy involving more than one medication has shown promise in the treatment of a number of diseases. A key challenge is to concurrently ensure effective doses for each medication. Therefore, there is an urgent need for developing dual or multi-drug delivery systems to attain sustained and predictable release profiles for individual drugs. Chapter 5 presents a simple and versatile approach to developing dual drug delivery systems. Both electrospinning and electrospraying were employed to fabricate composite membranes that were composed of microfibrinous matrices interspersed with microspheres. Two different composite membranes were fabricated including PLA phenytoin fibre/ PLGA lacosamide sphere composite membranes and PLA lacosamide fibre/ PLGA dexamethasone sphere composite membranes, respectively. The resultant composite membranes exhibited favourable thermal and mechanical properties. In contrast to loading dual or multiple drugs into the same micro- or nano- structure, these dual microstructural composite membranes show not only controllable dosage but also different release rates for each drug independently. Moreover, the release profile of each drug can be predictable using mathematical modelling.

On-demand drug delivery is becoming feasible through the application of appropriate stimuli-responsive materials. In addition to the above passive drug delivery systems, we have also developed 3D electrically responsive system for programmed drug delivery in Chapter 6. 3D printed (selective laser melting) interdigitated Ti_6Al_4V electrodes were used for electrodeposition of conductive polymer coatings (polypyrrole) doped with an anti-epilepsy prodrug, fosphenytoin. We have shown that drug release from the 3D conductive electrodes is precisely controlled by biphasic electrical stimulation. Moreover, dual drug delivery is achieved by further coating of the 3D electrodes with dexamethasone-loaded biodegradable microspheres. The interdigitated electrodes can be served as multi-function drug delivery systems. These 3D printed electrodes represent a novel electrically on-demand drug delivery system for treatment of central nervous system diseases including epilepsy.

Chapter 7 gives the main research conclusion and the prospect of further research work.

List of Abbreviations

2D; Two-dimensional

3D; Three-dimensional

A; Ampere

ACN; acetonitrile

aCSF; artificial cerebrospinal fluid

AEDs; Anti-epilepsy drugs

Ag/AgCl; Silver/Silver chloride

AR; Aspect ratio

BBB; Blood-brain barrier

BDNF; Brain-derived neurotrophic factor

CAD; Computer-aided design

CE; Counter electrode

CNS; Central nervous system

CNT; Carbon nanotube

CO₂; Carbon dioxide

CPs; Conducting polymers

CPD; Critical Point Drying

CV; Cyclic voltammetry

DDS; Drug delivery system

DNA; Deoxyribonucleic acid

EIS; Electrochemical impedance spectroscopy

FDA; Food and Drug Administration

FEG; Field emission gun

GABA; gamma-aminobutyric acid

cm; Centimetre

d ; Diameter of the microcapsules

Dex; Dexamethasone

D_e ; Effective diffusivity

DMF; Dimethylformamide

DMEM; Dulbecco modified eagle medium

EGF; Epidermal growth factor

GFAP; Glial fibrillary acidic protein

GF; Growth factor

GO; Graphene oxide

h; Hour

HPLC; High performance liquid chromatography

K; Liquid conductivity

kHz; Kilohertz

kV; Kilovolt

k Ω ; Kilo-ohm

LBL; Layer-by-layer

M; Molar

Min; Minute

mL; Millilitre

MPa; Megapascal

M_t ; Molar weight at any time

M_∞ ; Molar weight at infinite time

ng; Nanogram

NIH; National Institutes of Health

nm; Nanometre

NSCs; Neural stem cells

PBS; Phosphate buffer saline

PEDOT; Poly (3,4-ethylenedioxythiophene)

PHT; Phenytoin

PFA; Paraformaldehyde

PLA; Polylactic acid

PLGA; Poly (_{D,L}- lactic-*co*-glycolic acid)

PPy; Polypyrrole

Pt; Platinum

Q ; Liquid flow rate

RE; Reference electrode

s; Second

SEM; Scanning electron microscope

SLM; Selective laser melting

STDEV; Standard deviation

TGA; Thermogravimetric analysis

UV-vis; Ultraviolet-visible

V; Voltage

WE; Working electrode

ϵ ; Strain

γ ; Surface tension of solution

ϵ_0 ; Permittivity of vacuum

λ_n ; Roots of eigenfunctions

μg ; Microgram

μL ; Microlitre

ρ ; Density of solution

σ ; Stress

Contents

Dedication	i
Declaration.....	ii
Acknowledgements	iii
Publications	iv
Abstract.....	vii
List of Abbreviations	x
Contents	xv
List of Figures.....	xxii
List of Tables	xxx
1. CHAPTER 1: GENERAL INTRODUCTION.....	1
1.1 Drug delivery general introduction	2
1.1.1 Oral drug delivery.....	2
1.1.2 Transdermal drug delivery.....	4
1.1.3 Local drug delivery.....	6
1.1.4 Targeted drug delivery.....	7
1.2 Polymer for drug delivery	12
1.2.1 Biodegradable polymer.....	13
1.2.2 Conducting polymers.....	21

1.3 Technology in drug delivery	28
1.3.1 Electrospinning.....	32
1.3.2 Electrospraying.....	39
1.4 Highlights for epilepsy treatment.....	40
1.5 Aims and structure of this thesis	42
1.6 References	45
2. CHAPTER 2: GENERAL EXPERIMENTAL.....	63
2.1 Introduction	64
2.2 Reagents and materials.....	64
2.3 Fabrication methods	67
2.3.1 Electrojetting	67
2.3.2 Electropolymerization	69
2.4 General physicochemical characterization.....	70
2.4.1 Scanning electron microscopy.....	71
2.4.2 Thermogravimetric analysis	72
2.4.3 Tensile testing.....	73
2.4.4 Electrochemical impedance spectroscopy	74
2.4.5 Cyclic voltammetry	76
2.5 In vitro drug release study.....	77
2.5.1 Passive release study of electrojetted microcapsules	77

2.5.2 Electrically controlled release study of 3D printed electrodes with drug-laden coatings.....	78
2.5.3 High Performance Liquid Chromatography Analysis	79
2.6 References	81
3. CHAPTER 3: DEVELOPMENT OF DRUG-LOADED POLYMER	
MICROCAPSULES FOR TREATMENT OF EPILEPSY	84
3.1 Introduction	85
3.2 Materials and Methods	87
3.2.1 Materials	87
3.2.2 Microcapsule fabrication via electrojetting	87
3.2.3 Morphological and dimensional statistical analysis	88
3.2.4 <i>In vitro</i> drug release study	88
3.2.5 Mathematical modelling of the release profiles of the microcapsules	89
3.2.6 NSC culture and differentiation.....	90
3.2.7 NSC viability analysis	90
3.2.8 Scanning Electron Microscopy (SEM).....	91
3.3 Results and Discussion.....	91
3.3.1 Fabrication of lacosamide-loaded microcapsules by electrojetting.....	91
3.3.2 Dimensional and shape uniformity analysis	96
3.3.3 <i>In vitro</i> drug release and mathematical modelling study.....	100
3.3.4 Human neural stem cell viability and differentiation	105

3.4 Conclusion.....	111
3.5 References	112
4. CHAPTER 4: CORE-SHELL MICROCAPSULATION OF ANTI-EPILEPTIC DRUGS.....	118
4.1 Introduction	119
4.2 Materials and methods	121
4.2.1 Materials	121
4.2.2 Electrojetting (electrospinning and electrospraying).....	121
4.2.3 Morphological and dimensional statistical analysis	122
4.2.4 Determination of drug encapsulation efficiency	122
4.3 Results and Discussion.....	123
4.3.1 Preparation of various forms of electrojetted core-shell microcapsules.....	123
4.3.2 Morphological and dimensional statistical analysis	126
4.3.3 Drug encapsulation efficiency	133
4.3.4 In vitro drug release study	135
4.4 Conclusions	139
4.5 References	140
5. CHAPTER 5: DEVELOPMENT OF ELECTROSPUN AND ELECTROSPRAYED DUAL DRUG DELIVERY MATRICES.....	146
5.1 Introduction	147
5.2 Experimental	148

5.2.1 Materials	148
5.2.2 Fabrication of Composite matrices.....	148
5.2.3 Characterization and evaluation	150
5.2.4 In vitro drug release study and quantification of drug encapsulation efficiency...	150
5.3 Results and Discussion.....	152
5.3.1 Fabrication and selection of proper component	152
5.3.2 Fabrication of composite matrices containing two types of drugs	157
5.3.3 Thermal properties of composite matrices	161
5.3.4 Mechanical properties of the composite matrices	162
5.3.5 In vitro drug release study and mathematical simulation	164
5.4 Conclusions	172
5.5 References	173
6. CHAPTER 6: CONDUCTING AND BIODEGRADABLE POLYMERS	
COMBINED 3-DIMENSIONAL ELECTRODES DELIVERY SYSTEMS	178
6.1 Introduction	179
6.2 Experimental	181
6.2.1 Materials	181
6.2.2 3D printing of interdigitatedl electrodes.....	182
6.2.3 3D coating of fosphenytoin loaded conducting film	182
6.2.4 Electrospray coating of PLGA dexamethasone microspheres on the 3D electrodes	182

6.2.5 Scanning electron microscope	183
6.2.6 Electrochemical measurements	183
6.2.7 In vitro electrically controlled drug release	184
6.2.8 PLGA microsphere diametric statistics and drug release study	184
6.2.9 Determination of the amount of released fosphenytoin and dexamethasone	185
6.3 Results and Discussion.....	185
6.3.1 Fabrication and assembly of the interdigitated 3D electrodes.....	185
6.3.2 Scanning Electron Microscopy.....	188
6.3.3 Electrochemical impedance spectroscopy	192
6.3.4 Cyclic Voltammetry	193
6.3.5 Electrically controlled release of fosphenytoin	194
6.3.6 Drug release study of 3D electrode coated with PLGA/dexamethasone microspheres coating	200
6.4 Conclusion.....	205
6.5 References	206
7. CHAPTER 7: CONCLUSIONS AND FUTURE WORK.....	211
7.1 General Conclusion	212
7.2 Future work.....	214
7.2.1 Electrojetting biodegradable microcapsules	214
7.2.2 Electropolymerization of conducting polymer	216
7.3 References	218

List of Figures

Figure 1.1 The possible obstacles for oral delivery of biological therapeutics. Reproduced from reference [20].	3
Figure 1.2 Histological structure of human skin. Reproduced from reference [24].	5
Figure 1.3 Local drug delivery strategies for cancer treatment, including a) wafers in the brain, b) film in the lung, c) rod in the liver, d) gel in the intestine or stomach, d) nanoparticles in the ootheca. Reproduced from reference [31].	7
Figure 1.4 Schematic illustrations of passive targeting delivery compared with free drugs without a carrier. Reproduced from reference [40].	8
Figure 1.5 Schematic illustration of active targeting delivery, using folate modified nanocarrier as an example, receptor mediated. Reproduced from reference [40].	9
Figure 1.6 The blood-brain barrier (BBB) is mainly composed of vascular endothelial cells, highly connected by adherens and tight junctions, and a sparse layer of pericytes. Reproduced from reference [45].	11
Figure 1.7 Most commonly used biodegradable polyesters. a) L- and DL-PLA, b) PGA, c) PLGA, d) PCL.	15
Figure 1.8 The schematic illustration of erosion mechanisms: surface erosion (left) and bulk erosion (right). Reproduced from reference [71].	16
Figure 1.9 Mechanism of drug release from degradable polymers. Reproduced from reference [74].	18
Figure 1.10 Schematic illustration of the fabrication and function of the loperamide loaded PLGA nanoparticles. Reproduced from reference [75].	19

Figure 1.11 Schematic illustration of the composition of PLGA composite nanoparticles and their applications. Cited from reference [76].	20
Figure 1.12 The principle of electropolymerization of polypyrrole: the monomer is pyrrole, A^- is negative drug molecule, e^- is electronic charge. Cited from reference [101].	24
Figure 1.13 Schematic illustrations of the conduction process in polypyrrole.	26
Figure 1.14 The drug release from conducting polymer in response to electrical stimulation.	27
Figure 1.15 Timeline of nanotechnology-based drug delivery. Highlights of some delivery systems that serve as important milestones throughout the history of drug delivery. Cited from reference [130].	30
Figure 1.16 Nanotechnology-based synthetic methods: top-down or bottom-up engineering of individual components.	31
Figure 1.17 Schematics of the experimental setup used to perform electrospinning.	34
Figure 1.18 Schematic of the experimental setup used to perform electrospraying.	40
Figure 1.19 Schematic illustration of local treatment for epilepsy: a) the onset of pre-seizures; b) progression into an epileptic seizure event; c) implant local drug delivery system foci in effective seizure-controlling areas of the brain; d) return to normal situation. Reproduced from reference [174].	42
Figure 2.1 Photograph of NANON-01A electrojetting system.	68
Figure 2.2 Photograph of (A) CHI electrochemical workstation and, (B) schematic of the three-electrode system.	70
Figure 2.3 JSM7500FA Field Emission Scanning Electron Microscope from JEOL.	71
Figure 2.4 Thermogravimetric Analysis Instrument TA Q500.	72
Figure 2.5 Shimadzu EZ-L mechanical testing machine (A) and dog-bone sample (B).	74
Figure 2.6 The three-electrode system with a Luggin capillary for electrochemical testing.	75

Figure 2.7 The classical triangle waveform used in cyclic voltammetry.....	77
Figure 2.8 Applied potentials of the square wave, biphasic voltage stimulations used in the electrically controlled release study.....	78
Figure 2.9 Photograph of Agilent 1260 Infinity High Performance Liquid Chromatography system.	79
Figure 2.10 The pre-established calibration curves of model drugs used in this thesis.....	80
Figure 3.1 Schematic illustration of the electrospinning setup, with SEM images of electrospun PLGA/lacosamide microfibres.	92
Figure 3.2 Schematic illustration of the electro spraying setup, with SEM images of electro spray PLGA/lacosamide microspheres.	93
Figure 3.3 Scanning Electron Microscope (SEM) images of PLGA/lacosamide a, b) Flattened microspheres, c, d) Microspheres.	94
Figure 3.4 Scanning Electron Microscope images of PLGA/lacosamide Microfibres.....	95
Figure 3.5 Size of flattened microspheres, microspheres, and microfibres.	96
Figure 3.6 Size distributions of flattened microspheres, microspheres, and microfibres.	97
Figure 3.7 Aspect ratio of PLGA/lacosamide a, b) flattened microspheres and c, d) microspheres; Aspect ratio defined as the ratio of the l to w as shown in figures.....	98
Figure 3.8 Statistical results of aspect ratio, a) flattened microspheres and b) microspheres.....	99
Figure 3.9 Drug encapsulation efficiency of PLGA/lacosamide flattened microspheres, microspheres, and microfibres.....	100
Figure 3.10 Cumulative release profiles of various PLGA microcapsules.....	101
Figure 3.11 Comparison of the mathematical modelling results (linear) with experimental drug release profiles (dots).....	104
Figure 3.12 Human NSC viability and on a) microfibres and b) microspheres. NSCs were cultured with fibres and spheres following successful attachment.....	105

Figure 3.13 Human NSC viability and proliferation kinetics during culture with microfibres and microspheres.	106
Figure 3.14 Morphology of differentiated human NSCs during culture with microfibres and microspheres.	107
Figure 3.15 Morphology of differentiated human NSCs during conventional plate-based culture, used as the control for comparison.	108
Figure 3.16 Immunophenotyping of differentiated NSCs. DAPI (blue) colocalised with neuronal markers MAP2 (green), and TUJ1 (red), and glial marker GFAP (purple) expressed by differentiated NSCs cultured with microspheres. scale bar: 50 μ m.	109
Figure 3.17 Immunophenotyping of differentiated NSCs. DAPI (blue) colocalised with neuronal markers MAP2 (green) and TUJ1 (red), and glial marker GFAP (purple) expressed by differentiated NSCs cultured with microfibres. Scale bar: 50 μ m.	110
Figure 4.1 Schematic illustration of the electrojetting setup, electrospinning of core-shell microfibres.	124
Figure 4.2 Schematic illustration of the electrojetting setup, electrospraying of core-shell microspheres.	125
Figure 4.3 Scanning Electron Microscope (SEM) images of various core-shell PLGA microcapsules; a, b) Microflakes, c, d) Flattened microspheres, e, f) Microspheres.	127
Figure 4.4 Scanning Electron Microscope images of various core-shell PLGA a, b) Microspheres-fibres, c, d) Beaded microfibres.	128
Figure 4.5 Scanning Electron Microscope images of various core-shell PLGA a, b) Microfibres.	129
Figure 4.6 Schematic illustration of the detection points of the sizes of the fabricated core-shell microflakes, flattened microspheres, microspheres, microspheres-fibres, beaded microfibres, and microfibres. The d is from the detection points as shown in figure.	130

Figure 4.7 Size of the core-shell microflakes, flattened microspheres, microspheres, microspheres-fibres, beaded microfibrils, and microfibrils.....	131
Figure 4.8 Size distribution of each type of core-shell microcapsules.	132
Figure 4.9 Drug encapsulation efficiency of the core-shell microflakes, flattened microspheres, microspheres, microspheres-fibres, beaded microfibrils, and microfibrils.	134
Figure 4.10 Cumulative release of lacosamide from the fabricated core-shell PLGA microcapsules including microflakes, microspheres, microspheres-fibers, and microfibrils in aCSF (pH 7.4) at 37 °C over 104 days.	135
Figure 4.11 The release profiles of the core-shell microcapsules including microflakes, microspheres, microspheres-fibers, and microfibrils in the first 20 days.	136
Figure 4.12 Comparison of the release profile of the microspheres to that of core-shell microspheres.	137
Figure 4.13 Comparison of the release profile of the microfibrils with that of core-shell microfibrils.	138
Figure 5.1 Scanning electron microscope images of electrosprayed PLA erythrocyte-like microspheres.	152
Figure 5.2 Scanning electron microscope images of electrosprayed PLA microfibrils with two kinds of PLA microspheres, b) microspheres and c) beaded microspheres.	153
Figure 5.3 Scanning electron microscope images of electrosprayed PLA a,b) beaded microfibre and c,d) microfibrils.	154
Figure 5.4 Scanning electron microscope images of electrosprayed a,b) PLGA flattened microspheres, c,d) PLGA microspheres.	155
Figure 5.5 Schematic of the fabrication process of dual drug delivery composite matrices by using combinatorial electrospinning and electrospraying; the stable Taylor core of PLA solution (containing phenytoin or lacosamide) tend to form microfibrils, and the unstable	

Taylor core of PLGA solution (containing lacosamide or dexamethasone) tend to form microspheres.	157
Figure 5.6 Scanning electron microscope images of PLA phenytoin microfibrils/ PLGA lacosamide microspheres composite matrices; fewer microspheres indicate lower drug ratio.	158
Figure 5.7 Scanning electron microscope images of PLA lacosamide microfibrils/ PLGA dexamethasone microspheres composite matrices, more microspheres indicate higher drug ratio.	160
Figure 5.8 Thermogravimetric analyses (TGA) results of the as-fabricated PLGA microspheres, PLA microfibrils matrices and composite matrices which contain drugs.	161
Figure 5.9 Typical tensile stress-strain results of as-fabricated PLA microfibrils matrices and composite matrices which contain drugs.	163
Figure 5.10 Drug encapsulation efficiency testing results of PLA fibres and PLGA spheres in composite matrices.....	164
Figure 5.11 Cumulative release of each drug from PLA phenytoin microfibrils-PLGA lacosamide microspheres composite matrices.	166
Figure 5.12 Cumulative release of each drug from PLA lacosamide microfibril/PLGA dexamethasone microspheres composite matrices.....	167
Figure 5.13 Dimensional statistical analysis results of diameters including PLA phenytoin fibres, PLGA lacosamide spheres, PLA lacosamide fibres, PLGA dexamethasone spheres.	168
Figure 5.14 Diameters distribution of PLA phenytoin microfibrils, PLGA lacosamide microspheres, PLA lacosamide microfibril, and PLGA dexamethasone microspheres.....	169
Figure 5.15 Mathematical modelling of drug release of PLA phenytoin fibres and PLGA lacosamide spheres (solid curves: theory fitting results, symbols and standard deviations: experimental sampling points).....	170

Figure 5.16 Mathematical modelling of drug release of PLA lacosamide fibres and PLGA dexamethasone spheres.....	171
Figure 6.1 Schematic illustration of the fabrication procedures of a) electropolymerization of PPy fos-phenytoin on the 3D printed electrodes; b) electrospayed PLGA microspheres coating on 3D electrodes.....	186
Figure 6.2 Schematic of fabrication procedures of a) assembly process of two interdigitated PPy fos-phenytoin coated electrodes; b) assembly process of interdigitated PPy fos-phenytoin coated electrode and electrospay PLGA microspheres coated 3D electrode on insulated base.	187
Figure 6.3 Scanning Electron Microscopy images of a,b) a whole 3D electrode and individual post; c,d) high magnification of the bare 3D electrode.	189
Figure 6.4 Scanning Electron Microscopy images of the PPy-fosphenytoin coating.....	190
Figure 6.5 Scanning Electron Microscopy images of electrospayed PLGA dexamethasone coated 3D electrode. The arrows are pointing to the gaps between the microspheres.	191
Figure 6.6 The electrochemical testing results of Impedance spectra for bare 3D electrode, PLGA dexamethasone microspheres coated 3D electrode, and PPy fos-phenytoin modified 3D electrode.	192
Figure 6.7 Cyclic voltammograms of the bare 3D electrode, PLGA dexamethasone microspheres coated 3D electrode, and PPy fos-phenytoin modified 3D electrode.....	194
Figure 6.8 Electrically controlled fos-phenytoin release: a) cumulative release profile using repeated square wave, biphasic voltage stimulation (-1 V for 5s, followed by 0 V for 5s) to determine the total available drug.	195
Figure 6.9 Cumulative release profiles in response to milder electrical square wave, biphasic voltage stimulation (-0.5 V for 5s, followed by 0.5 V for 5s), and without electrical stimulation.....	196

Figure 6.10 Release amount under 120 cycles of different square wave, biphasic voltage stimulation, where the negative phase is -0.25, -0.5, -1 V, positive phase is 0.5 V. 197

Figure 6.11 Comparison of the release amount from a single 3D electrode with that from two interdigitated 3D electrodes. 198

Figure 6.12 SEM images of the PPy fos-phenytoin coating after 1200 cycles of electrical square wave, biphasic voltage stimulation (-0.5 V for 5s, followed by 0.5 V for 5s), no obvious delamination or breakdown was observed on the surface of the PPy coating. 199

Figure 6.13 Cumulative release of PLGA dexamethasone microspheres coating in aCSF (pH 7.4) at 37 °C..... 200

Figure 6.14 Diameters distribution of the dexamethasone PLGA microspheres..... 202

Figure 6.15 Comparison of the mathematical modelling results with the experimental drug release profiles of electrospray PLGA dexamethasone microspheres coating. 203

Figure 6.16 SEM images of PLGA dexamethasone microspheres coating after more than three months release incubation. It shows that the PLGA retained its spherical structure. ... 204

Figure 7.1 SEM images of PPy/graphene oxide/fosphenytoin coated on the surface of 3D printed electrode..... 217

List of Tables

Table 1.1 Examples of commonly used biodegradable aliphatic polyesters and their thermal, mechanical, biodegradable properties.....	14
Table 1.2 Typical conducting polymers and their structures.	22
Table 1.3 Examples of electrospun synthetic and biopolymers that have been used for drug delivery applications [158-160].	36
Table 2.1 Information on Reagents and Materials.	64
Table 4.1 Microcapsules with various structures and their respective fabrication conditions.	126
Table 5.1 HPLC testing parameters for the drugs including mobile phase, UV-Vis detection wavelength, and mobile phase flow rate.	151
Table 5.2 Microcapsules with various polymers, structure, and their respective fabrication conditions.	156
Table 5.3 Mechanical properties of electrospun PLA microfibre and the composite matrices.	162

CHAPTER 1: GENERAL

INTRODUCTION

1.1 Drug delivery general introduction

Advanced systems for drug delivery have attracted tremendous interest recently, in particular in the field of developing technologies concerning drug formulation, route of administration, site targeting, metabolism, and toxicity [1-12]. These technologies aim to deliver pharmaceutical agents to the site of action in order to maximize the therapeutic effect, minimize side effects, and enhance patient compliance. Unfortunately, there are two types of barriers to these delivery processes; (i) the complexity of the paths to reach the target disease site, and (ii) the limitation of tools to control the delivery behaviour [6, 13]. When the administered drug (free without a carrier) arrives into the human bloodstream, it will undergo various metabolic processes, such as renal clearance and distribution in non-target tissues [14]. Usually, these metabolic processes reduce the drug concentration and therapeutic effect at target tissues and increase the toxic side effects. However, due to the development of materials science and pharmaceutics, a wide range of carriers with multiple functions, diverse architectures, and special surface properties have been investigated [11, 15, 16].

1.1.1 Oral drug delivery

The most favourable drug administration is oral dosage, near 80% of the worldwide market [17]. It is patient friendly, non-painful, and convenient for self-medication. Compared to the administration via injection (subcutaneous, intramuscular, and intravenous delivery, etc.), oral delivery reduces the risk of disease transmission, cost, while increasing patient compliance. However, with the development of new therapeutics, more and more biotechnology-based drugs such as peptides, proteins, and other macromolecular drugs have been very effective in treating various diseases. Because of their structures, effective administration by oral route presents a significant challenge [18, 19].

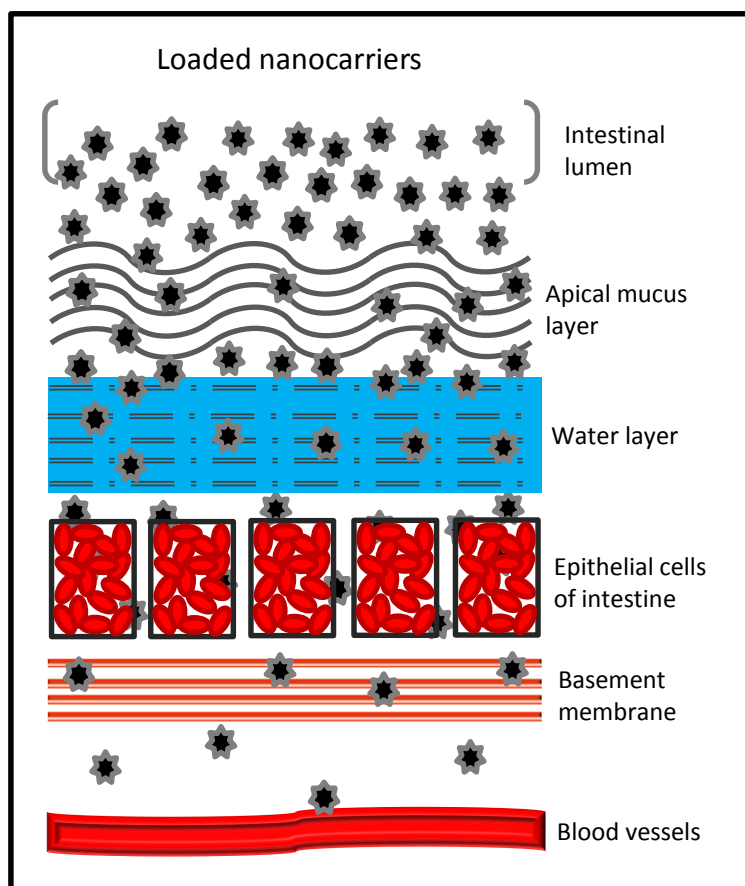


Figure 1.1 The possible obstacles for oral delivery of biological therapeutics. Reproduced from reference [20].

Due to gastrointestinal barriers (**Figure 1.1**), these biological therapeutics have poor oral bioavailability and are rarely used for direct oral administration [20, 21]. Therefore, it is necessary to design effective drug delivery systems in order to improve their bioavailability. Tremendous attempts have been made to overcome the challenges presented by the gastrointestinal barriers for oral delivery of therapeutic peptides and proteins, among which novel nanocarriers have shown their potential for improved oral administration [20]. The nanocarriers include nanoemulsions, dendrimers, micelles, liposomes, solid lipid nanoparticles and biodegradable polymeric nanoparticles [22]. However, each type of the

nanocarriers has their own limitations, and much work still needs to be done in order to gain wide clinical acceptance [23].

1.1.2 Transdermal drug delivery

Transdermal drug delivery has attracted tremendous interest and provides an attractive alternative to oral delivery and hypodermic injections [3, 24]. Besides being non-invasive and easily self-administered, in some cases, it can improve patient compliance and provide a release for long periods of time. Compared with oral administration, transdermal delivery has a particular advantage which can avoid the first-pass effect of the liver that can prematurely metabolize drugs [25]. Transdermal delivery also has advantages compared with hypodermic injection, which is painful and generates dangerous medical waste. Additionally, transdermal delivery systems are generally inexpensive compared to hypodermic injections, and would be only slightly more expensive than a tablet.

The first systemic transdermal delivery was approved by the Food and Drug Administration (FDA) in 1979 and used for motion sickness treatment. Until now, more than one billion transdermal patches are produced every year. However, only a limited number of drugs are amenable to administration by transdermal delivery, which is one of the greatest challenges for this administration method [24]. This limitation is ascribed to the inherent skin barrier function. Skin is the largest organ of the human body with a very low permeability for foreign molecules. As shown in **Figure 1.2**, the outmost layer is the stratum corneum. There are tremendous lipids organized in bilayer structures between corneocytes which provide a primary barrier to drug molecular penetration. The middle layer is viable epidermis. It

possesses the function for stratum corneum continuous renewing. The inner fibrous layer is the dermis, which provides the mechanical support for the skin [26].

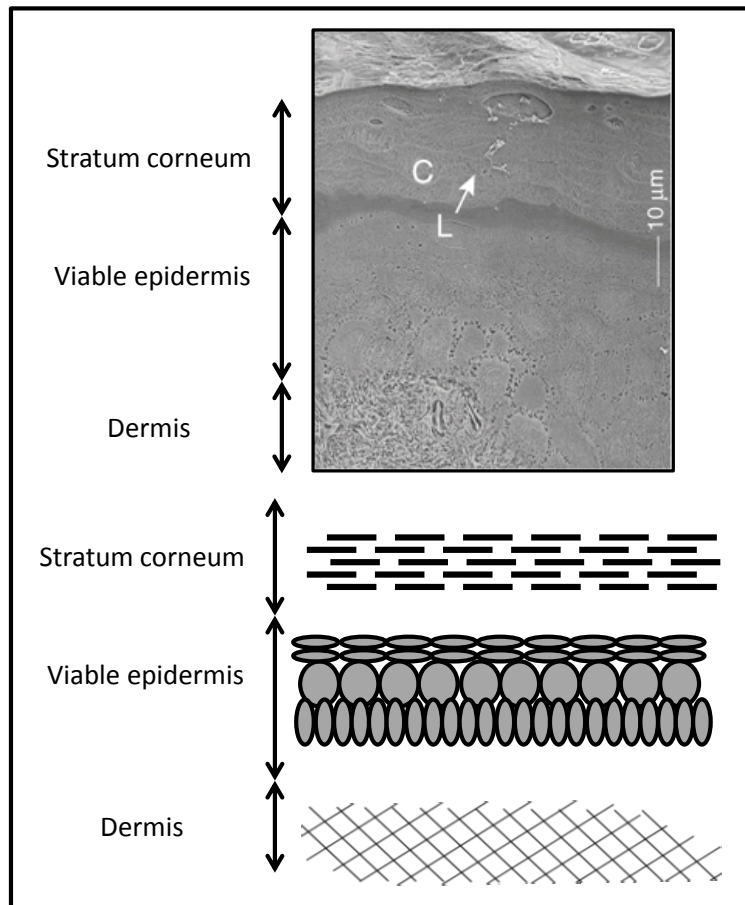


Figure 1.2 Histological structure of human skin. Reproduced from reference [24].

Transdermal delivery systems can be divided into three generations:

- 1st generation consists mostly of the patches produced today. The therapeutics in these patches can cross the skin but with little or no enhancement in penetration rate. For example, the nicotine patches had helped smokers and increased their lifespan [27].

- 2nd generation of transdermal delivery systems have been developed for delivery of small molecules with enhanced skin permeability and driving forces.
- 3rd generation of transdermal delivery systems enable transdermal delivery of not only small molecule drugs, but also biological macromolecules, such as virus-based and other vaccines et al. This generation enables stronger disruption of the stratum corneum barrier, and is thereby a most effective transdermal delivery system [28]. However, the third generation of transdermal delivery systems are still at an early developmental stage.

1.1.3 Local drug delivery

In systemic drug delivery, the drug enters into the blood circulation system where the concentration can quickly drop below an effective level. In addition, too much drug distributes to non-target tissues with only a small portion of the drug reaching the target site. To increase the dosage to the target tissues in these situations, re-administration is required, which unfortunately leads to an increased risk of overdose and the possibility of serious side effects [29].

Local drug delivery, also known as regional drug delivery, is an approach which has been developed to improve the selectivity of therapeutic reagents for target tissues. Compared with the systemic drug delivery routes, local delivery could significantly increase the drug concentrations at the disease site, thereby reducing drug loading dosage required since it is effective at avoiding the anatomic or physiological barriers, which lead to rapid drug elimination during the systemic circulation or in non-target tissue [30]. As shown in **Figure**

1.3, one of a most typical example of local drug delivery study is implanting these delivery systems next to tumours for continuously long period release [31].

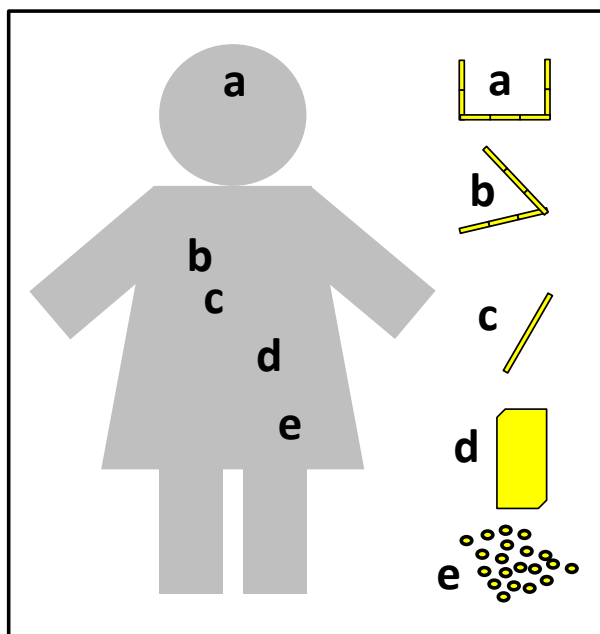


Figure 1.3 Local drug delivery strategies for cancer treatment, including a) wafers in the brain, b) film in the lung, c) rod in the liver, d) gel in the intestine or stomach, d) nanoparticles in the ootheca. Reproduced from reference [31].

1.1.4 Targeted drug delivery

The concept of targeted drug delivery was first proposed by Ehrlich at the beginning of the last century [32]. Until recent decades, targeted drug delivery has been approaching the forefront of biomedical research [33-38]. By combination of therapeutic reagents with a smart carrier, targeted drug delivery systems can be selectively accumulated in targeted cell, tissue, and organ. Because of the concentration of drugs in target sites, it can significantly

reduce the frequency of the dosage taken, fluctuation in circulating drug levels, and side effects associated with drug toxicity in non-targeted areas [34].

1.1.4.1 Kinds of targeting strategies

There are two kinds of strategies used for the targeted delivery of polymer encapsulated drug to cancerous tissue: passive targeting and active targeting [39]. Passive targeting relies on the Enhanced Permeation and Retention (EPR) effect. As a result, the concentration of the drug delivery systems in tumour tissue can be much higher than those in normal tissue (**Figure 1.4**).

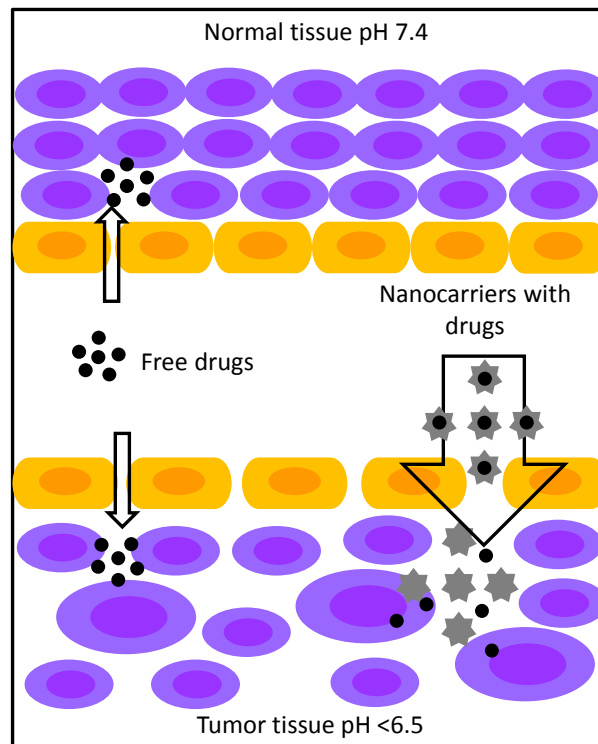


Figure 1.4 Schematic illustrations of passive targeting delivery compared with free drugs without a carrier. Reproduced from reference [40].

However, due to the presence of various biological barriers in the human body, the actual concentration of a drug at the tumour site can be low, yielding a low therapeutic efficacy [41]. Different from passive targeting, active targeting conjugates target molecules on the surface of polymer encapsulated drug particle (**Figure 1.5**). It can recognize and bind to specific ligands on the cancer cells [39]. This approach significantly increases the drug concentration in the tumour site by both local and systemic administration.

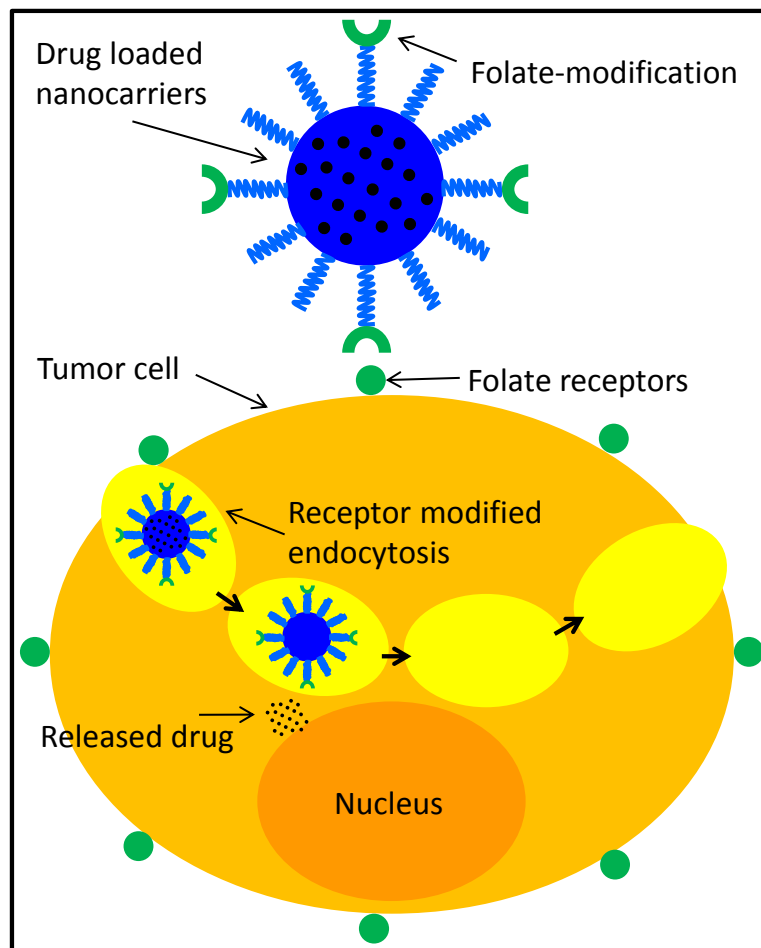


Figure 1.5 Schematic illustration of active targeting delivery, using folate modified nanocarrier as an example, receptor mediated. Reproduced from reference [40].

1.1.4.2 Application in cancer therapy

Cancer therapy is one of the most important applications of targeted drug delivery [37]. Cancer is a group of diseases involving abnormal cell growth, which causes nearly 14.6% of human deaths each year [42]. It was considered incurable, but most patients diagnosed and treated at an early stage will survive today. There are over 100 known cancers that affect humans, for most of them; chemotherapy has become an integral component of cancer treatment. However, chemotherapeutic agents typically have poor specificity in reaching tumour tissue and are often restricted by dose-limiting toxicity. Development of proper target polymer encapsulation drug delivery can provide a more efficient and less harmful solution to overcome the limitations.

1.1.4.3 Application in brain-related diseases

Another interesting and important application of targeted drug delivery is the development of nanoparticles for delivery of drugs to brain-related diseases [43-45]. Compared with delivery targeting to other organs, drug delivery to the brain is more challenging; since drugs have to cross the blood brain barrier (BBB) before reaching the targets. The BBB serves to restrict the movement of substances between the CNS and the blood circulation. It is formed primarily by endothelial cells which form complex, tight junctions (**Figure 1.6**) with substantial transendothelial electrical resistance, creating a physical barrier that severely limits paracellular transport across the BBB [43].

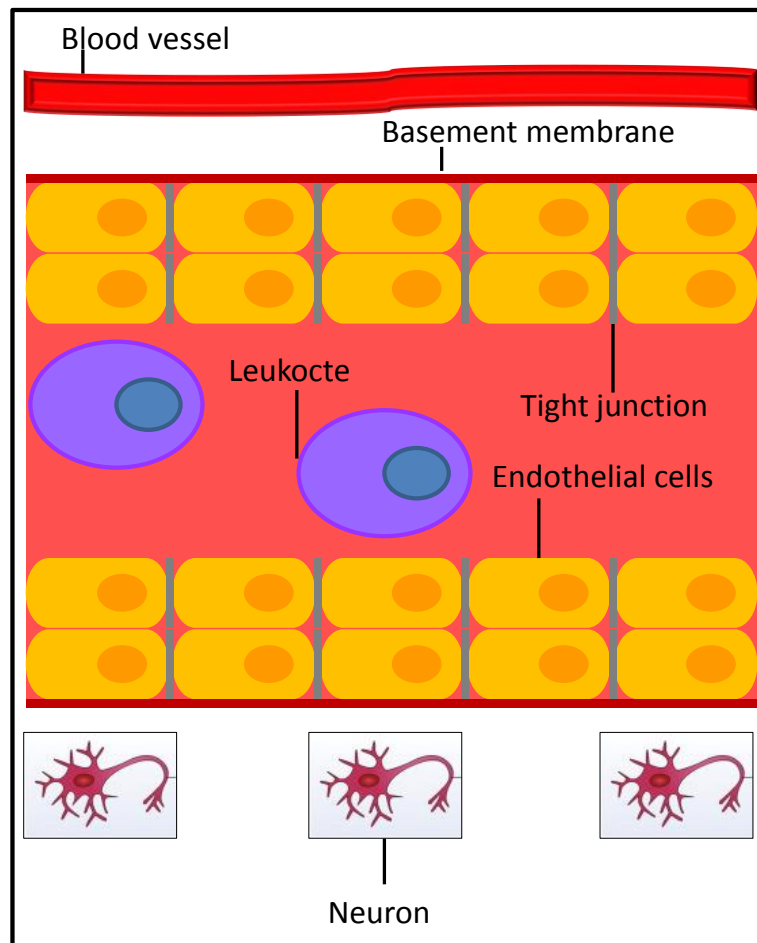


Figure 1.6 The blood-brain barrier (BBB) is mainly composed of vascular endothelial cells, highly connected by adherens and tight junctions, and a sparse layer of pericytes. Reproduced from reference [45].

In order to deliver the drugs to the brain, tremendous efforts have been made to develop nanoparticle-based targeted drug delivery for systemic delivery of therapeutic reagent [45-47]. Usually, the nanoparticle-based targeted drug delivery surface is modified to specifically recognize and bind exclusively to the surface of diseased cells [47]. The nanoparticle-based targeted drug delivery systems include polymer nanoparticles and micelles, liposomes, nanoscale ceramics, and nanoscale carbon et al. This nanoscale targeted drug delivery has

been designed to improve delivery efficiency, drug nanomedicine, and to reduce off-target effects of drug payload.

1.2 Polymer for drug delivery

Spurred by progress in materials science and fabrication techniques, a wide range of materials have been applied in drug delivery as carriers. Among them, polymers are one of the most commonly used materials [48-53]. Due to their diversity in chemistry, architecture, and dimension, polymer materials can meet the increasing requirements of developing new drug delivery systems [54]. Most of the well-developed polymeric carriers are compatible with the drug to form stable delivery systems during synthesis, storage, and administration process.

The first investigation of controlled release from polymers was conducted by Folkman and Long in 1964 using silicone rubber [55]. Later, in the 1970s, the biodegradable polymers were applied as drug delivery materials [56]. At that time, the concept of “drug delivery” is limited to achieving sustained long period of the releasing time. Today, after nearly half a century of development drug delivery systems possess more smart release behaviours and diversity in functions. During this time, a large number of polymers including different kinds of natural, semi-natural, and synthetic polymers have been investigated. And several polymer-based drug delivery systems have been “Regulatory Approved,” reaching the market [57]. There are several important characteristics of polymeric carriers such as molecular weight and its distribution, shape (architecture), size, and surface properties including hydrophobicity, hydrophilicity, and charge density. Considerations of these important

characteristics, the biodegradable polymer and conducting polymer have received tremendous interest in drug delivery research.

1.2.1 Biodegradable polymer

The polymers used for therapeutic applications can be divided into two main classes: biostable polymers and biodegradable polymers [58]. Biostable polymers have been used for a long time both for permanently and temporarily in drug delivery. However, soon after they emerged, biodegradable polymers have received great interest for temporary therapeutic applications [59-63].

Prior to the Second International Scientific Workshop on Biodegradable Polymers and Plastics at Montpellier, France, there were many definitions of the term “biodegradable polymers.” It was at this workshop that a unified definition of the degradable polymer was established as “*a polymer in which the degradation is mediated at least partially by a biological system.*” According to resources, the biodegradable polymers can be either natural or synthetic. No matter natural or synthetic, the desirable characteristics of polymer carriers are biocompatible with the human body, nontoxic, and biodegradable [64-66]. Application of natural biodegradable polymers for drug delivery is still attracting research since these polymers are naturally available, relatively inexpensive. However, for the selection of a biodegradable polymer carrier, there is a criterion that the mechanical properties and the degradable rate should match to the needs of the clinical application [67]. Therefore, the synthetic biodegradable polymers have their own advantage from these perspectives.

1.2.1.1 Biodegradable polyesters

Table 1.1 Examples of commonly used biodegradable aliphatic polyesters and their thermal, mechanical, biodegradable properties.

Polymer	T _m (°C)	T _g (°C)	Tensile modulus (MPa)	Degradation time (Months)
poly(glycolic acid)	225-230	35-40	7	6-12
L- poly(lactic acid)	173-178	60-65	2.7	>24
DL-poly(lactic acid)	Amorphous	55-60	1.9	12-16
poly(ε-caprolactone)	58-63	-65--60	0.4	>24
poly(lactic-co-glycolic acid)	Amorphous	50-55	2.0	5-6

(85/15)

The most widely investigated synthetic biodegradable polymers used in biomedicine for drug delivery are aliphatic polyesters such as poly(glycolic acid) (PGA), poly(lactic acid), poly(lactic-co-glycolic acid) (PLGA) and poly(ε-caprolactone) (PCL) respectively; as shown in **Table 1.1** and **Figure 1.7** [65].

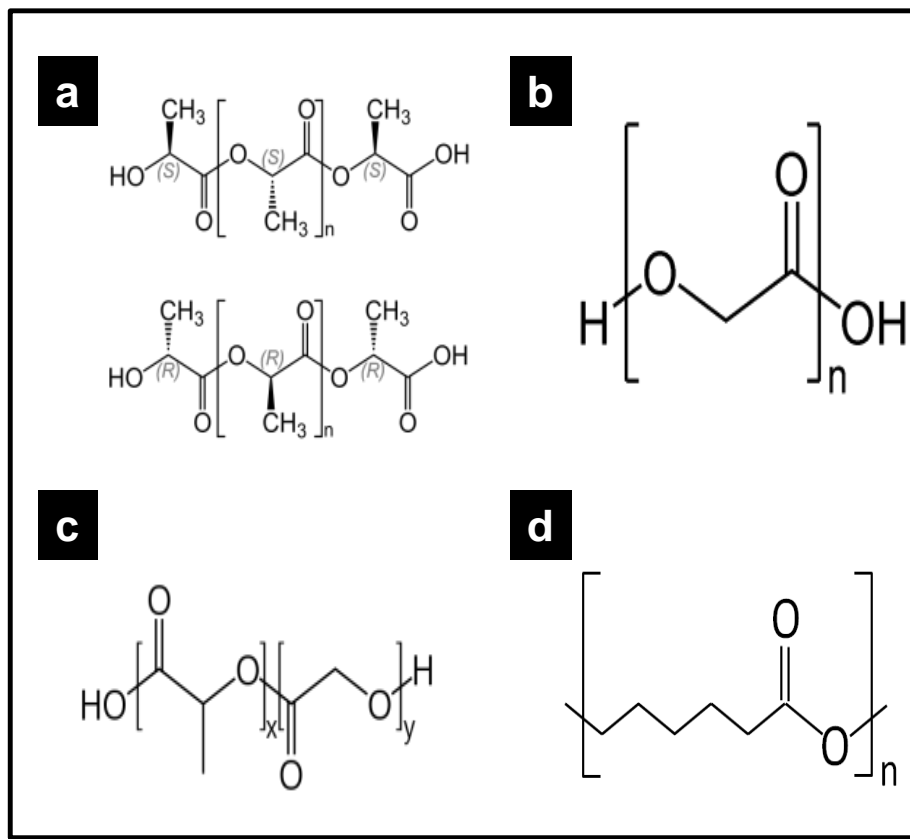


Figure 1.7 Most commonly used biodegradable polyesters. a) L- and DL-PLA, b) PGA, c) PLGA, d) PCL.

These aliphatic polyesters are derived from the lactic and glycolic acids monomers. Compared to some natural biodegradable polymers (such as collagen, gelatin, chitosan, and alginate), these synthetic biodegradable polymers are commercially available in different compositions and molecular weights, and which allow control of degradation rate of the polymers. Those early investigations demonstrated the well biocompatible, nontoxic, and predictable properties of these aliphatic polyesters [68-70].

1.2.1.2 Erosion and drug release mechanisms

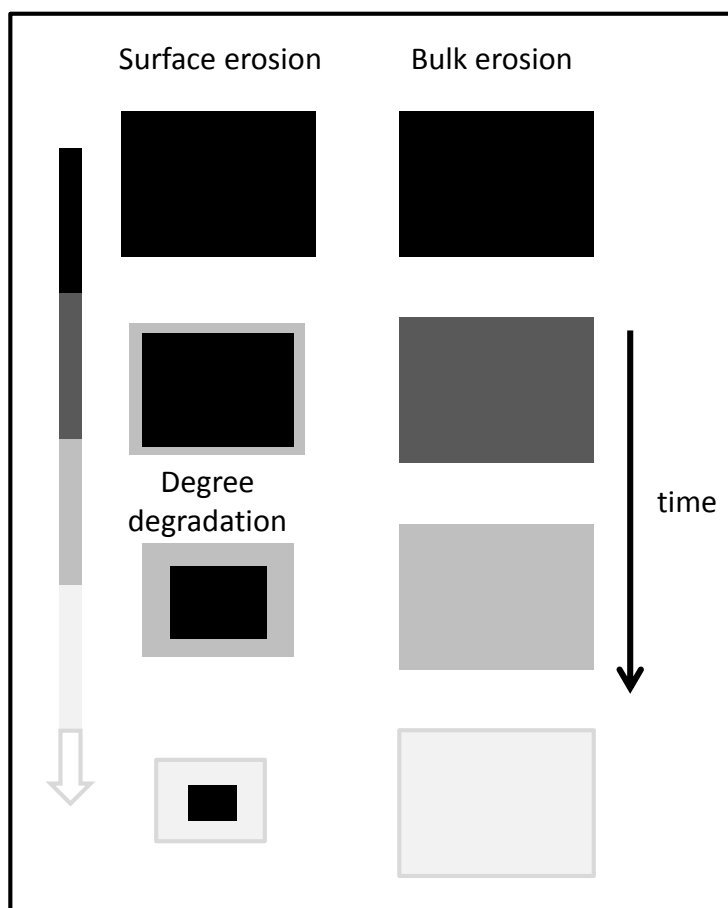


Figure 1.8 The schematic illustration of erosion mechanisms: surface erosion (left) and bulk erosion (right). Reproduced from reference [71].

The aforesaid polyesters are generally prepared by ring-opening polymerization of the cyclic esters. The degradation describes the process of polymer chain cleavage, leading to molecular weight loss. And the degradation results in the subsequent erosion of the polymer. For the biodegradable polymers, there are two kinds of erosion mechanisms: bulk erosion and surface erosion [71]. Bulk erosion is also known as homogeneous erosion; surface erosion is also known as heterogeneous erosion (as shown in **Figure 1.8**). Due to water penetration into the polymer bulk being faster than polymer degradation, bulk erosion occurs all over the polymer

cross-section. In contrast, for surface erosion biodegradable polymer, the degradation is faster than the penetration of water into the bulk. However, for most biodegradable polymers, both of these two mechanisms would occur with the erosion mechanisms having consequences on the drug release mechanisms.

The drug release mechanisms from these biodegradable polymer matrices can be divided into three kinds: (i) diffusion controlled, (ii) swelling controlled, and (iii) erosion controlled (**Figure 1.9**). Degradation of the polyesters starts with the hydrolytic breakage of the ester bonds. It occurs randomly via hydrolytic ester cleavage when water penetration into the polymers leads to the subsequent erosion. Many parameters affect the degradation rate; including molecular weight, polydispersity and crystallinity, polymer composition, and all these factors can be used to control drug release [72]. For example, the copolymer PLGA, which is a copolymer consisting of lactic acid and glycolic acid, the rate of degradation increases with the ratio of glycolic acid to lactic acid. As an exception to this rule, when the ratio of lactic acid and glycolic acid is 50/50, the rate of degradation is the fastest, approximately two months in vivo [73].

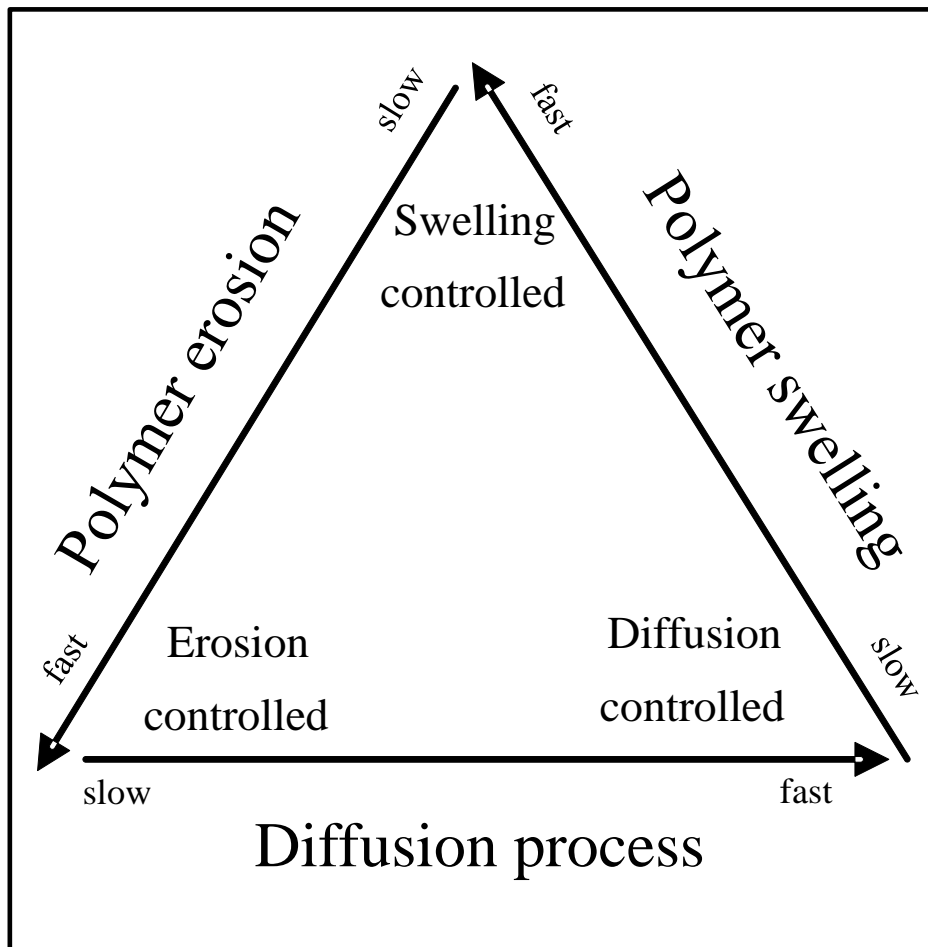


Figure 1.9 Mechanism of drug release from degradable polymers. Reproduced from reference [74].

1.2.1.3 Application in drug delivery

Recently, a wealth of studies has been conducted using PLGA, PLA as carriers for drug delivery. In order to efficiently transport to the central nervous system through the blood-brain barrier, Fornaguera *et al.* used nano-emulsion with a low-energy method to fabricate loperamide loaded PLGA nanoparticles (as shown in **Figure 1.10**) [75]. Firstly, non-loaded polymeric O/W (Oil phase/Water phase) nanoemulsion was prepared. Then, the emulsions with 90 wt% of aqueous phase content and 70/30 O/W ratio was selected as a compromise between 50 nm droplet and low surfactant contents. After that, the nano-emulsions were

reformulated containing 0.1 wt% drug in the oil phase and the droplet size around 100 nm. Then, the drug-loaded PLGA nanoparticles were finally obtained by solvent evaporation. This is a methodology which can be easily applied to the scalable production of nanoparticles of biodegradable polymers (PLGA).

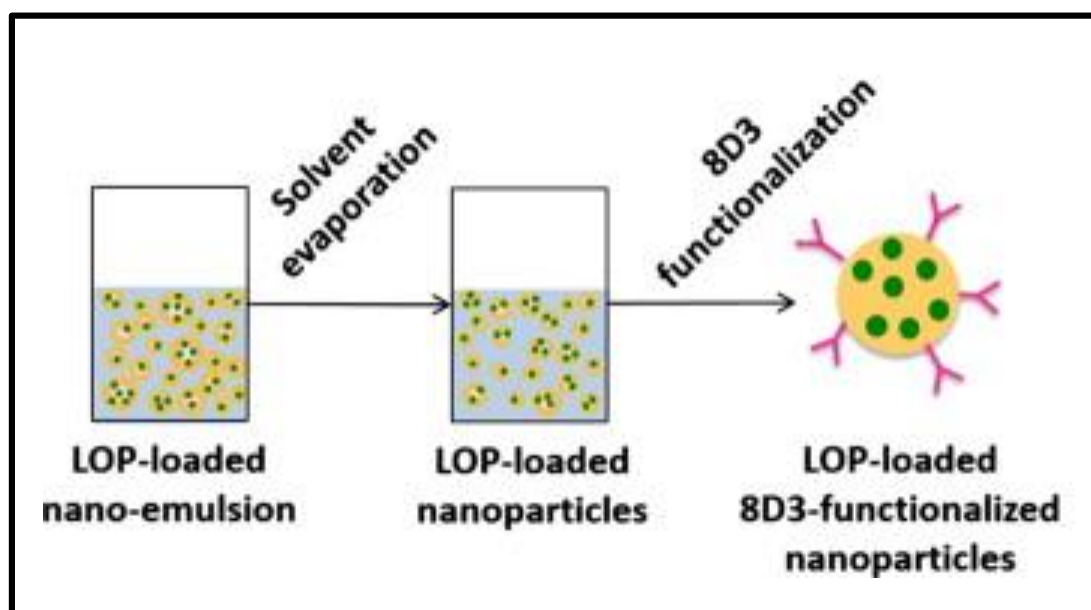


Figure 1.10 Schematic illustration of the fabrication and function of the loperamide loaded PLGA nanoparticles. Reproduced from reference [75].

Ye *et al.* developed biodegradable polymeric vesicles as a nanocarrier system both for multimodal bioimaging and anticancer drug delivery [76]. They synthesized PLGA-SPION-Mn:ZnS vesicles as a multifunctional drug delivery system. It used the biodegradable polymer as a shell containing multiple imaging agents and anti-cancer drug (**Figure 1.11**). This drug delivery system showed enhanced imaging contrast, improved cell uptake, and enhanced fluorescence visualization. It also exhibited both high entrapment efficiency for the lipophilic drug busulfan and sustained drug release. The *in vivo* results confirmed the

biodistribution to different tissues. Wan *et al.* developed PLGA microparticles by using the spray-drying method. They used different molecular weight PLGA and different solvent mixtures, which resulted in different drug diffusion rates during the process of microparticle formation and the drug release profiles were dependent on the solvent composition.

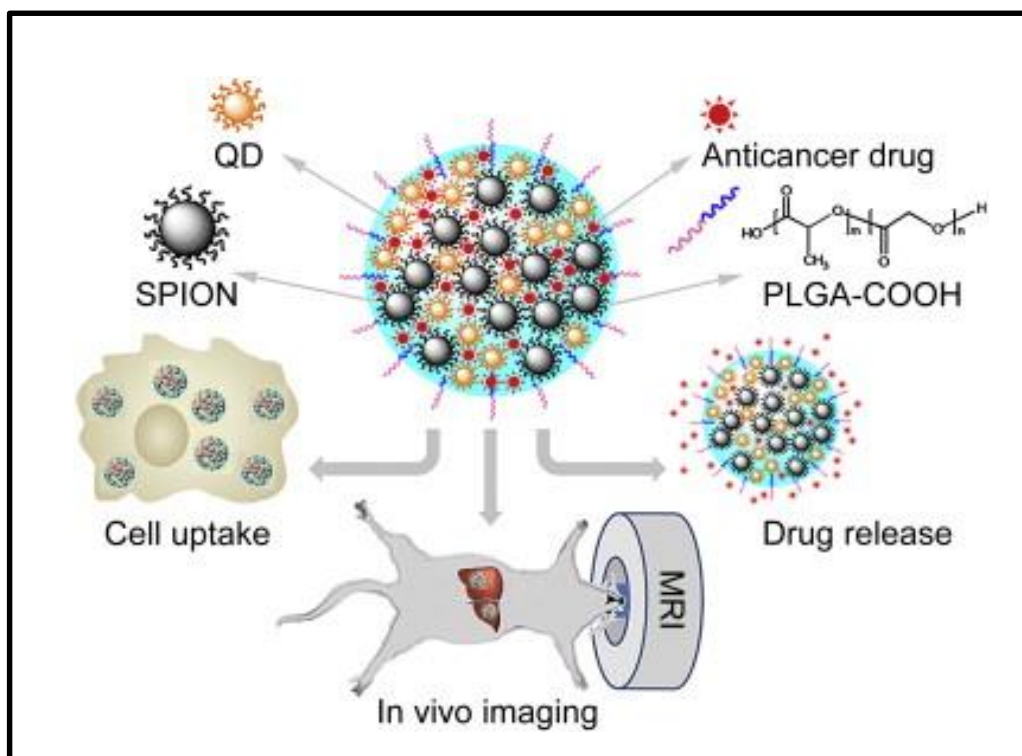


Figure 1.11 Schematic illustration of the composition of PLGA composite nanoparticles and their applications. Cited from reference [76].

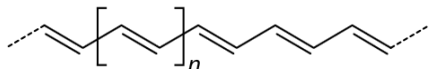
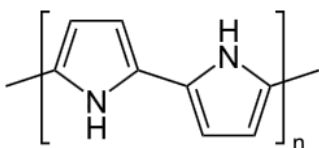
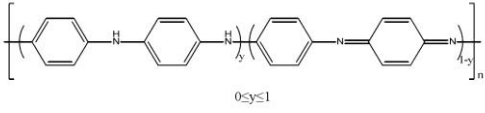
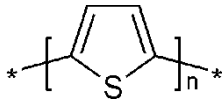
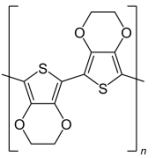
Combining different biodegradable polymers or other polymers together to form a composite carrier is also an attractive research area. PLGA nanoparticle was coated with a layer of polydopamine. Then a layer of poly(ethylene glycol) was formed and the drug loading content achieved a 3.8-fold increase [77]. Covalent surface modified PLGA microparticle demonstrated enhanced durable binding on targeted cells and ultra-high cytostatic efficacy

[78]. Chitosan was also used to modify PLGA nanoparticles, and it showed a positive charge surface and affected the drug release profile [79]. Other interesting work is that of the fabrication of a hybrid dendrimer hydrogel/PLGA nanoparticle which can enhance drug bioavailability, reduce dosing frequency, and substantially enhance sustaining drug activity [80].

1.2.2 Conducting polymers

Conducting polymers can be categorized as intrinsic conducting polymers or composite conducting polymers [81]. Here the focus is on intrinsic conducting polymers. Conductive polymers are organic polymers with metallic electrical properties [82]. The first conducting polymer, polyacetylene (PAC) was discovered in 1977 at Tokyo Institute of Technology by Shirakawa *et al.* [83]. Until now, after several decades investigation and development, a series of conducting polymers have found use in a wide range of applications both in research and industry [84-90]. The most widely applied conducting polymers are polypyrrole (PPy) [91, 92], polyaniline (PANi) [93, 94], polythiophene (PT) [95], and poly(3'4-ethylenedioxythiophene) (PEDOT) [96, 97] (**Table 1.2**).

Table 1.2 Typical conducting polymers and their structures.

Name	Molecular structure
polyacetylene (PAC)	
polypyrrole (PPy)	
polyaniline (PANi)	
polythiophene (PT)	
poly(3,4-ethylenedioxythiophene) (PEDOT)	

1.2.2.1 Synthesis of conducting polymer

Conducting polymers can be synthesized by chemical or electrochemical means, and involves oxidative polymerization [82, 98]. Usually, the conducting polymers used for drug delivery

are synthesised by using electrochemical oxidation. Compared to chemical polymerization, the electrochemical polymerization process can be easily controlled by adjusting the amount, and rate of charge passed during growth. Even the morphology and electromechanical properties can be controlled [99].

The electrochemical oxidation in conducting polymer preparation process is usually carried out using two-electrode or three-electrode systems with a reference electrode, a counter electrode, and a working electrode [100]. The reference electrode is often silver/silver chloride (Ag/AgCl), the counter electrode usually is platinum, and the conducting polymer is deposited on the surface of the working electrode. Synthesis can be performed using either constant potential, constant current or cyclic voltammetry which is referred to as potentiostatic mode, galvanostatic mode, and potentiodynamic mode respectively.

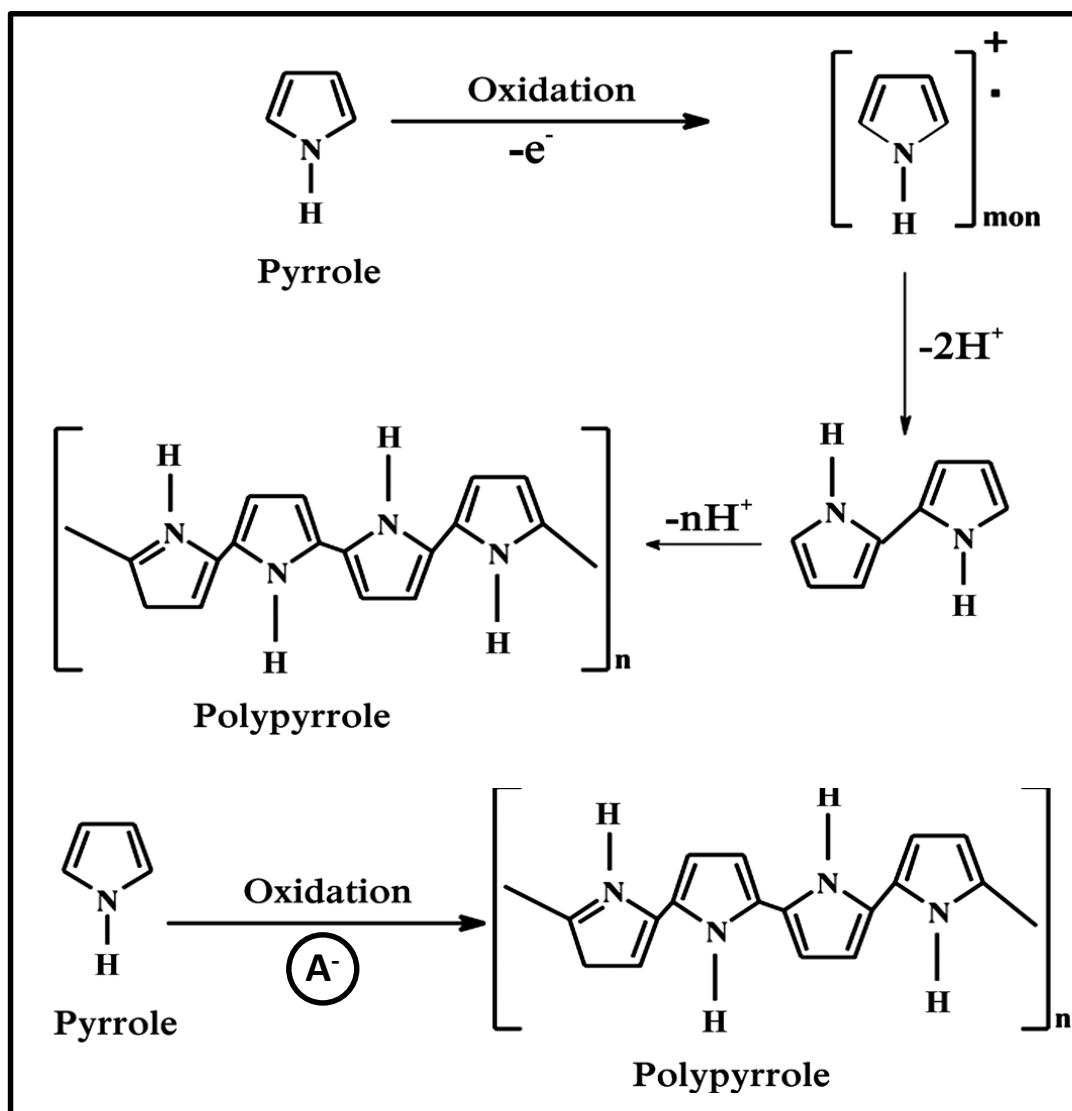


Figure 1.12 The principle of electropolymerization of polypyrrole: the monomer is pyrrole, A^- is negative drug molecule, e^- is electronic charge. Cited from reference [101].

Many parameters affect the final conducting polymer properties. However, the key process is related to doping which incorporates anionic molecules into the polymer backbone [102]. Take polypyrrole preparation for example, where the dopant is A^- (inserted into polypyrrole backbone to alter the electrical characteristic), the pyrrole monomers would be electrochemically oxidized and polymerized on the surface of the working electrode. At the initiation, pyrrole monomers are oxidised to radical cations. Then the radical cations dimerise

with radical-radical coupling at α positions. The neutral dimer can then be oxidised to a radical and later react with a monomer, dimer or oligomeric radical to grow the chain (as shown in **Figure 1.12**) [101, 103].

1.2.2.2 Properties of conducting polymer

The inherent conductivity is attributable to the uninterrupted and ordered π -conjugated structure of the polymer backbone (**Table 1.2**) [104]. The contiguous sp^2 hybridized carbon centres have high mobility when the polymers are doped by oxidation, which is responsible for the electrical conductivity of the polymers. There is a one-dimensional electronic band within the conducting polymers, and the electrons within this band would become mobile electrons when holes are formed (empty of electron). The free electrons move along the polymer backbone and result in the conductivity of the polymers (**Figure 1.13**). The degree of conductivity depends on the electrons density and mobility, which can span several orders of magnitude [105].

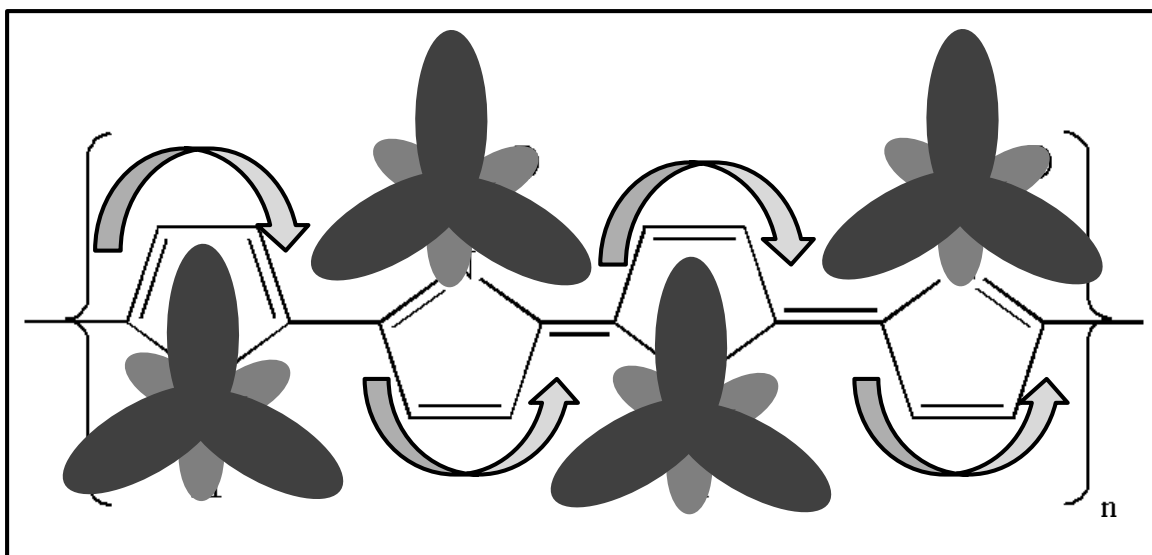


Figure 1.13 Schematic illustrations of the conduction process in polypyrrole.

The mechanical properties of most conducting polymers are poor. They are brittle and easily destroyed. The processability of conducting polymers is also poor. Most of them are not soluble in common solvents, and cannot be melt processed. However, some polymers such as polypyrrole and poly(3,4-ethylenedioxythiophene) have good biocompatibility and have been widely applied in biomedical areas. Studies have shown that bioactive molecules can be incorporated into the conducting polymers to enhance their biocompatibility [106, 107]. Moreover, the cellular reactions associated with implanted devices can be modulated by stimulation via the conducting polymer [108].

1.2.2.3 Application in drug delivery

In drug delivery applications, negatively charged drugs or biomolecules have been incorporated into conductive polymers such as Polypyrrole or PEDOT, during the process of oxidative polymerization to maintain charge neutrality.

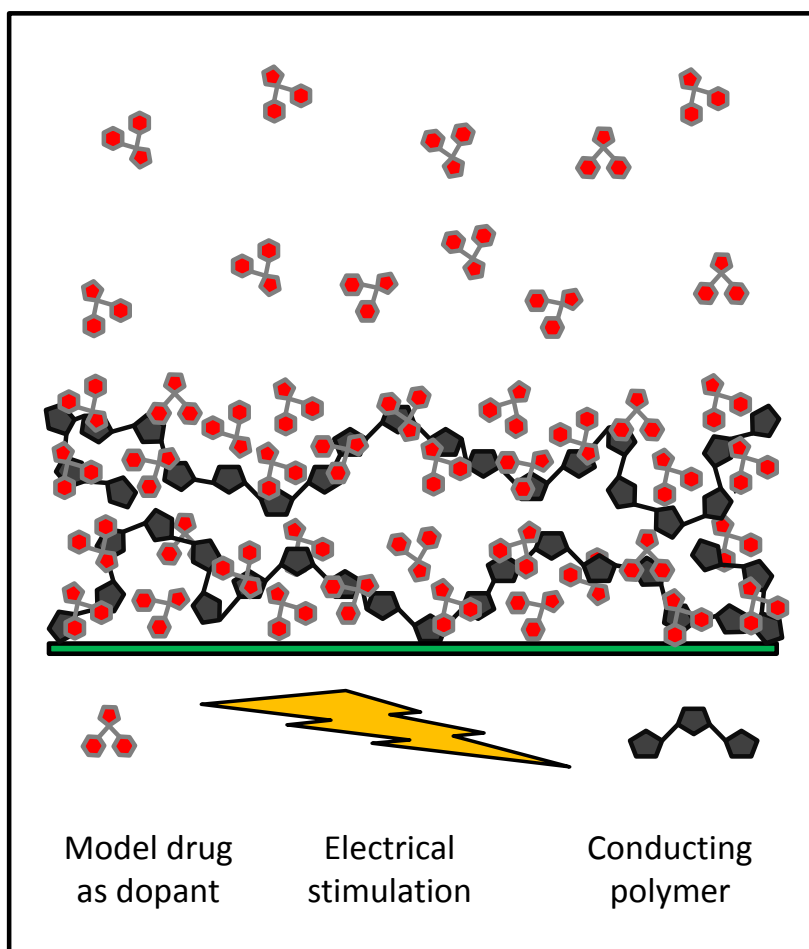


Figure 1.14 The drug release from conducting polymer in response to electrical stimulation.

The electrically triggered release involves a synergistic process of electrochemical reduction/oxidation and electrically driven movement of these charged molecules (dopant). In drug delivery studies, charged drugs or biomolecules could be incorporated into the PPy coating [109, 110]. When the PPy coating is electrochemically reduced, the doped molecules will be released (**Figure 1.14**). The release of the drug is associated with the change of the overall net charge along the PPy backbone in the oxidized form.

Many parameters affect the amount of drug released and the release rate from conducting polymers. As mentioned above, the conducting polymers for drug delivery applications are usually deposited on the electrode as a film. Therefore, the total amount of the incorporated drugs is related to the film thickness and density. Increasing the thickness and density will lead to increased drug loading. However, the available drug for releasing is not linearly increased with the thickness of the film. The thinner film could release a higher percentage of the incorporated drugs [111, 112]. Actually, the releasing amount from conducting polymer is a surface area dependent process, with drug releasing more efficiently from the surface than the bulk of the film [113].

It has been demonstrated that the media used for release studies, with variations of *pH*, ionic strength, influence the release profile from a conductive polymer [114]. However, electrical stimulation parameters are key determining factors, affecting both the release amount and release rate [115]. Potential sweeping has been used to release the drugs [116, 117]. Another frequently applied electrical stimulation waveform is pulsed potential which changes the potential instantaneously between set potentials [118, 119]. In addition, there is a clinical stimulation to stimulate the conducting polymers by using a biphasic, charge balanced, and high frequency current stimulation [120].

1.3 Technology in drug delivery

To overcome the problems raised by present drug administration, advanced nanotechnology for fabricating nano- and micro-scale drug delivery systems has gained tremendous attention [39, 121-129]. Compared with conventional technology, nanotechnology may revolutionise

the rules and possibilities of drug discovery and change the landscape of pharmaceutical industries [121, 130-133]. By application of nanotechnology to fabricate proper drug delivery systems, it is possible to achieve improvement of pharmacokinetics and pharmacodynamics including but not limited to the following aspects: (1) delivery of poor water soluble or very short circulating half-life drugs which demonstrates potent biological activity; (2) passive targeting or active targeting delivery of drugs to specific tissue or even into the single cell; (3) transcytosis of drugs across special biological barriers such as skin or blood brain barrier; (4) for combination therapy involving co-delivery of dual or multiple drugs; (5) delivery of macromolecular drugs to intracellular sites of action; (6) for other biological applications to deliver diagnostic or visualisation agent et al.

Liposomes are the first nanotechnology drug delivery system developed in the 1960s [134]. While the first controlled release polymer system for delivery of macromolecules was reported in 1976 [135]. The first long circulating liposomes were described in 1987, and the concept was later named “stealth liposomes” [136]. After that, the use of polyethylene glycol (PEG) and polyesters such as PLA and PLGA was increased in the 1990s. A variety of nanotechnology fabricated nanomaterials and devices for drug delivery systems were developed (**Figure 1.15**).

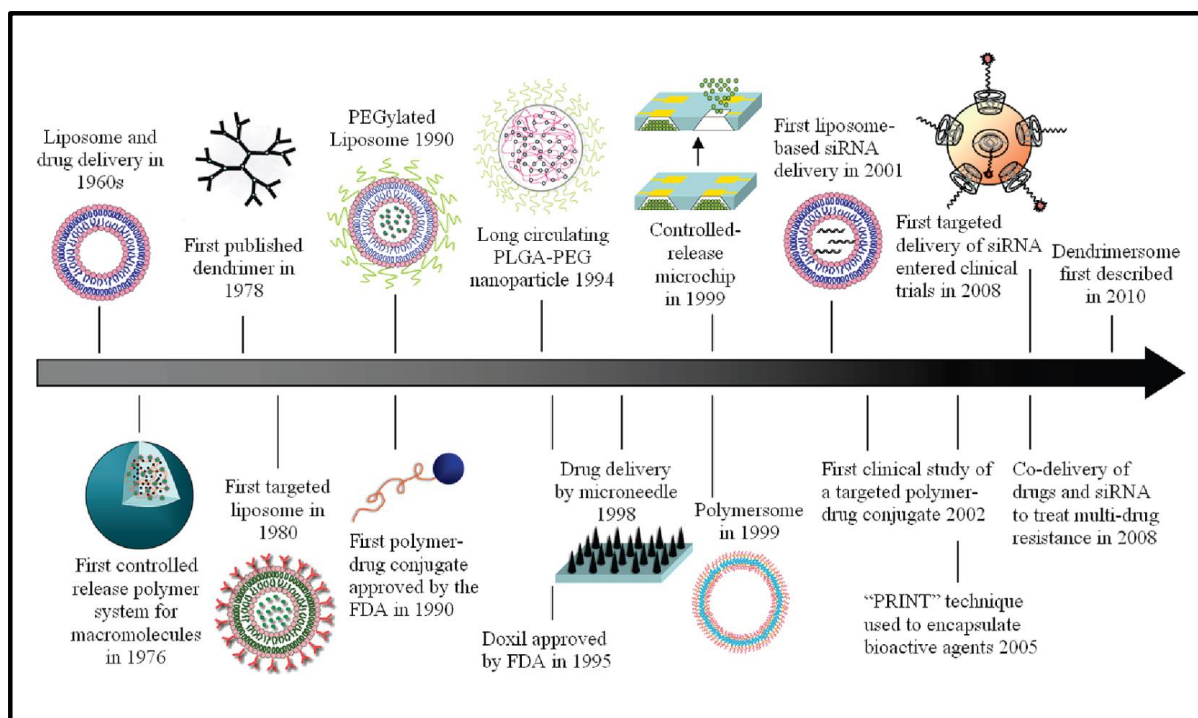


Figure 1.15 Timeline of nanotechnology-based drug delivery. Highlights of some delivery systems that serve as important milestones throughout the history of drug delivery. Cited from reference [130].

Among them, more than two dozen therapeutic delivery systems have been approved for clinical use. Most of the clinical use delivery systems can be divided into either liposomal drugs or polymer-drug conjugates [137]. In the future, it is important to continue using nanotechnology to develop entirely new therapeutics delivery systems which differ from these two kinds [130, 138].

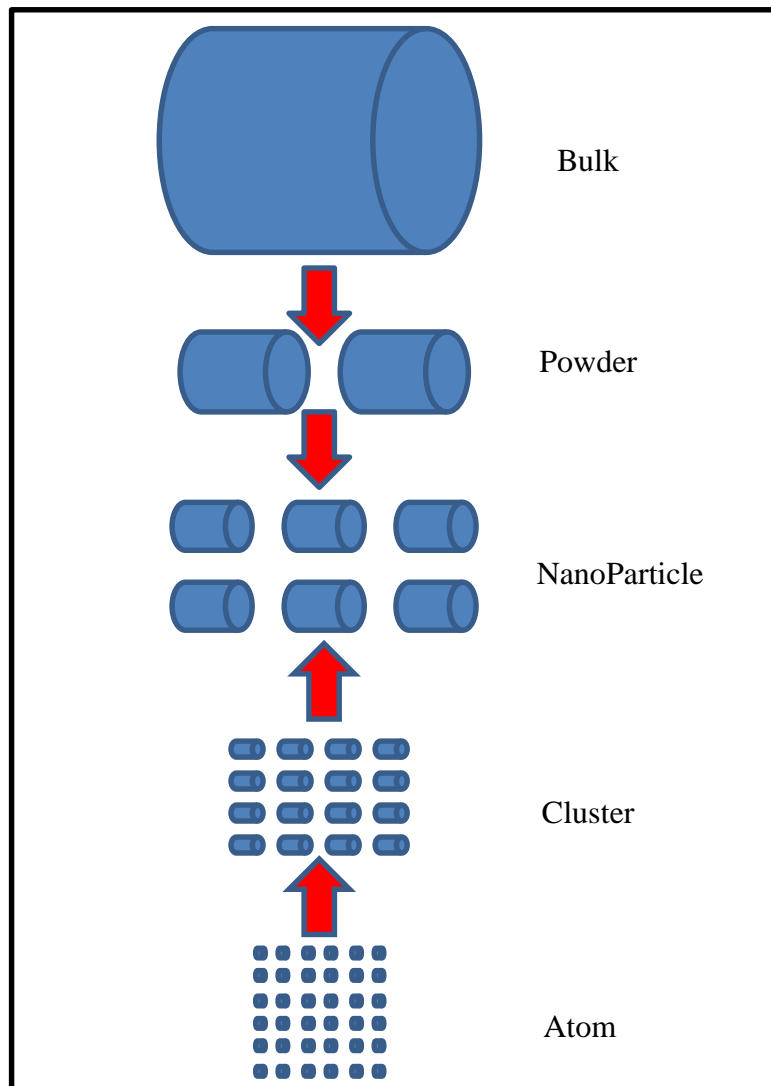


Figure 1.16 Nanotechnology-based synthetic methods: top-down or bottom-up engineering of individual components.

Nanotechnology-based synthetic methods are most commonly developed on the basis of two rational designs: either top-down or bottom-up engineering of individual components [122, 139]. The top-down process involves starting with a larger object and breaking it up into nanostructures, while the bottom-up technique refers to synthesis based on atom-by-atom or molecule-by-molecule arrangement in a controlled manner, which is usually regulated by thermodynamic means (as demonstrated in **Figure 1.16**). There are many nanotechnology

methods for fabricating drug delivery systems. Here, the focus is on technologies for fabricating nano- or micro-scale polymeric fibres and particles including electrospinning and electrospraying which are extensively used in this thesis.

1.3.1 Electrospinning

Electrospinning is a simple and effective method to fabricate polymer fibres with diameters ranging from several nanometres to tens of micrometres [140-146]. The simple procedure, possible large-scale production, and wide variety of suitable polymer materials, make electrospinning an attractive technique for biomedical applications such as tissue engineering, wound repairing, and drug delivery.

1.3.1.1 Electrospinning history

The term “electrospinning” is derived from electrostatic spinning, which has been extensively used since the 1990s [140, 147]. However, the application of electrostatic forces to fabricate fibres can be traced back more than two centuries. In 1745, Bose first demonstrated the use of high electric potentials to fabricate aerosols. In 1882, Lord Rayleigh conducted an in-depth investigation and calculated the charges number that was required to overcome the surface tension of a droplet [148]. At the beginning of the last century, Cooley and Morton developed the first device which can use an electrical charge to spray liquids. From 1934 to 1944, Anton Formhals described the first experimental setup to use electrostatic forces to generate polymeric fibres [149]. Cellulose acetate fibres with small diameters were firstly successfully prepared. Formhals also had a patent for fabrication of composites fibres at that time [150].

After Formhals, more works have been reported focusing on the better understanding of the process of electrospinning. In 1969, Taylor investigated the polymer droplet formation at the end of a capillary [151]. When an electric field is applied, the pendant droplet becomes a cone due to the electrostatic forces being balanced with the surface tension. This cone is now known as “Taylor cone”. Taylor also found that the diameters of the formed fibres are much thinner than the diameter of the applied capillary. It is because of the fibre jet is emitted from the apex of the core. After Taylor, Baumgarten used a high-speed camera to observe a single fibre formation from the droplet. In 1971, Baumgarten firstly conducted the studies on the effects of processing parameters and solution properties on the electrospun fibre structures [152]. Despite these early investigations, electrospinning had not widely been used until the 1990s. In the 1990s, the Reneker group rediscovered and spread the investigation and application of the electrospinning technology. After that, electrospinning has received extensive research interest [153, 154].

1.3.1.2 Electrospinning setup and parameters

A typical electrospinning setup consists of three major components: (a) a high voltage power supply; (b) a spinneret connected with solution supplier; and (c) a conductive grounded collector. This is schematically shown in **Figure 1.17**. After feeding a polymer solution to the spinneret, a droplet of the polymer solution is formed at the tip of the spinneret due to surface tension. Application of an electric field between the spinneret and collector adds electrical charges to the droplet. It leads to an electrical force directly opposite to the surface tension. With increasing voltage of the electric field, the number of surface charges increases until the electrical force overcomes the surface tension at which point the liquid polymer solution would be ejected towards the collector. During the movement process of the solution, the

solvent evaporates and finally polymer fibres would form on the surface of the collector [155]. Development of more advanced systems that enable production of core-shell fibres, tri-axial fibres, multi-tubes fibres, oriented fibres, twisted fibres, and patterned fibres mats can be achieved by refitting the spinnerets and/or collectors.

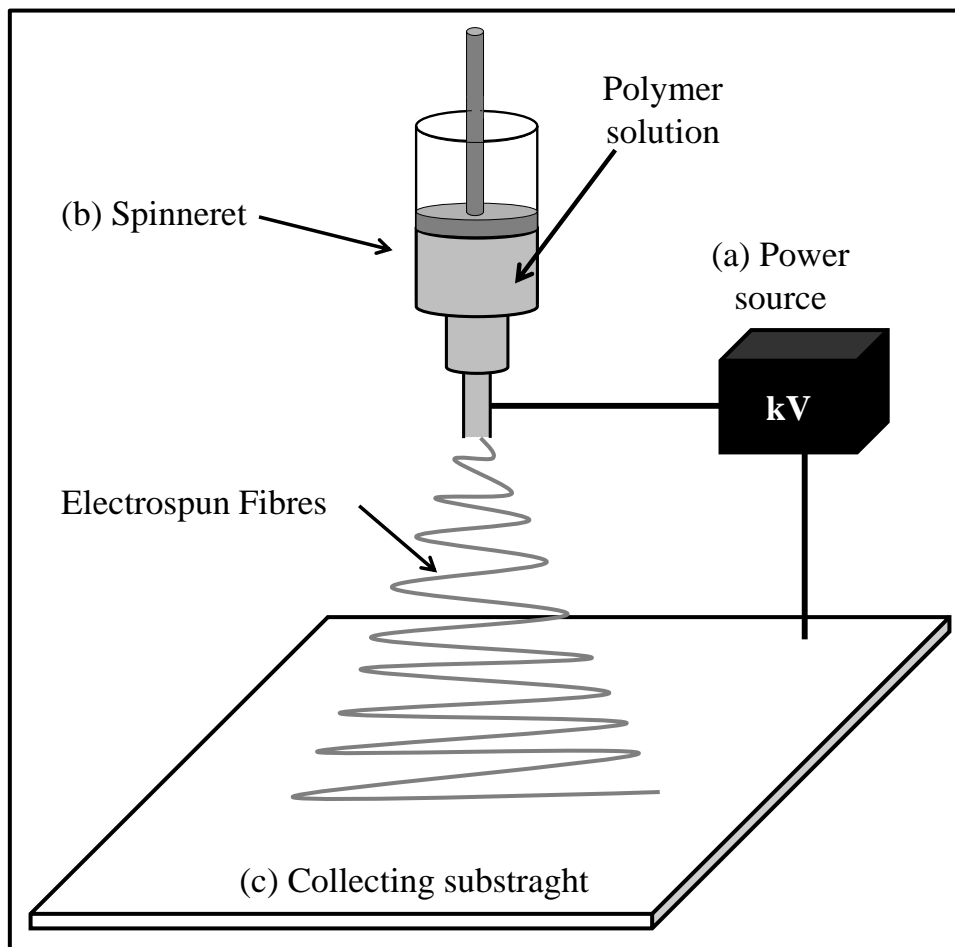


Figure 1.17 Schematics of the experimental setup used to perform electrospinning.

Although electrospinning is simple and easy to manipulate, there are still a range of processing parameters which can influence the final fibre structure and morphology. All the parameters can be summarized and divided into three groups: (a) solution properties

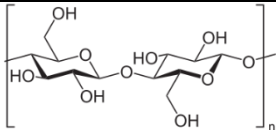
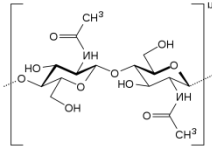
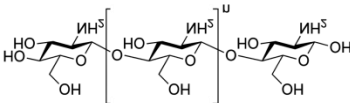
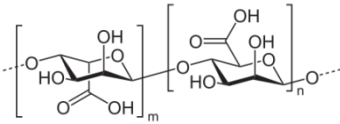
such viscosity, elasticity, conductivity, and surface tension; (b) governing variables such as hydrostatic pressure in the capillary tube, electric potential between spinneret and collector, and the distance between the spinneret and collector; (c) ambient parameters such as solution and air temperature, humidity, and air velocity in the electrospinning environment [155-157].

1.3.1.3 Application of electrospinning to drug delivery systems

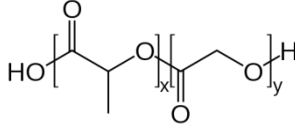
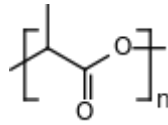
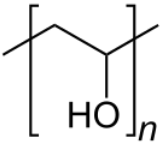
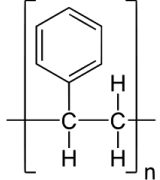
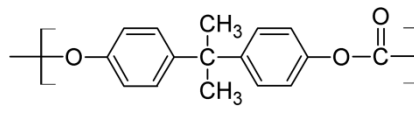
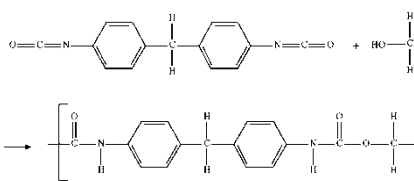
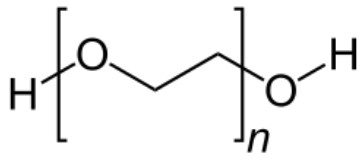
Electrospinning has been explored in a wide variety of biomedical application such as tissue engineering, drug delivery, and biosensors. Applications in drug delivery for fabrication of carriers, electrospinning affords flexibility in materials selections; both biodegradable and non-degradable polymers can be electrospun into fibres. **Table 1.3** lists the examples of synthetic and biopolymers that have been electrospun to produce nano- or micro-scale fibres for use in drug delivery. These matrices have been utilized for delivery of a number of drugs including antibiotics, anti-inflammatory drugs, anticancer drugs, proteins, DNA, and RNA [158].

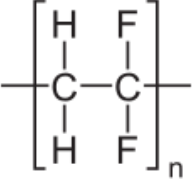
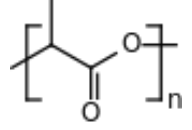
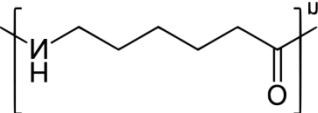
For drug delivery applications, electrospun fibres received much attention because of their peculiar structures. The thinner fibres possess large surface area to volume ratios. The porosity of the fibrous mats dramatically further increases the surface areas. Compared with other polymeric structures, it not only overcomes the limitation of high drug uptake, but also surmounts the constraint of drug diffusion [159]. This significantly increases the drug release efficiency. Besides these, it is easy to control the properties of the electrospun mats such as porosity, diameters, and morphology which can regulate the release kinetics.

Table 1.3 Examples of electrospun synthetic and biopolymers that have been used for drug delivery applications [158-160].

Polymer	Structure	Polymer Information	Solvent	Concentration
Cellulose		Surgical cotton (1140 polymerization)	8 wt% LiCl/DMAc	1-3 wt%
Cellulose Acetate	N/A	Molecular weight 30 k	Acetone/Water	10 wt%
Chitin		Molecular weight 920 k	HFIP	3-6 wt%
Chitosan		Molecular weight 210 k	TFA	7 wt%
Alginate		Molecular weight 196 k	water	0.25-2 wt%
Collagen	N/A	From Kensey Nash	HFP	10 wt%
Gelatin	N/A	From Aldrich	TFE	7.5 wt%
Silk	N/A	Bombyx mori	LiBr/water	0.45 g/ml

silk cocoons

PLGA		60 k	DMF/ Dichloroform	1g/8ml
PLA		109 k	Dichloroform	5 wt%
PVA		65 k	water	8-16 wt%
PS		190 k	THF	18-35 wt%
PC		80 k	DMF/chloroform m	17 wt%
PU		400D	DMF	21 wt%
PEO		400 k	water	7-10 wt%

PVDF		107 k	DMF	20 wt%
PCL		50 k	Chloroform/met hanol	12 wt%
Nylon 6		10 k	Formic acid	10 wt%

Electrospinning can be used to load drugs by various methods including coating, embedding, and encapsulating drugs which lead to well-controlled drug release kinetics. In cases where both the polymer matrix and drug are soluble in the same solvent, the drug can be incorporated into the polymer by directly dissolving in the polymer solution [160]. When they cannot be dissolved in the same solvent, the drug can be dissolved in a solvent that is miscible with the polymer solution [161]. By these ways, after the electrospinning, the drug would be embedded in the polymeric fibres. The drug can also be encapsulated in the polymer using coaxial and emulsion electrospinning [162]. Other popular methods of drug loading adopted are: where the electrospun fibrous mats are immersed in a drug solution, or surface coating [163]. Therefore, in these two cases, the drug release mechanisms are diffusion from the polymer matrix or desorption from the fibre surface.

1.3.2 Electrospaying

Electrospaying is also another electro-hydrodynamic fabrication method widely applied in drug delivery [164-167]. Actually, electrospaying is considered as “sister” technology to electrospinning (**Figure 1.18**). The only difference is that electrospinning is used for nano-microfibre fabrication; while electrospaying is used to produce nano- or micro-particles.

As introduced in the electrospinning part, the polymer solution at the tip of the spinneret would form a Taylor cone. When the electrostatic repulsion surpasses the surface tension, liquid ejection will occur at the surface of the Taylor cone. If the Taylor cone is stable, the liquid jet will undergo a whipping or bending motion process, which leads to the formation of fibres. However, if the Taylor cone is unstable, the liquid jet will break up into droplets and finally form particles [168]. The different properties of the Taylor cone lead to the difference between electrospinning and electrospaying. It also depends on the chain entanglement density of the polymer solution [169]. From the perspective of electrospaying, limiting chain entanglements will help generate smaller droplets and more uniform microbeads. Chain entanglements within the drop eventually limit the subdivision of these drops [170, 171]. During the movement of these drops, the solvent evaporates rapidly. Finally, the polymeric particles with nano-size or micro-size will form on the surface of the collector.

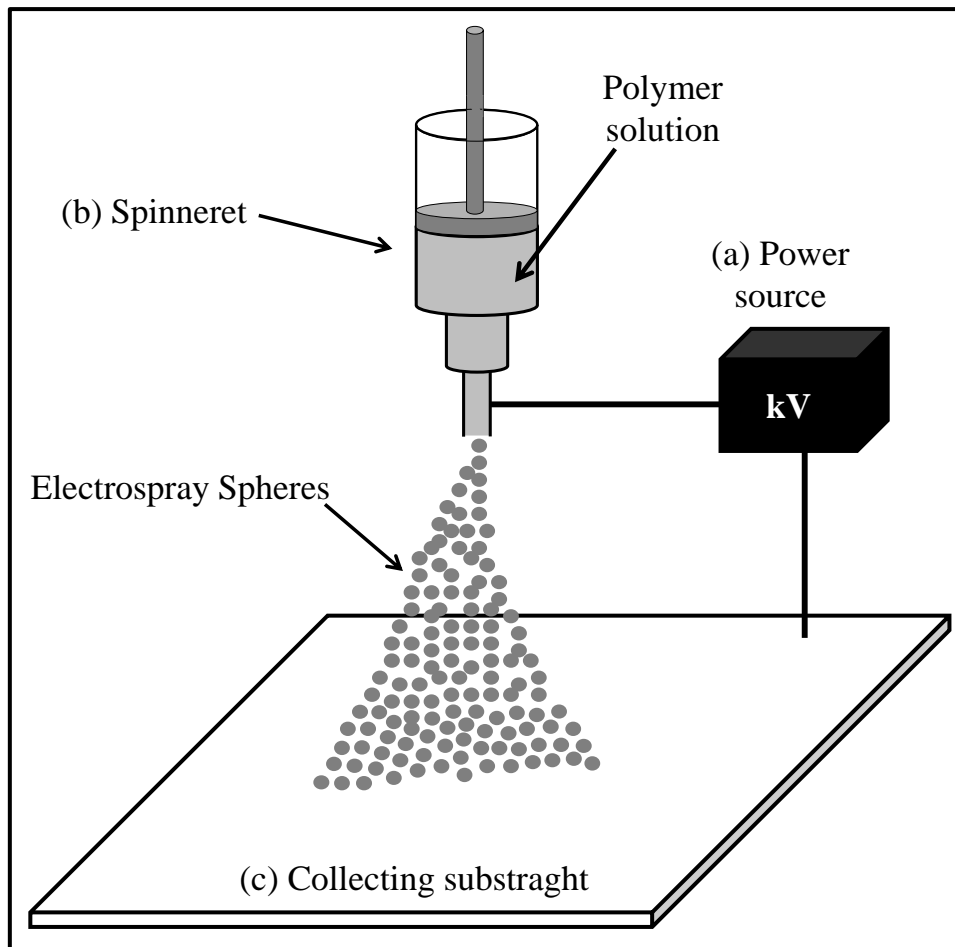


Figure 1.18 Schematic of the experimental setup used to perform electrospaying.

1.4 Highlights for epilepsy treatment

According to the World Health Organisation, epilepsy is the world's most common serious brain disorder; it is more than three times as common as multiple sclerosis, Parkinson's disease, and cerebral palsy. It is estimated that around 50 million people in the world have epilepsy at any one time [172]. Data from Epilepsy Action Australia shows that 800,000 people in Australia will be diagnosed with epilepsy at some stage in their lifetime and up to 5% of the world's population may have a seizure at some time in their lives. Also, it is estimated that over 225,000 Australians are living with epilepsy. Approx. 3% to 3.5% of Australians will experience epilepsy at some point in their lives [173]. Moreover, the impact

of epilepsy is not only on the person with epilepsy but also the family, and indirectly the community is affected. This data and situation highlight the significance to develop effective polymeric nano- or micro-structural drug delivery for local treatment of epilepsy.

Therapeutic interventions for epilepsy currently control seizures in only around 70% of affected individuals with the remaining people being unresponsive to the current therapeutic interventions [174-177]. The reasons for this are not currently well understood, but there is a lot of evidence to suggest that a major reason is the presence of blood-brain barrier [175]. Side effects associated with systemic administration of anti-convulsant drugs include nausea, rashes, weight changes and dizziness. These side effects are major factors limiting the drugs' effectiveness in controlling epileptic seizures by preventing the use of higher doses [178-180]. Development of effective polymeric nano- or micro-structural drug delivery systems holds great potential for local treatment of epilepsy. They could be used in the treatment of multiple independent foci, as well as treatment of seizure foci in eloquent areas of the brain (**Figure 1.19**). Local direct delivery may also avoid potential problems of whole-brain and systemic toxicity encountered in current drug delivery systems.

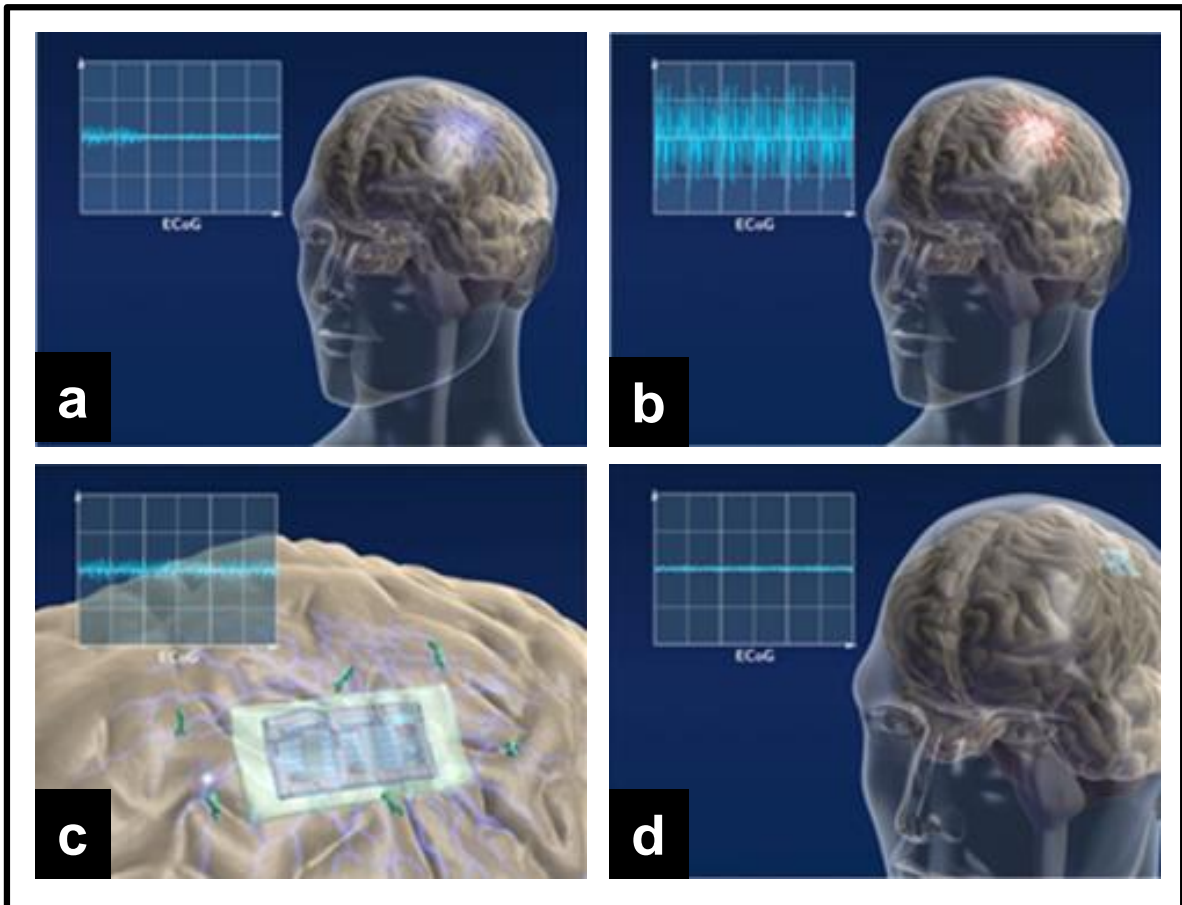


Figure 1.19 Schematic illustration of local treatment for epilepsy: a) the onset of pre-seizures; b) progression into an epileptic seizure event; c) implant local drug delivery system foci in effective seizure-controlling areas of the brain; d) return to normal situation. Reproduced from reference [174].

1.5 Aims and structure of this thesis

This thesis aims to develop novel structured implantable or injectable drug delivery systems for local treatment of central nervous system disorders such as epilepsy. A variety of biodegradable polymer microcapsules and 3D conducting polymer drug delivery systems have been fabricated by electrojetting and electropolymerization techniques, respectively.

These delivery systems have been systematically characterised, and shown their ability to control the release profiles of anti-epileptic drugs.

The investigated biodegradable drug delivery microcapsules will possess controllable and uniform morphology with narrow size distribution, high efficiency drug encapsulation, sustained and predictable drug release characteristics, and neuro-cytocompatibility. Studies will also investigate conducting polymer drug delivery systems that will enable electrically controlled properties, sustained near-linear release, flexible dosage control, and super stability. Moreover, combined with biodegradable microspheres which contain different drugs, two interdigitated electrodes may serve as a multi-functional drug delivery system.

The structure of this thesis is summarised in the following sections:

Chapter 1 presents the general introduction and related literature review of this research field.

Chapter 2 describes the general experimental method relevant to fabrication, characterization, and drug delivery evaluation.

Chapter 3 describes the preparation and characterization of electrojetted PLGA microcapsules containing the anti-epilepsy drug, including flattened microspheres, microspheres, and microfibres. Different microcapsules lead to the variably controllable drug release profiles, and human neural stem cell culture demonstrates the neuro-cytocompatibility of the microcapsules.

Chapter 4 describes the development of a series of core-shell structural microcapsules using novel core-shell electrojetting. A more hydrophobic polymer shell acts as a barrier component to control the rate of drug release from the polymeric core, which leads to prolonged drug release profiles.

Chapter 5 investigates the dual drug delivery systems which are composed of electrospun microfibres with electrospray microspheres as a composite membrane. These composite membranes contain two kinds of drugs, and display stable thermal and mechanical properties, and have promising potential for combined therapy.

Chapter 6 describes an electrically on-demand drug delivery system that consists of three-dimensional printed interdigitated electrodes drug delivery systems coated by electropolymerization of a conducting polymer film and electrospray of biodegradable polymer microspheres. The interdigitated structure provided flexible drug delivery combinations both for mono drug delivery and dual drug delivery systems.

Chapter 7 provides a summary of the thesis and highlight directions for future research.

1.6 References

- [1] Langer R. New methods of drug delivery. *Science* 1990;249:1527-33.
- [2] Langer R. Drugs on target. *Science* 2001;293:58-9.
- [3] Prausnitz MR, Mitragotri S, Langer R. Current status and future potential of transdermal drug delivery. *Nat Rev Drug Discov* 2004;3:115-24.
- [4] Medina SH, El-Sayed MEH. Dendrimers as carriers for delivery of chemotherapeutic agents. *Chemical Reviews* 2009;109:3141-57.
- [5] de Bono JS, Ashworth A. Translating cancer research into targeted therapeutics. *Nature* 2010;467:543-9.
- [6] Allen TM, Cullis PR. Drug delivery systems: Entering the mainstream. *Science* 2004;303:1818-22.
- [7] Mitragotri S, Lahann J. Materials for drug delivery: Innovative solutions to address complex biological hurdles. *Advanced Materials* 2012;24:3717-23.
- [8] Siepmann J, Siegel RA, Rathbone MJ. *Fundamentals and applications of controlled release drug delivery*: Springer Science & Business Media; 2011.
- [9] Cannon RE, Peart JC, Hawkins BT, Campos CR, Miller DS. Targeting blood-brain barrier sphingolipid signaling reduces basal P-glycoprotein activity and improves drug delivery to the brain. *Proceedings of the National Academy of Sciences* 2012;109:15930-5.
- [10] Hsia Y, Bale JB, Gonen S, Shi D, Sheffler W, Fong KK, Nattermann U, Xu C, Huang P-S, Ravichandran R, Yi S, Davis TN, Gonen T, King NP, Baker D. Design of a hyperstable 60-subunit protein icosahedron. *Nature* 2016;535:136-9.
- [11] Mura S, Nicolas J, Couvreur P. Stimuli-responsive nanocarriers for drug delivery. *Nat Mater* 2013;12:991-1003.

- [12] Yun YH, Lee BK, Park K. Controlled drug delivery: Historical perspective for the next generation. *Journal of Controlled Release* 2015;219:2-7.
- [13] Kearney CJ, Mooney DJ. Macroscale delivery systems for molecular and cellular payloads. *Nat Mater* 2013;12:1004-17.
- [14] Liu S. The role of coordination chemistry in the development of target-specific radiopharmaceuticals. *Chemical Society Reviews* 2004;33:445-61.
- [15] Farokhzad OC, Langer R. Nanomedicine: Developing smarter therapeutic and diagnostic modalities. *Advanced Drug Delivery Reviews* 2006;58:1456-9.
- [16] Doshi N, Mitragotri S. Designer biomaterials for nanomedicine. *Advanced Functional Materials* 2009;19:3843-54.
- [17] Morishita M, Peppas NA. Advances in oral drug delivery: improved bioavailability of poorly absorbed drugs by tissue and cellular optimization. *Advanced Drug Delivery Reviews* 2012;64:479.
- [18] Morishita M, Peppas NA. Is the oral route possible for peptide and protein drug delivery? *Drug Discovery Today* 2006;11:905-10.
- [19] Colombo P, Sonvico F, Colombo G, Bettini R. Novel platforms for oral drug delivery. *Pharmaceutical Research* 2009;26:601-11.
- [20] Mukhopadhyay P, Mishra R, Rana D, Kundu PP. Strategies for effective oral insulin delivery with modified chitosan nanoparticles: A review. *Progress in Polymer Science* 2012;37:1457-75.
- [21] Sant S, Tao SL, Fisher OZ, Xu Q, Peppas NA, Khademhosseini A. Microfabrication technologies for oral drug delivery. *Advanced Drug Delivery Reviews* 2012;64:496-507.
- [22] Mei L, Zhang Z, Zhao L, Huang L, Yang X-L, Tang J, Feng S-S. Pharmaceutical nanotechnology for oral delivery of anticancer drugs. *Advanced Drug Delivery Reviews* 2013;65:880-90.

- [23] Nicolas J, Mura S, Brambilla D, Mackiewicz N, Couvreur P. Design, functionalization strategies and biomedical applications of targeted biodegradable/biocompatible polymer-based nanocarriers for drug delivery. *Chemical Society Reviews* 2013;42:1147-235.
- [24] Prausnitz MR, Langer R. Transdermal drug delivery. *Nat Biotech* 2008;26:1261-8.
- [25] Williams A. Transdermal and topical drug delivery: from theory to clinical practice: Pharmaceutical Press London; 2003.
- [26] Bouwstra JA, de Graaff A, Gooris GS, Nijse J, Wiechers JW, van Aelst AC. Water distribution and related morphology in human stratum corneum at different hydration levels. *Journal of Investigative Dermatology* 2003;120:750-8.
- [27] Henningfield JE. Nicotine medications for smoking cessation. *New England Journal of Medicine* 1995;333:1196-203.
- [28] Santini JJT, Richards AC, Scheidt R, Cima MJ, Langer R. Microchips as controlled drug-delivery devices. *Angewandte Chemie International Edition* 2000;39:2396-407.
- [29] Heyder J. Deposition of inhaled particles in the human respiratory tract and consequences for regional targeting in respiratory drug delivery. *Proceedings of the American Thoracic Society* 2004;1:315-20.
- [30] Bhattarai N, Gunn J, Zhang M. Chitosan-based hydrogels for controlled, localized drug delivery. *Advanced Drug Delivery Reviews* 2010;62:83-99.
- [31] Wolinsky JB, Colson YL, Grinstaff MW. Local drug delivery strategies for cancer treatment: Gels, nanoparticles, polymeric films, rods, and wafers. *Journal of Controlled Release* 2012;159:14-26.
- [32] Ehrlich P. *Collected studies on immunity*: Wiley; 1906.
- [33] Allen TM. Long-circulating (sterically stabilized) liposomes for targeted drug delivery. *Trends in Pharmacological Sciences* 1994;15:215-20.

- [34] Sudimack J, Lee RJ. Targeted drug delivery via the folate receptor. *Advanced Drug Delivery Reviews* 2000;41:147-62.
- [35] Gu FX, Karnik R, Wang AZ, Alexis F, Levy-Nissenbaum E, Hong S, Langer RS, Farokhzad OC. Targeted nanoparticles for cancer therapy. *Nano Today* 2007;2:14-21.
- [36] Zhan C, Li C, Wei X, Lu W, Lu W. Toxins and derivatives in molecular pharmaceuticals: Drug delivery and targeted therapy. *Advanced Drug Delivery Reviews* 2015;90:101-18.
- [37] Ashley CE, Carnes EC, Phillips GK, Padilla D, Durfee PN, Brown PA, Hanna TN, Liu J, Phillips B, Carter MB, Carroll NJ, Jiang X, Dunphy DR, Willman CL, Petsev DN, Evans DG, Parikh AN, Chackerian B, Wharton W, Peabody DS, Brinker CJ. The targeted delivery of multicomponent cargos to cancer cells by nanoporous particle-supported lipid bilayers. *Nat Mater* 2011;10:389-97.
- [38] Johnstone TC, Suntharalingam K, Lippard SJ. The next generation of platinum drugs: targeted Pt(II) agents, Nanoparticle delivery, and Pt(IV) prodrugs. *Chemical Reviews* 2016;116:3436-86.
- [39] Ferrari M. Cancer nanotechnology: opportunities and challenges. *Nat Rev Cancer* 2005;5:161-71.
- [40] Ganta S, Devalapally H, Shahiwala A, Amiji M. A review of stimuli-responsive nanocarriers for drug and gene delivery. *Journal of Controlled Release* 2008;126:187-204.
- [41] Brigger I, Dubernet C, Couvreur P. Nanoparticles in cancer therapy and diagnosis. *Advanced Drug Delivery Reviews* 2002;54:631-51.
- [42] Stewart B, Wild CP. *World cancer report 2014. World 2016.*
- [43] Patel T, Zhou J, Piepmeier JM, Saltzman WM. Polymeric nanoparticles for drug delivery to the central nervous system. *Advanced Drug Delivery Reviews* 2012;64:701-5.

- [44] Cecchelli R, Berezowski V, Lundquist S, Culot M, Renftel M, Dehouck M-P, Fenart L. Modelling of the blood-brain barrier in drug discovery and development. *Nat Rev Drug Discov* 2007;6:650-61.
- [45] Saraiva C, Praça C, Ferreira R, Santos T, Ferreira L, Bernardino L. Nanoparticle-mediated brain drug delivery: Overcoming blood–brain barrier to treat neurodegenerative diseases. *Journal of Controlled Release* 2016;235:34-47.
- [46] Miura Y, Takenaka T, Toh K, Wu S, Nishihara H, Kano MR, Ino Y, Nomoto T, Matsumoto Y, Koyama H, Cabral H, Nishiyama N, Kataoka K. Cyclic RGD-linked polymeric micelles for targeted delivery of platinum anticancer drugs to glioblastoma through the blood–brain tumor barrier. *ACS Nano* 2013;7:8583-92.
- [47] Krol S. Challenges in drug delivery to the brain: Nature is against us. *Journal of Controlled Release* 2012;164:145-55.
- [48] Langer R, Peppas NA. Advances in biomaterials, drug delivery, and bionanotechnology. *AIChE Journal* 2003;49:2990-3006.
- [49] Qiu LY, Bae YH. Polymer Architecture and Drug Delivery. *Pharmaceutical Research* 2006;23:1-30.
- [50] Duncan R, Vicent MJ. Polymer therapeutics-prospects for 21st century: The end of the beginning. *Advanced Drug Delivery Reviews* 2013;65:60-70.
- [51] Gaspar R, Duncan R. Polymeric carriers: Preclinical safety and the regulatory implications for design and development of polymer therapeutics. *Advanced Drug Delivery Reviews* 2009;61:1220-31.
- [52] Kim SW, Petersen RV, Feijen J. Polymeric drug delivery systems. *Drug Design* 2016;10:193-250.
- [53] Merino S, Martín C, Kostarelos K, Prato M, Vázquez E. Nanocomposite hydrogels: 3D polymer–nanoparticle synergies for on-demand drug delivery. *ACS Nano* 2015;9:4686-97.

- [54] Torchilin VP. Structure and design of polymeric surfactant-based drug delivery systems. *Journal of Controlled Release* 2001;73:137-72.
- [55] Folkman J, Long DM. The use of silicone rubber as a carrier for prolonged drug therapy. *Journal of Surgical Research* 1964;4:139-42.
- [56] Jalil R, Nixon J. Microencapsulation using poly (L-lactic acid) IV: Release properties of microcapsules containing phenobarbitone. *Journal of microencapsulation* 1990;7:53-66.
- [57] Dawidczyk CM, Kim C, Park JH, Russell LM, Lee KH, Pomper MG, Searson PC. State-of-the-art in design rules for drug delivery platforms: Lessons learned from FDA-approved nanomedicines. *Journal of Controlled Release* 2014;187:133-44.
- [58] Ebnesajjad S. *Handbook of biopolymers and biodegradable plastics: properties, processing and applications*: William Andrew; 2012.
- [59] Jiang W, Gupta RK, Deshpande MC, Schwendeman SP. Biodegradable poly(lactic-co-glycolic acid) microparticles for injectable delivery of vaccine antigens. *Advanced Drug Delivery Reviews* 2005;57:391-410.
- [60] Lu Y, Chen SC. Micro and nano-fabrication of biodegradable polymers for drug delivery. *Advanced Drug Delivery Reviews* 2004;56:1621-33.
- [61] Ma PX, Zhang R. Microtubular architecture of biodegradable polymer scaffolds. *Journal of Biomedical Materials Research* 2001;56:469-77.
- [62] Orloff LA, Domb AJ, Teomim D, Fishbein I, Golomb G. Drug delivery strategies for restenosis biodegradable implant strategies for inhibition of restenosis. *Advanced Drug Delivery Reviews* 1997;24:3-9.
- [63] Suzuki K, Price J. Microencapsulation and dissolution properties of a neuroleptic in a biodegradable polymer, poly (d, l-lactide). *Journal of pharmaceutical sciences* 1985;74:21-4.
- [64] Mogoşanu GD, Grumezescu AM. Natural and synthetic polymers for wounds and burns dressing. *International Journal of Pharmaceutics* 2014;463:127-36.

- [65] Tian H, Tang Z, Zhuang X, Chen X, Jing X. Biodegradable synthetic polymers: Preparation, functionalization and biomedical application. *Progress in Polymer Science* 2012;37:237-80.
- [66] Kumbar S, Laurencin C, Deng M. *Natural and synthetic biomedical polymers*: Newnes; 2014.
- [67] Li S, Vert M. Biodegradation of Aliphatic Polyesters. In: Scott G, editor. *Degradable polymers: Principles and applications*. Dordrecht: Springer Netherlands; 2002. p. 71-131.
- [68] Frazza EJ, Schmitt EE. A new absorbable suture. *Journal of Biomedical Materials Research* 1971;5:43-58.
- [69] Brady JM, Cutright DE, Miller RA, Battistone GC, Hunsuck EE. Resorption rate, route of elimination, and ultrastructure of the implant site of polylactic acid in the abdominal wall of the rat. *Journal of Biomedical Materials Research* 1973;7:155-66.
- [70] Bostman O, Vainionpaa S, Hirvensalo E, Makela A, Vihtonen K, Tormala P, Rokkanen P. Biodegradable internal fixation for malleolar fractures. A prospective randomised trial. *Bone & Joint Journal* 1987;69-B:615-9.
- [71] Burkersroda Fv, Schedl L, Göpferich A. Why degradable polymers undergo surface erosion or bulk erosion. *Biomaterials* 2002;23:4221-31.
- [72] Li S, Vert M. Biodegradation of aliphatic polyesters. *Degradable polymers*: Springer; 2002. p. 71-131.
- [73] Astete CE, Sabliov CM. Synthesis and characterization of PLGA nanoparticles. *Journal of Biomaterials Science, Polymer Edition* 2006;17:247-89.
- [74] Winzenburg G, Schmidt C, Fuchs S, Kissel T. Biodegradable polymers and their potential use in parenteral veterinary drug delivery systems. *Advanced Drug Delivery Reviews* 2004;56:1453-66.

- [75] Fornaguera C, Dols-Perez A, Calderó G, García-Celma MJ, Camarasa J, Solans C. PLGA nanoparticles prepared by nano-emulsion templating using low-energy methods as efficient nanocarriers for drug delivery across the blood–brain barrier. *Journal of Controlled Release* 2015;211:134-43.
- [76] Ye F, Barrefelt Å, Asem H, Abedi-Valugerdi M, El-Serafi I, Saghafian M, Abu-Salah K, Alrokayan S, Muhammed M, Hassan M. Biodegradable polymeric vesicles containing magnetic nanoparticles, quantum dots and anticancer drugs for drug delivery and imaging. *Biomaterials* 2014;35:3885-94.
- [77] Amoozgar Z, Wang L, Brandstoeffer T, Wallis SS, Wilson EM, Goldberg MS. Dual-layer surface coating of PLGA-based nanoparticles provides slow-release drug delivery to achieve metronomic therapy in a paclitaxel-resistant murine ovarian cancer model. *Biomacromolecules* 2014;15:4187-94.
- [78] Neutsch L, Wirth EM, Spijker S, Pichl C, Kählig H, Gabor F, Wirth M. Synergistic targeting/prodrug strategies for intravesical drug delivery — Lectin-modified PLGA microparticles enhance cytotoxicity of stearyl gemcitabine by contact-dependent transfer. *Journal of Controlled Release*;169:62-72.
- [79] Wang Y, Li P, Kong L. Chitosan-modified PLGA nanoparticles with versatile surface for improved drug delivery. *AAPS PharmSciTech* 2013;14:585-92.
- [80] Yang H, Tyagi P, Kadam RS, Holden CA, Kompella UB. Hybrid Dendrimer Hydrogel/PLGA Nanoparticle platform sustains drug delivery for one week and antiglaucoma effects for four days following one-time topical administration. *ACS Nano* 2012;6:7595-606.
- [81] Skotheim TA. *Handbook of conducting polymers*: CRC press; 1997.
- [82] Wallace GG, Teasdale PR, Spinks GM, Kane-Maguire LA. *Conductive electroactive polymers: intelligent polymer systems*: CRC press; 2008.

- [83] Shirakawa H, Louis EJ, MacDiarmid AG, Chiang CK, Heeger AJ. Synthesis of electrically conducting organic polymers: halogen derivatives of polyacetylene, $(CH)_x$. *Journal of the Chemical Society, Chemical Communications* 1977:578-80.
- [84] Baughman RH. Conducting polymer artificial muscles. *Synthetic Metals* 1996;78:339-53.
- [85] Schmidt CE, Shastri VR, Vacanti JP, Langer R. Stimulation of neurite outgrowth using an electrically conducting polymer. *Proceedings of the National Academy of Sciences* 1997;94:8948-53.
- [86] Abidian MR, Kim DH, Martin DC. Conducting-polymer nanotubes for controlled drug release. *Advanced Materials* 2006;18:405-9.
- [87] Ghosh S, Inganäs O. Conducting polymer hydrogels as 3D electrodes: applications for supercapacitors. *Advanced Materials* 1999;11:1214-8.
- [88] Ghosh S, Kouamé NA, Ramos L, Remita S, Dazzi A, Deniset-Besseau A, Beaunier P, Goubard F, Aubert P-H, Remita H. Conducting polymer nanostructures for photocatalysis under visible light. *Nat Mater* 2015;14:505-11.
- [89] Gerard M, Chaubey A, Malhotra BD. Application of conducting polymers to biosensors. *Biosensors and Bioelectronics* 2002;17:345-59.
- [90] Mawad D, Stewart E, Officer DL, Romeo T, Wagner P, Wagner K, Wallace GG. A single component conducting polymer hydrogel as a scaffold for tissue engineering. *Advanced Functional Materials* 2012;22:2692-9.
- [91] Kanazawa KK, Diaz A, Geiss RH, Gill WD, Kwak JF, Logan JA, Rabolt JF, Street GB. 'Organic metals': polypyrrole, a stable synthetic 'metallic' polymer. *Journal of the Chemical Society, Chemical Communications* 1979:854-5.
- [92] Vernitskaya TyV, Efimov ON. Polypyrrole: a conducting polymer; its synthesis, properties and applications. *Russian Chemical Reviews* 1997;66:443-57.

- [93] Huang W-S, Humphrey BD, MacDiarmid AG. Polyaniline, a novel conducting polymer. Morphology and chemistry of its oxidation and reduction in aqueous electrolytes. *Journal of the Chemical Society, Faraday Transactions 1: Physical Chemistry in Condensed Phases* 1986;82:2385-400.
- [94] Wu C-G, Bein T. Conducting polyaniline filaments in a mesoporous channel host. *Science* 1994;1757-9.
- [95] Waltman RJ, Bargon J, Diaz A. Electrochemical studies of some conducting polythiophene films. *The Journal of Physical Chemistry* 1983;87:1459-63.
- [96] Groenendaal L, Jonas F, Freitag D, Pielartzik H, Reynolds JR. Poly (3, 4-ethylenedioxythiophene) and its derivatives: past, present, and future. *Advanced Materials* 2000;12:481-94.
- [97] Bubnova O, Khan ZU, Malti A, Braun S, Fahlman M, Berggren M, Crispin X. Optimization of the thermoelectric figure of merit in the conducting polymer poly(3,4-ethylenedioxythiophene). *Nat Mater* 2011;10:429-33.
- [98] Tallman DE, Spinks G, Dominis A, Wallace GG. Electroactive conducting polymers for corrosion control. *Journal of Solid State Electrochemistry* 2002;6:73-84.
- [99] Ding J, Liu L, Spinks GM, Zhou D, Wallace GG, Gillespie J. High performance conducting polymer actuators utilising a tubular geometry and helical wire interconnects. *Synthetic Metals* 2003;138:391-8.
- [100] Pringle JM, Forsyth M, Wallace GG, MacFarlane DR. Solution-surface electropolymerization: a route to morphologically novel poly (pyrrole) using an ionic liquid. *Macromolecules* 2006;39:7193-5.
- [101] Dubal DP, Lee SH, Kim JG, Kim WB, Lokhande CD. Porous polypyrrole clusters prepared by electropolymerization for a high performance supercapacitor. *Journal of Materials Chemistry* 2012;22:3044-52.

- [102] Baba A, Tian S, Stefani F, Xia C, Wang Z, Advincula RC, Johannsmann D, Knoll W. Electropolymerization and doping/dedoping properties of polyaniline thin films as studied by electrochemical-surface plasmon spectroscopy and by the quartz crystal microbalance. *Journal of Electroanalytical Chemistry* 2004;562:95-103.
- [103] John R, Wallace GG. The use of microelectrodes to probe the electropolymerization mechanism of heterocyclic conducting polymers. *Journal of Electroanalytical Chemistry and Interfacial Electrochemistry* 1991;306:157-67.
- [104] Inzelt G. *Conducting polymers: a new era in electrochemistry*: Springer Science & Business Media; 2012.
- [105] McCoy CH, Wrighton MS. Potential-dependent conductivity of conducting polymers yields opportunities for molecule-based devices: a microelectrochemical push-pull amplifier based on two different conducting polymer transistors. *Chemistry of materials* 1993;5:914-6.
- [106] Wallace GG, Kane-Maguire LA. Manipulating and monitoring biomolecular interactions with conducting electroactive polymers. *Advanced Materials* 2002;14:953-60.
- [107] Goding J, Gilmour A, Martens P, Poole-Warren L, Green R. Small bioactive molecules as dual functional co-dopants for conducting polymers. *Journal of Materials Chemistry B* 2015;3:5058-69.
- [108] Gilmour A, Woolley A, Poole-Warren L, Thomson C, Green R. A critical review of cell culture strategies for modelling intracortical brain implant material reactions. *Biomaterials* 2016;91:23-43.
- [109] Wadhwa R, Lagenaur CF, Cui XT. Electrochemically controlled release of dexamethasone from conducting polymer polypyrrole coated electrode. *Journal of Controlled Release* 2006;110:531-41.
- [110] Jeon G, Yang SY, Byun J, Kim JK. Electrically actuable smart nanoporous membrane for pulsatile drug release. *Nano Letters* 2011;11:1284-8.

- [111] Zhang H, Xiong L, Liao X, Huang K. Controlled-release system of small molecules triggered by the photothermal effect of polypyrrole. *Macromolecular Rapid Communications* 2016;37:149-54.
- [112] Zhang B, Molino PJ, Harris AR, Yue Z, Moulton SE, Wallace GG. Conductive and protein resistant polypyrrole films for dexamethasone delivery. *Journal of Materials Chemistry B* 2016;4:2570-7.
- [113] Luo X, Cui XT. Electrochemically controlled release based on nanoporous conducting polymers. *Electrochemistry Communications* 2009;11:402-4.
- [114] Lin Y, Wallace GG. Factors influencing electrochemical release of 2,6-anthraquinone disulphonic acid from polypyrrole. *Journal of Controlled Release* 1994;30:137-42.
- [115] Weaver CL, LaRosa JM, Luo X, Cui XT. Electrically controlled drug delivery from graphene oxide Nanocomposite Films. *ACS Nano* 2014;8:1834-43.
- [116] Leprince L, Dogimont A, Magnin D, Demoustier-Champagne S. Dexamethasone electrically controlled release from polypyrrole-coated nanostructured electrodes. *Journal of Materials Science: Materials in Medicine* 2010;21:925-30.
- [117] Jiang S, Sun Y, Cui X, Huang X, He Y, Ji S, Shi W, Ge D. Enhanced drug loading capacity of polypyrrole nanowire network for controlled drug release. *Synthetic Metals* 2013;163:19-23.
- [118] Ge J, Neofytou E, Cahill TJ, Beygui RE, Zare RN. Drug Release from Electric-Field-Responsive Nanoparticles. *ACS Nano* 2012;6:227-33.
- [119] Luo X, Matranga C, Tan S, Alba N, Cui XT. Carbon nanotube nanoreservoir for controlled release of anti-inflammatory dexamethasone. *Biomaterials* 2011;32:6316-23.
- [120] Thompson BC (2009). The controlled release of neurotrophic proteins from the conducting polymer polypyrrole to improve the nerve/cochlear implant interface. Doctoral dissertation, University of Wollongong, Wollongong.

- [121] Farokhzad OC, Langer R. Impact of nanotechnology on drug delivery. *ACS Nano* 2009;3:16-20.
- [122] Whitesides GM. The 'right' size in nanobiotechnology. *Nat Biotech* 2003;21:1161-5.
- [123] Parveen S, Misra R, Sahoo SK. Nanoparticles: a boon to drug delivery, therapeutics, diagnostics and imaging. *Nanomedicine: Nanotechnology, biology and medicine* 2012;8:147-66.
- [124] Kesharwani P, Jain K, Jain NK. Dendrimer as nanocarrier for drug delivery. *Progress in Polymer Science* 2014;39:268-307.
- [125] Wang Y, Zhao Q, Han N, Bai L, Li J, Liu J, Che E, Hu L, Zhang Q, Jiang T, Wang S. Mesoporous silica nanoparticles in drug delivery and biomedical applications. *Nanomedicine: Nanotechnology, Biology and Medicine* 2015;11:313-27.
- [126] Alderton GK. Nanotechnology: Improving drug delivery with algae. *Nat Rev Cancer* 2016;16:5-.
- [127] Liu T, Wang C, Gu X, Gong H, Cheng L, Shi X, Feng L, Sun B, Liu Z. Drug delivery with PEGylated MoS₂ nano-sheets for combined photothermal and chemotherapy of cancer. *Advanced Materials* 2014;26:3433-40.
- [128] Qian C, Yu J, Chen Y, Hu Q, Xiao X, Sun W, Wang C, Feng P, Shen Q-D, Gu Z. Anticancer therapy: Light-activated hypoxia-responsive nanocarriers for enhanced anticancer therapy (*Adv. Mater.* 17/2016). *Advanced Materials* 2016;28:3226-.
- [129] da Silva PB, de Freitas ES, Bernegossi J, Gonzalez ML, Sato MR, Leite CQF, Pavan FR, Chorilli M. Nanotechnology-based drug delivery systems for treatment of tuberculosis-A review. *Journal of Biomedical Nanotechnology* 2016;12:241-60.
- [130] Shi J, Votruba AR, Farokhzad OC, Langer R. Nanotechnology in drug delivery and tissue engineering: From discovery to applications. *Nano Letters* 2010;10:3223-30.

- [131] Yang K, Feng L, Liu Z. Stimuli responsive drug delivery systems based on nano-graphene for cancer therapy. *Advanced Drug Delivery Reviews* 2016; 105: 228-241.
- [132] Blanco E, Shen H, Ferrari M. Principles of nanoparticle design for overcoming biological barriers to drug delivery. *Nat Biotech* 2015;33:941-51.
- [133] Levy-Nissenbaum E, Radovic-Moreno AF, Wang AZ, Langer R, Farokhzad OC. Nanotechnology and aptamers: applications in drug delivery. *Trends in Biotechnology* 2008;26:442-9.
- [134] Bangham A, Standish MM, Watkins J. Diffusion of univalent ions across the lamellae of swollen phospholipids. *Journal of molecular biology* 1965;13:238-252, IN26-IN27.
- [135] Langer R, Folkman J. Polymers for the sustained release of proteins and other macromolecules. 1976; 263: 797-800.
- [136] Allen T, Chonn A. Large unilamellar liposomes with low uptake into the reticuloendothelial system. *FEBS letters* 1987;223:42-6.
- [137] Wagner V, Dullaart A, Bock A-K, Zweck A. The emerging nanomedicine landscape. *Nature biotechnology* 2006;24:1211-7.
- [138] Pamies P, Stoddart A. Materials for drug delivery. *Nat Mater* 2013;12:957-.
- [139] Alexis F, Rhee J-W, Richie JP, Radovic-Moreno AF, Langer R, Farokhzad OC. New frontiers in nanotechnology for cancer treatment. *Urologic oncology: Seminars and original investigations* 2008;26:74-85.
- [140] Doshi J, Reneker DH. Electrospinning process and applications of electrospun fibers. *Industry Applications Society Annual Meeting, 1993, Conference Record of the 1993 IEEE1993*. p. 1698-703 vol.3.
- [141] Huang Z-M, Zhang YZ, Kotaki M, Ramakrishna S. A review on polymer nanofibers by electrospinning and their applications in nanocomposites. *Composites Science and Technology* 2003;63:2223-53.

- [142] Dzenis Y. Spinning continuous fibers for nanotechnology. *Science* 2004;304:1917-9.
- [143] Papkov D, Zou Y, Andalib MN, Goponenko A, Cheng SZD, Dzenis YA. Simultaneously strong and tough ultrafine continuous nanofibers. *ACS Nano* 2013;7:3324-31.
- [144] Chen Y, Han D, Ouyang W, Chen S, Hou H, Zhao Y, Fong H. Fabrication and evaluation of polyamide 6 composites with electrospun polyimide nanofibers as skeletal framework. *Composites Part B: Engineering* 2012;43:2382-8.
- [145] Jiang T, Carbone EJ, Lo KWH, Laurencin CT. Electrospinning of polymer nanofibers for tissue regeneration. *Progress in Polymer Science* 2015;46:1-24.
- [146] Sill TJ, von Recum HA. Electrospinning: Applications in drug delivery and tissue engineering. *Biomaterials* 2008;29:1989-2006.
- [147] Fong H, Chun I, Reneker DH. Beaded nanofibers formed during electrospinning. *Polymer* 1999;40:4585-92.
- [148] Greiner A, Wendorff JH. Electrospinning: A eascinating method for the preparation of ultrathin fibers. *Angewandte Chemie International Edition* 2007;46:5670-703.
- [149] Formhals A. Process and apparatus for preparing artificial threads. US Patent, 1975504. 1934.
- [150] Anton F. Artificial thread and method of producing same. Google Patents; 1940.
- [151] Taylor G. Electrically driven jets. *Proceedings of the Royal Society of London A: Mathematical, Physical and Engineering Sciences: The Royal Society*; 1969. p. 453-75.
- [152] Baumgarten PK. Electrostatic spinning of acrylic microfibers. *Journal of Colloid and Interface Science* 1971;36:71-9.
- [153] Li D, Xia Y. Electrospinning of nanofibers: Reinventing the wheel? *Advanced Materials* 2004;16:1151-70.

- [154] Ding Y, Hou H, Zhao Y, Zhu Z, Fong H. Electrospun polyimide nanofibers and their applications. *Progress in Polymer Science* 2016; 61: 67-103.
- [155] Huang Z-M, Zhang Y-Z, Kotaki M, Ramakrishna S. A review on polymer nanofibers by electrospinning and their applications in nanocomposites. *Composites Science and Technology* 2003;63:2223-53.
- [156] Doshi J, Reneker DH. Electrospinning process and applications of electrospun fibers. *Industry Applications Society Annual Meeting, 1993, Conference Record of the 1993 IEEE: IEEE; 1993. p. 1698-703.*
- [157] Fong H, Chun I, Reneker D. Beaded nanofibers formed during electrospinning. *Polymer* 1999;40:4585-92.
- [158] Yoo HS, Kim TG, Park TG. Surface-functionalized electrospun nanofibers for tissue engineering and drug delivery. *Advanced Drug Delivery Reviews* 2009;61:1033-42.
- [159] Zeng J, Xu X, Chen X, Liang Q, Bian X, Yang L, Jing X. Biodegradable electrospun fibers for drug delivery. *Journal of Controlled Release* 2003;92:227-31.
- [160] Kim TG, Lee DS, Park TG. Controlled protein release from electrospun biodegradable fiber mesh composed of poly(ϵ -caprolactone) and poly(ethylene oxide). *International Journal of Pharmaceutics* 2007;338:276-83.
- [161] Maretschek S, Greiner A, Kissel T. Electrospun biodegradable nanofiber nonwovens for controlled release of proteins. *Journal of Controlled Release* 2008;127:180-7.
- [162] Viry L, Moulton SE, Romeo T, Suhr C, Mawad D, Cook M, Wallace GG. Emulsion-coaxial electrospinning: designing novel architectures for sustained release of highly soluble low molecular weight drugs. *Journal of Materials Chemistry* 2012;22:11347-53.
- [163] Tungprapa S, Jangchud I, Supaphol P. Release characteristics of four model drugs from drug-loaded electrospun cellulose acetate fiber mats. *Polymer* 2007;48:5030-41.

- [164] Chakraborty S, Liao IC, Adler A, Leong KW. Electrohydrodynamics: A facile technique to fabricate drug delivery systems. *Advanced Drug Delivery Reviews* 2009;61:1043-54.
- [165] Wu Y, MacKay JA, R. McDaniel J, Chilkoti A, Clark RL. Fabrication of elastin-like polypeptide nanoparticles for drug delivery by electrospraying. *Biomacromolecules* 2009;10:19-24.
- [166] Arya N, Chakraborty S, Dube N, Katti DS. Electrospraying: A facile technique for synthesis of chitosan-based micro/nanospheres for drug delivery applications. *Journal of Biomedical Materials Research Part B: Applied Biomaterials* 2009;88B:17-31.
- [167] Nguyen DN, Clasen C, Van den Mooter G. Pharmaceutical applications of electrospraying. *Journal of Pharmaceutical Sciences* 2016;105:2601-20.
- [168] Sridhar R, Lakshminarayanan R, Madhaiyan K, Amutha Barathi V, Lim KHC, Ramakrishna S. Electrosprayed nanoparticles and electrospun nanofibers based on natural materials: applications in tissue regeneration, drug delivery and pharmaceuticals. *Chemical Society Reviews* 2015;44:790-814.
- [169] Shenoy SL, Bates WD, Frisch HL, Wnek GE. Role of chain entanglements on fiber formation during electrospinning of polymer solutions: good solvent, non-specific polymer–polymer interaction limit. *Polymer* 2005;46:3372-84.
- [170] Tang K, Gomez A. Generation by electrospray of monodisperse water droplets for targeted drug delivery by inhalation. *Journal of Aerosol Science* 1994;25:1237-49.
- [171] Almería B, Fahmy TM, Gomez A. A multiplexed electrospray process for single-step synthesis of stabilized polymer particles for drug delivery. *Journal of Controlled Release* 2011;154:203-10.
- [172] http://www.who.int/mental_health/neurology/epilepsy/en/.
- [173] <http://www.epilepsy.org.au/about-epilepsy/understanding-epilepsy/facts-statistics>.

- [174] Muller R, Yue Z, Ahmadi S, Ng W, Grosse WM, Cook MJ, Wallace GG, Moulton SE. Development and validation of a seizure initiated drug delivery system for the treatment of epilepsy. *Sensors and Actuators B: Chemical* 2016;236:732-40.
- [175] Cook MJ, O'Brien TJ, Berkovic SF, Murphy M, Morokoff A, Fabinyi G, D'Souza W, Yerra R, Archer J, Litewka L, Hosking S, Lightfoot P, Ruedebusch V, Sheffield WD, Snyder D, Leyde K, Himes D. Prediction of seizure likelihood with a long-term, implanted seizure advisory system in patients with drug-resistant epilepsy: a first-in-man study. *The Lancet Neurology* 2013;12:563-71.
- [176] Kwan P, Brodie MJ. Early identification of refractory epilepsy. *New England Journal of Medicine* 2000;342:314-9.
- [177] Steinlein OK, Mulley JC, Propping P, Wallace RH, Phillips HA, Sutherland GR, Scheffer IE, Berkovic SF. A missense mutation in the neuronal nicotinic acetylcholine receptor α 4 subunit is associated with autosomal dominant nocturnal frontal lobe epilepsy. *Nat Genet* 1995;11:201-3.
- [178] Paschal AM, Hawley SR, Romain TS, Ablah E. Measures of adherence to epilepsy treatment: Review of present practices and recommendations for future directions. *Epilepsia* 2008;49:1115-22.
- [179] Kwan P, Brodie MJ. Phenobarbital for the treatment of epilepsy in the 21st Century: A Critical Review. *Epilepsia* 2004;45:1141-9.
- [180] Meyer A-C, Dua T, Ma J, Saxena S, Birbeck G. Global disparities in the epilepsy treatment gap: a systematic review. *Bulletin of the World Health Organization* 2010;88:260-6.

**CHAPTER 2: GENERAL
EXPERIMENTAL**

2.1 Introduction

In this chapter, the general materials, experimental techniques, and instruments used in this thesis are briefly described. These include the reagents list, synthesis methods, physiochemical characterization, and in vitro drug release studies. More details regarding specific procedures will be presented in the experimental section of each chapter.

2.2 Reagents and materials

The materials used in this thesis are summarized in **Table 2.1**.

Table 2.1 Information on Reagents and Materials.

Name	Detailed Information	Company
1. Drug Carriers		
Poly(D,L lactic-co-glycolic acid) (85/15)	$M_w \sim 60,000$ Da, molar ratio of lactide to glycolide 85/15	Purac, Singapore
Poly(D,L lactic-co-glycolic acid) (75/25)	$M_w \sim 60,000$ Da, molar ratio of lactide to glycolide 75/25	Purac, Singapore
Poly(lactic acid)	$M_w \sim 180,000$ Da	Purac, Singapore

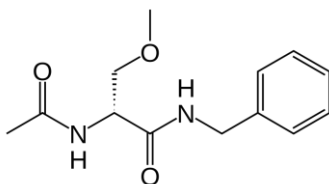
Pyrrole monomer

Fresh distilled before use

Sigma-Aldrich

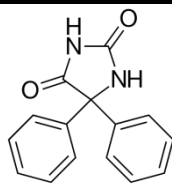
2. Model Drugs

Lacosamide



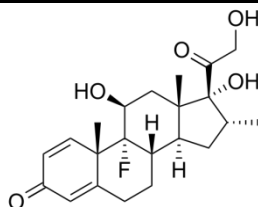
UCB Pharma Pty Ltd

Phenytoin



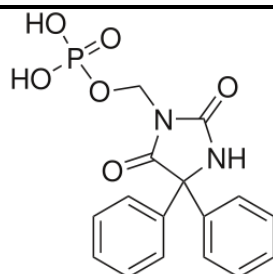
Sigma-Aldrich

Dexamethasone



Sigma-Aldrich

fosPhenytoin



Sigma-Aldrich

3. Release Media related

Phosphate buffered saline	Preparation to 0.001M/L	Sigma-Aldrich
---------------------------	-------------------------	---------------

Milli-Q water	Resistivity is 18.2 M Ω ·cm at	IPRI
---------------	---------------------------------------	------

25 °C

Sodium chloride	Analytical Reagent	Sigma-Aldrich
-----------------	--------------------	---------------

Potassium chloride	Analytical Reagent	Alfa Aesar
--------------------	--------------------	------------

Magnesium chloride	Analytical Reagent	Alfa Aesar
--------------------	--------------------	------------

Calcium chloride	Analytical Reagent	Sigma-Aldrich
------------------	--------------------	---------------

4. Solvents and others

Chloroform	Chemical Pure	Tokyo Chemical Industry
------------	---------------	-------------------------

Dimethylformamide	Chemical Pure	Sigma-Aldrich
-------------------	---------------	---------------

Methanol	HPLC Grade	Honeywell
----------	------------	-----------

Acetonitrile	HPLC Grade	Honeywell
--------------	------------	-----------

Trifluoroacetic acid	Analytical Reagent	Chemical Supply
Orthophosphoric acid	Analytical Reagent	Sigma-Aldrich
Paraformaldehyde	For biological purpose	Sigma-Aldrich
Ethanol	For biological purpose	Chemical Supply

2.3 Fabrication methods

2.3.1 Electrojetting

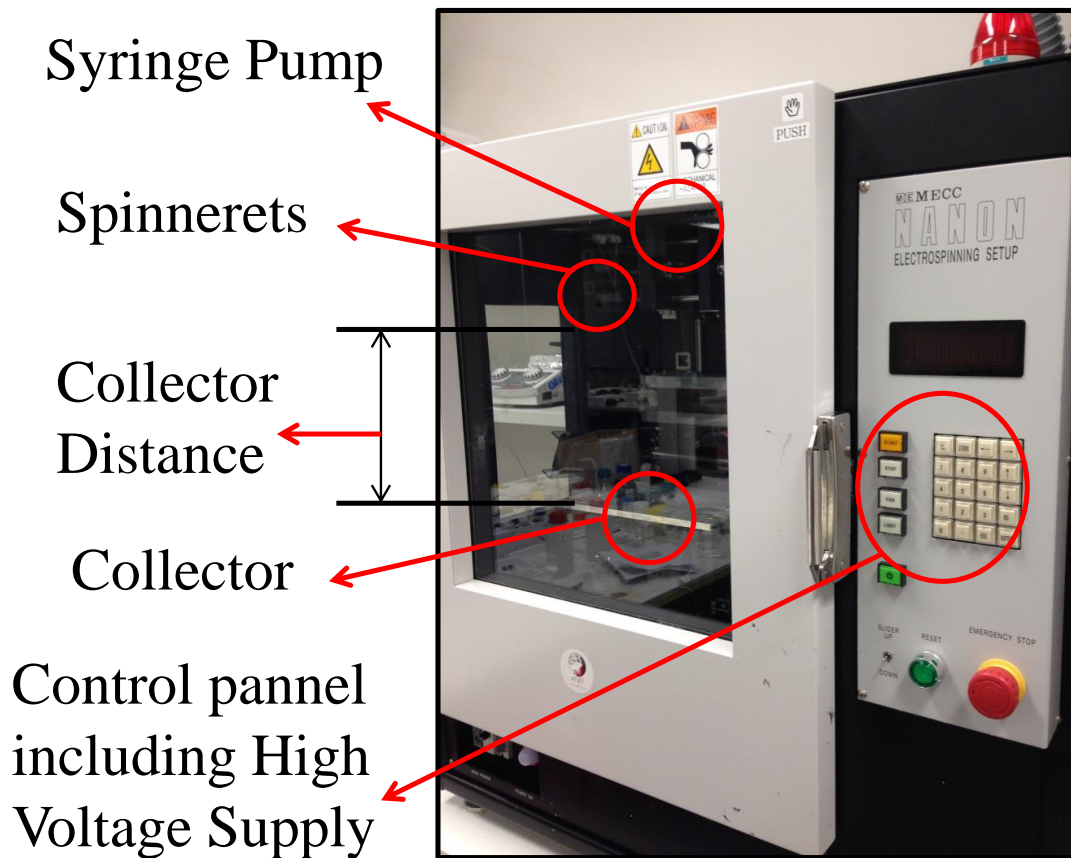


Figure 2.1 Photograph of NANON-01A electrojetting system.

Electrojetting including electrospinning and electrospraying is a simple and versatile technique to fabricate nano-/micro- fibre and particle [1-4]. All electrojetting experiments were conducted using a NANON-01A electrojetting system which was purchased from MECC Co. Ltd, Japan (**Figure 2.1**). The system is composed of several main parts including high voltage power supply, syringe and pump, spinnerets, collector, and Controller panel. Both the spinnerets and collectors can be replaced, depending on the application requirement. Two kinds of spinnerets are used in this thesis: single tube spinnerets and co-axial spinnerets. Two kinds of the collector are used: rotating drum and metal plate. The programming controller panel is used to set parameters such as voltage, feeding volume, and rate of the solution, the rotation speed of collector, spinnerets movement, etc. The chamber of the

NANON-01A system can maintain the electrojetting in a stable atmospheric environment with constant temperature and moisture.

2.3.2 Electropolymerization

Electropolymerization involves the oxidation of the heteroarene to afford radical cations that couple to form oligomers. The oligomers precipitate to nucleate polymerization on the electrode surface [5, 6]. In this study, electropolymerization was conducted by using a CHI 600 electrochemical system from CH Instruments, Inc. (**Figure 2.2**). The instrument contains a potentiostat with a potential control range of ± 10 V; the current range is ± 250 mA. It is also available with a wide variety of electrochemical techniques and is capable of integrated simulation and fitting software functions for detecting Electrochemical impedance spectroscopy (EIS) and Cyclic voltammetry (CV). A standard three-electrode cell with a stainless steel mesh counter electrode (CE) and Ag/AgCl reference electrode (RE) were used for conducting polymer electrochemical synthesis. The printed 3D Ti-6Al-4V electrode was used as the working electrode (WE). The electrodes used in this study were 1 cm by 1 cm by 1 cm and contain 54 posts. Each post has a ~ 500 μm diameter and 8 mm height.

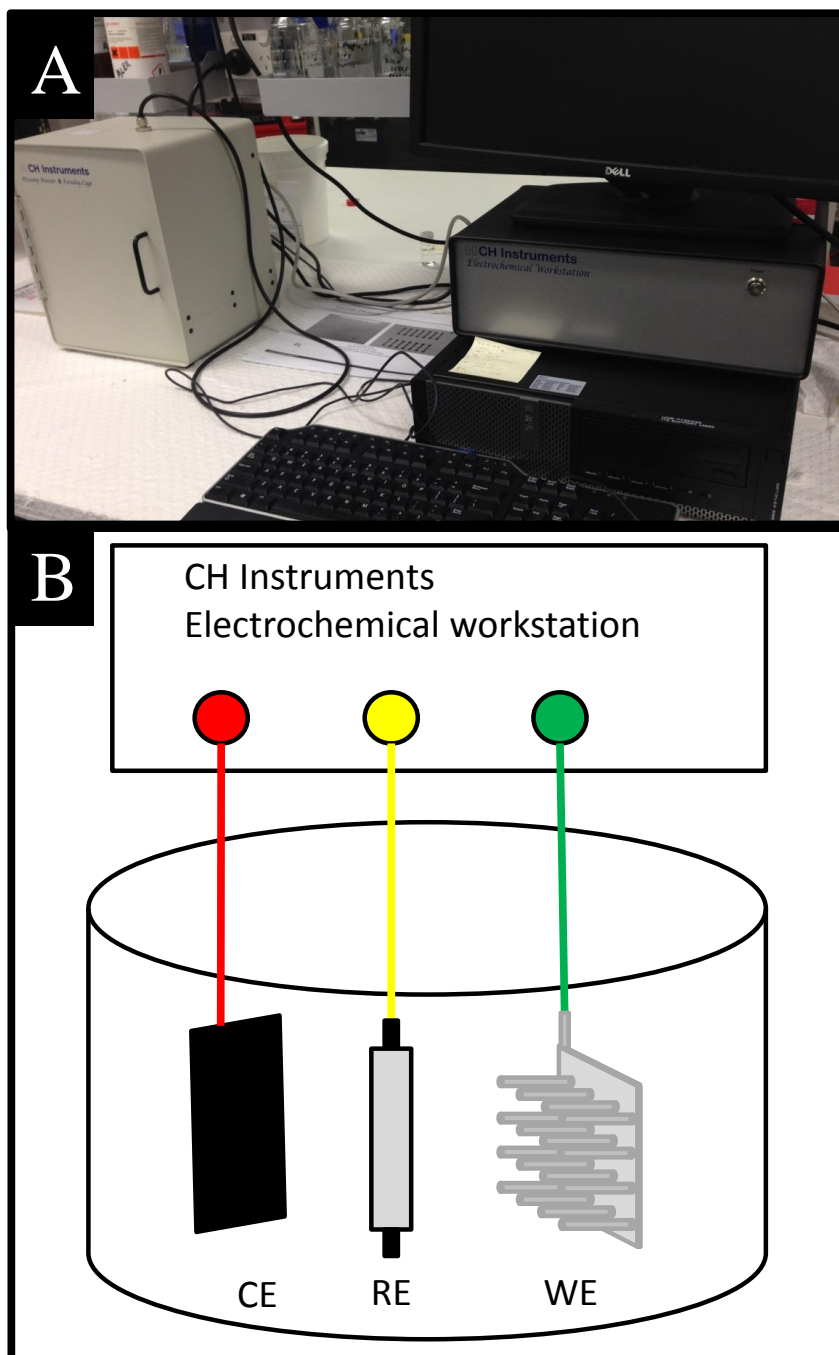


Figure 2.2 Photograph of (A) CHI electrochemical workstation and, (B) schematic of the three-electrode system.

2.4 General physicochemical characterization

2.4.1 Scanning electron microscopy

Scanning Electron Microscopy (SEM) is used to observe the microstructure of the materials. In this thesis, all SEM images were obtained using a JSM7500FA Field Emission Scanning Electron Microscope from JEOL Ltd., Japan (**Figure 2.3**). The sample is dried using a vacuum oven at room temperature to remove any residual organic solvent or moisture. Typically, the sample is attached to the testing plate with conductive tape. Before SEM testing, the nonconductive sample is coated with a thin layer of gold to avoid charge accumulation.



Figure 2.3 JSM7500FA Field Emission Scanning Electron Microscope from JEOL.

2.4.2 Thermogravimetric analysis

Thermogravimetric Analysis (TGA) is used to investigate the pyrolysis and combustion behaviour of the materials [7]. TGA is performed on a TGA Instrument Q500 from TA Instruments, UK (**Figure 2.4**). It can provide information regarding reactions occurring during the materials pyrolysis process; such as number and sequence and activation energy etc. Typically, the sample weight is ~10 mg, the heating rate is set at 10 °C/min, and the TGA curves are recorded from 50 to 800 °C. In order to eliminate the moisture interference, the sample is dried in a vacuum oven overnight before TGA testing.

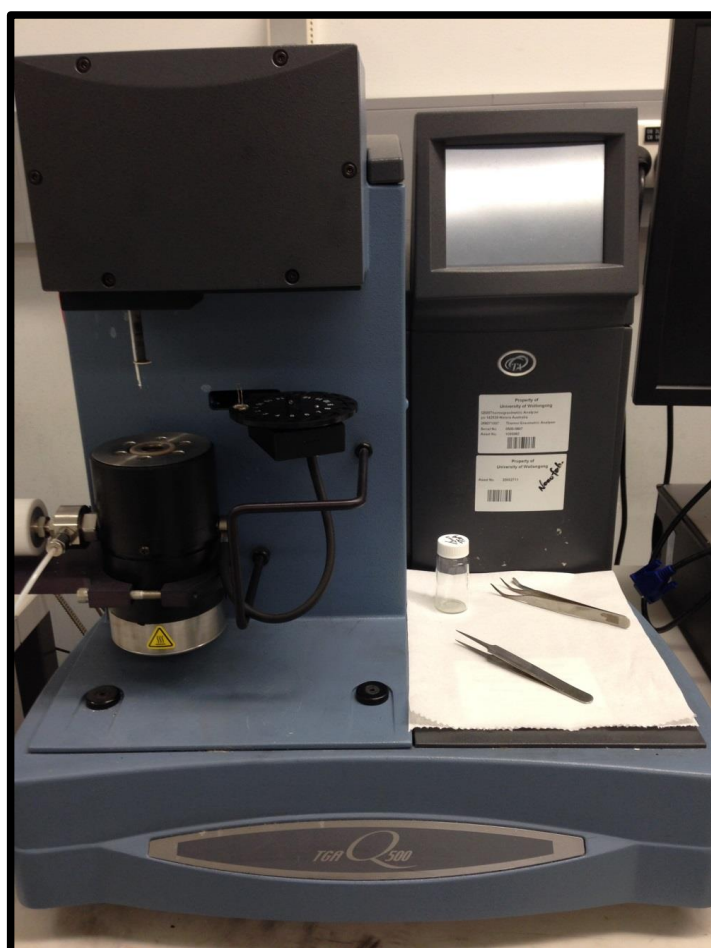


Figure 2.4 Thermogravimetric Analysis Instrument TA Q500.

2.4.3 Tensile testing

Tensile testing is commonly used to obtain mechanical properties of materials [8]. The sample used for tensile testing is typically made into a dog-bone shape, subjected to controlled tension until mechanical failure. The result of tensile testing is given as a stress-strain curve. From this curve, mechanical information such as tensile strength, tensile modulus, yield strength (not for all kinds of materials), elongation at break can be determined. The tensile testing is performed by using a commercial Shimadzu EZ-L mechanical testing machine (**Figure 2.5**). The sample is gripped by the machine at the two ends. It is important to make sure that the sample is held tightly without slippage or failure in the gripped parts.

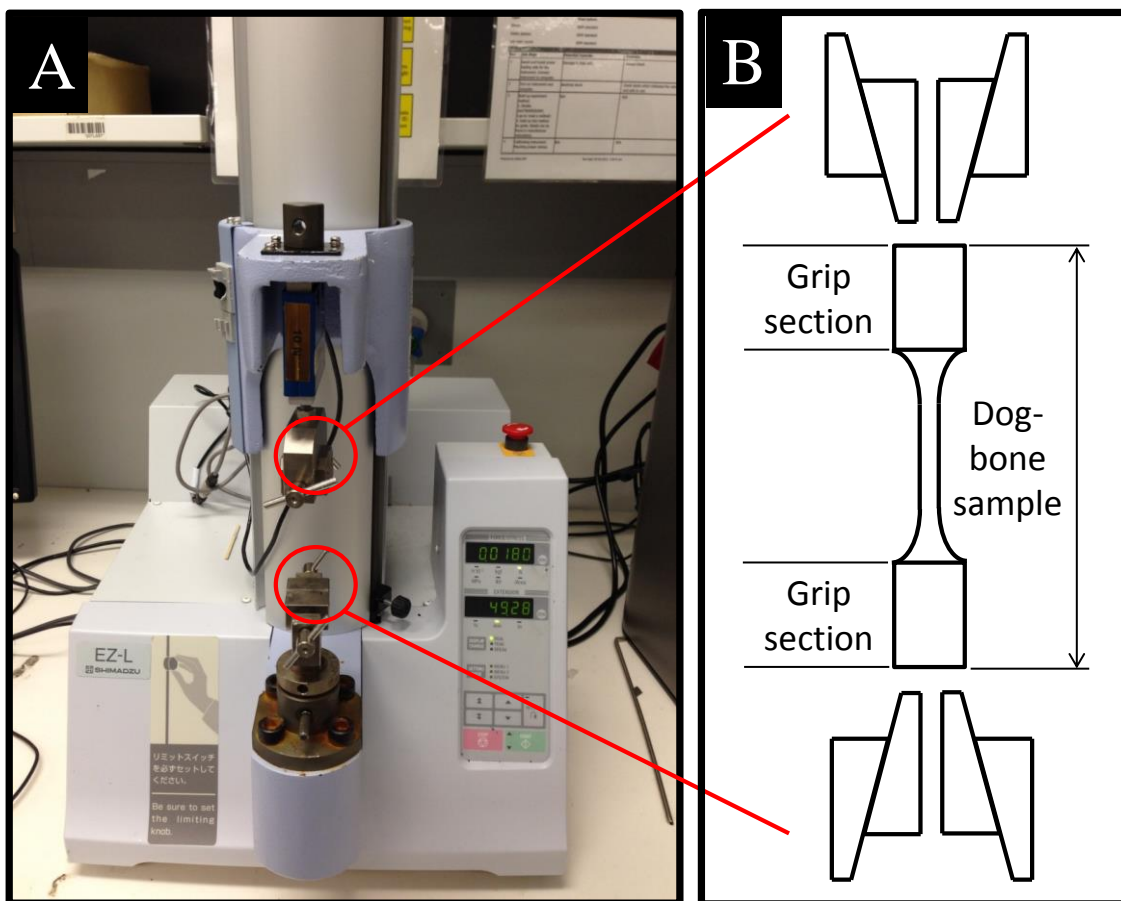


Figure 2.5 Shimadzu EZ-L mechanical testing machine (A) and dog-bone sample (B).

2.4.4 Electrochemical impedance spectroscopy

Electrochemical impedance spectroscopy (EIS) is a powerful diagnostic tool which can be used to characterize the interface between the electronic and ionic conductor in electrochemical systems [9]. When conducting impedance testing, a frequency response analyser is used to impose a small amplitude AC signal to the electrochemical systems and then measuring the current through the systems.

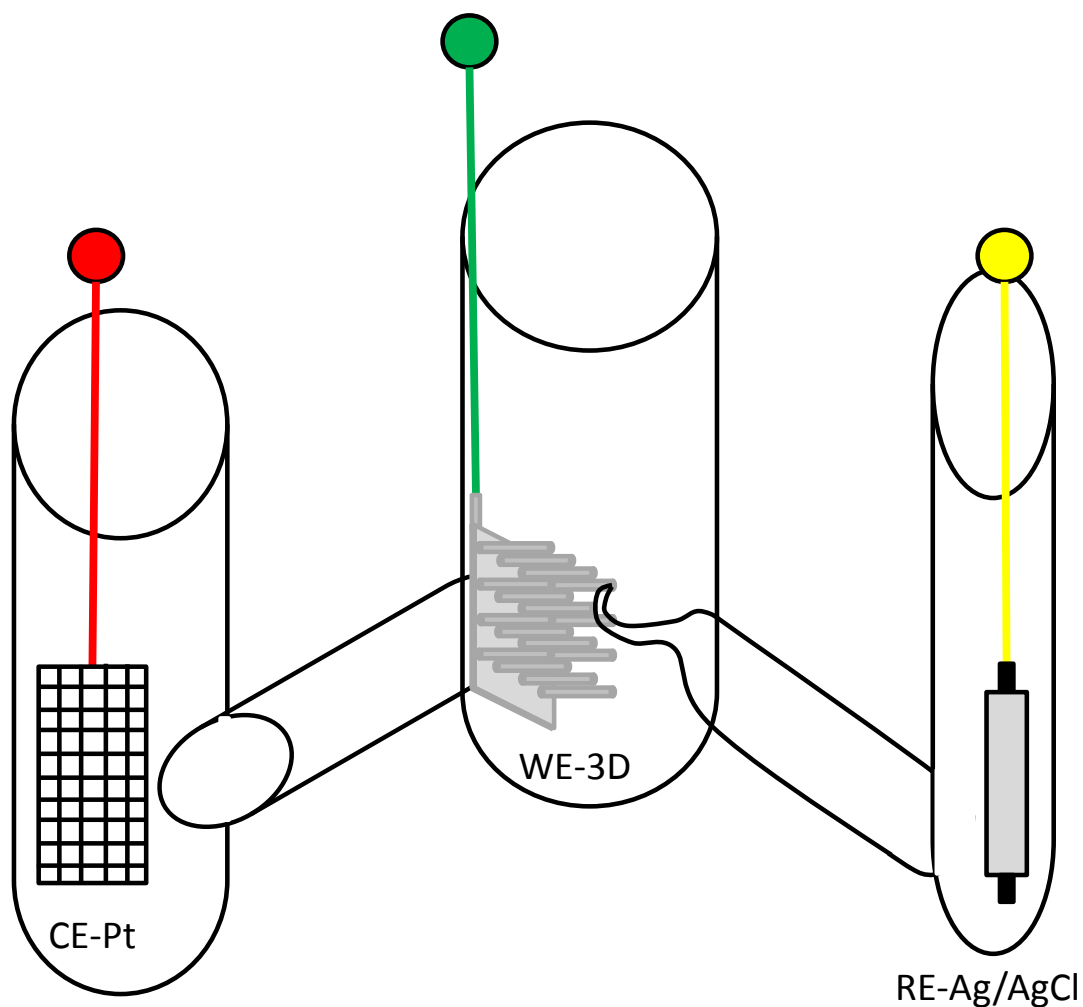


Figure 2.6 The three-electrode system with a Luggin capillary for electrochemical testing.

EIS is measured using a Gamry EIS 3000 TM system with Gamry framework software employing a three-electrode system (**Figure 2.6**). The system is made of glass, with a Luggin capillary in order to minimize the impact of uncompensated electrolyte resistance [10]. The frequency range was from 0.1 Hz to 100 kHz, and the AC perturbation was 5 mV at open circuit potential. Data presentation is shown as a Bode Plot in this study. The impedance is plotted with log frequency on the X-axis and the absolute values of the impedance on the Y-axis.

2.4.5 Cyclic voltammetry

Cyclic voltammetry (CV) is widely used to study the mechanism, kinetics, electrochemical active surface area, and thermodynamics of electrochemical reactions [11]. In cyclic voltammetry, the electrode potential ramps linearly versus time as shown in **Figure 2.7**. These ramps can be repeated many times according to experimental requirement. The rate of voltage change is the scan rate in mV/s. The potential is applied between the working electrode and the reference electrode, and the current is measured between the working electrode and the counter electrode. The data is expressed as current vs. applied potential. In CV, the current flow is a result of the oxidation/reduction process. It is important and useful in the characterization of materials' electroactivity. In this study, the CV experiment was performed using a CHI 600 electrochemical system from CH Instruments, USA. It is tested in a three-electrode system, using Ag/AgCl reference electrode and Pt mesh as the counter electrode in aCSF (artificial Cerebral Spinal Fluid) solution.

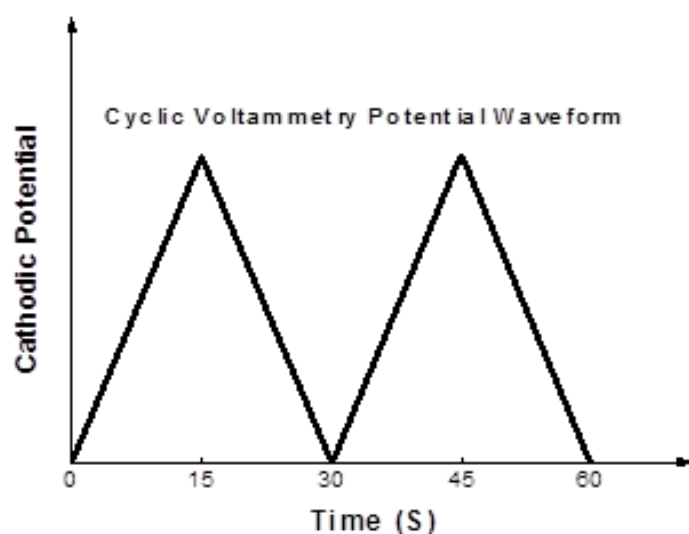


Figure 2.7 The classical triangle waveform used in cyclic voltammetry.

2.5 In vitro drug release study

2.5.1 Passive release study of electrojetted microcapsules

Drug release study of electrojetted microcapsules including microparticles, microfibrils, and their hybrid structures is conducted by using a SW23 shaking water bath from John Morris Scientific Pty Ltd. The water bath is designed to control the temperature and deliver a smooth reciprocal shaking motion (60 rPm). All samples are immersed in aCSF in a glass vial and incubated in the shaking water bath. The temperature is set at 37 °C. At appropriate time intervals, the release medium was withdrawn and replaced with an equal volume of fresh aCSF.

2.5.2 Electrically controlled release study of 3D printed electrodes with drug-laden coatings

The electrically controlled release is carried out in a three-electrode system by using CHI 600 electrochemical system from CH Instruments, USA. An Ag/AgCl electrode is used as a reference electrode; the stainless steel mesh is used as counter electrode. For two interdigitated electrodes release study, one electrode is used as the counter electrode. A square wave, biphasic voltage stimulation is used for electrical stimulation to trigger drug release. The detailed information relating to voltage stimulation is shown in **Figure 2.8**. After several stimulations, the released solution is sampled each time.

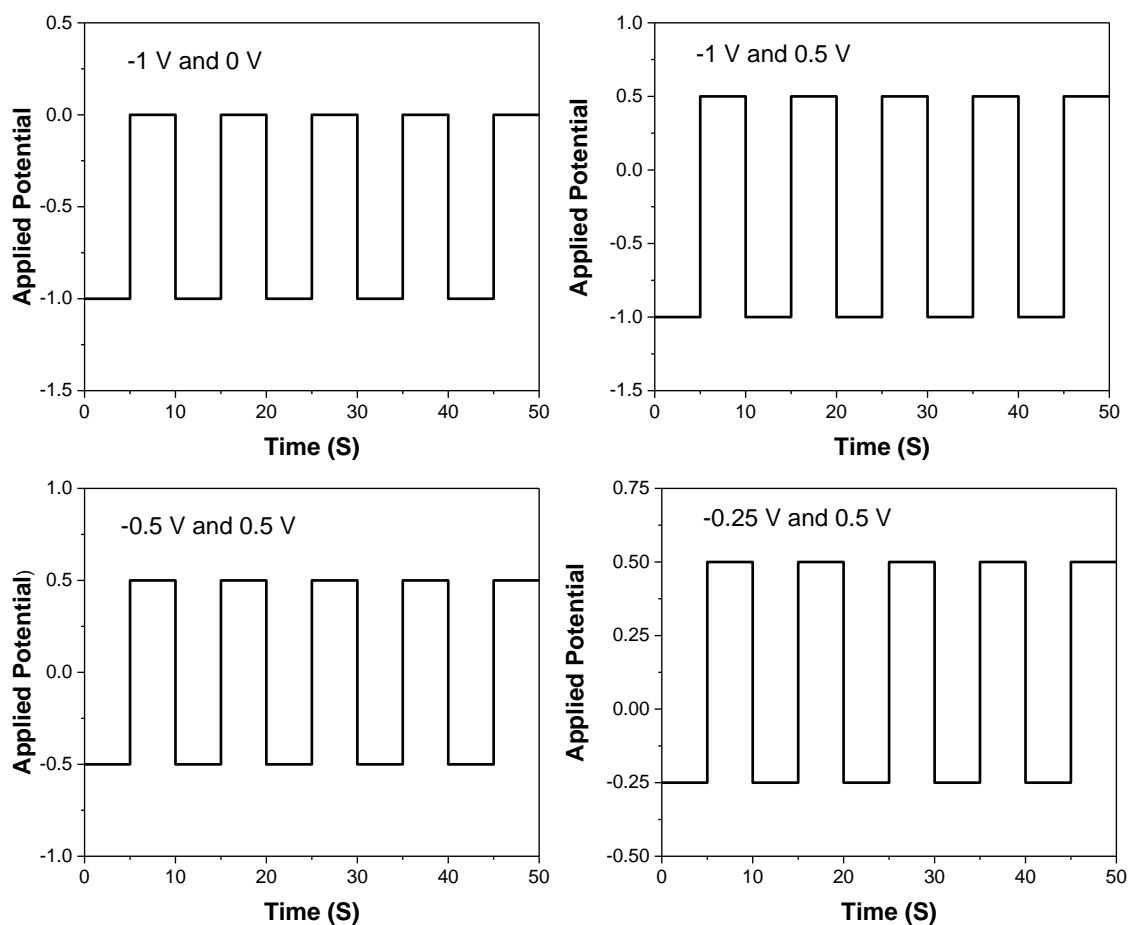


Figure 2.8 Applied potentials of the square wave, biphasic voltage stimulations used in the electrically controlled release study.

2.5.3 High Performance Liquid Chromatography Analysis

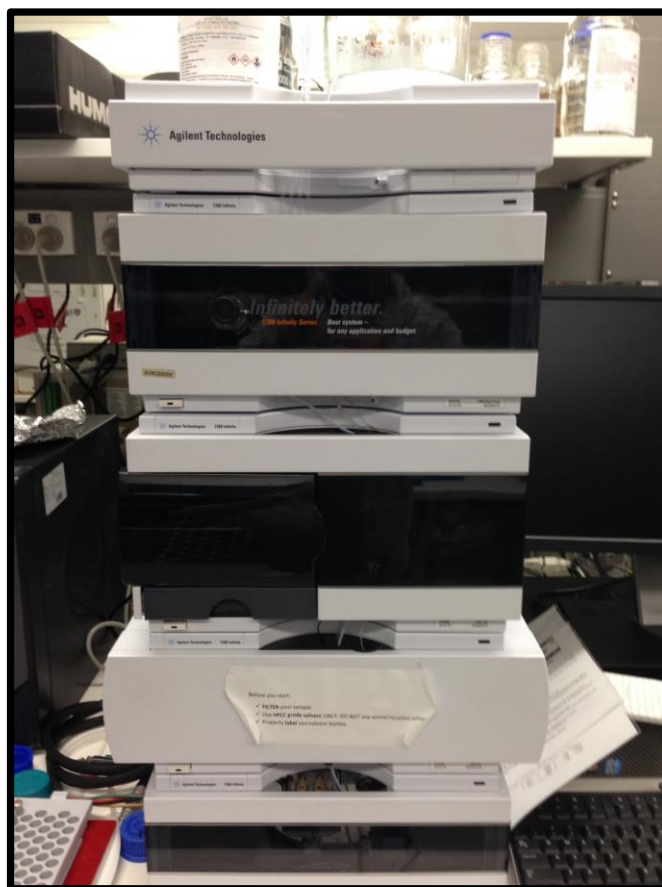


Figure 2.9 Photograph of Agilent 1260 Infinity High Performance Liquid Chromatography system.

High Performance Liquid Chromatography (HPLC) has wide application in analytical chemistry for separation, identification, quantification of chemical components in a mixture [12]. HPLC analysis of aCSF containing released drugs was conducted on an Agilent 1260 Infinity HPLC system (**Figure 2.9**). The analytical column used here is an Atlantis® T3 C18 column (5 μm , 250 mm \times 4.60 mm). The mobile phase, mobile phase flow rate and the UV-vis detection wavelength are detailed in each chapter. The amounts of released drugs are

calculated according to pre-established calibration curves (**Figure 2.10**). All the error bars data shown in figure are expressed as mean \pm standard division.

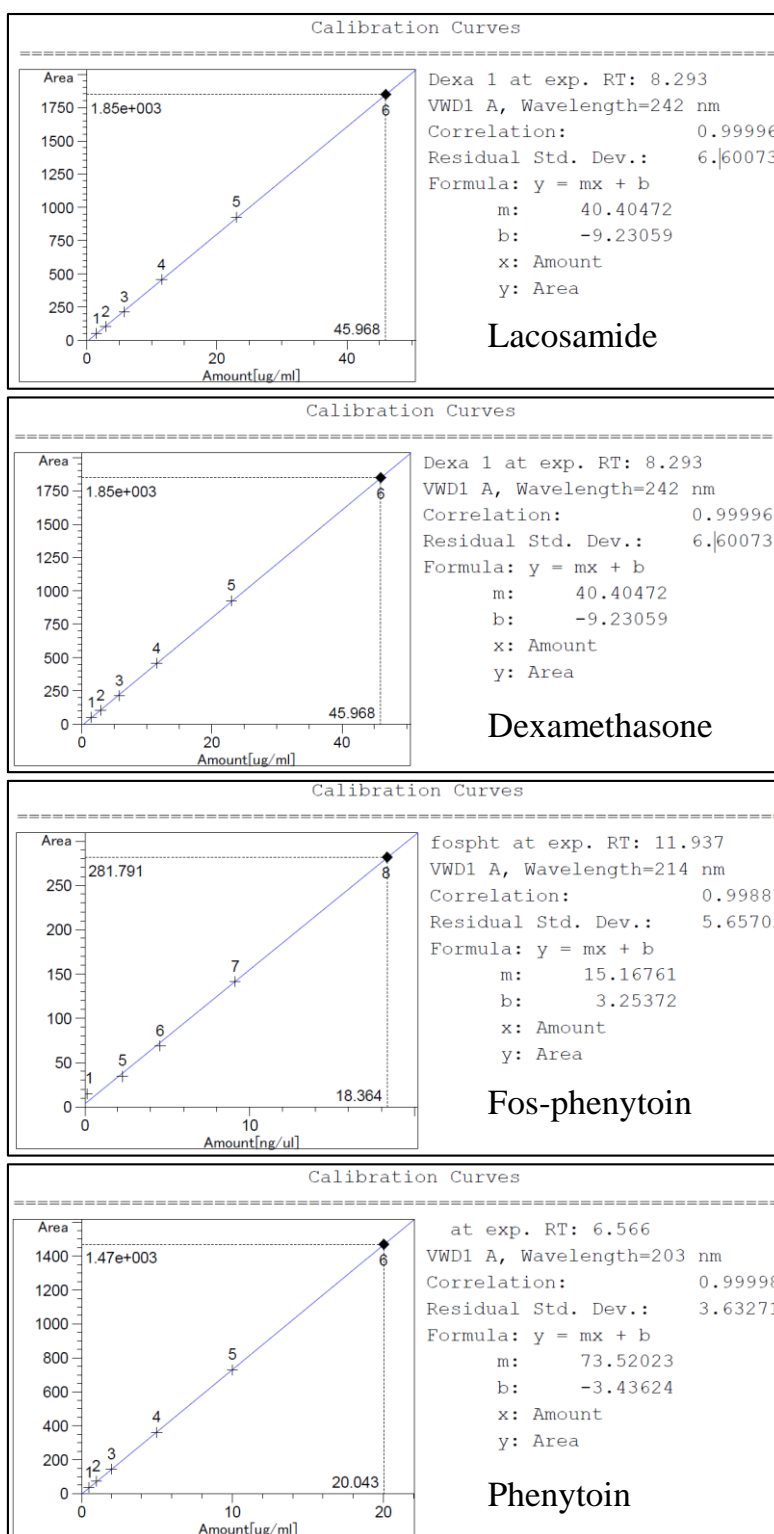


Figure 2.10 The pre-established calibration curves of model drugs used in this thesis

2.6 References

- [1] Doshi J, Reneker DH. Electrospinning process and applications of electrospun fibers. Industry Applications Society Annual Meeting, 1993, Conference Record of the 1993 IEEE1993. p. 1698-703 vol.3.
- [2] Huang Z-M, Zhang YZ, Kotaki M, Ramakrishna S. A review on polymer nanofibers by electrospinning and their applications in nanocomposites. *Composites Science and Technology* 2003;63:2223-53.
- [3] Gañán-Calvo AM, Dávila J, Barrero A. Current and droplet size in the electrospraying of liquids. Scaling laws. *Journal of Aerosol Science* 1997;28:249-75.
- [4] Jaworek A, Sobczyk AT. Electrospraying route to nanotechnology: An overview. *Journal of Electrostatics* 2008;66:197-219.
- [5] Zhou M, Heinze J. Electropolymerization of pyrrole and electrochemical study of polypyrrole: 1. Evidence for structural diversity of polypyrrole. *Electrochimica Acta* 1999;44:1733-48.
- [6] Pringle JM, Forsyth M, Wallace GG, MacFarlane DR. Solution-surface electropolymerization: a route to morphologically novel poly (pyrrole) using an ionic liquid. *Macromolecules* 2006;39:7193-5.
- [7] Broido A. A simple, sensitive graphical method of treating thermogravimetric analysis data. *Journal of Polymer Science Part A-2: Polymer Physics* 1969;7:1761-73.
- [8] Nicholas T. Tensile testing of materials at high rates of strain. *Experimental Mechanics* 1981;21:177-85.
- [9] Orazem ME, Tribollet B. *Electrochemical impedance spectroscopy*: John Wiley & Sons; 2011.

- [10] van der Vliet D, Strmcnik DS, Wang C, Stamenkovic VR, Markovic NM, Koper MTM. On the importance of correcting for the uncompensated Ohmic resistance in model experiments of the Oxygen Reduction Reaction. *Journal of Electroanalytical Chemistry* 2010;647:29-34.
- [11] Lyons M. *Electroactive Polymer Electrochemistry: Part 1: Fundamentals*: Springer Science & Business Media; 2013.
- [12] Parris NA. *Instrumental liquid chromatography: a practical manual on high-performance liquid chromatographic methods*: Elsevier; 2000.

**CHAPTER 3: DEVELOPMENT OF
DRUG-LOADED POLYMER
MICROCAPSULES FOR
TREATMENT OF EPILEPSY**

3.1 Introduction

Approximately 90% of the new drugs that are successful in preclinical studies fail in clinical trials[1]. The high failure rate in new drug development is not due to a lack of drug potency, but rather due to toxicity, side effects, and poor pharmacokinetics and pharmacodynamics. A promising strategy for overcoming these drawbacks is to develop an appropriate drug delivery system for targeted and efficient application. For treatment of brain diseases, such as epilepsy, Parkinson's disease, Huntington's disease, Alzheimer's disease, and brain tumours, drug delivery to the central nervous system (CNS) represents a unique challenge. This is due to a number of factors, in particular the presence of physical permeability barriers such as the blood-brain barrier (BBB) and the blood-cerebrospinal fluid (blood-CSF) barrier, and expression of multidrug drug efflux transporters at the barriers, which work collectively to restrict the entry of many pharmaceuticals into to the brain [2-6]. The low brain permeability of many drugs is responsible for drug resistance in the therapies for many diseases. In the case of epilepsy, 30-40% of patients remain drug resistant with poor clinical outcomes, and this represents a significant hurdle for medication therapy of intractable epilepsy [7].

In order to deliver drugs to the brain, considerable effort has been made to develop nanocarriers for systemic delivery of therapeutics [8-14]. Compared to systemic drug delivery, local drug delivery to the site of action offers the potential to improve the therapeutic efficacy of epilepsy medication. It directly bypasses the physical brain barriers, which may result in improved drug delivery efficiency and bio-distribution. Consequently, a lower therapeutic dosage may be required, with a concomitant reduction in side effects [15-17]. These advantages have motivated the research and development of local drug delivery systems for treatment of epilepsy [18-21]. For example, Williamson *et al.* developed an

organic electronic ion pump, composed of poly(3,4-ethylenedioxythiophene) doped with polystyrene sulfonate electrodes, for on-demand and site-specific delivery of an inhibitory neurotransmitter, gamma-aminobutyric acid (GABA). The delivery of GABA was shown to result in quick and localized suppression of epileptiform activity [21]. Pritchard *et al.* developed silk fibroin coatings on solid reservoirs of the anticonvulsant adenosine. By modulating the coating thickness and crystallinity, sustained release of adenosine with various release profiles including zero-order release profiles was achieved over a period of two weeks [19].

Lacosamide, the R-enantiomer of 2-acetamido-N-benzyl-3-methoxypropionamide, is a novel antiepilepsy drug. Based on the efficacy and therapeutic index observed in a range of animal models of epilepsy at the National Institute of Health (NIH) Anticonvulsant Screening Program, lacosamide warranted further evaluation and was subsequently developed as an AED for both oral and intravenous use. It is suggested that lacosamide has a dual action underlying its anticonvulsant and analgesic properties. It has also been found that lacosamide selectively enhances slow inactivation of voltage-gated sodium channels without affecting fast inactivation [7].

This chapter aims to fabricate microcapsules using a simple electrojetting (electrospinning and electrospraying) technology, for the sustained delivery of antiepilepsy drugs (AEDs). The microcapsules include flattened microspheres, microspheres, and microfibres, which have controllable uniform morphology and size distribution, enable high-efficiency drug encapsulation, and have release profiles that agree well with the mathematical simulation model results, and thus are predictable. Importantly, the microcapsules are compatible with

human NSCs (Neural Stem Cells) and derivative neurons and neuroglia, which is indicative of clinical compliance for therapeutic use. These microcapsules can be utilized as injectable/implantable systems for site-specific delivery of AEDs.

3.2 Materials and Methods

3.2.1 Materials

The anti-epilepsy drug, lacosamide, was provided by UCB Pharma Pty Ltd. Poly(D,L- lactic-co-glycolic acid) ($M_w \sim 60,000$ Da, with a 75/25 molar ratio of lactide to glycolide) (PLGA 75/25) was purchased from Purac, Singapore. Chloroform, methanol, and acetonitrile were all analytical grade from Sigma-Aldrich. All the others chemicals and reagents were purchased from Sigma-Aldrich and used as received.

3.2.2 Microcapsule fabrication via electrojetting

The microcapsules, including microspheres and microfibres, were fabricated using NANON-01A electrospinning system (MECC Co. Ltd, Japan) at ambient temperature. A range of PLGA/lacosamide (w/w, 10/1) solutions were prepared in chloroform, with the PLGA concentration varying from 1.5 wt%, 4.5 wt%, to 14.0 wt%, respectively. After encapsulation efficiency testing, drug loadings of 8.91 %, 9.20 %, and 9.23 % were achieved. For electrojetting, each solution was loaded into a plastic syringe equipped with a 23-gauge

stainless steel needle. The distance between the tip of the needle and the aluminium foil was 12 cm, and the voltage was 10 kV for electrospaying and 21 kV for electrospinning. The feed rate was controlled at 0.5 mL/h using a syringe pump, and the electrojetted samples were collected using aluminium foil.

3.2.3 Morphological and dimensional statistical analysis

A field emission scanning electron microscope (FESEM, JEOL JSM-7500FA) was used to examine the morphologies of the as-fabricated microcapsules. The samples were sputter-coated with 20 nm gold prior to SEM testing. The dimensional statistical analysis was conducted by quantitatively evaluating the high-magnification SEM micrographs using the imaging software, Leica Application Suite.

3.2.4 *In vitro* drug release study

The drug release was conducted in artificial cerebrospinal fluid (aCSF) at 37 °C in a shaking water bath. Each sample was immersed in 1 mL of aCSF, and the released solution was removed at various time points and replaced with 1 mL of fresh aCSF. All samples were kept at -20 °C, before being analysed by high performance liquid chromatography (HPLC). HPLC analysis was conducted using an Agilent 1260 Infinity HPLC system. The analytical column used was an Atlantis® T3 C18 column (5 µm, 250 mm × 4.60 mm). The mobile phase consisted of Milli-Q water, acetonitrile (HPLC grade) and methanol (HPLC grade) (65:26.2:8.8, v/v/v). The mobile phase flow rate was 0.8 mL/min, and the UV-vis detection wavelength was 210 nm [20]. The amounts of released drug were calculated according to a pre-established calibration curve. An extraction method was used to determine the drug

encapsulation efficiencies of the as-fabricated core-shell microcapsules. Briefly, each sample (1 cm × 1 cm) was placed into 1 mL methanol for 12 hours, after which the methanol was removed and replenished with 1 mL of fresh methanol. This extraction procedure was repeated four times, with each methanol sample being allowed to evaporate to leave the residual drug behind, which was reconstituted using artificial cerebrospinal fluid (aCSF, 0.866 wt% NaCl, 0.224 wt% KCl, 0.0164 wt% MgCl₂·6H₂O, and 0.0206 wt% CaCl₂·6H₂O in 0.001M Phosphate Buffer Solution). Each aCSF sample was then analysed for drug content using HPLC. The 4th reconstituted sample revealed an absence of the drug, indicating that the entire drug had been extracted from the electrojetted sample [22].

3.2.5 Mathematical modelling of the release profiles of the microcapsules

The release profiles of the microcapsules were simulated using Fick's second law of diffusion subject to appropriate boundary conditions [23, 24]. When the surface resistance to mass transfer at the surface is negligible, the fraction of the drug released from the microcapsules (M_t/M_∞) at any time (t) can be expressed as follows:

$$\frac{M_t}{M_\infty} = 1 - \sum_{n=0}^{\infty} \frac{2i}{\lambda_n^2} e^{-\frac{4\lambda_n^2 D_e t}{d^2}} \quad (3.1)$$

Where, d is the diameter of the microcapsules, D_e is the effective diffusivity of drug, $i = (2, 3, 3)$ and $\lambda_n = (n\pi)$ for flattened microspheres and microspheres, $\lambda_n = (2.41, 5.52, 8.65, 11.8, 14.93 \dots)$ for microfibre [25] (International system of units). The mathematical modelling study are based on equation (1), using MATLAB Curve Fitting Toolbox.

3.2.6 NSC culture and differentiation

Working stocks of human NSCs (ReNcell CX, SCC007, Millipore) were maintained under 5% CO₂ at 37 °C, seeding at a density of 2 – 3 x 10⁶ cells in proliferation medium comprising NeuroCult NS-A (#5751, Stem Cell Technologies) with 2 µg/mL heparin, 20 ng/mL FGF2 and 20 ng/mL EGF (AF-100-15, Peprotech) on laminin (L6274, Life Technologies) coated 6-well plates (Greiner Bio-One). Cells were passaged at confluency every 5-7 days by digesting in TrypLE (Life Technologies) for 3 min at 37 °C. Differentiation of NSCs was performed 3 days after initially seeding in proliferation medium, using neural differentiation medium comprising two parts DMEM/F-12 (11330-032, Life Technologies), one part Neurobasal (21103-049, Life Technologies) supplemented with 0.5% N2 (17502048, Gibco) and 50 ng/mL brain-derived neurotrophic factor (BDNF, 450-02, Peprotech) for up to 10 days.

3.2.7 NSC viability analysis

PrestoBlue™ cell viability reagent was used for NSC viability studies, according to the manufacturer's instructions. Briefly, cells were incubated with the reagent in culture medium for 1 hr at 37 °C. Following incubation, for each sample, 100 µL supernatant was transferred to a well of a 96-well plate and screened by a microplate reader (POLARstar Omega) to read fluorescence intensity. After processing, samples were rinsed in culture medium and returned to culture, with the process repeated for each time point until the study was completed.

3.2.8 Scanning Electron Microscopy (SEM)

SEM was performed as previously described [26]. Briefly, samples were fixed in 3.7% paraformaldehyde (PFA) for 10 min and then serially dehydrated in 30%, 50%, 70%, 85%, 95%, and 100% ethanol before Critical Point Drying using a LeicaEMCPD030 instrument. The samples were then coated with 20 nm platinum followed by imaging with a JEOL JSM-7500FA.

3.3 Results and Discussion

3.3.1 Fabrication of lacosamide-loaded microcapsules by electrojetting

Electrojetting is an electrohydrodynamic process. It is a simple, versatile and cost effective technology that employs an electrically charged jet of a polymer solution to fabricate nano- or micro- scale fibres (i.e., electrospinning) or particles (i.e., electrospraying) [27-31]. Electrojetting is governed by the interactions between the electrostatic repulsion induced by an applied electric field and surface tension of a liquid droplet. At the tip of the capillary, due to the electrostatic repulsion and the surface tension, the hemispherical surface of the polymer droplet is distorted into a conical shape that is known as the Taylor cone. When the electrostatic repulsion surpasses the surface tension, liquid ejection will occur at the surface of the Taylor cone. Electrospinning (as is illustrated in **Figure 3.1**) typically occurs when the polymer concentration and molecular weight are sufficiently high so that the Taylor cone is stable, and the fluid does not break up into droplets but forms a stable liquid jet. The liquid jet

will undergo a whipping or bending motion process, giving rise to the formation of fibres [27].

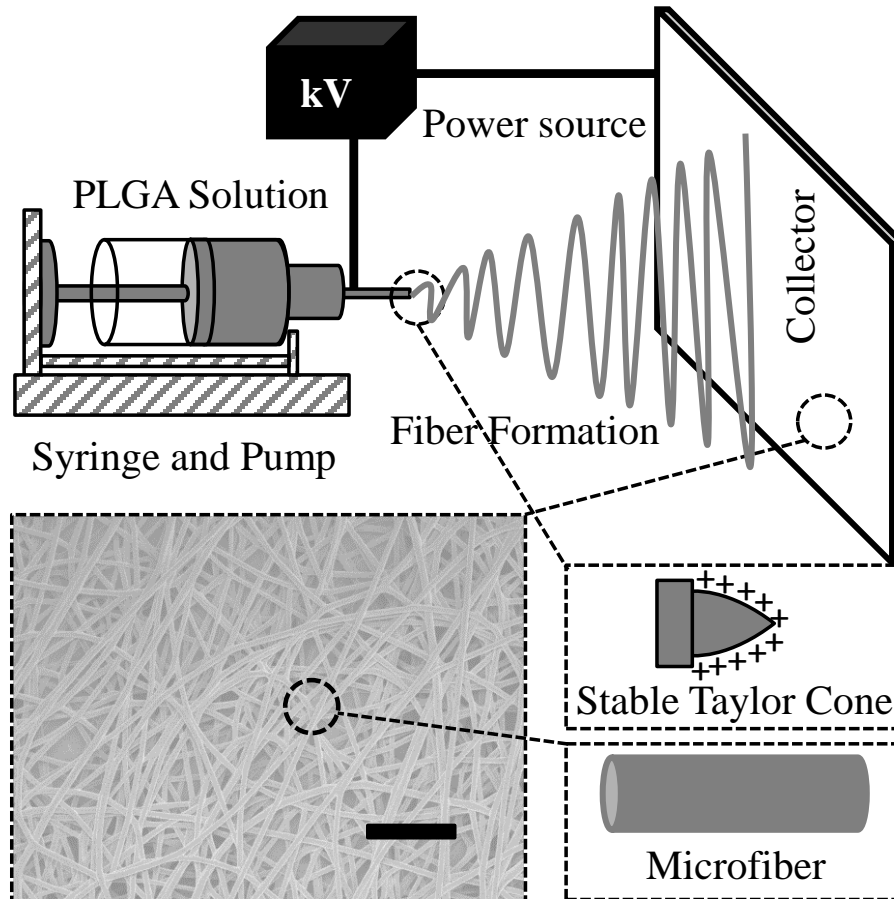


Figure 3.1 Schematic illustration of the electrospinning setup, with SEM images of electrospun PLGA/lacosamide microfibres. The scale bar is 10 μm .

However, when the polymer concentration is below a threshold and/or the polymer molecular weight is low enough, the Taylor cone becomes unstable, and the liquid jet breaks up due to varicose instabilities and hence fine droplets are formed. The electrostatic forces among the droplets enable self-dispersing of the droplets in space with minimal droplet agglomeration. Further evaporation of the solvent leads to concentration and solidification of the droplets,

i.e., the formation of the polymeric microspheres. This process is also known as electrospaying, which is illustrated in **Figure 3.2** [32].

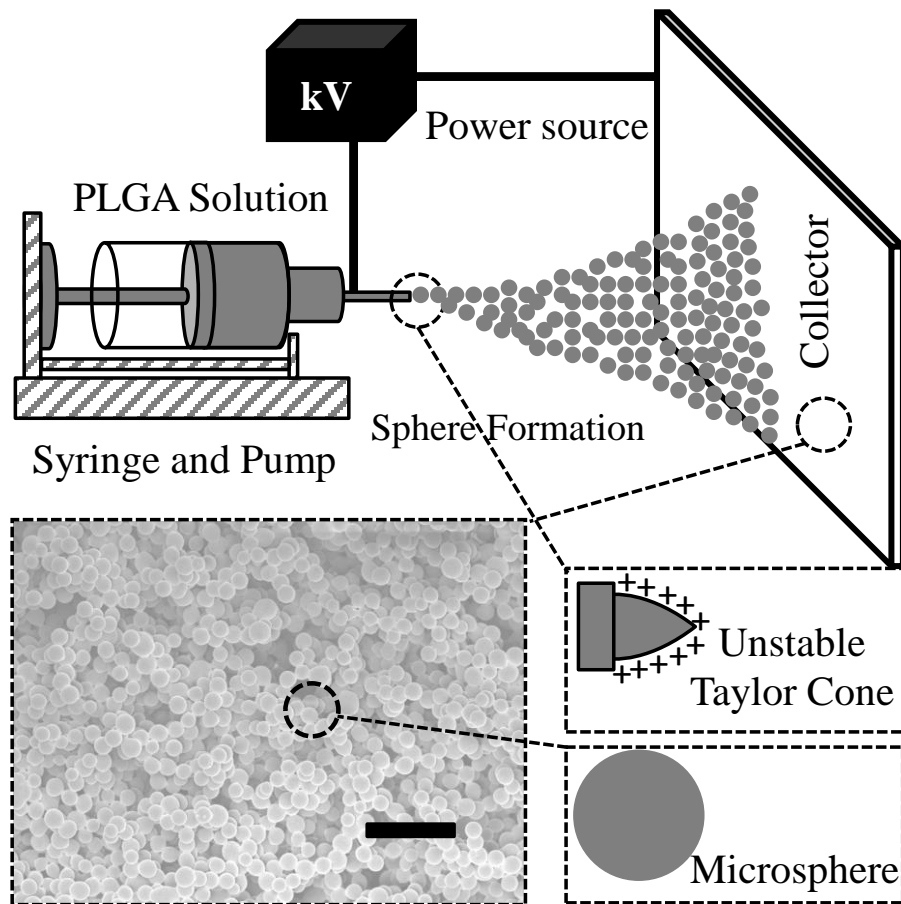


Figure 3.2 Schematic illustration of the electrospaying setup, with SEM images of electrospay PLGA/lacosamide microspheres. The scale bar is 10 μm .

Therefore, under a given electric field, the difference between electrospinning and electrospaying lies in the chain entanglement density of the polymer solution [30]. In this study, the only variable affecting the chain entanglement density is the PLGA concentration. The final electrojetted structure is mainly determined by the PLGA concentration. By

carefully varying the PLGA concentration in the solutions, three kinds of microcapsules have been fabricated, including flattened microspheres, microspheres, and microfibres.

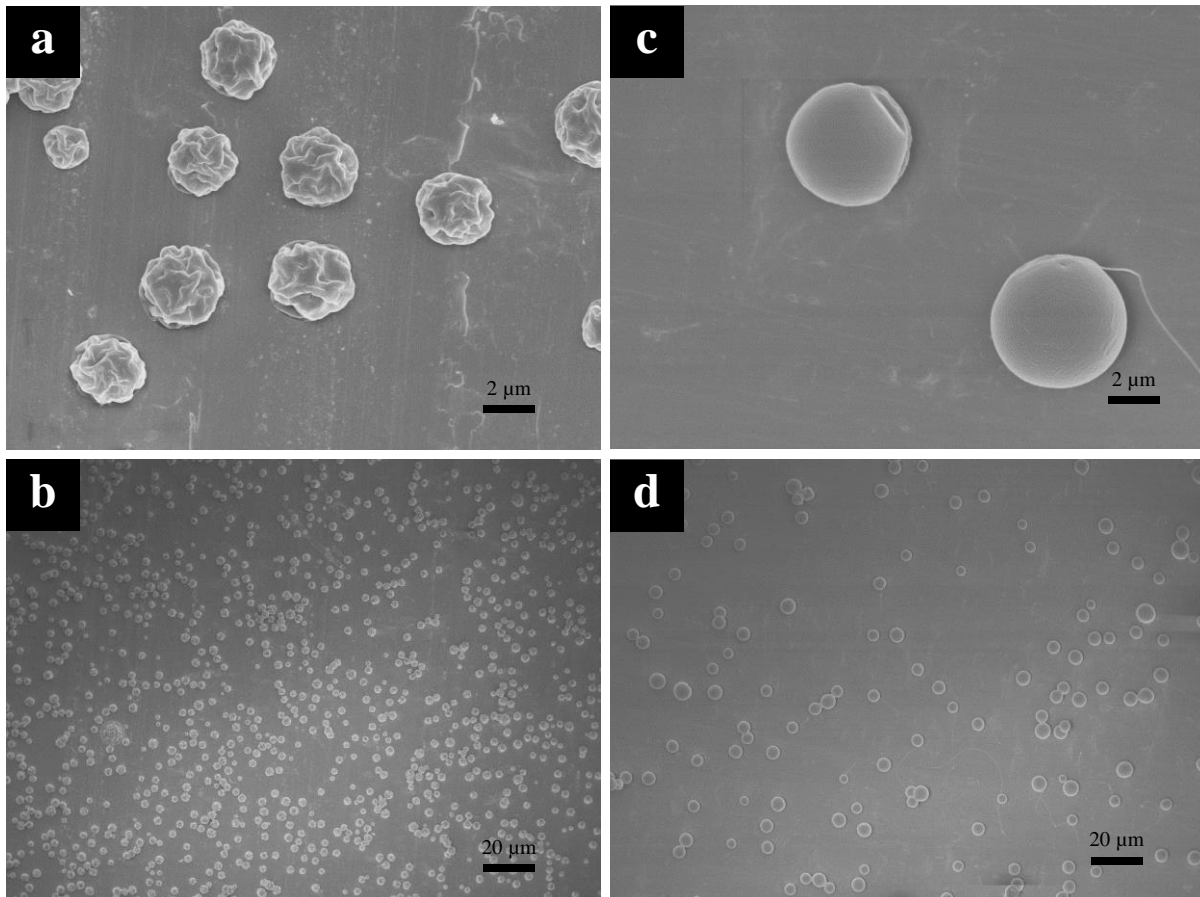


Figure 3.3 Scanning Electron Microscope (SEM) images of PLGA/lacosamide a, b) Flattened microspheres, c, d) Microspheres.

Here shown are the SEM micrographs of lacosamide-loaded flattened microspheres (obtained from 1.5 wt% PLGA and at 10 kV), microspheres (obtained from 4.5 wt% PLGA and at 10 kV), and microfibres (obtained from 14 wt% PLGA and at 21 kV). Our study shows that electrospinning led to the formation of either flattened microspheres or microspheres (**Figure 3.3**), while electrospinning led to the formation of microfibres (**Figure 3.4**).

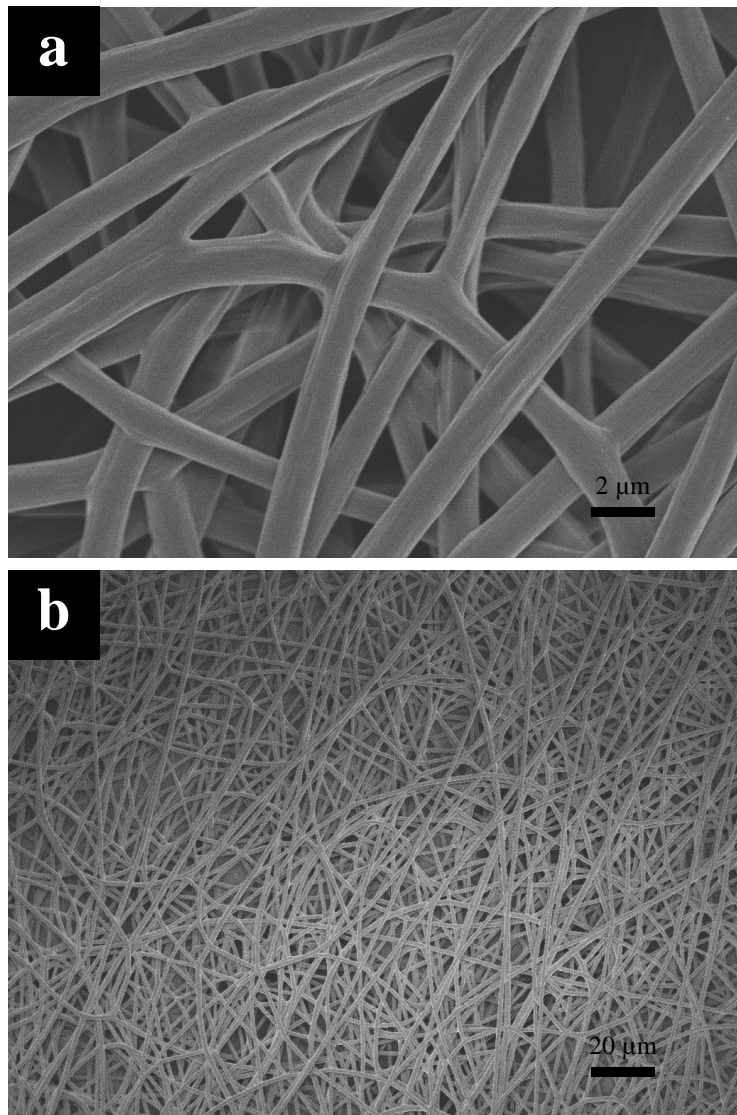


Figure 3.4 Scanning Electron Microscope images of PLGA/lacosamide Microfibres.

These results are consistent with the previous studies, where the polymer concentration is demonstrated to be the most critical parameter in determining the morphology of electrojetted microcapsules [24, 30]. In the current study, at a low PLGA concentration such as 1.5 wt% and 4.5 wt%, even with an increased applied voltage of up to 21 kV, only micro-spherical structures were fabricated.

3.3.2 Dimensional and shape uniformity analysis

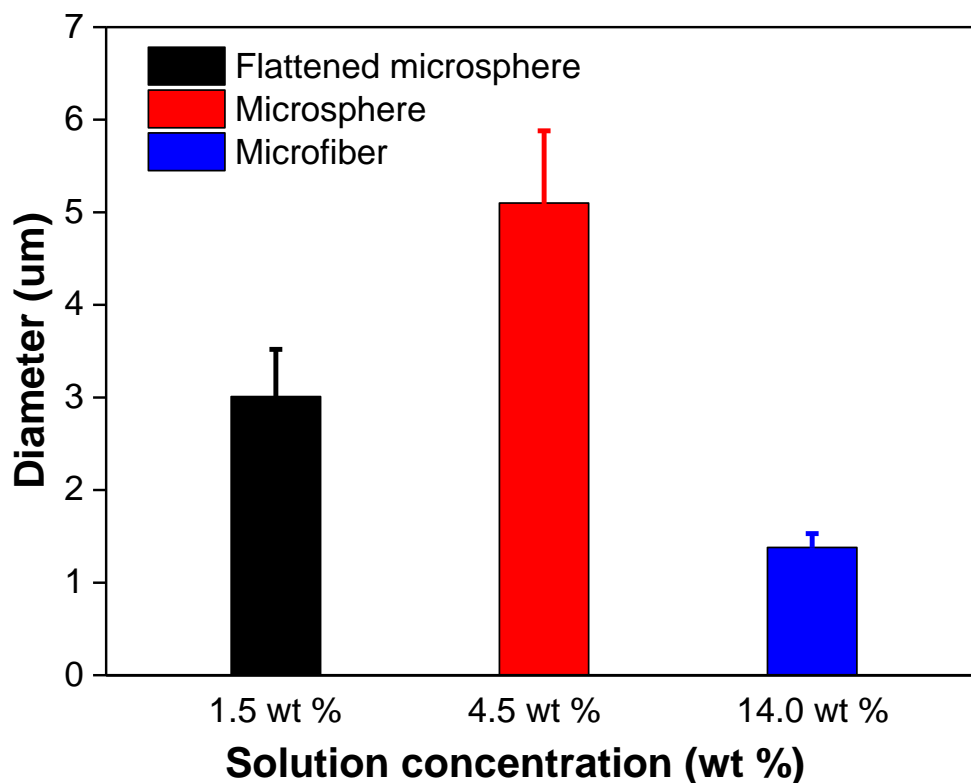


Figure 3.5 Size of flattened microspheres, microspheres, and microfibres.

Evaluation of the dimensional and shape uniformity was conducted by analysis of the SEM images of the as-prepared microcapsules. As shown in **Figure 3.5**, the diameters are $3.01 \pm 0.51 \mu\text{m}$ for the flattened microspheres, $5.10 \pm 0.78 \mu\text{m}$ for the microspheres, and $1.38 \pm 0.15 \mu\text{m}$ for the microfibres, respectively. The diameter distribution of each kind of the

microcapsules is shown in **Figure 3.6**, respectively. All the as-fabricated microcapsules demonstrate uniform morphology with narrow size distribution.

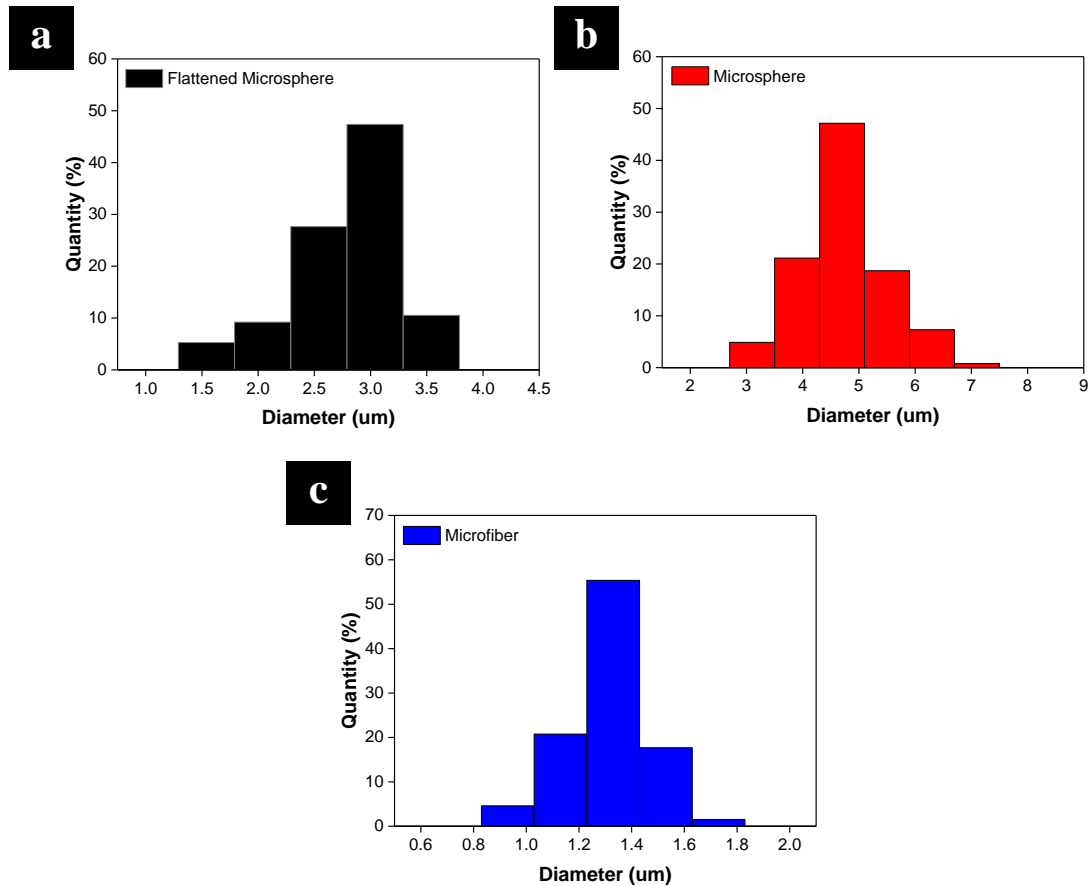


Figure 3.6 Size distributions of flattened microspheres, microspheres, and microfibres.

For electrospinning, as the PLGA concentration is high at 14 wt%, sufficient polymer entanglements are present and responsible for the formation of a stable liquid jet of PLGA that undergo continuous stretching during the whipping or bending motion process. Compared to the microcapsules produced by electrospray, the diameters of the electrospun microfibres are much thinner [33].

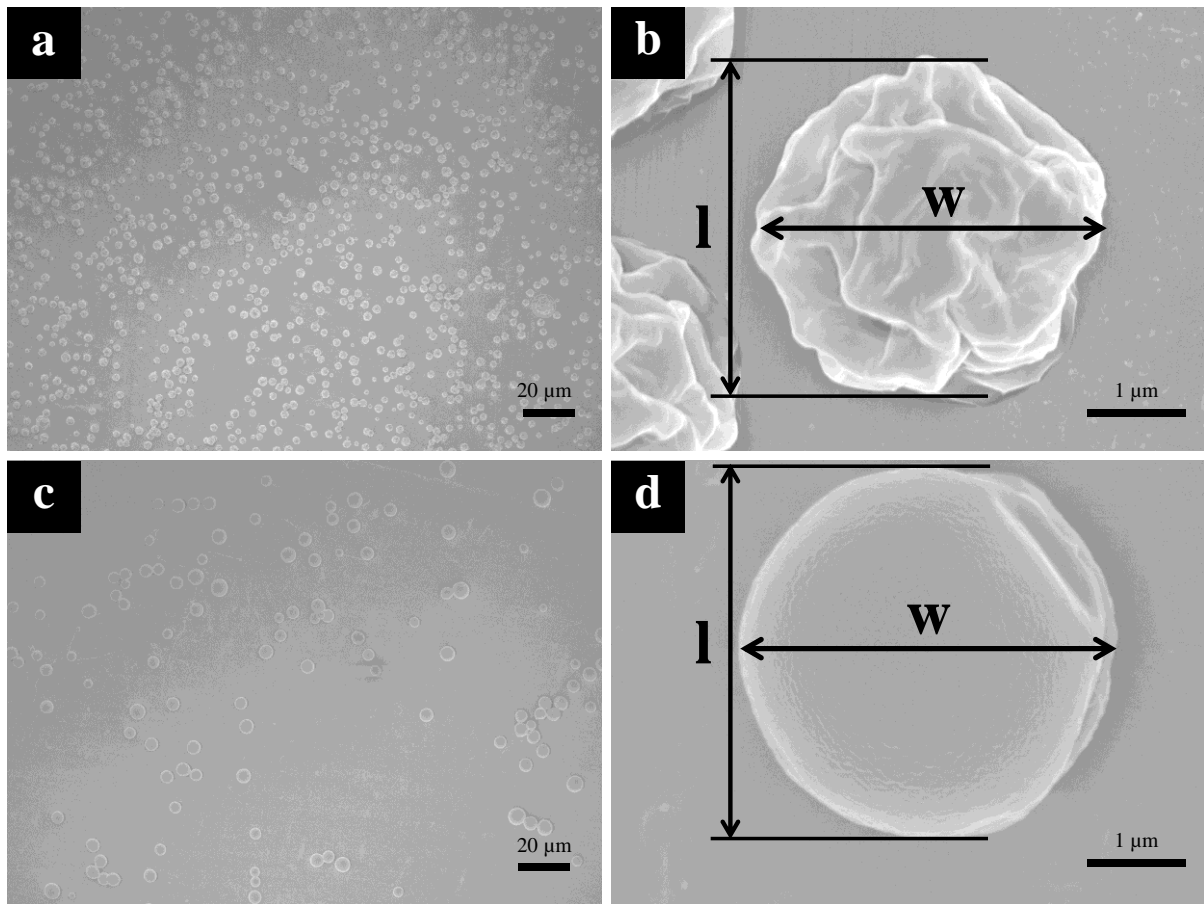


Figure 3.7 Aspect ratio of PLGA/lacosamide a, b) flattened microspheres and c, d) microspheres; Aspect ratio defined as the ratio of the l to w as shown in figures.

For electrospaying, the dimension and shape of the microcapsules are controlled by these two processes: rapid solvent evaporation of the droplets, and polymer diffusion during evaporation. However, rapid solvent evaporation and polymer diffusion do not necessarily lead to spherical microspheres. When a lower PLGA concentration, such as 1.5 wt%, was used in this present work, flattened morphology is formed. This is probably due to incomplete solvent evaporation, as such the electrospayed microcapsules are still in liquid form when reaching the collector [34]. Increasing the polymer concentration to 4.5 wt% prompts the

formation of spherical microspheres with increased particle sizes; since increasing the polymer concentration leads to an increase in the solution viscosity and a reduction in the surface tension. In accordance with Hartman's study, decreasing the surface tension results in increasing the size of electrospay PLGA microspheres [35].

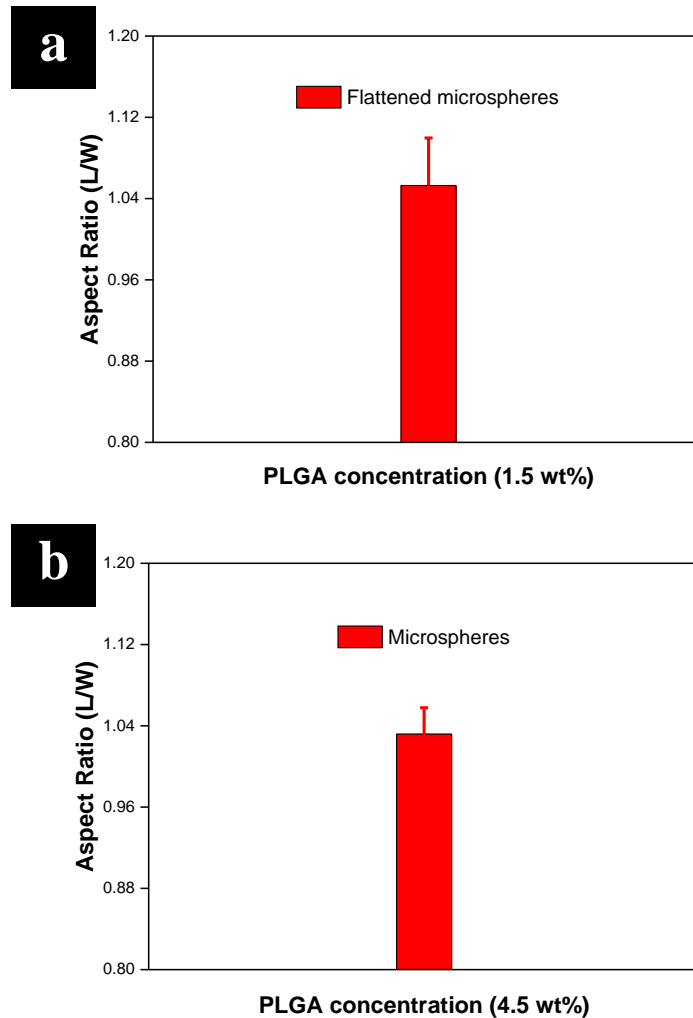


Figure 3.8 Statistical results of aspect ratio, a) flattened microspheres and b) microspheres.

Aspect ratio (AR), expressed as l to w (shown in **Figure 3.7**), is an important parameter to evaluate the shape uniformity of the particles. The dimensions of flattened microspheres and microspheres were measured in two perpendicular directions. The AR of the microspheres is

1.03 for the microspheres, and 1.05 for the flattened microspheres (**Figure 3.8**). Both kinds of microcapsules possess excellent shape uniformity.

3.3.3 *In vitro* drug release and mathematical modelling study

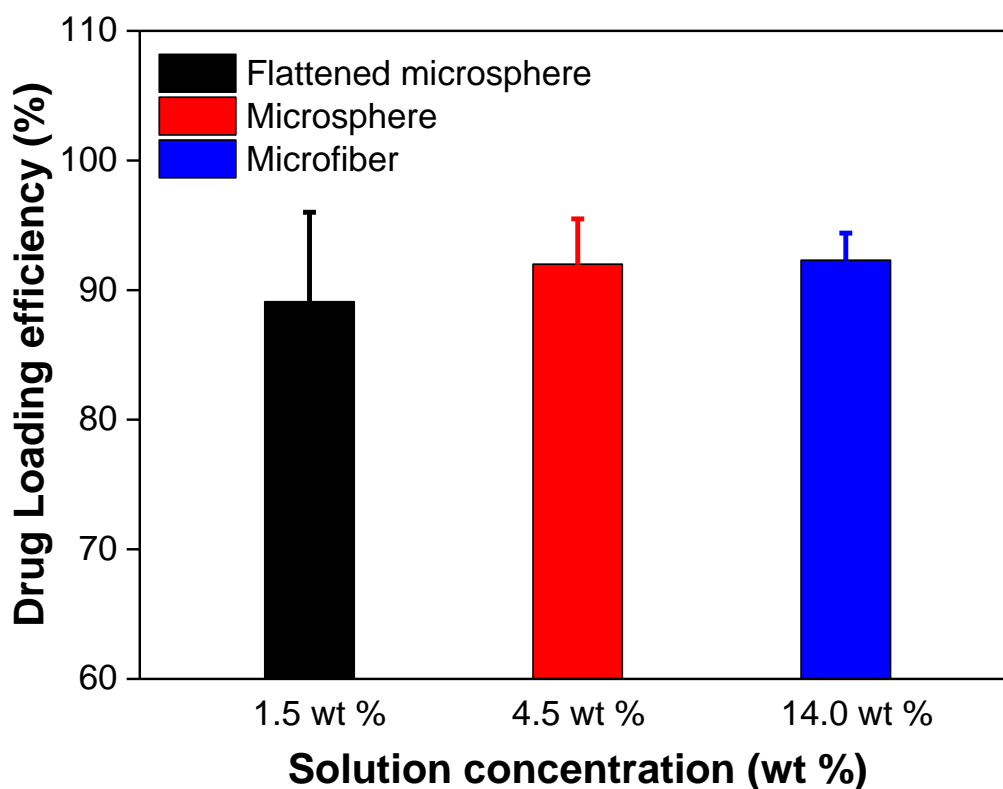


Figure 3.9 Drug encapsulation efficiency of PLGA/lacosamide flattened microspheres, microspheres, and microfibres.

As shown in **Figure 3.9**, all the microcapsules exhibit ultra-high drug encapsulation efficiency. They are 89.1 ± 6.9 % for flattened microspheres, 92.0 ± 3.5 % for microspheres, and 92.3 ± 2.1 % for microfibres. These encapsulation efficiencies are significantly greater than those prepared using other techniques, including emulsion, suspension, and emulsion

polymerization [36], solvent evaporation [36, 37], spray drying [38], and layer-by-layer encapsulation [39].

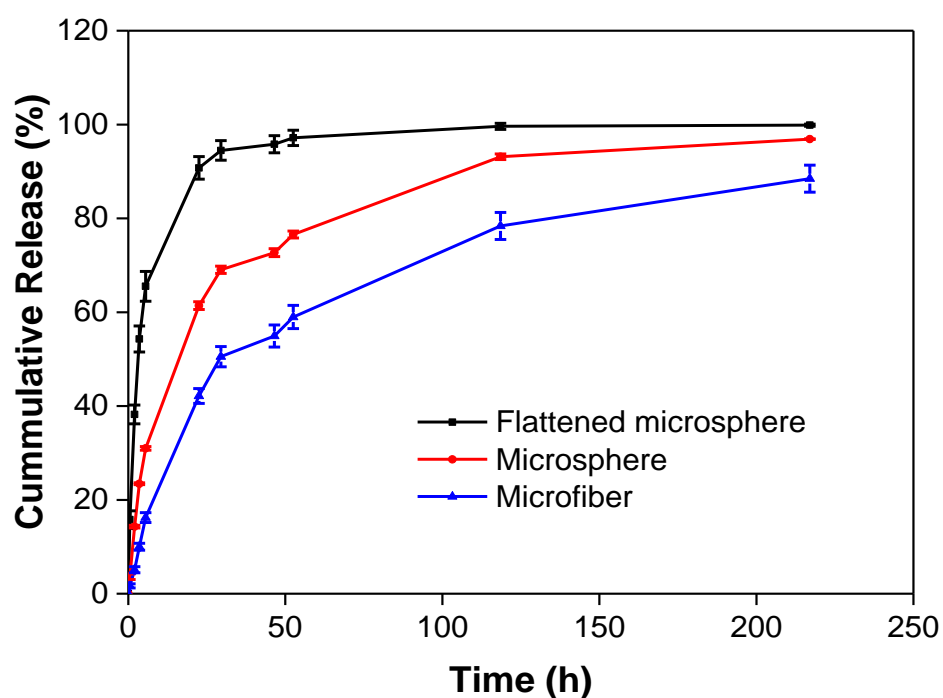


Figure 3.10 Cumulative release profiles of various PLGA microcapsules.

Figure 3.10 shows the *in vitro* drug release profiles of the flattened microspheres, microspheres, and microfibres. The release profiles vary significantly with the shape and morphology of the microcapsules. While the microfibres demonstrate the least initial burst release, the flattened microspheres exhibit the most rapid release characteristics, with more than 95% of the lacosamide being eluted within ~52 hours. Within the same period, the cumulative release of the lacosamide from the microspheres and microfibres is approximately 74% and 55% of the respective total drug loading.

From the perspective of clinical application, for short term seizure prophylaxis, such as after brain surgery, quick early release to a therapeutic level would be preferred. However, the microfibres are more clinically useful as they afford a longer duration of release. An ideal implantable seizure control device should further improve the kinetics to provide as even and as long-term release as possible over the duration of the implant [18]. The fabrication methods demonstrated here have the potential for further improvement after easy modification. For example, application of core-shell spinnerets to fabricate core-shell microfibres can significantly prolong release time [16]. Besides these, use of a more hydrophobic polymer as drug carrier is another promising option.

Typically, drug release from biodegradable microcapsules is controlled by diffusion at an initial stage and then a combination of diffusion and erosion at the later stage [40]. During incubation in the release medium, drug diffusion occurs initially within a thin surface layer, and subsequently with water penetration into the bulk of the microcapsules, enhanced diffusive transport of the remaining lacosamide in the microcapsules occurs. Therefore, the morphology and dimension of the PLGA microcapsules have a significant influence on the release of lacosamide. Most of the reported mathematical modelling studies for biodegradable microcapsules drug delivery systems are based on a single, zero-order process; or a process that is governed only by diffusional mass transfer or chemical reactions [41]. In order to more accurately predict drug release kinetics for biodegradable microcapsules, mathematical models that take account of the effects of composition and geometry (size and shape) on the drug release are required.

In this study, it is assumed that drug release from those microcapsules is predominantly diffusion-controlled within the period of study. This assumption is based on our and others' *in vitro* studies that showed minimal polymer degradation of the microcapsules within a period of up to three weeks [20, 24, 41]. According to Fick's second law of diffusion, the fraction of the released drug from the microcapsules (M_t/M_∞) at any time (t) can be expressed as equation (1). In this model, a well-mixed external aqueous phase with a negligibly small drug concentration is assumed. And the drug is assumed to be homogeneously distributed throughout the polymer matrix with an initial drug concentration higher than the solubility of the drug in the polymer. For the microfibrils geometry, the drug diffusional release is considered from a cylindrical matrix. The eigenvalues λ_n , the roots of eigenfunctions are $\lambda_n=2.41, 5.52, 8.65, 14.93$, and so on [25]. The mathematical model can be expressed as:

$$\frac{M_t}{M_\infty} = 1 - \sum_{n=0}^{\infty} \left(\frac{4}{(\lambda_n)^2}\right) e^{-\frac{4\lambda_n^2 D_e t}{d^2}} \quad (3.2)$$

For the flattened microspheres and microspheres geometry, the diffusional drug release is considered from a spherical matrix. The eigenvalues λ_n , the roots of eigenfunctions are $n\pi$.

The equation (3.1) can be expressed as:

$$\frac{M_t}{M_\infty} = 1 - \sum_{n=0}^{\infty} \left(\frac{6}{(n\pi)^2}\right) e^{-\frac{4\lambda_n^2 D_e t}{d^2}} \quad (3.3)$$

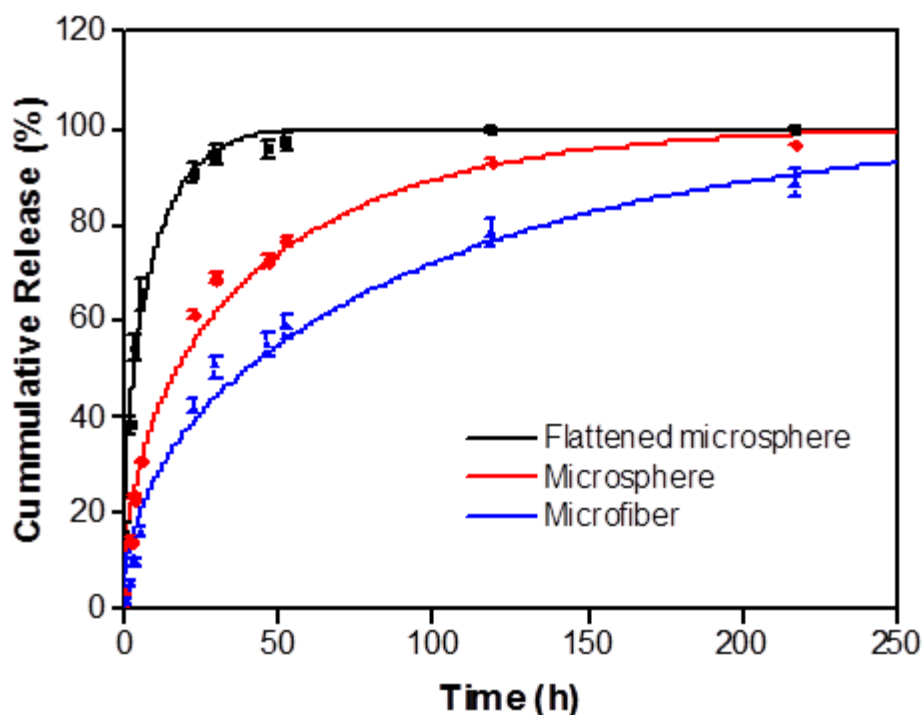


Figure 3.11 Comparison of the mathematical modelling results (linear) with experimental drug release profiles (dots).

Figure 3.11 shows the least-squares fitting results by applying these mathematical models. The initial drug loading is determined by encapsulation efficiency testing results of HPLC. Our results demonstrated that drug release profiles using the above models could be predicted with a very good agreement with the experimental drug release data. The computed effective diffusivities (D_e) are 3.29×10^{-12} cm²/min for flattened microspheres, 1.89×10^{-12} cm²/min for microspheres, and 1.23×10^{-13} cm²/min for microfibres, well within the range of values

previously reported for hydrophobic drugs in PLGA microcapsules [23]. Compared with the flattened microspheres and microspheres, the microfibrils possess the lowest effective diffusivities (D_e) during this time-dependent diffusion process.

3.3.4 Human neural stem cell viability and differentiation

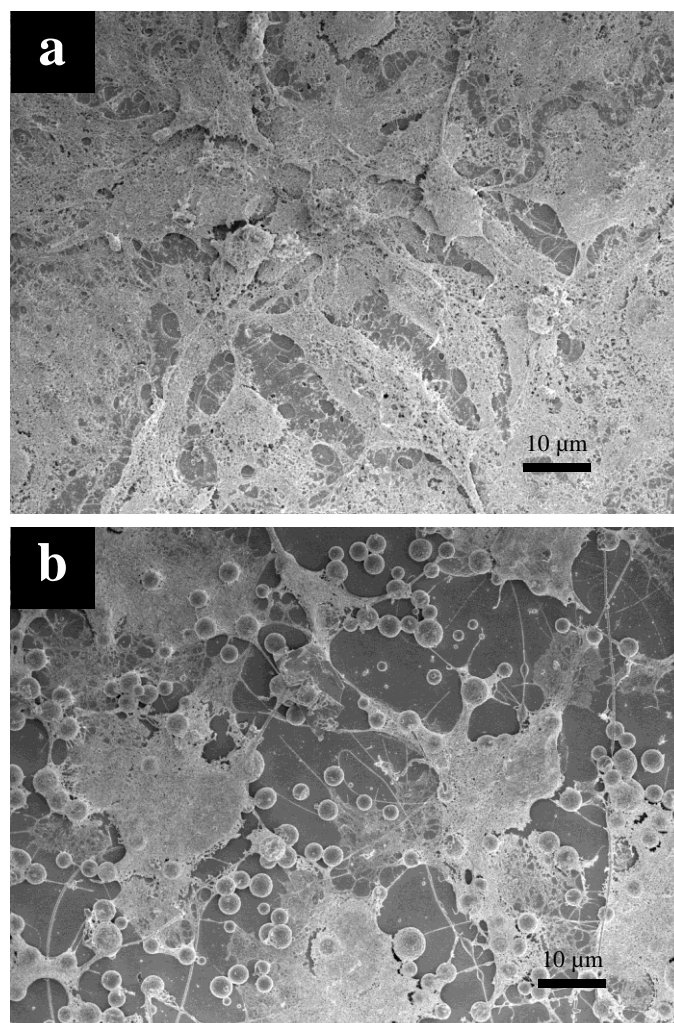


Figure 3.12 Human NSC viability and on a) microfibrils and b) microspheres. NSCs were cultured with fibres and spheres following successful attachment.

Demonstration of neuro-cytopatibility of these electrojetted spheres and fibres was carried out by using clinically relevant human brain tissue derived NSCs and their differentiation to neurons and supporting neuroglia.

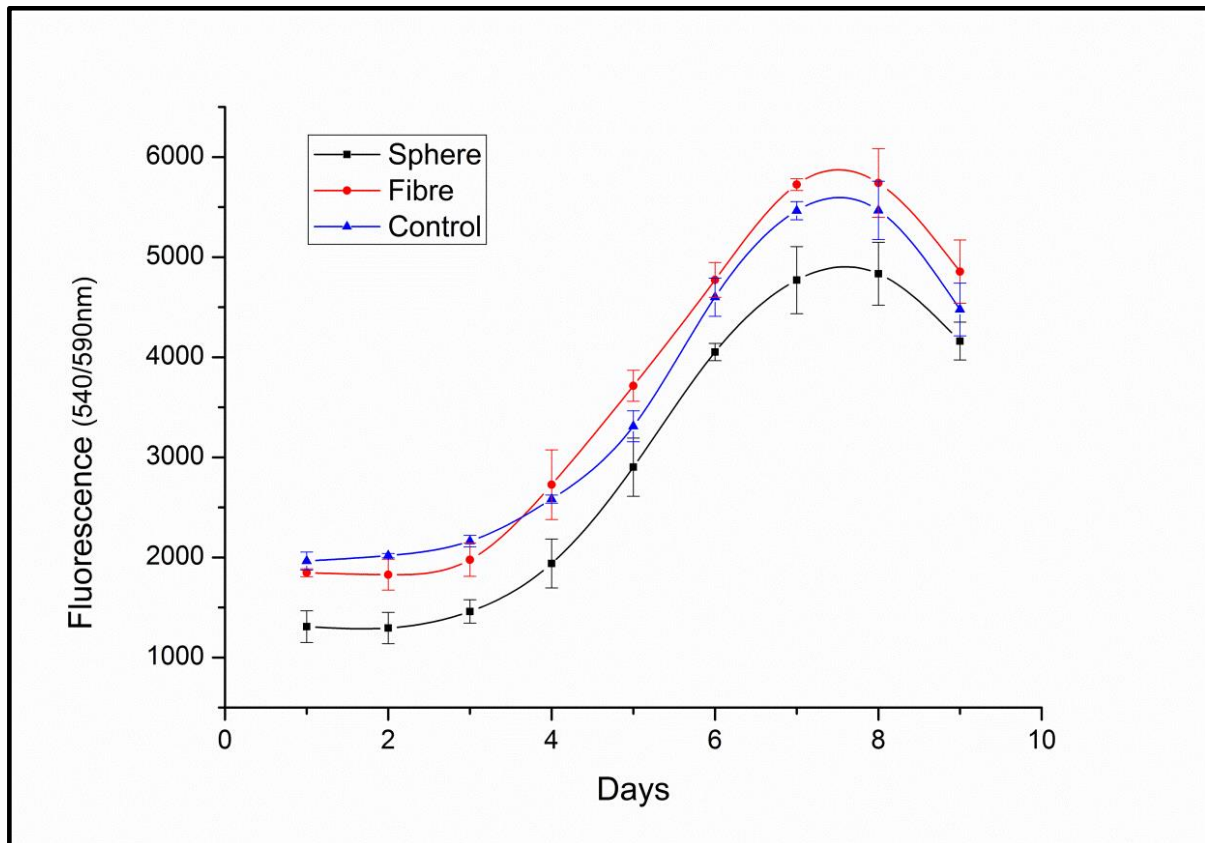


Figure 3.13 Human NSC viability and proliferation kinetics during culture with microfibres and microspheres.

Neurocompatibility was supported by cell attachment (**Figure 3.12**) and viability (**Figure 3.13**) during extended cell culture with fibres and spheres. NSC viability studies indicated cell proliferation on all substrates (**Figure 3.14**), similar to the control (**Figure 3.15**).

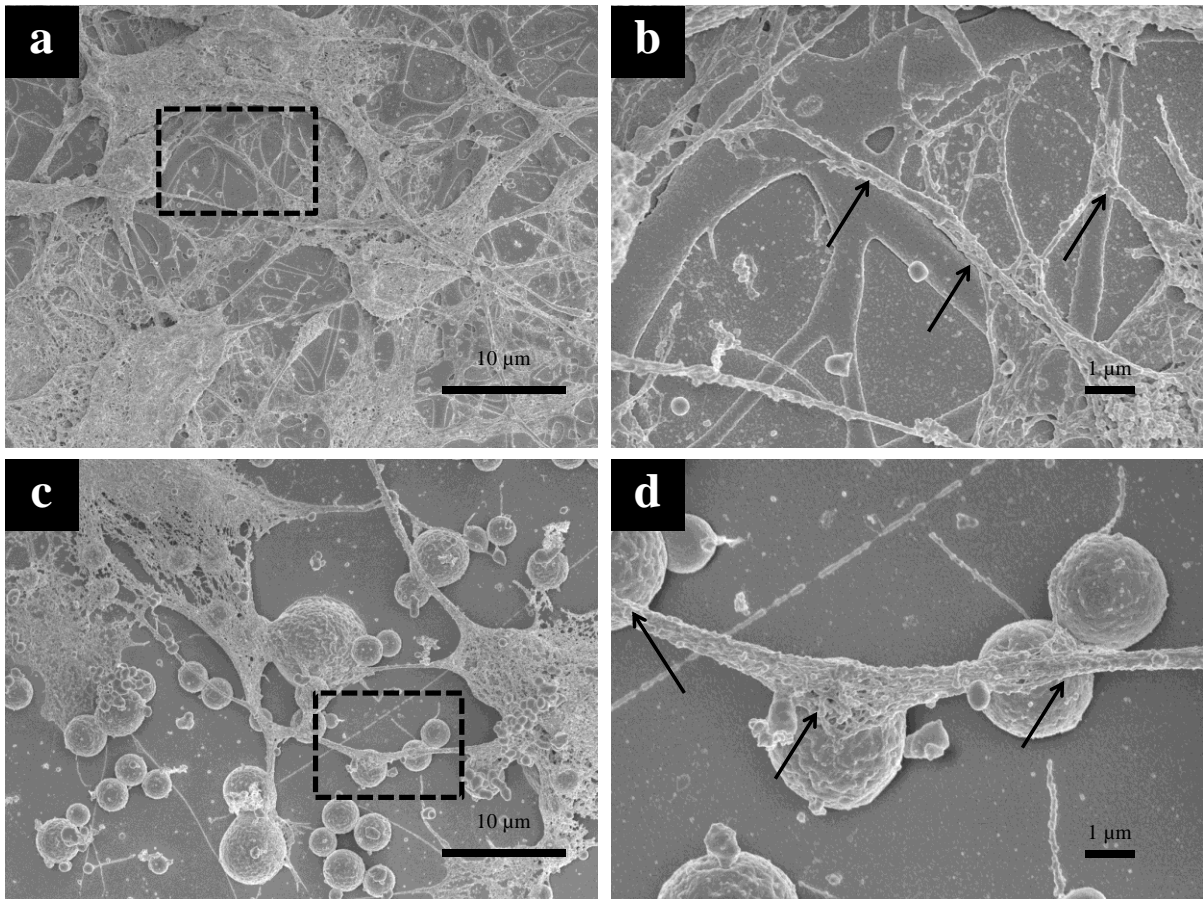


Figure 3.14 Morphology of differentiated human NSCs during culture with microfibres and microspheres.

In all cases, quantitative measurement of cell viability marker PrestoBlue® supported normal growth kinetics, with cell proliferation increasing exponentially up to 8 days culture. As expected, cell viability decreased following peak cell growth, reflecting the limits of culture due to media exhaustion [42].

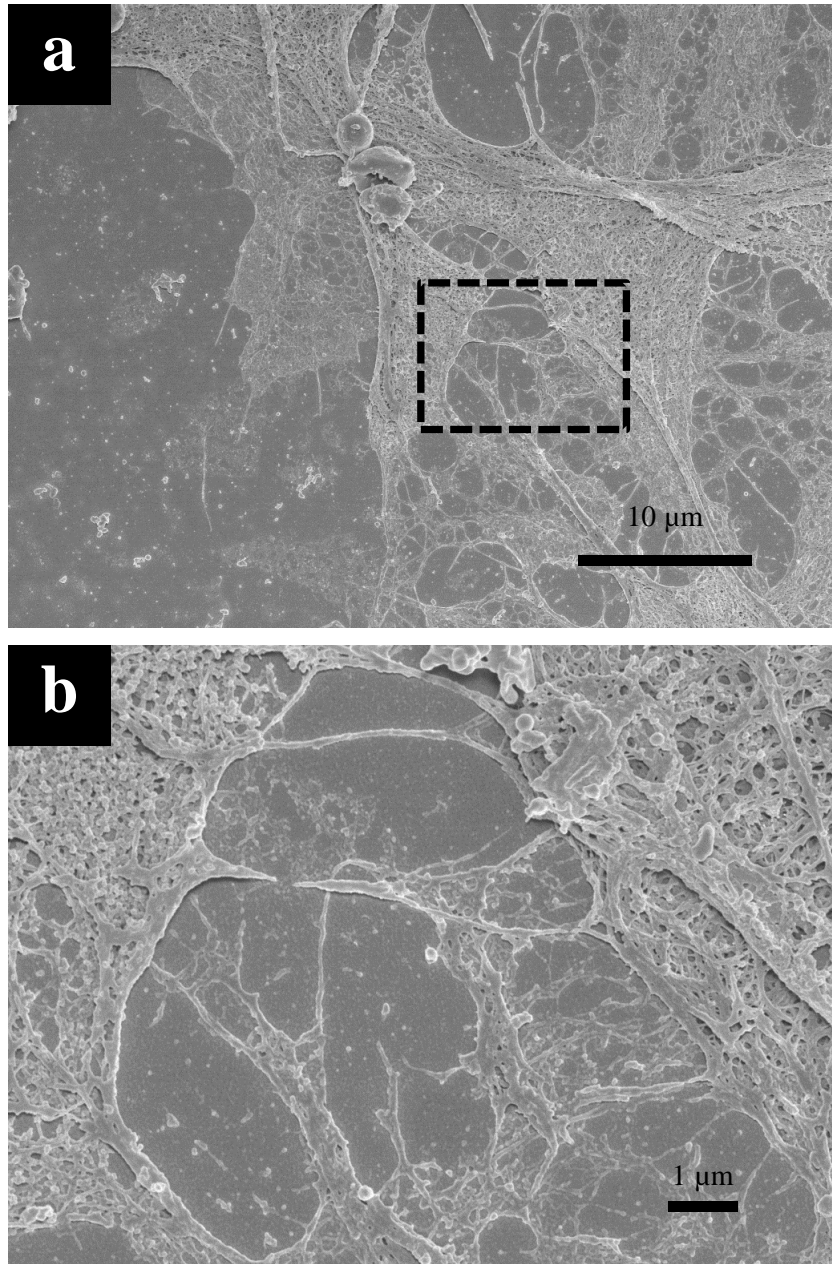


Figure 3.15 Morphology of differentiated human NSCs during conventional plate-based culture, used as the control for comparison.

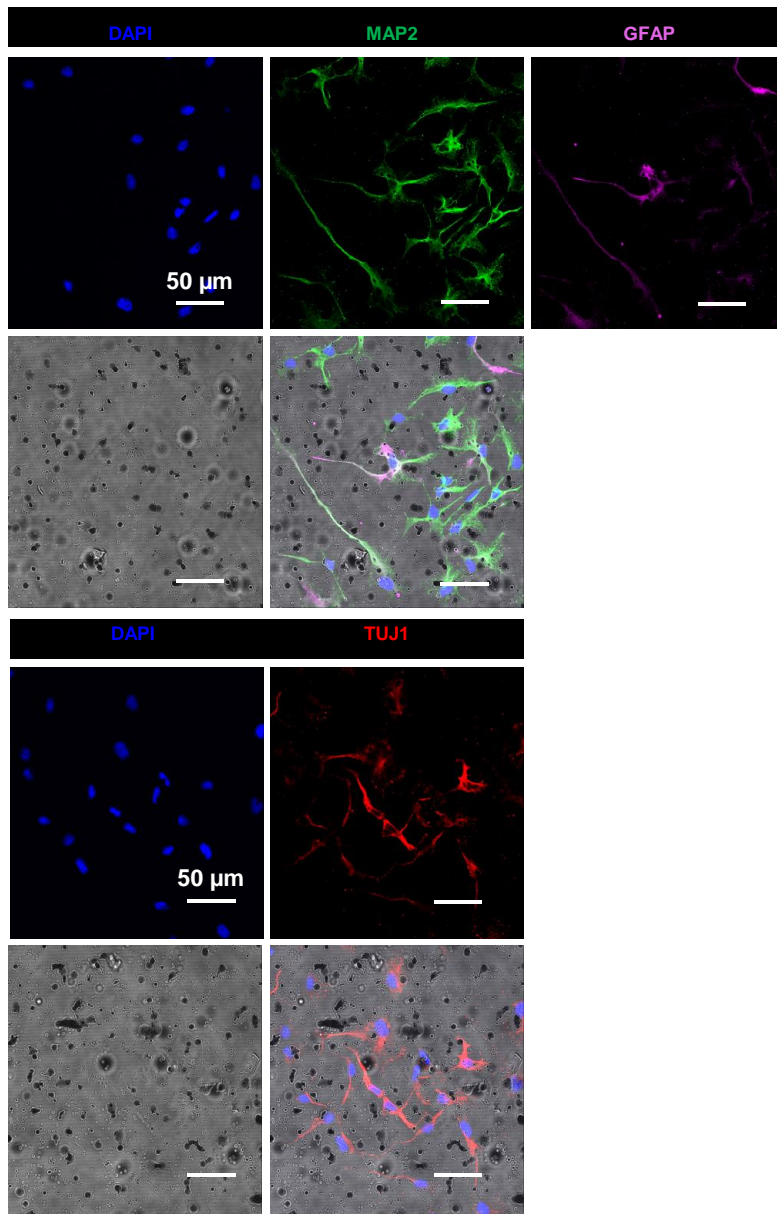


Figure 3.16 Immunophenotyping of differentiated NSCs. DAPI (blue) colocalised with neuronal markers MAP2 (green), and TUJ1 (red), and glial marker GFAP (purple) expressed by differentiated NSCs cultured with microspheres. scale bar: 50 μm .

Importantly, differentiation of NSCs resulted in neuronal cells cultured for up to 10 days with densely packed neurites adhering to the fibres and spheres. Immunophenotyping confirmed

successful differentiation and co-culture of spheres and fibres with MAP2 and TUJ1 expressing neurons (**Figure 3.16**) and GFAP expressing glial cells (**Figure 3.17**).

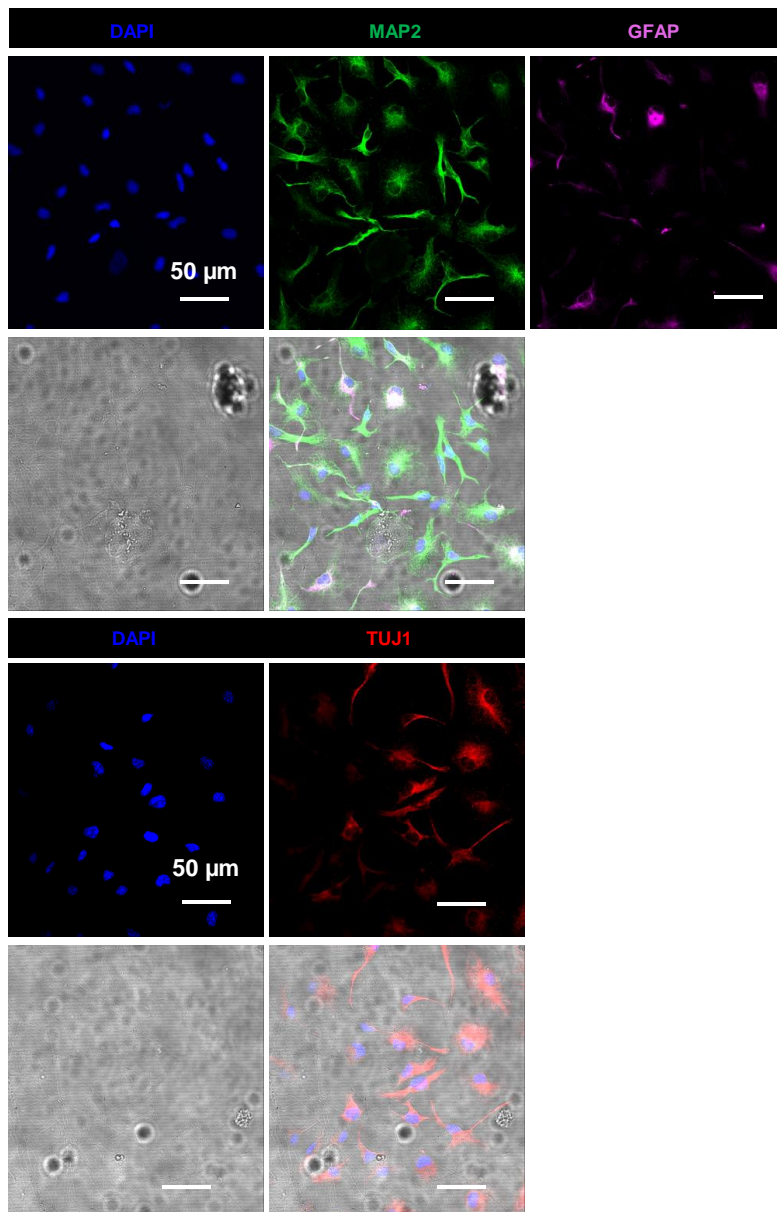


Figure 3.17 Immunophenotyping of differentiated NSCs. DAPI (blue) colocalised with neuronal markers MAP2 (green) and TUJ1 (red), and glial marker GFAP (purple) expressed by differentiated NSCs cultured with microfibres. Scale bar: 50 μm.

3.4 Conclusion

In conclusion, microstructured drug delivery systems have been fabricated by using a simple electrojetting (electrospraying and electrospinning) technology for local delivery of AEDs. These microcapsules have demonstrated a number of advantages, including controllable and uniform morphology and narrow size distribution, high efficiency drug encapsulation, sustained and predictable drug release characteristics, and neuro-cytocompatibility as evidenced by human NSC support and differentiation. Our findings broadly support the utility and efficacy of the local drug delivery systems for treating human brain disorders such as epilepsy. In addition, the method presented here could be applicable to the fabrication of other microstructured delivery systems using different drugs and/or polymers.

3.5 References

- [1] Hay M, Thomas DW, Craighead JL, Economides C, Rosenthal J. Clinical development success rates for investigational drugs. *Nat Biotech* 2014;32:40-51.
- [2] Abbott NJ, Ronnback L, Hansson E. Astrocyte-endothelial interactions at the blood-brain barrier. *Nat Rev Neurosci* 2006;7:41-53.
- [3] Cecchelli R, Berezowski V, Lundquist S, Culot M, Renftel M, Dehouck M-P, Fenart L. Modelling of the blood-brain barrier in drug discovery and development. *Nat Rev Drug Discov* 2007;6:650-61.
- [4] Loscher W, Potschka H. Drug resistance in brain diseases and the role of drug efflux transporters. *Nat Rev Neurosci* 2005;6:591-602.
- [5] Abbott NJ, Khan EU, Rollinson CM, Reichel A, Janigro D, Dombrowski SM, Dobbie MS, Begley DJ. Drug resistance in epilepsy: the role of the blood-brain barrier. *Novartis Foundation Symposium: Chichester; New York; John Wiley; 1999; 2002. p. 38-53.*
- [6] Engelhardt B, Sorokin L. The blood–brain and the blood–cerebrospinal fluid barriers: function and dysfunction. *Seminars in Immunopathology* 2009;31:497-511.
- [7] Cook MJ, O'Brien TJ, Berkovic SF, Murphy M, Morokoff A, Fabinyi G, D'Souza W, Yerra R, Archer J, Litewka L, Hosking S, Lightfoot P, Ruedebusch V, Sheffield WD, Snyder D, Leyde K, Himes D. Prediction of seizure likelihood with a long-term, implanted seizure advisory system in patients with drug-resistant epilepsy: a first-in-man study. *The Lancet Neurology* 2013;12:563-71.
- [8] Tiwari SB, Amiji MM. A review of nanocarrier-based CNS delivery systems. *Current Drug Delivery* 2006;3:219-32.
- [9] Miura Y, Takenaka T, Toh K, Wu S, Nishihara H, Kano MR, Ino Y, Nomoto T, Matsumoto Y, Koyama H, Cabral H, Nishiyama N, Kataoka K. Cyclic RGD-linked

polymeric micelles for targeted delivery of platinum anticancer drugs to glioblastoma through the blood–brain tumor barrier. *ACS Nano* 2013;7:8583-92.

[10] Krol S. Challenges in drug delivery to the brain: Nature is against us. *Journal of Controlled Release* 2012;164:145-55.

[11] Chen Y, Liu L. Modern methods for delivery of drugs across the blood–brain barrier. *Advanced drug delivery reviews* 2012;64:640-65.

[12] Wohlfart S, Gelperina S, Kreuter J. Transport of drugs across the blood–brain barrier by nanoparticles. *Journal of Controlled Release* 2012;161:264-73.

[13] Fornaguera C, Dols-Perez A, Calderó G, García-Celma MJ, Camarasa J, Solans C. PLGA nanoparticles prepared by nano-emulsion templating using low-energy methods as efficient nanocarriers for drug delivery across the blood–brain barrier. *Journal of Controlled Release* 2015;211:134-43.

[14] Mo J, He L, Ma B, Chen T. Tailoring particle size of mesoporous silica nanosystem to antagonize glioblastoma and overcome blood–brain barrier. *ACS Applied Materials & Interfaces* 2016;8:6811-25.

[15] Mura S, Nicolas J, Couvreur P. Stimuli-responsive nanocarriers for drug delivery. *Nat Mater* 2013;12:991-1003.

[16] Bauquier SH, Jiang JL, Yue Z, Lai A, Chen Y, Moulton SE, McLean KJ, Vogrin S, Halliday AJ, Wallace G. Antiepileptic effects of lacosamide loaded polymers implanted subdurally in GAERS. *International Journal of Polymer Science* 2016; 6594960, 10 pages.

[17] Hironaka K, Yamazaki Y, Hirai Y, Yamamoto M, Miyake N, Miyake K, Okada T, Morita A, Shimada T. Enzyme replacement in the CSF to treat metachromatic leukodystrophy in mouse model using single intracerebroventricular injection of self-complementary AAV1 vector. *Scientific Reports* 2015;5:13104.

- [18] Halliday AJ, Moulton SE, Wallace GG, Cook MJ. Novel methods of antiepileptic drug delivery — polymer-based implants. *Advanced Drug Delivery Reviews* 2012;64:953-64.
- [19] Pritchard EM, Szybala C, Boison D, Kaplan DL. Silk fibroin encapsulated powder reservoirs for sustained release of adenosine. *Journal of Controlled Release* 2010;144:159-67.
- [20] Chen Y, Yue Z, Moulton SE, Hayes P, Cook MJ, Wallace GG. A simple and versatile method for microencapsulation of anti-epileptic drugs for focal therapy of epilepsy. *Journal of Materials Chemistry B* 2015;3:7255-61.
- [21] Williamson A, Rivnay J, Kergoat L, Jonsson A, Inal S, Uguz I, Ferro M, Ivanov A, Sjöström TA, Simon DT, Berggren M, Malliaras GG, Bernard C. Controlling epileptiform activity with organic electronic ion pumps. *Advanced Materials* 2015;27:3138-44.
- [22] Salonen J, Laitinen L, Kaukonen AM, Tuura J, Björkqvist M, Heikkilä T, Vähä-Heikkilä K, Hirvonen J, Lehto VP. Mesoporous silicon microparticles for oral drug delivery: Loading and release of five model drugs. *J Control Release* 2005;108:362-74.
- [23] Arifin DY, Lee LY, Wang C-H. Mathematical modeling and simulation of drug release from microspheres: Implications to drug delivery systems. *Advanced Drug Delivery Reviews* 2006;58:1274-325.
- [24] Fattahi P, Borhan A, Abidian MR. Microencapsulation of chemotherapeutics into monodisperse and tunable biodegradable polymers via electrified liquid jets: control of size, shape, and drug release. *Advanced Materials* 2013;25:4555-60.
- [25] Watson GN. *A treatise on the theory of Bessel functions*: Cambridge university press; 1995.
- [26] Xie J, MacEwan MR, Schwartz AG, Xia Y. Electrospun nanofibers for neural tissue engineering. *Nanoscale* 2010;2:35-44.
- [27] Dzenis Y. Spinning continuous fibers for nanotechnology. *Science* 2004;304:1917-9.

- [28] Chen Y, Han D, Ouyang W, Chen S, Hou H, Zhao Y, Fong H. Fabrication and evaluation of polyamide 6 composites with electrospun polyimide nanofibers as skeletal framework. *Composites Part B: Engineering* 2012;43:2382-8.
- [29] Tian Y, Wu G, Tian X, Tao X, Chen W. Novel erythrocyte-like graphene microspheres with high quality and mass production capability via electrospray assisted self-assembly. *Scientific Reports* 2013;3:3327.
- [30] Shenoy SL, Bates WD, Frisch HL, Wnek GE. Role of chain entanglements on fiber formation during electrospinning of polymer solutions: good solvent, non-specific polymer–polymer interaction limit. *Polymer* 2005;46:3372-84.
- [31] Padmakumar S, Joseph J, Neppalli MH, Mathew SE, Nair SV, Shankarappa SA, Menon D. Electrospun polymeric core–sheath yarns as drug eluting surgical sutures. *ACS Applied Materials & Interfaces* 2016;8:6925-34.
- [32] Bock N, Dargaville TR, Woodruff MA. Electro spraying of polymers with therapeutic molecules: State of the art. *Progress in Polymer Science* 2012;37:1510-51.
- [33] Zheng J, Zhang H, Zhao Z, Han CC. Construction of hierarchical structures by electrospinning or electro spraying. *Polymer* 2012;53:546-54.
- [34] Almería B, Deng W, Fahmy TM, Gomez A. Controlling the morphology of electrospray-generated PLGA microparticles for drug delivery. *Journal of Colloid and Interface Science* 2010;343:125-33.
- [35] Hartman RPA, Brunner DJ, Camelot DMA, Marijnissen JCM, Scarlett B. Jet break-up in electrohydrodynamic atomization in the core-jet mode. *Journal of Aerosol Science* 2000;31:65-95.
- [36] Freiberg S, Zhu XX. Polymer microspheres for controlled drug release. *Int J Pharmaceut* 2004;282:1-18.

- [37] Chung T-W, Huang Y-Y, Liu Y-Z. Effects of the rate of solvent evaporation on the characteristics of drug loaded PLLA and PDLLA microspheres. *Int J Pharmaceut* 2001;212:161-9.
- [38] Louey M, Van Oort M, Hickey A. Aerosol dispersion of respirable particles in narrow size distributions produced by jet-milling and spray-drying techniques. *Pharmaceutical Research* 2004;21:1200-6.
- [39] Wang C, Ye W, Zheng Y, Liu X, Tong Z. Fabrication of drug-loaded biodegradable microcapsules for controlled release by combination of solvent evaporation and layer-by-layer self-assembly. *Int J Pharmaceut* 2007;338:165-73.
- [40] Fu K, Pack D, Klibanov A, Langer R. Visual evidence of acidic environment within degrading poly(lactic-co-glycolic acid) (PLGA) microspheres. *Pharm Res* 2000;17:100-6.
- [41] Faisant N, Siepmann J, Benoit JP. PLGA-based microparticles: elucidation of mechanisms and a new, simple mathematical model quantifying drug release. *European Journal of Pharmaceutical Sciences* 2002;15:355-66.
- [42] Gu Q, Tomaskovic-Crook E, Lozano R, Chen Y, Kapsa RM, Zhou Q, Wallace GG, Crook JM. Functional 3D neural mini-tissues from printed gel-based bioink and human neural stem cells. *Advanced Healthcare Materials* 2016; 5: 1429-1438.

**CHAPTER 4: CORE-SHELL
MICROCAPSULATION OF ANTI-
EPILEPTIC DRUGS**

4.1 Introduction

Epilepsy is a long-term neurological disorder, affecting more than 60 million people worldwide. It is characterized by recurrent and unpredictable seizures, which can cause loss of consciousness, falls and injury, psychosocial disability, and even mortality. Medication provided via oral administration is the first approach to epilepsy treatment, but controls only up to 70% of the cases, whilst the rest of the patients remain incompletely responsive to medication [1, 2]. The reasons for this are not yet fully understood, but there is a significant body of evidence pointing to the blood-brain barrier (BBB) [3]. The BBB protects the brain from harmful blood-borne substances and microorganisms by separating the brain parenchyma from the circulating blood. Such self-protection also poses an obstacle to drug delivery to the brain. Nearly 100% of high molecular weight drugs and >98% of low molecular weight drugs are excluded from the brain [4-6]. For instance, a typical dosage of an antiepilepsy drug (AED), such as lacosamide (used in this study), is 400 - 500 mg per day [7, 8] by oral administration. However, the actual amount of lacosamide arriving at the sites of seizures is very limited due to the limited ability of the drug to cross the BBB [3]. Moreover, this high systemic dosage causes serious whole body side-effects, such as rashes, nausea, and weight changes.

For patients whose seizures cannot be controlled by medications, surgery represents an alternative option, which can be provided only to appropriately selected patients, where the seizure origin in the brain can be localized. In addition, a comprehensive pre-surgical assessment must be conducted in order to ensure the benefits of the operation. Following surgical therapy, the patients still need to take AEDs for a long time to prevent epilepsy relapse [9, 10].

To improve epilepsy control, local drug delivery through microinjection or implantation in the brain to bypass the BBB may offer an innovative approach to improve the efficacy of the medication. This approach can significantly reduce the dosage of AEDs, while concurrently minimising the side effects associated with systemic administration of AEDs [11, 12]. In addition, compared to surgical resection, direct injection or implantation would significantly reduce potential brain damage [13].

An ideal local drug delivery system should be biocompatible, biodegradable and exhibit an optimal drug release profile pertaining to the targeted application. It should also be amenable to fabrication and large scale production. Poly(lactic-*co*-glycolic acid) (PLGA) has been intensively studied for local drug delivery [14-16]. In particular, it has been explored in treating central nervous system disorders, such as Alzheimer's [17, 18] and Parkinson's [19, 20] diseases, as well as in treating brain injury [21], demonstrating excellent brain biocompatibility. Lacosamide was selected as a model drug based on its efficacy and therapeutic index [22]. In terms of material fabrication, electrojetting, such as electrospinning and electrospraying, has attracted tremendous interest in recent years [23-28]. It is a low-cost and versatile technique for uniform fabrication of polymer structures ranging from nanoscale to microscale [29-31]. However, only limited studies have been undertaken on the electrojetted systems in terms of morphology, drug encapsulation efficiency and drug release characteristics [31, 32]. Moreover, to the best of our knowledge, no study has yet to be reported on core-shell structured electrojetted systems.

This chapter aims to apply a novel electrojetting technique for the fabrication of core-shell microspheres and microfibers, where AED-laden polymer cores are surrounded by drug-free

polymer shells that act as a barrier in order to regulate drug release characteristics. A variety of core-shell PLGA/lacosamide microcapsules, including microflakes, flattened microspheres, microspheres, microsphere-fibres, beaded microfibrils, and microfibrils, have been developed with narrow size distribution and uniform morphology. These systems demonstrated high efficiency in drug encapsulation and sustained drug release characteristics, which makes them promising candidates as injectable microspheres and polymer implants for local drug delivery for epilepsy control.

4.2 Materials and methods

4.2.1 Materials

Poly(D,L-lactic-*co*-glycolic acid) (PLGA) ($M_w \sim 60,000$ Da) with various molar ratio of lactide to glycolide, including PLGA 75/25 (lactide/glycolide = 75/25) and PLGA 85/15 (lactide/glycolide = 85/15), were purchased from Purac, Singapore, and used as received. Lacosamide, an anti-epilepsy drug, was provided by UCB Pharma Pty Ltd. All the other chemicals and reagents were purchased from Sigma-Aldrich.

4.2.2 Electrojetting (electrospinning and electrospraying)

A range of solutions of PLGA 75/25 and lacosamide were prepared as the core solutions for electrojetting. In these solutions, the ratio of polymer/drug (w/w) was kept constant at 10/1, while the polymer concentration was varied from 0.75 to 15 wt%. After encapsulation efficiency testing, drug loadings of 9.06 %, 9.11 %, 9.40 %, 9.53 %, 9.49 %, and 9.92 % were achieved. A range of drug-free PLGA 85/15 solutions were prepared as the shell solutions for electrojetting, with the polymer concentration ranging from 0.5 to 10 wt%.

Electrojetting (electrospinning and electrospraying, respectively) was conducted at room temperature using a NANON-01A electrospinning system (MECC Co. Ltd, Japan). A coaxial spinneret with 0.2 mm core and 0.8 mm sheath nozzles were connected to the core and shell solutions. The distance from the spinneret tip to the collector was maintained at 12 cm, and the applied voltage for electrospinning and electrospraying was 21 kV and 10 kV, respectively. The feed rate was 0.1 mL/h for the core solutions and 0.4 mL/h for the shell solutions. Aluminium foil was used to collect the fabricated core-shell microcapsules, and the samples were further dried in a vacuum oven at room temperature for 48 hours to remove any residual organic solvent.

4.2.3 Morphological and dimensional statistical analysis

The morphologies of the as-prepared microcapsules were examined using a Field Emission Scanning Electron Microscope (FESEM, JEOL JSM-7500FA). The samples were sputter-coated with 20 nm gold to avoid charge accumulation. The dimensional statistical analysis was conducted by analysis of the SEM micrographs using the imaging software, Leica Application Suite. All data were expressed as mean \pm standard deviation (SD).

4.2.4 Determination of drug encapsulation efficiency

An extraction method was used to determine the drug encapsulation efficiencies of the as-fabricated core-shell microcapsules. Briefly, each sample (1 cm \times 1 cm) was placed into 1 mL methanol for 12 hours, after which the methanol was removed and replenished with 1 mL of fresh methanol. This extraction procedure was repeated four times with each methanol sample allowed to evaporate to leave residual drug behind. And the methanol extracts were quantified by HPLC to determine the respective drug encapsulation efficiency.

The details of the HPLC testing method were refer to previous work [33]. The amounts of released drug were calculated according to a pre-established calibration curve that was obtained by plotting the peak areas against respective concentrations of a range of standard lacosamide solutions prepared in aCSF.

4.2.5 *In vitro* drug release study

In vitro drug release was conducted in artificial cerebrospinal fluid (aCSF). Each sample (1 cm × 1 cm) was incubated in 1 ml of aCSF at 37 °C in a shaking water bath. At appropriate time intervals, the release medium was withdrawn and replaced with 1mL of fresh aCSF. The released samples were stored at -20 °C prior to the HPLC analysis for quantification of the amounts of the lacosamide released. The results were shown as cumulative release vs time. A line was used to connect the sample dots of the appropriate time intervals. The results were quite different from the modelled data presented in Chapter 3.

4.3 Results and Discussion

4.3.1 Preparation of various forms of electrojetted core-shell microcapsules

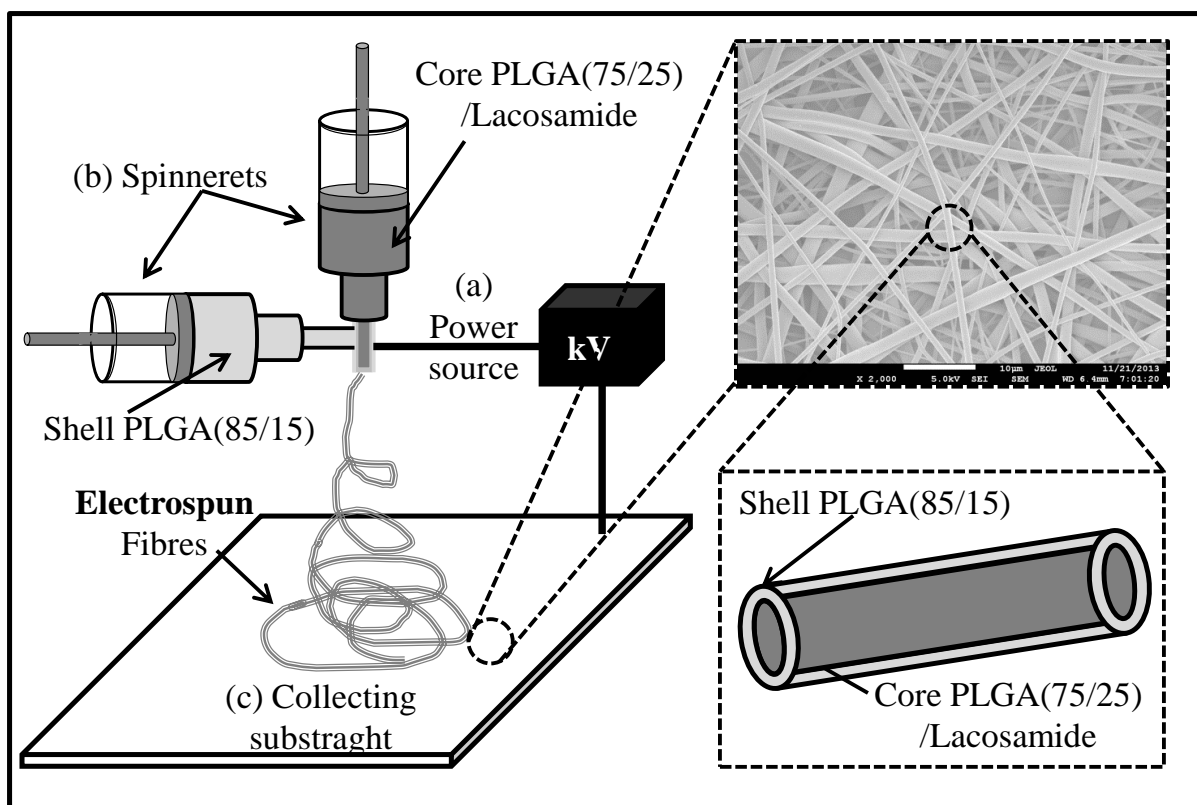


Figure 4.1 Schematic illustration of the electrojetting setup, electrospinning of core-shell microfibres.

Electrojetting, including electrospinning and electrospraying, represents a simple and versatile method for producing monodisperse polymeric spheres and fibres at the nano- and micro-scale [23, 34]. Electrojetting is governed by the interactions between the electrostatic repulsion induced by an applied electric field and surface tension of a liquid droplet. When the electrostatic repulsion surpasses the surface tension to a critical point, liquid ejection will occur at the surface of the droplet. The liquid jet will undergo a whipping process, which leads to the formation of either fibres (electrospinning, as shown in **Figure 4.1**), or spheres (electrospraying, as shown in **Figure 4.2**) at the nano- or micro-scale. Therefore, the final electrojetted structure is determined by the electric force applied and the properties of polymer solutions. The polymer solution properties are governed by the molecular weight and concentration of the polymer, as well as the solvent properties.

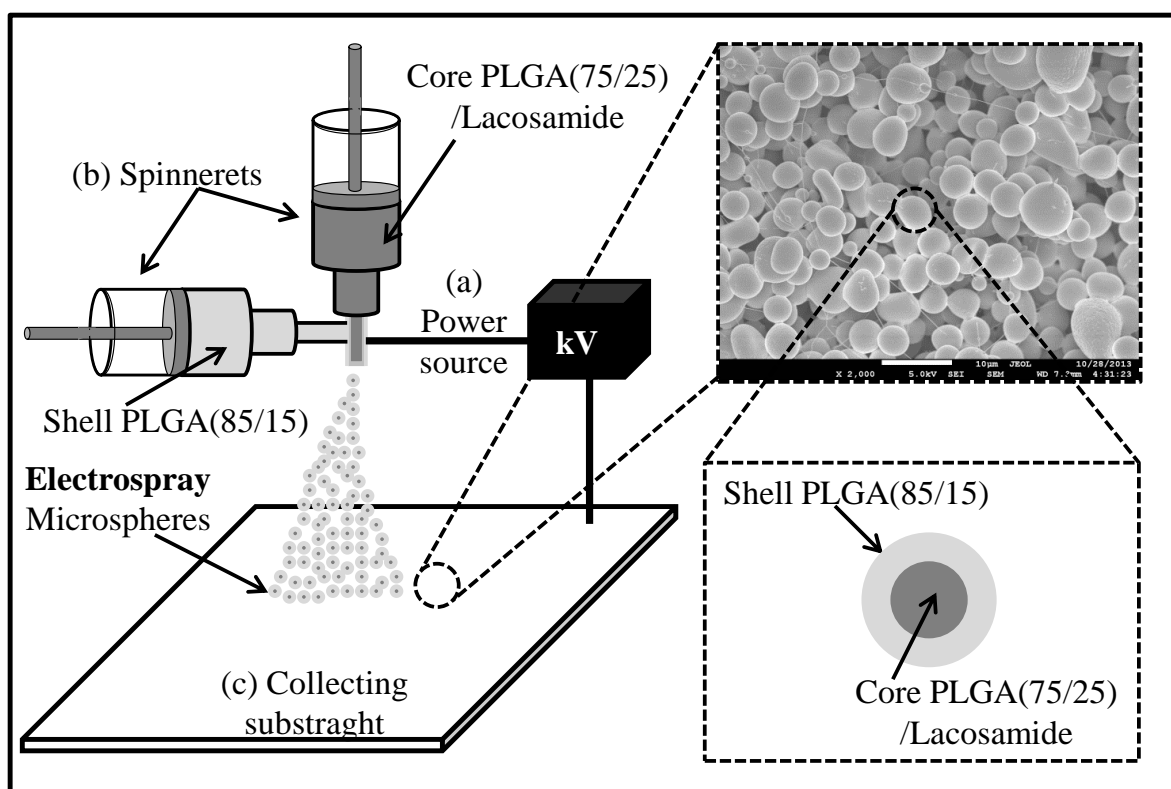


Figure 4.2 Schematic illustration of the electrojetting setup, electrospinning of core-shell microspheres.

In this study, PLGA 75/25 and lacosamide were used as the core structural materials, whilst PLGA 85/15, a more hydrophobic copolymer, was used as the shell material [35]. Chloroform was used as the solvent, with a low boiling point of 61.2 °C. By adjusting the applied voltage and screening of the concentrations of the core and shell solutions, microcapsules with various shapes, including microflakes, flattened microspheres, microspheres, microspheres-fibres, beaded microfibres, and microfibres, were successfully fabricated.

Table 4.1 Microcapsules with various structures and their respective fabrication conditions.

Sample Code	Core PLGA (75/25) concentration (wt %)	Shell PLGA (85/15) concentration (wt %)	Applied Voltage (kV)	Type of microcapsule formed
S0w	0.75	0.5	10	Microflakes
S2w	3	2	10	Flattened microspheres
S4w	6	4	10	Microspheres
S5w	7.5	5	10	Microspheres-fibres
S8w	12	8	21	Beaded microfibres
S10w	15	10	21	Microfibres

These microstructures, together with their respective fabrication conditions, including the concentrations of the core and shell solutions and voltage, are summarised in **Table 4.1**. For electrospaying of microflakes, flattened microspheres, microspheres or microspheres-fibres, a 10 kV voltage was used, whereas for electrospinning of beaded microfibres or microfibres, a 21 kV voltage was used.

4.3.2 Morphological and dimensional statistical analysis

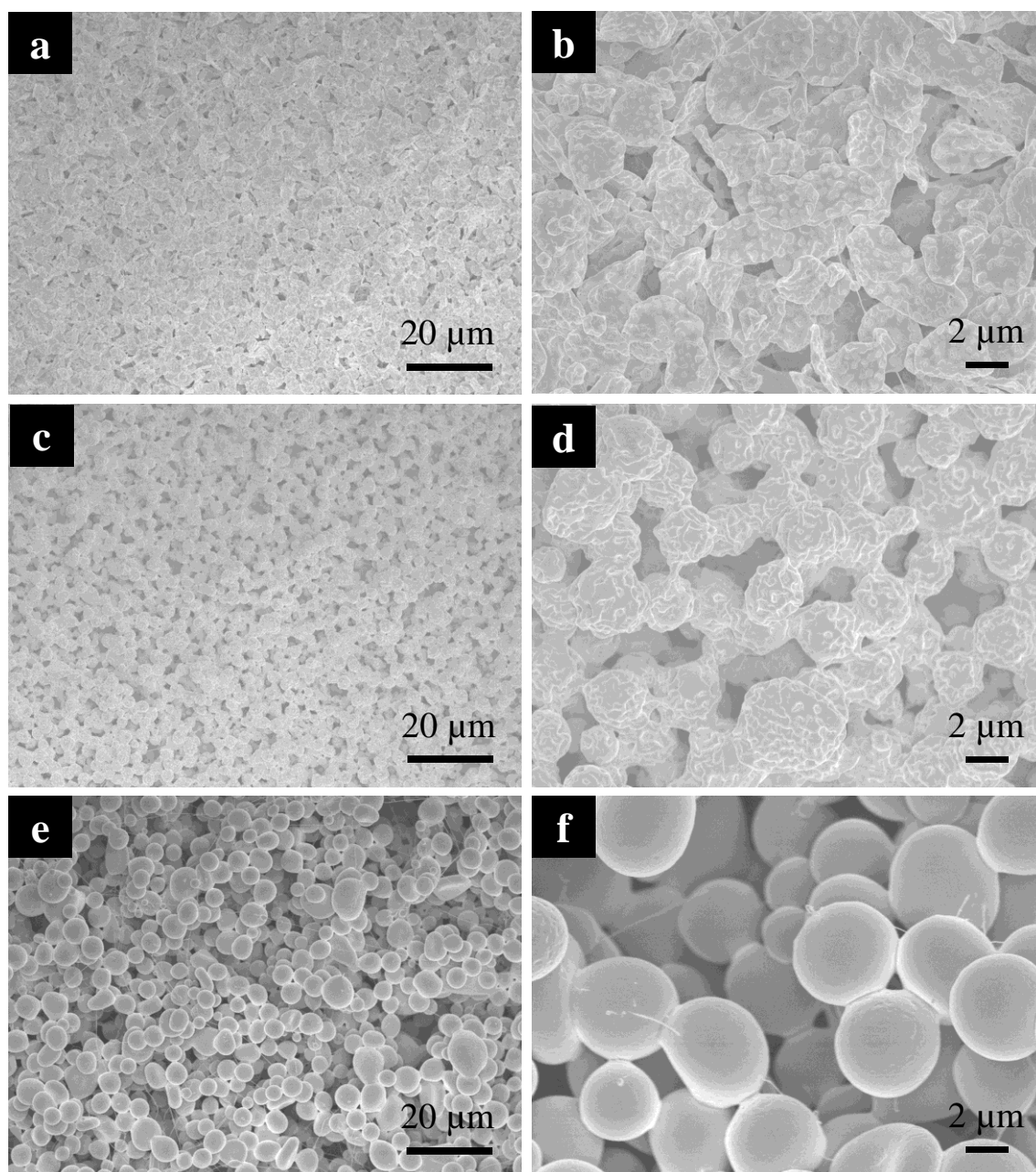


Figure 4.3 Scanning Electron Microscope (SEM) images of various core-shell PLGA microcapsules; a, b) Microflakes, c, d) Flattened microspheres, e, f) Microspheres.

During the electrojetting process for fabrication of the microflakes or flattened microspheres, both the polymer concentrations in the core and shell solutions are very low (**Table 4.1**). This results in the rapid collapse of PLGA microcapsules during solvent evaporation and polymer solidification, to produce the microflakes (**Figure 4.3 a,b**) and flattened microspheres

(**Figure 4.3 c,d**) with a rough, pitted and porous surface topography [36]. At higher PLGA concentrations, such as 6 wt% of the core solution and 4 wt% of the shell solution, microspheres (**Figure 4.3 e,f**) are produced, exhibiting a much smoother surface.

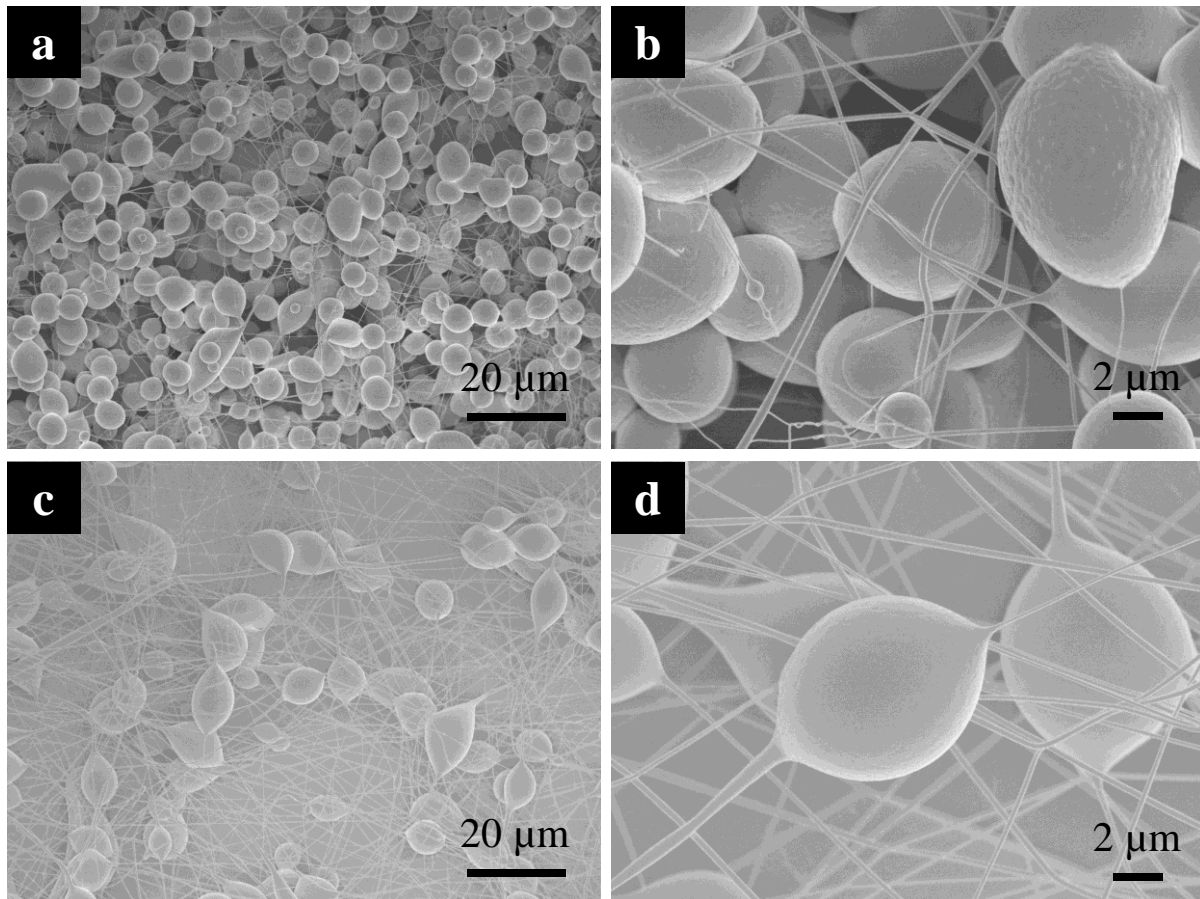


Figure 4.4 Scanning Electron Microscope images of various core-shell PLGA a, b) Microspheres-fibres, c, d) Beaded microfibres.

Further increasing the PLGA concentrations to 7.5 wt% for the core and 5 wt% for the shell results in the concurrent formation of microspheres and microfibres (**Figure 4.4**), where the diameters of fibres are much thinner than those of the microspheres. The portion of the microfibres in the microcapsules increases with increasing polymer concentrations.

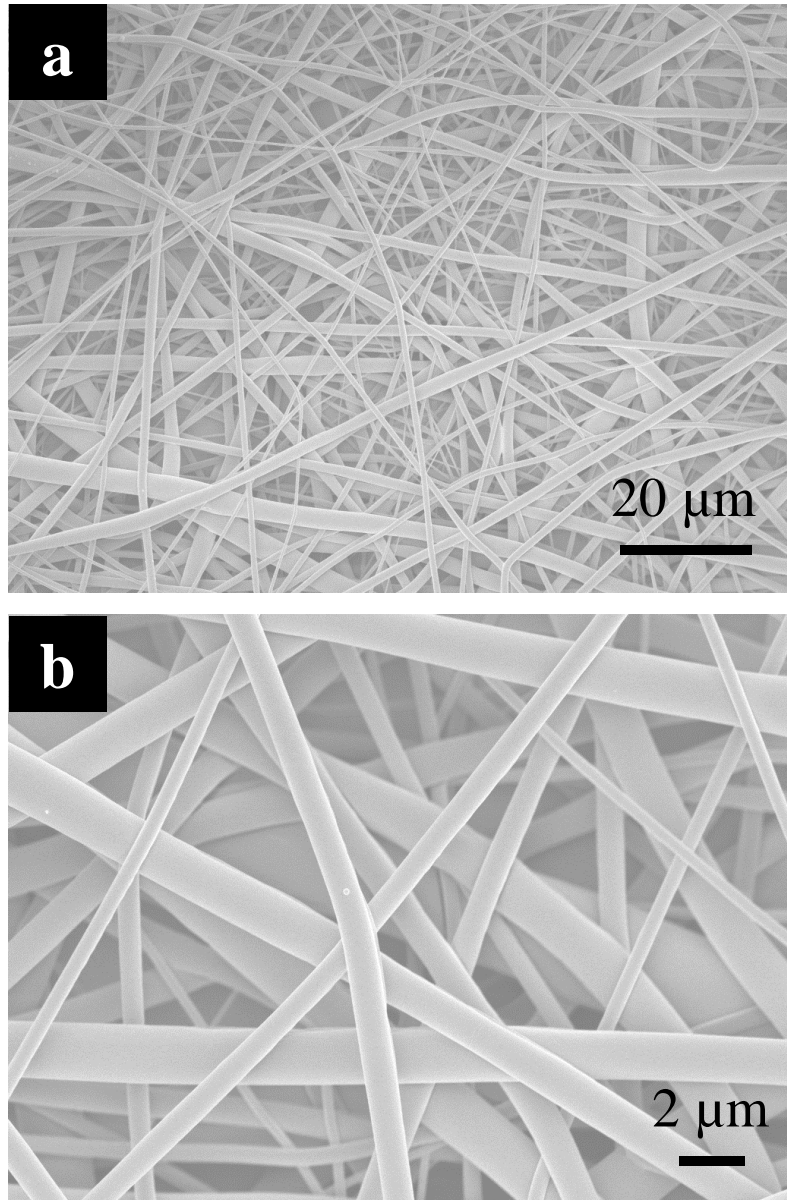


Figure 4.5 Scanning Electron Microscope images of various core-shell PLGA a, b) Microfibres.

When the polymer concentration reaches 15 wt% for the core and 10 wt% for the shell, only microfibres (**Figure 4.5**) are produced.

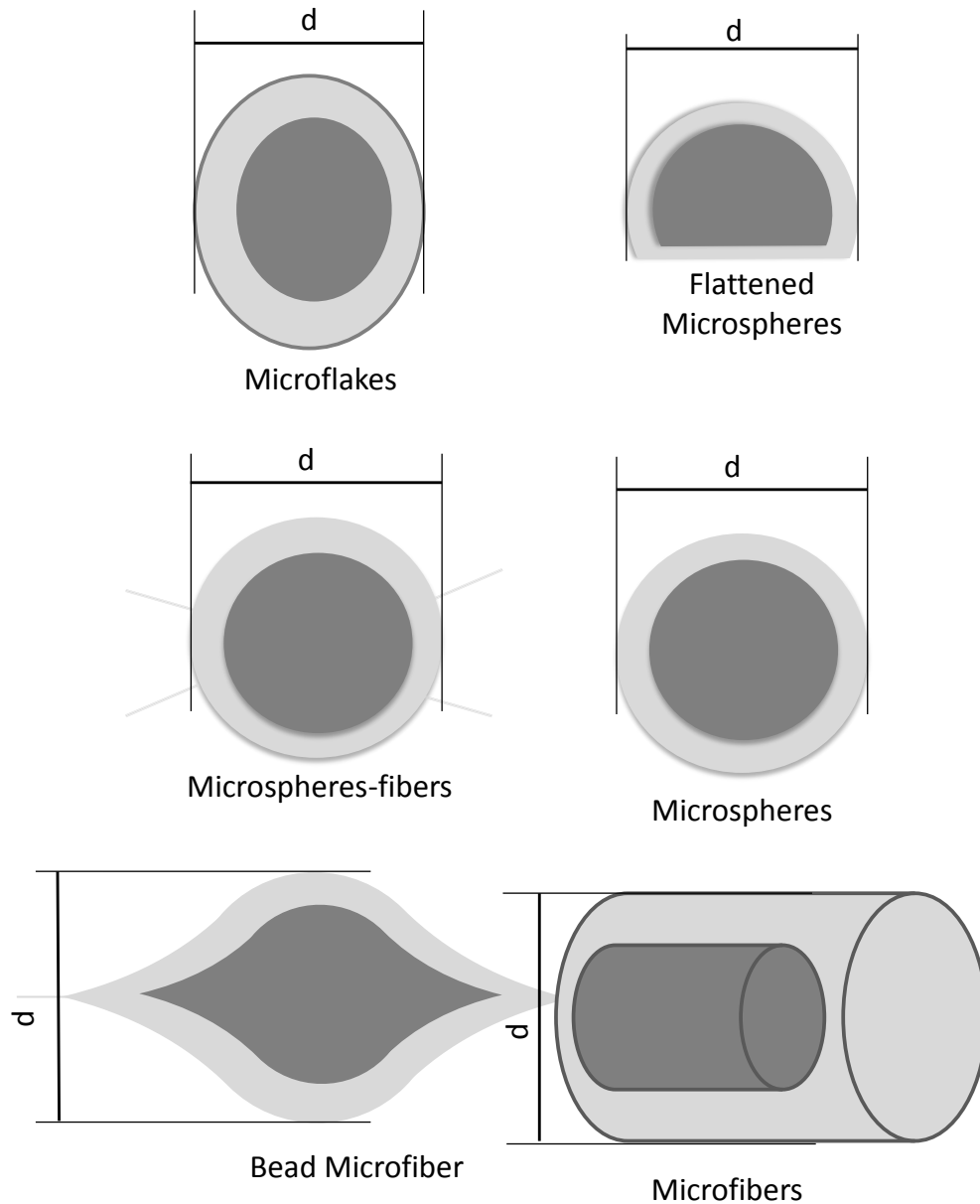


Figure 4.6 Schematic illustration of the detection points of the sizes of the fabricated core-shell microflakes, flattened microspheres, microspheres, microspheres-fibres, beaded microfibres, and microfibres. The d is from the detection points as shown in figure.

Our work demonstrates the critical roles of both the polymer concentrations of the core and shell solutions in controlling the shape and morphologies of the electrojetted core-shell microcapsules. A similar concentration effect has recently been reported in a range of PLGA

microcapsules that were produced by electrojetting a single solution and thus do not possess the core-shell structures [31].

In order to evaluate the shape, size and size distribution of the as-prepared microcapsules, a Leica Application Suite was used to analyse the SEM images. The detection points of the sizes of the microcapsules are schematically illustrated in **Figure 4.6**.

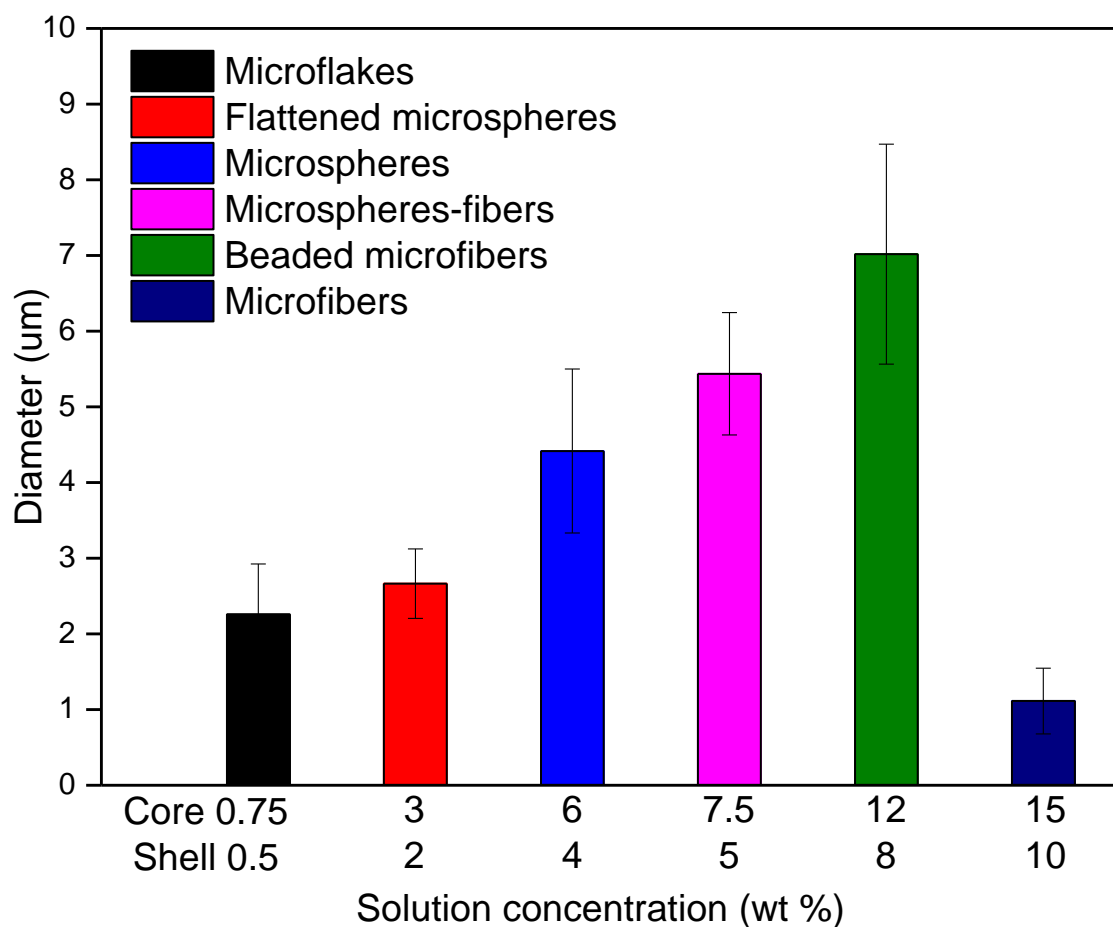


Figure 4.7 Size of the core-shell microflakes, flattened microspheres, microspheres, microspheres-fibres, beaded microfibres, and microfibres.

The sizes of the microflakes, flattened microspheres, microspheres, microspheres-fibres, beaded microfibres, and microfibres are presented in **Figure 4.7**. The size distributions of each kind of microcapsules are shown in **Figure 4.8**.

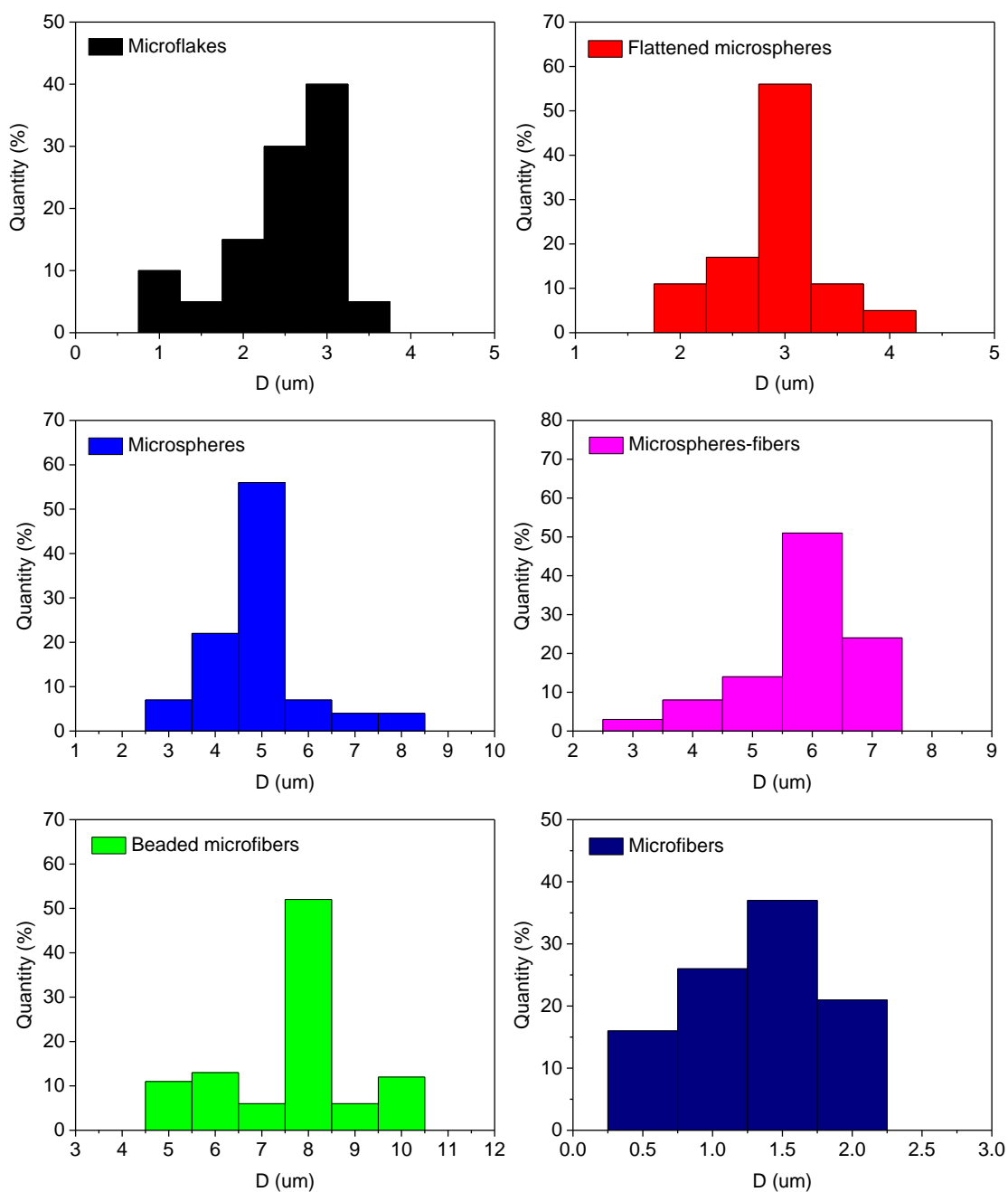


Figure 4.8 Size distribution of each type of core-shell microcapsules.

Each type of the electrojetted core-shell microcapsules exhibits a narrow size distribution and uniform morphology. With an increase in the PLGA concentrations, the dimension of the respective microcapsules firstly increased, and then decreased in the case of microfibres. The

diameters are 2.26 ± 0.67 μm for the microflakes, 2.67 ± 0.46 μm for the flattened microspheres, 4.42 ± 1.08 μm for the microspheres, 5.35 ± 0.94 μm for the microspheres-fibres, 7.02 ± 1.45 μm for the beaded microfibrils, and 1.11 ± 0.43 μm for the microfibrils, respectively.

In accordance with Hartman's study [37], the dimension of PLGA microspheres formed using electrospraying is governed by the surface tension of the polymer solution, as shown in Equation (4.1):

$$d \sim \left(\frac{\rho \varepsilon_0 Q^3}{\gamma K} \right)^{1/6} \quad (4.1)$$

Where d is the droplet size, ρ is the density of solution, ε_0 is the permittivity of vacuum, Q is the liquid flow rate, γ is the surface tension of solution in ambient air, and K is the liquid conductivity (International system of units). Increasing the polymer concentration leads to an increase in the solution viscosity, and a reduction in the surface tension (γ), and consequently an increase in microsphere size (d) (Equation 4.1) [37]. When the polymer concentration becomes sufficiently high, the solution can endure continuous and longer stretching from the nozzle tip to the collector, which gives rise to much thinner microfibrils through the mechanism of electrospraying.

4.3.3 Drug encapsulation efficiency

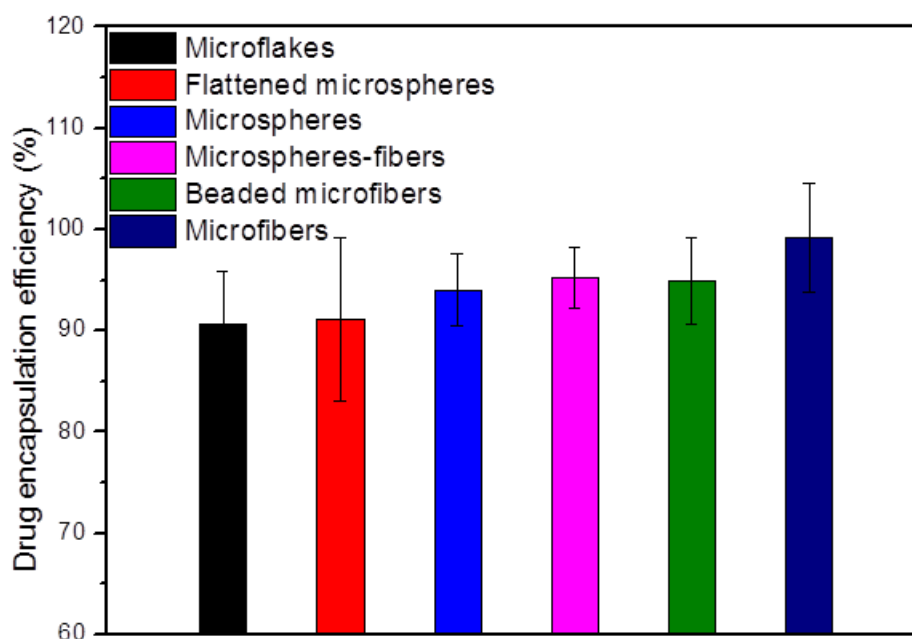


Figure 4.9 Drug encapsulation efficiency of the core-shell microflakes, flattened microspheres, microspheres, microspheres-fibres, beaded microfibres, and microfibres.

It is shown in **Figure 4.9** that all the fabricated core-shell microcapsules exhibit > 90% drug encapsulation efficiencies. The core-shell microfibres demonstrate the highest drug encapsulation efficiency ($99.2 \pm 5.4\%$). These encapsulation efficiencies are greater than those prepared using other techniques, including emulsion, suspension, and emulsion polymerization [38], solvent evaporation [38, 39], spray drying [40], layer-by-layer [41]. This can be ascribed to i) the inherent core-shell structures where the drug is encapsulated in the core and further protected by a shell of more hydrophobic polymer and ii) the fast solidification of the microcapsules at room temperature due to the use of a low boiling point solvent, chloroform [31, 42].

4.3.4 In vitro drug release study

The representative *in vitro* release profiles of lacosamide from the fabricated PLGA microflakes, microspheres, microspheres-fibres, and microfibres are shown in **Figure 4.10**.

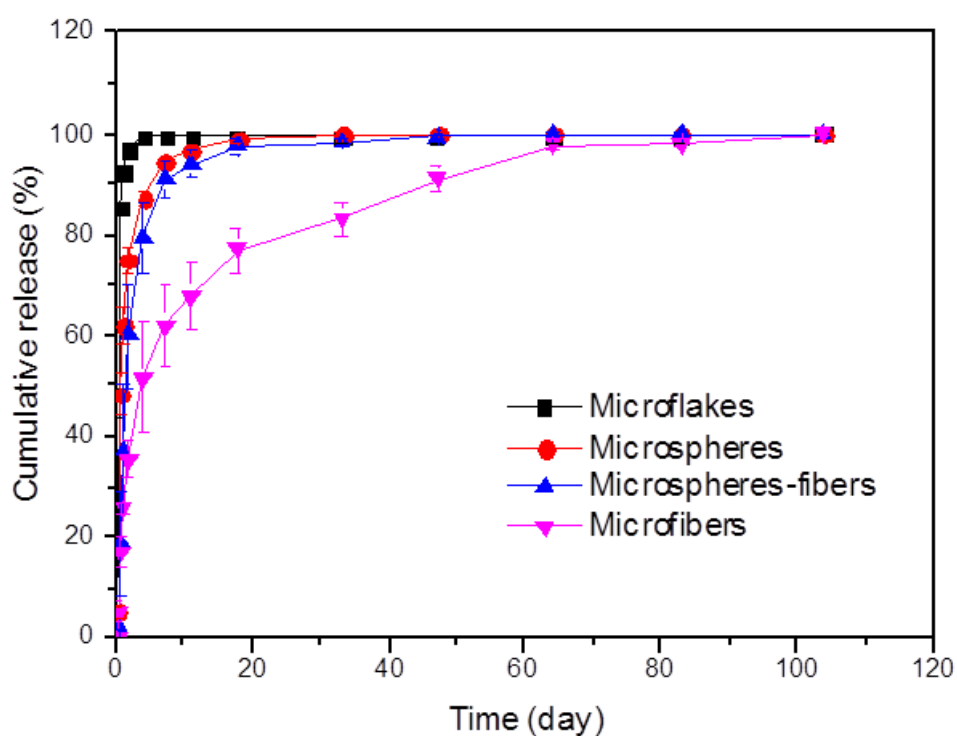


Figure 4.10 Cumulative release of lacosamide from the fabricated core-shell PLGA microcapsules including microflakes, microspheres, microspheres-fibers, and microfibers in aCSF (pH 7.4) at 37 °C over 104 days.

The sustained release characteristics demonstrated by all the microcapsules could be attributable to their core-shell structures, where the drug-free polymer shells present an additional barrier to the drug elution from the core [35]. The release profiles varied significantly with the shape and morphologies of the microcapsules. The microflakes exhibited the most rapid release characteristics, with > 96% of the encapsulated lacosamide being eluted within ~43 hours. Within the same period, the cumulative release of the lacosamide from the microspheres, microspheres-fibres, and microfibres, was approximately 75%, 60%, and 35% of the respective total drug loading. Compared to the microflakes, microspheres, and microsphere-fibres, microfibres exhibited significantly less initial burst release.

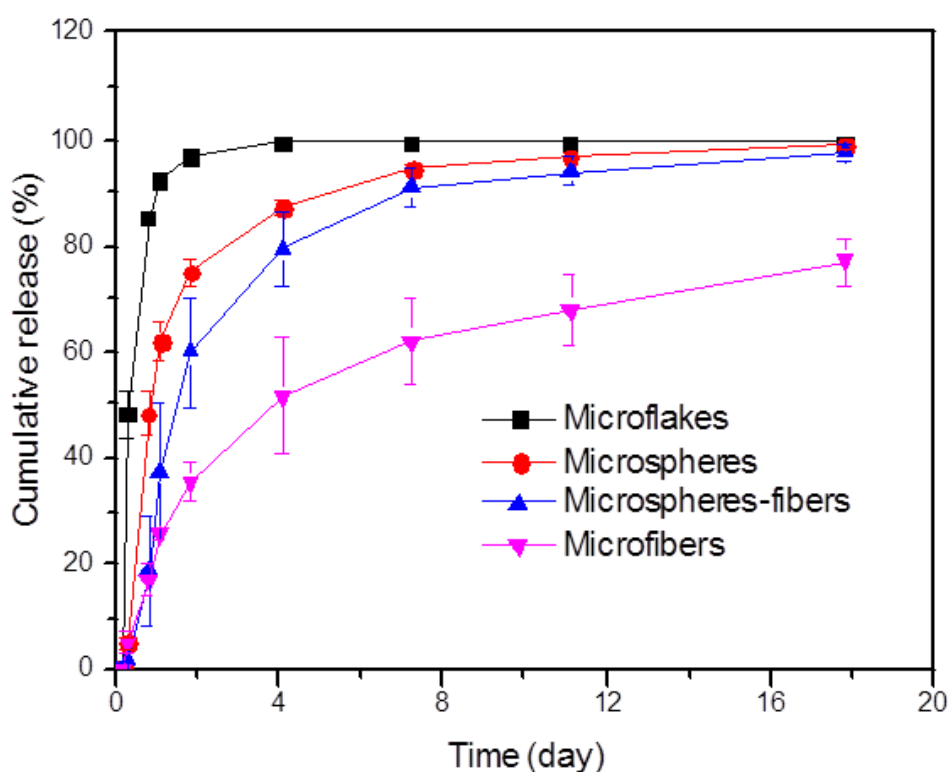


Figure 4.11 The release profiles of the core-shell microcapsules including microflakes, microspheres, microspheres-fibers, and microfibers in the first 20 days.

It is also noted that there is no significant mass loss in the microcapsules after a prolonged incubation in aCSF (104 days), other than that arising from the drug elution. This suggests minimal polymer degradation of the electrojetted microcapsules taking place within this period, which also indicates that the drug release from these microcapsules is predominantly diffusion controlled. The morphology and dimension of the PLGA microcapsules had a significant influence in the lacosamide release characteristics.

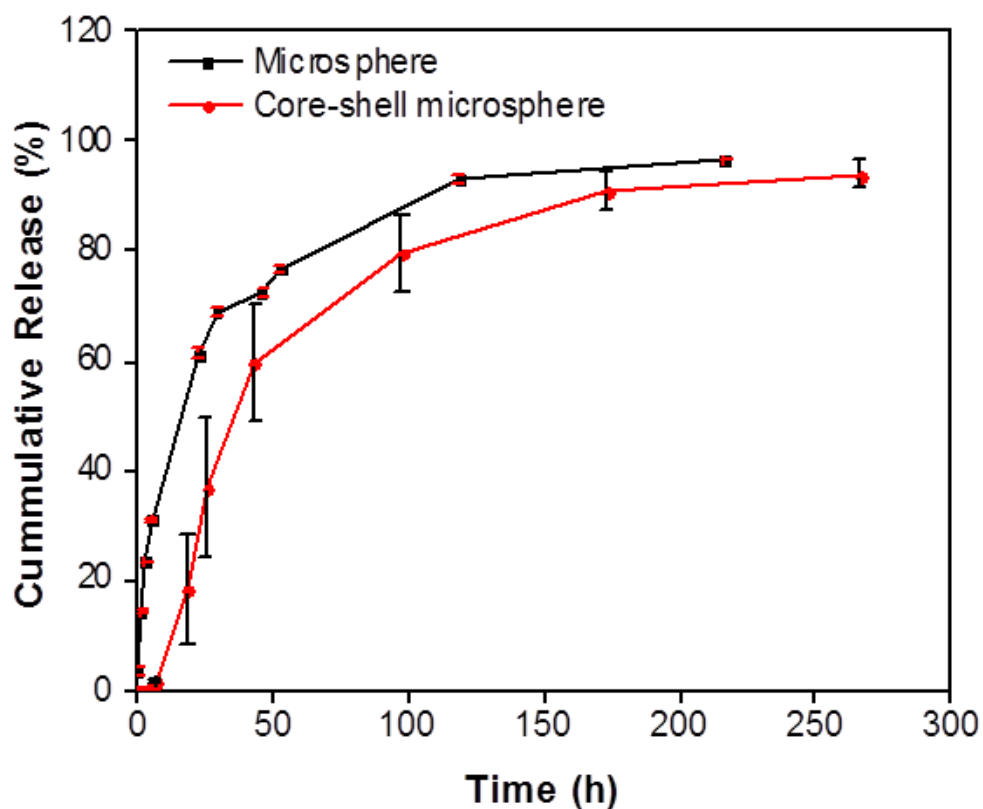


Figure 4.12 Comparison of the release profile of the microspheres to that of core-shell microspheres.

For the microcapsules with dominant sphere/particulate shape, including microflakes, microspheres, microspheres-fibres, the release rate decreased with increasing microcapsule dimension (**Figure 4.7** and **Figure 4.11**). With an increase in the sizes of the microcapsules, the surface area to volume ratios of the microcapsules decrease, and this leads to slower water penetration rates into the microcapsules and thus slower drug release profiles. Compared with the microspheres (**Figure 4.12**) and microfibrils (**Figure 4.13**) without core-shell structure, the core-shell structured microspheres and microfibrils exhibit significantly slower release.

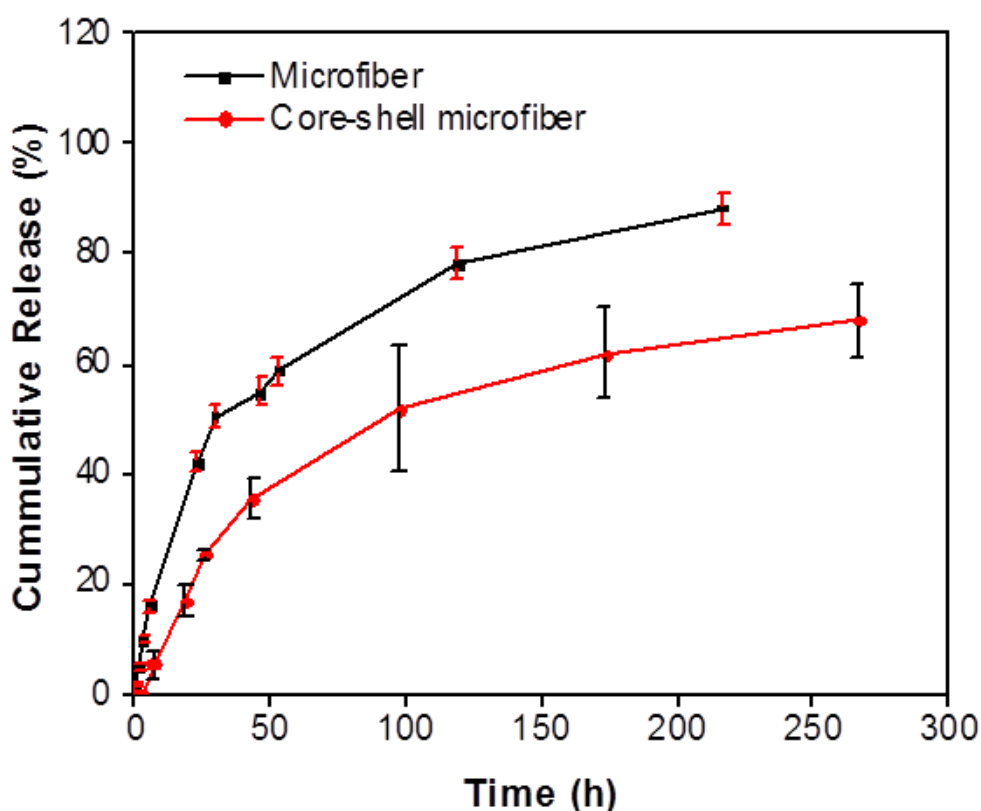


Figure 4.13 Comparison of the release profile of the microfibrils with that of core-shell microfibrils.

These microcapsules can serve as injectable microparticulate systems or polymer implants, for the local pharmaceutical intervention of epilepsy, as well as treatments for other neurological disorders, such as Parkinson's disease, Huntington's disease, and Alzheimer's disease. Compared with the systemic administration that requires high dosages, local implantation or injection using these drug-eluting microcapsules can significantly reduce the dosage and side effects. Moreover, these drug release studies demonstrate that the daily release dosage of these systems could be readily tailored by varying the shape and size of the microcapsules.

4.4 Conclusions

In summary, a variety of core-shell structured PLGA microcapsules containing an anti-epilepsy drug, lacosamide, have been fabricated by a novel electrojetting technique. These microcapsules, including microflakes, flattened microspheres, microspheres, microspheres-fibres, beaded microfibrils, and microfibrils, all demonstrated narrow size distribution and uniform morphology, high efficiency of drug encapsulation and sustained drug release characteristics. The release profile of lacosamide varies with the morphologies and shape of the core-shell microcapsules and thus can be readily controlled over long periods of time.

4.5 References

- [1] Cook MJ, O'Brien TJ, Berkovic SF, Murphy M, Morokoff A, Fabinyi G, D'Souza W, Yerra R, Archer J, Litewka L, Hosking S, Lightfoot P, Ruedebusch V, Sheffield WD, Snyder D, Leyde K, Himes D. Prediction of seizure likelihood with a long-term, implanted seizure advisory system in patients with drug-resistant epilepsy: a first-in-man study. *The Lancet Neurology* 2013;12:563-71.
- [2] Kwan P, Brodie MJ. Early identification of refractory epilepsy. *New England Journal of Medicine* 2000;342:314-9.
- [3] Oby E, Janigro D. The blood–brain barrier and epilepsy. *Epilepsia* 2006;47:1761-74.
- [4] Abbott NJ. Anatomy and physiology of the blood–brain barriers. In: Hammarlund-Udenaes M, de Lange ECM, Thorne RG, editors. *Drug Delivery to the Brain*: Springer New York; 2014. p. 3-21.
- [5] Wang ZH, Wang ZY, Sun CS, Wang CY, Jiang TY, Wang SL. Trimethylated chitosan-conjugated PLGA nanoparticles for the delivery of drugs to the brain. *Biomaterials* 2010;31:908-15.
- [6] Pardridge WM. Blood–brain barrier delivery. *Drug Discovery Today* 2007;12:54-61.
- [7] Halász P, Kälviäinen R, Mazurkiewicz-Beldzińska M, Rosenow F, Doty P, Hebert D, Sullivan T, on behalf of the SPSG. Adjunctive lacosamide for partial-onset seizures: Efficacy and safety results from a randomized controlled trial. *Epilepsia* 2009;50:443-53.
- [8] Stöhr T, Kupferberg HJ, Stables JP, Choi D, Harris RH, Kohn H, Walton N, White HS. Lacosamide, a novel anti-convulsant drug, shows efficacy with a wide safety margin in rodent models for epilepsy. *Epilepsy Research* 2007;74:147-54.
- [9] Blumer D, Wakhlu S, Davies K, Hermann B. Psychiatric outcome of temporal lobectomy for epilepsy: Incidence and treatment of psychiatric complications. *Epilepsia* 1998;39:478-86.

- [10] Sindou M, Guenot M, Isnard J, Ryvlin P, Fischer C, Mauguière F. Temporo-mesial epilepsy surgery: Outcome and complications in 100 consecutive adult patients. *Acta Neurochir (Wien)* 2006;148:39-45.
- [11] Ortinski P, Meador KJ. Cognitive side effects of antiepileptic drugs. *Epilepsy & Behavior* 2004;5, Supplement 1:60-5.
- [12] Perucca P, Gilliam FG. Adverse effects of antiepileptic drugs. *The Lancet Neurology* 2012;11:792-802.
- [13] Bennewitz MF, Saltzman WM. Nanotechnology for delivery of drugs to the brain for epilepsy. *Neurotherapeutics* 2009;6:323-36.
- [14] Edwards DA, Hanes J, Caponetti G, Hrkach J, Ben-Jebria A, Eskew ML, Mintzes J, Deaver D, Lotan N, Langer R. Large porous particles for pulmonary drug delivery. *Science* 1997;276:1868-72.
- [15] Grayson ACR, Choi IS, Tyler BM, Wang PP, Brem H, Cima MJ, Langer R. Multi-pulse drug delivery from a resorbable polymeric microchip device. *Nat Mater* 2003;2:767-72.
- [16] Acharya S, Sahoo SK. PLGA nanoparticles containing various anticancer agents and tumour delivery by EPR effect. *Advanced Drug Delivery Reviews* 2011;63:170-83.
- [17] Mathew A, Fukuda T, Nagaoka Y, Hasumura T, Morimoto H, Yoshida Y, Maekawa T, Venugopal K, Kumar DS. Curcumin loaded-PLGA nanoparticles conjugated with tet-1 peptide for potential use in alzheimer's disease. *Plos One* 2012;7:e32616.
- [18] Zhang P, Chen L, Gu W, Xu Z, Gao Y, Li Y. In vitro and in vivo evaluation of donepezil-sustained release microparticles for the treatment of Alzheimer's disease. *Biomaterials* 2007;28:1882-8.
- [19] Wen Z, Yan Z, Hu K, Pang Z, Cheng X, Guo L, Zhang Q, Jiang X, Fang L, Lai R. Odorranalectin-conjugated nanoparticles: Preparation, brain delivery and pharmacodynamic

study on Parkinson's disease following intranasal administration. *J Control Release* 2011;151:131-8.

[20] Fernández M, Negro S, Slowing K, Fernández-Carballido A, Barcia E. An effective novel delivery strategy of rasagiline for Parkinson's disease. *Int J Pharmaceut* 2011;419:271-80.

[21] Manickam DS, Brynskikh AM, Kopanic JL, Sorgen PL, Klyachko NL, Batrakova EV, Bronich TK, Kabanov AV. Well-defined cross-linked antioxidant nanozymes for treatment of ischemic brain injury. *J Control Release* 2012;162:636-45.

[22] Chung S, Sperling MR, Biton V, Krauss G, Hebert D, Rudd GD, Doty P, on behalf of the SPSG. Lacosamide as adjunctive therapy for partial-onset seizures: A randomized controlled trial. *Epilepsia* 2010;51:958-67.

[23] Greiner A, Wendorff JH. Electrospinning: A fascinating method for the preparation of ultrathin fibers. *Angewandte Chemie International Edition* 2007;46:5670-703.

[24] Arya N, Chakraborty S, Dube N, Katti DS. Electrospaying: A facile technique for synthesis of chitosan-based micro/nanospheres for drug delivery applications. *Journal of Biomedical Materials Research Part B: Applied Biomaterials* 2009;88B:17-31.

[25] Kenawy E-R, Bowlin GL, Mansfield K, Layman J, Simpson DG, Sanders EH, Wnek GE. Release of tetracycline hydrochloride from electrospun poly(ethylene-co-vinylacetate), poly(lactic acid), and a blend. *J Control Release* 2002;81:57-64.

[26] Kaassis AYA, Young N, Sano N, Merchant HA, Yu D-G, Chatterton NP, Williams GR. Pulsatile drug release from electrospun poly(ethylene oxide)-sodium alginate blend nanofibres. *Journal of Materials Chemistry B* 2014;2:1400-7.

[27] Lu W, Sun J, Jiang X. Recent advances in electrospinning technology and biomedical applications of electrospun fibers. *Journal of Materials Chemistry B* 2014;2:2369-80.

- [28] Hu X, Liu S, Zhou G, Huang Y, Xie Z, Jing X. Electrospinning of polymeric nanofibers for drug delivery applications. *J Control Release* 2014;185:12-21.
- [29] Reneker DH, Yarin AL, Fong H, Koombhongse S. Bending instability of electrically charged liquid jets of polymer solutions in electrospinning. *Journal of Applied Physics* 2000;87:4531-47.
- [30] Chen Y, Han D, Ouyang W, Chen S, Hou H, Zhao Y, Fong H. Fabrication and evaluation of polyamide 6 composites with electrospun polyimide nanofibers as skeletal framework. *Composites Part B: Engineering* 2012;43:2382-8.
- [31] Fattahi P, Borhan A, Abidian MR. Microencapsulation of chemotherapeutics into monodisperse and tunable biodegradable polymers via electrified liquid jets: Control of size, shape, and drug release. *Advanced Materials* 2013;25:4555-60.
- [32] Fattahi P, Borhan A, Abidian MR. Characterization of the size, shape, and drug encapsulation efficiency of PLGA microcapsules produced via electrojetting for drug delivery to brain tumors. *Neural Engineering (NER), 2013 6th International IEEE/EMBS Conference on 2013*. p. 953-6.
- [33] Martinez SE, Bowen KA, Remsberg CM, Takemoto JK, Wright HM, Chen-Allen AV, Davies NM. High-performance liquid chromatographic analysis of lacosamide in canine serum using ultraviolet detection: application to pre-clinical pharmacokinetics in dogs. *Biomedical Chromatography* 2012;26:606-9.
- [34] Gupta P, Elkins C, Long TE, Wilkes GL. Electrospinning of linear homopolymers of poly(methyl methacrylate): exploring relationships between fiber formation, viscosity, molecular weight and concentration in a good solvent. *Polymer* 2005;46:4799-810.
- [35] Viry L, Moulton SE, Romeo T, Suhr C, Mawad D, Cook M, Wallace GG. Emulsion-coaxial electrospinning: designing novel architectures for sustained release of highly soluble low molecular weight drugs. *Journal of Materials Chemistry* 2012;22:11347-53.

- [36] Almería B, Deng W, Fahmy TM, Gomez A. Controlling the morphology of electrospray-generated PLGA microparticles for drug delivery. *Journal of Colloid and Interface Science* 2010;343:125-33.
- [37] Hartman RPA, Brunner DJ, Camelot DMA, Marijnissen JCM, Scarlett B. Jet break-up in electrohydrodynamic atomization in the core-jet mode. *Journal of Aerosol Science* 2000;31:65-95.
- [38] Freiberg S, Zhu XX. Polymer microspheres for controlled drug release. *Int J Pharmaceut* 2004;282:1-18.
- [39] Chung T-W, Huang Y-Y, Liu Y-Z. Effects of the rate of solvent evaporation on the characteristics of drug loaded PLLA and PDLLA microspheres. *Int J Pharmaceut* 2001;212:161-9.
- [40] Louey M, Van Oort M, Hickey A. Aerosol dispersion of respirable particles in narrow size distributions produced by jet-milling and spray-drying techniques. *Pharmaceutical Research* 2004;21:1200-6.
- [41] Wang C, Ye W, Zheng Y, Liu X, Tong Z. Fabrication of drug-loaded biodegradable microcapsules for controlled release by combination of solvent evaporation and layer-by-layer self-assembly. *Int J Pharmaceut* 2007;338:165-73.
- [42] Anderson JM, Shive MS. Biodegradation and biocompatibility of PLA and PLGA microspheres. *Advanced Drug Delivery Reviews* 2012;64, Supplement:72-82.

**CHAPTER 5: DEVELOPMENT OF
ELECTROSPUN AND
ELECTROSPRAYED DUAL DRUG
DELIVERY MATRICES**

5.1 Introduction

The packaging and delivery of drugs to a specific location in the human body via biomaterials systems has been approaching the forefront of biomedical research for the past few decades [1-5]. Most of the drug delivery systems have been developed focusing on the achievement of mono drug release by developing a wide variety of biomaterial carriers. However, there are many situations that require multiple medications. Combination therapy with drugs of different therapeutic effects provides an effective strategy in the treatment of diseases [6]. Studies also show that combined therapy with two or more drugs provides a promising strategy to suppress drug resistance as different drugs possess different therapeutic effects at various pathological stages [7]. A variety of drug combinations can induce synergism and have shown promise in preventing disease recurrence [8-13].

One major challenge of combination therapy is to ensure effective dose for each drug independently. In order to overcome this challenge, one of the most popular approaches is to load multiple therapeutic agents into one delivery system and then concurrently deliver them to the site of action [8, 12, 14, 15]. A number of such drug delivery systems, including nanoscale and microscale particles, have been developed, for delivery of multiple drugs. However, fine control of the dosage and release kinetics remains a challenge. Besides, the complexity of the materials for use in the human body creates additional regulatory challenges. In addition, our limited understanding of the interactions between these new synthesis compounds and the body, especially the diseased part environment presents hurdles [1, 16]. The complicated fabrication process also makes it difficult to mass produce and apply it widely to clinical use of the drug delivery systems.

This chapter aims to use combinatorial electrospinning and electrospraying, to fabricate composite matrices as dual drug delivery vehicles. The composite structures of fibrous matrices with microparticles dual drug delivery systems demonstrated well-controlled internal structures, with uniform morphology and favourable thermal and mechanical properties. The drug release study shows that the daily dosage and release kinetics of these systems can be tailored by varying the shape and size of the polymeric carriers. In addition, the release behaviour of these dual drug delivery systems can be predicted using mathematical modelling.

5.2 Experimental

5.2.1 Materials

Poly(D,L lactic-co-glycolic acid) (PLGA) with a molar ratio of lactide to glycolide, 75 to 25, and polylactic acid (PLA), were purchased from Purac, Singapore, and used as received. The anti-epilepsy drug, lacosamide, was provided by UCB Pharma Pty Ltd. Phenytoin and dexamethasone were purchased from Sigma-Aldrich. All the others chemicals and reagents not mentioned above were purchased from Sigma-Aldrich and used as received without further purification.

5.2.2 Fabrication of Composite matrices

The polymer solutions for electrosprayed spheres were prepared by dissolving PLA and PLGA separately with the drug in chloroform. And the polymer solution for electrospun

fibres was prepared by dissolving PLA and drug in chloroform/DMF (volume ratio, 4/1). The solvent and a mixture solvent of the electrospinning and electrospraying conditions were optimized to obtain bead-free PLA fibres and uniform spherical PLA, PLGA spheres. In these solutions, the ratio of polymer/drug (w/w) was kept constant at 10/1, while the polymer concentration varied from 0.75 to 9.6 wt%. After encapsulation efficiency testing, drug loadings were achieved, which were 9.72 % for PLA phenytoin microfibres, 9.06 % for PLGA lacosamide microspheres, 9.35 % for PLA lacosamide microfibres, and 9.10 % for PLGA dexamethasone microspheres.

Composite dual drug delivery systems were formed by combinatorial electrospinning and electrospraying from two opposing spinnerets onto a rotating mandrel at room temperature [17, 18]. The solutions were loaded into plastic syringes with 23-gauge stainless steel needle independently. For electrospinning microfibres, the injection rate was 0.3 mL/h, the applied voltage was 21 kV, and the distance from the tip of the needle to collector mandrel was 15 cm. For electrospraying microspheres, the injection rate was 0.5 mL/h, the applied voltage was 10 kV, and the distance from the tip of the needle to collector mandrel was 12 cm. The rotation speed of the mandrel was set as 0.2 m/s. The low enough rotation speed can prevent microfibres alignment [19]. In order to obtain a homogeneous mixture of the microfibres and the microspheres, a dielectric tap was attached to the rotating mandrel to delimit the deposition area. The charged electrospraying microspheres are very sensitive to the electrostatic field and can be confined with a dielectric tap [18]. In order to remove possible residual organic solvent, all the samples were further dried in a vacuum oven at room temperature for 48 hours.

5.2.3 Characterization and evaluation

A Field Emission Scanning Electron Microscope (FESEM, JEOL JSM-7500FA) was used to examine the morphologies of the as-fabricated microcapsules. Before the SEM examination, the specimens were sputter-coated with gold to avoid charge accumulation. Dimensional statistical analysis was conducted by analysis of the SEM micrographs using the imaging software, Leica Application Suite. All data were expressed as the mean \pm standard deviation (STDEV). Thermogravimetric analyses (TGA) were carried out by using Q500 (TA Instruments), the heating rate was set at 10 °C/min, and the TGA curves were recorded from 50 to 800 °C under 15 ml/min flow of N₂. The amounts of samples for the TGA analyses were ~ 10 mg to avoid possible thermal lag. For testing the mechanical properties of composite matrices, the prepared matrices were cut into standard dumbbell-shaped specimens, and the test was performed by using a commercial mechanical Shimadzu EZ-L testing machine at the crosshead speed of 5 mm/min. Five specimens were tested for each sample, and the average values with respective standard deviations were calculated.

5.2.4 In vitro drug release study and quantification of drug encapsulation efficiency

In vitro drug release was conducted in artificial cerebrospinal fluid (aCSF) at 37 °C in a shaking water bath. At appropriate sample time, the release medium was withdrawn and replaced with equal amount of fresh aCSF. The released samples were analysed using the HPLC to determine the amounts of drug released.

HPLC analysis was conducted using an Agilent 1260 Infinity HPLC system. The analytical column used was an Atlantis® T3 C18 column (5 μ m, 250 mm \times 4.60 mm). The testing

parameters for the three drugs are summarised in **Table 5.1**. The amounts of released drug were calculated according to a pre-established calibration curve in aCSF [20-22]. The drug encapsulation efficiency was determined by using an extraction method according to our previous work [17]. Briefly, each sample (1 cm × 1 cm) was placed into 1 mL methanol for 12 hours, after which the methanol was removed and replenished with 1 mL of fresh methanol. This extraction procedure was repeated four times, with each methanol sample being allowed to evaporate to leave the residual drug behind, which was reconstituted using aCSF. The drug content was then analysed using HPLC as described above.

Table 5.1 HPLC testing parameters for the drugs including mobile phase, UV-Vis detection wavelength, and mobile phase flow rate.

Name of drug	Mobile phase (v to v)	Detection wavelength (nm)	Flow rate (mL/min)
Lacosamide	Milli-Q water, acetonitrile, and methanol (65:26.2:8.8)	210	0.8
Phenytoin	Milli-Q water and acetonitrile (50:50)	203	1.4
Dexamethasone	Milli-Q water and acetonitrile (35:65) with 0.1 % trifluoroacetic acid	242	1.0

5.3 Results and Discussion

5.3.1 Fabrication and selection of proper component

The process parameters including choosing of polymer, preparation of the solution, conditions of electrospinning and electro spraying et al. were optimized in order to achieve steady and repeatable formation of beaded-free microfibres and proper spherical microparticles.

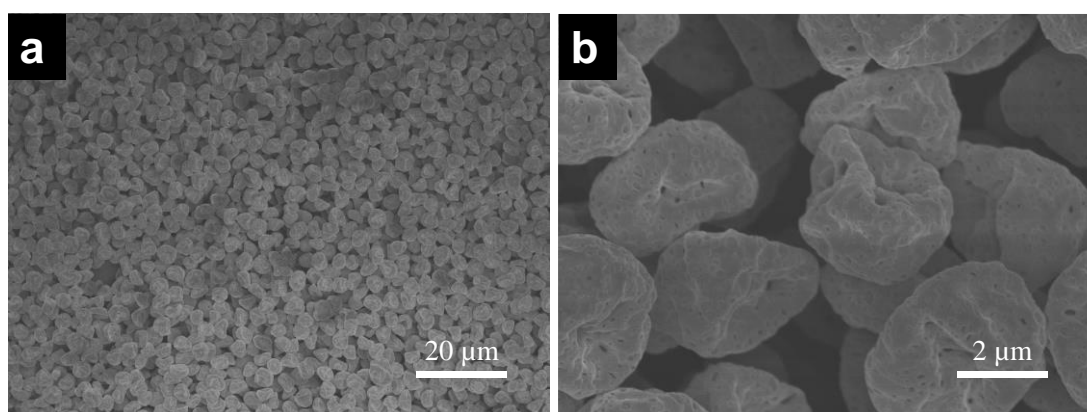


Figure 5.1 Scanning electron microscope images of electrospayed PLA erythrocyte-like microspheres.

As discussed in chapter 3, the electrojetted polymeric structures mainly depend on the polymer concentration and electrojetting parameters. Here, the focus is on discussion of the fabrication of PLA microspheres and microfibres. Similarly, by adjusting the polymer concentration and electro spraying parameters, erythrocyte-like PLA microspheres (**Figure 5.1**) were obtained. They were prepared using a polymer concentration of 0.75 wt%. All these erythrocyte-like PLA microspheres demonstrated narrow size distribution and uniform morphology. As the PLA concentration increased to 2 wt%, two kinds of microspheres, PLA

microspheres (**Figure 5.2b**), beaded microspheres (**Figure 5.2c**) with a certain amount of concomitant nanofibre were fabricated. It indicates that higher polymer concentrations tend to form fibres.

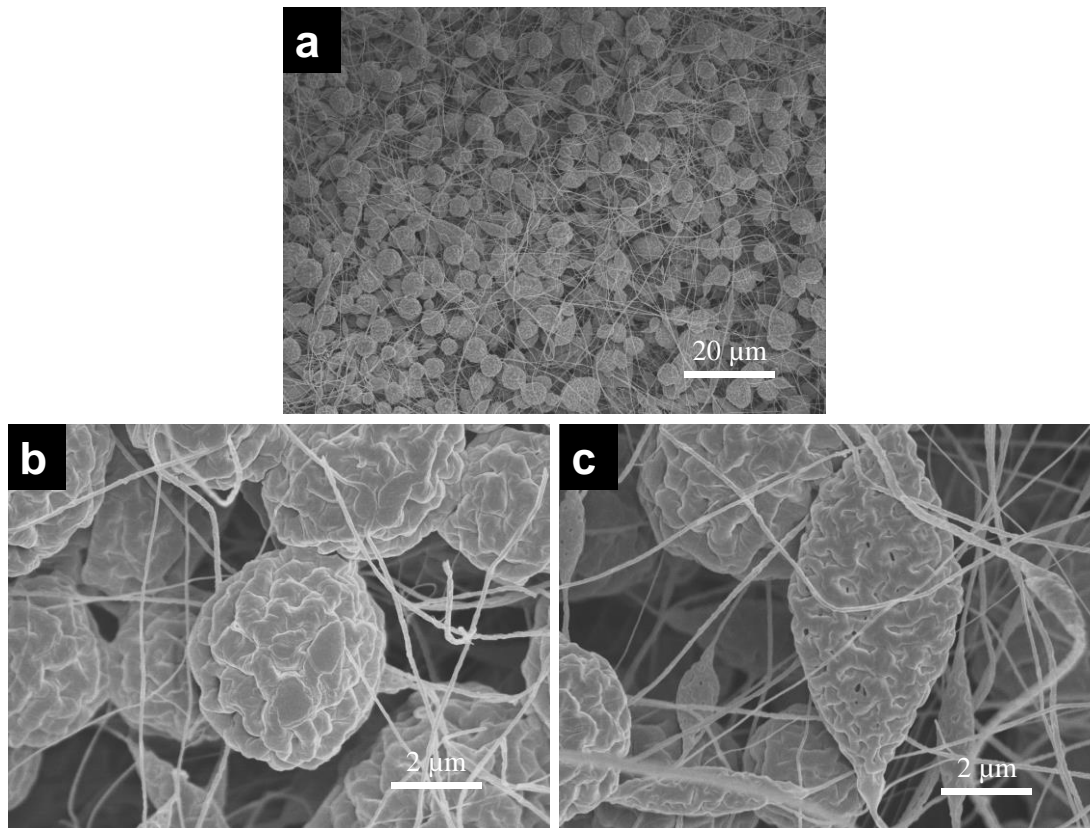


Figure 5.2 Scanning electron microscope images of electrospun PLA microfibres with two kinds of PLA microspheres, b) microspheres and c) beaded microspheres.

On further increase of PLA concentration to 4.5 wt%, PLA beaded microfibres appeared (**Figure 5.3 a,b**). This phenomenon agrees with former chapters' studies, and there is a transition stage between spherical structures and fibrous structures. Finally, when the polymer concentration was eventually increased to 9.6 wt%, the microfibres were formed, as shown in **Figure 5.3 c,d**.

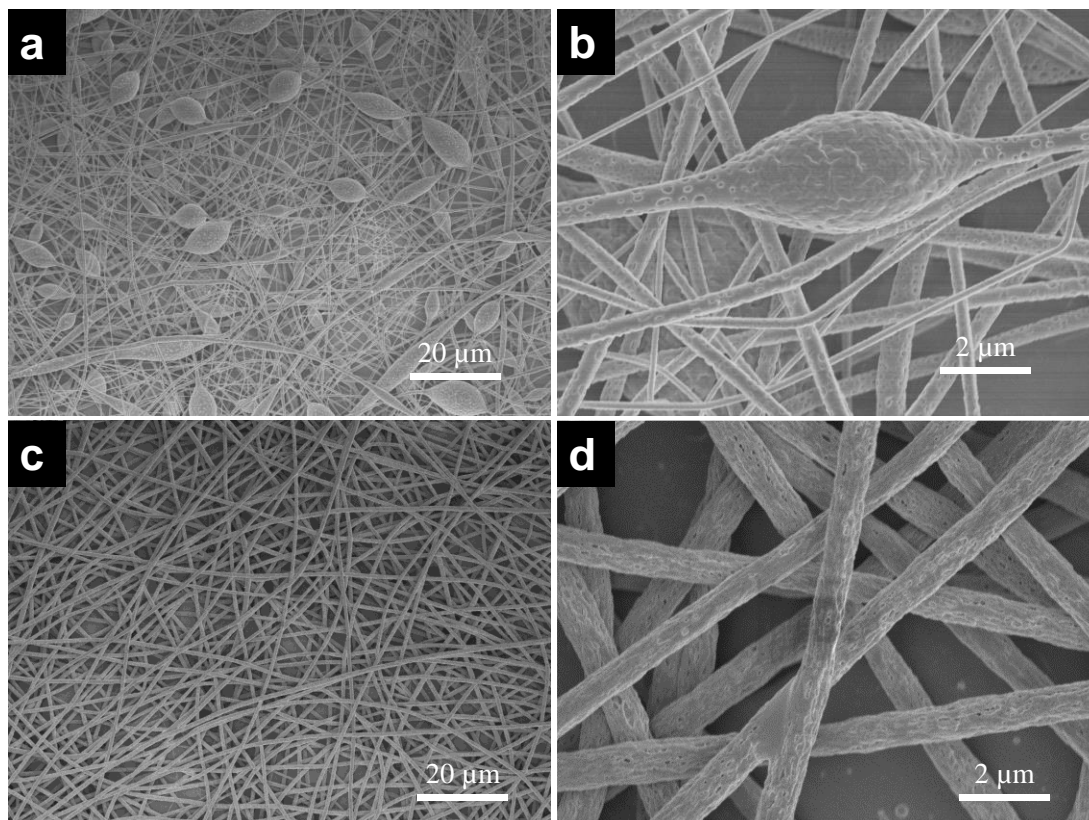


Figure 5.3 Scanning electron microscope images of electrospun PLA a,b) beaded microfibre and c,d) microfibres.

Both PLA and PLGA have been widely accepted for use in medical devices due to their excellent biocompatibility. The PLA and PLGA materials also exhibit low toxicity and immunogenicity, as well as well-defined biodegradation. Compared with PLGA, the absence of glycolic acid segments makes PLA more hydrophobic and results in longer degradation kinetics. Therefore, electrospun PLA was chosen rather than PLGA as a fibrous carrier in the composite matrices.

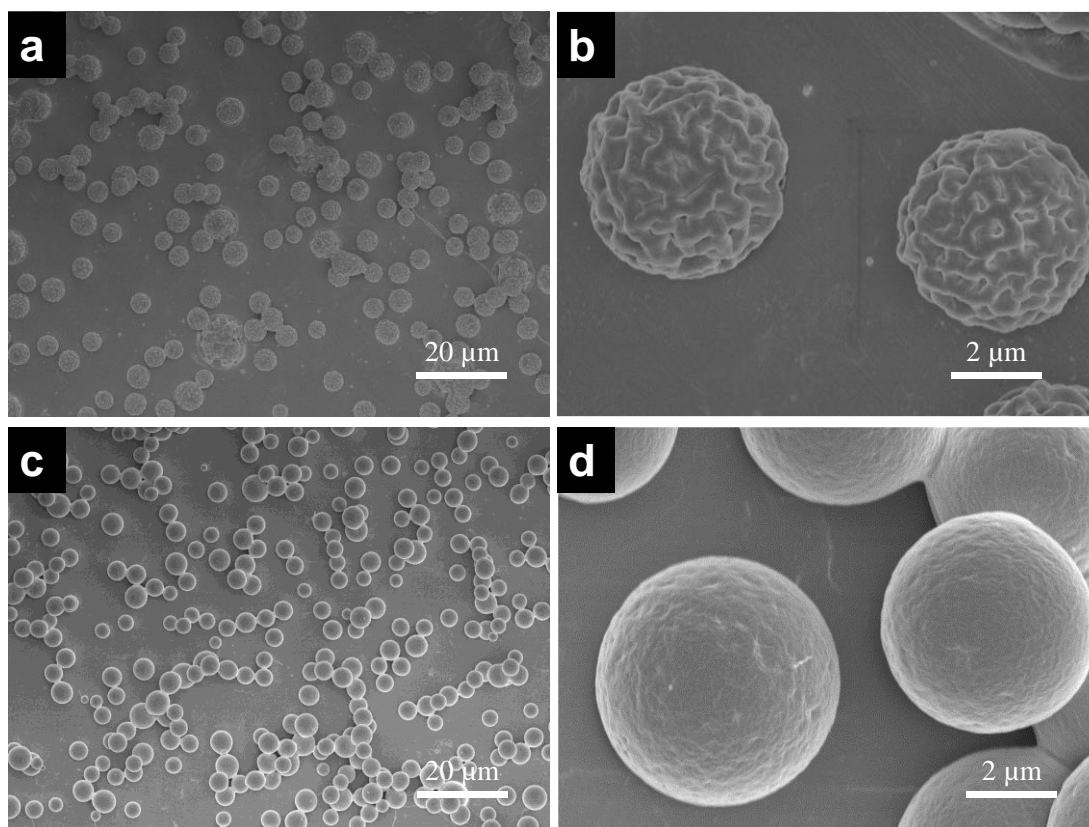


Figure 5.4 Scanning electron microscope images of electrospayed a,b) PLGA flattened microspheres, c,d) PLGA microspheres.

Firstly, erythrocyte-like PLA microspheres were used as a spherical component. Unfortunately, it was found that the erythrocyte-like PLA microspheres could not tightly incorporate into the PLA microfibrils matrices. Part of the erythrocyte-like PLA microspheres even dropped out from the composites matrices when it was incubating in the release medium aCSF. Then, as discussed in former chapters, flattened PLGA microspheres (3.5 wt%, **Figure 5.4 a,b**) and PLGA microspheres (4.5 wt%, **Figure 5.4 c,d**) were also tried as the spherical component. The outcome was that the Flattened PLGA microspheres could be firmly attached to the PLA microfibrils. The mechanism and more detailed information are

discussed and given below. All microcapsules with various polymers, structure, and their respective fabrication conditions are summarized in **Table 5.2**.

Table 5.2 Microcapsules with various polymers, structure, and their respective fabrication conditions.

Polymers	Solution concentrations (wt%)	Applied Voltage (kV)	Structure Type
PLA	0.75	10	Erythrocyte-like microspheres
PLA	2.0	10	Microspheres, beaded spheres, and fibres
PLA	4.5	21	Beaded microfibres
PLA	9.6	21	Microfibres
PLGA	3.5	10	Microspheres
PLGA	4.5	10	Flattened microspheres

5.3.2 Fabrication of composite matrices containing two types of drugs

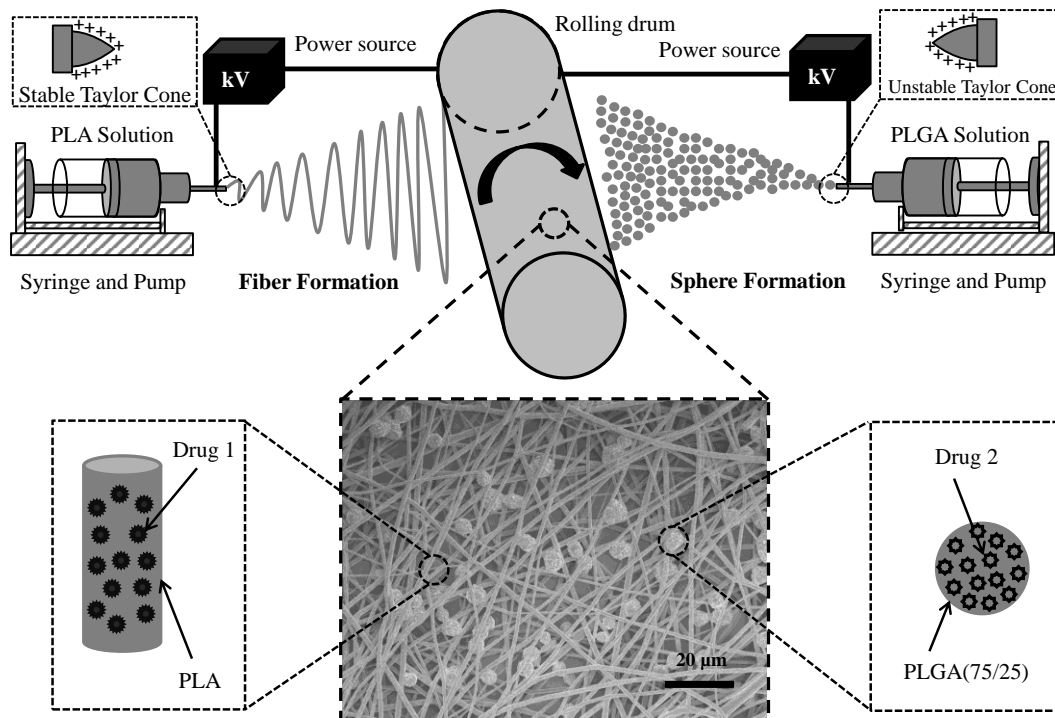


Figure 5.5 Schematic of the fabrication process of dual drug delivery composite matrices by using combinatorial electrospinning and electro spraying; the stable Taylor core of PLA solution (containing phenytoin or lacosamide) tend to form microfibrils, and the unstable Taylor core of PLGA solution (containing lacosamide or dexamethasone) tend to form microspheres.

Figure 5.5 shows the schematic fabrication process of composite matrices as dual drug delivery systems. In order to minimize the charge effect between electrospinning and electro spraying, PLGA microspheres were electro sprayed on one side of the rotation

mandrel, and PLA microfibres were electrospun on the other side, to generate the composite matrices.

Different from electrospinning, the Taylor core (as shown in **Figure 5.5**) is unstable in the electrospaying process, and the liquid jet is destabilized due to varicose instability, and hence fine droplets were formed [24].

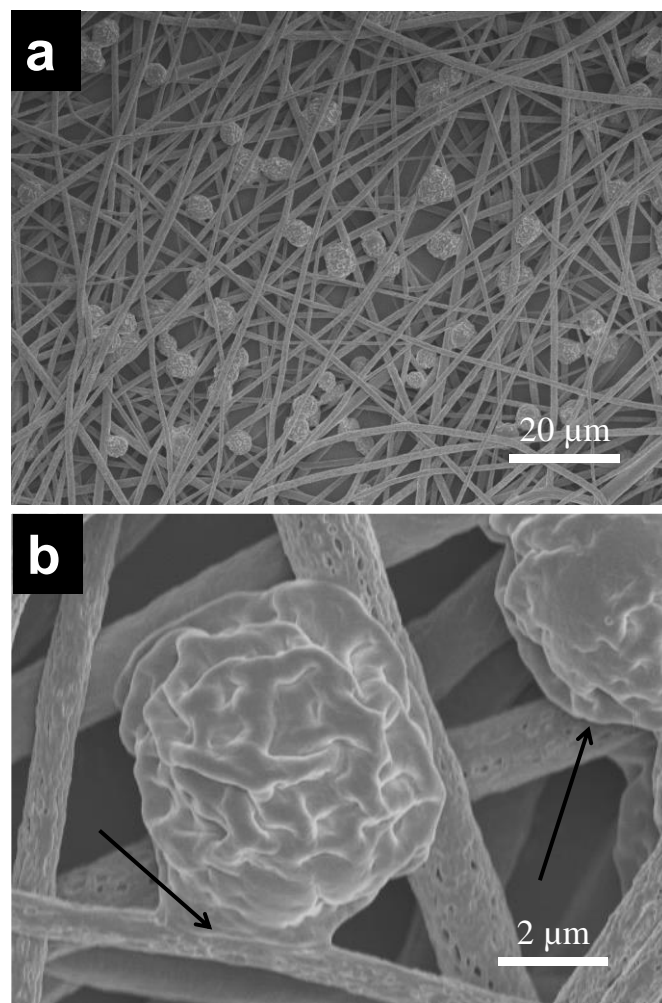


Figure 5.6 Scanning electron microscope images of PLA phenytoin microfibres/ PLGA lacosamide microspheres composite matrices; fewer microspheres indicate lower drug ratio.

While the drops move from the needle tip to the rotating mandrel, rapid solvent evaporation and polymer diffusion occurs. This leads to the formation of spherical microparticles. When a low concentration of PLGA, such as 3.5 wt%, was used in this work, flattened microspheres were formed. This is due to incomplete solvent evaporation, and, therefore, the electrospayed microcapsules are still partially dissolved when they reach the surface of the PLA microfibrils. Before hitting the surface of the PLA microfibrils, there is still a small amount of residual solvent in the PLGA microspheres; which makes the microspheres deform and flatten, and firmly attaching to the microfibril to form a conglomerated stable composite matrix structure [23]. When PLGA microspheres were electrospayed in combination with PLA microfibrils, a relatively uniform distribution within the microfibrils was observed (**Figure 5.6 and 5.7**). This results in the formation of composite matrices with randomly deposited microspheres and microfibrils.

As a proof of combined therapeutic conception, two composite matrices were fabricated. They contain different drugs: PLA phenytoin microfibrils/PLGA lacosamide microspheres composite matrices and PLA lacosamide microfibrils/PLGA dexamethasone microspheres composite matrices. In order to tailor the dosage ratio of two drugs in each composite matrix, the quantity of PLGA microspheres was roughly controlled by simply varying the duration of the electrospinning and the electrospaying. As a result, PLA phenytoin microfibrils were incorporated with fewer PLGA lacosamide microspheres, and PLA lacosamide microfibrils were incorporated with more PLGA dexamethasone microspheres. The SEM images (**Figure 5.6 and 5.7**) clearly show this quantitative difference of the two kinds of PLGA microspheres.

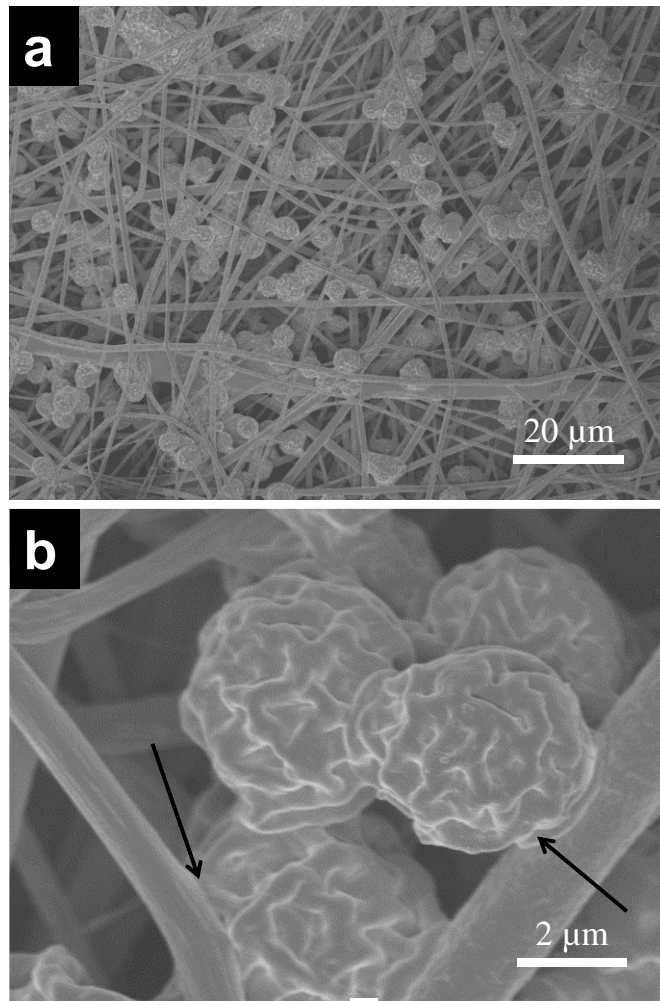


Figure 5.7 Scanning electron microscope images of PLA lacosamide microfibrils/ PLGA dexamethasone microspheres composite matrices, more microspheres indicate higher drug ratio.

5.3.3 Thermal properties of composite matrices

Thermogravimetric analysis (TGA) curves of the PLA microfibrils, PLA-phenytoin microfibrils/PLGA-lacosamide microspheres composites, PLA-lacosamide microfibrils/PLGA-dexamethasone microspheres composites and PLGA microspheres are presented in **Figure 5.8**.

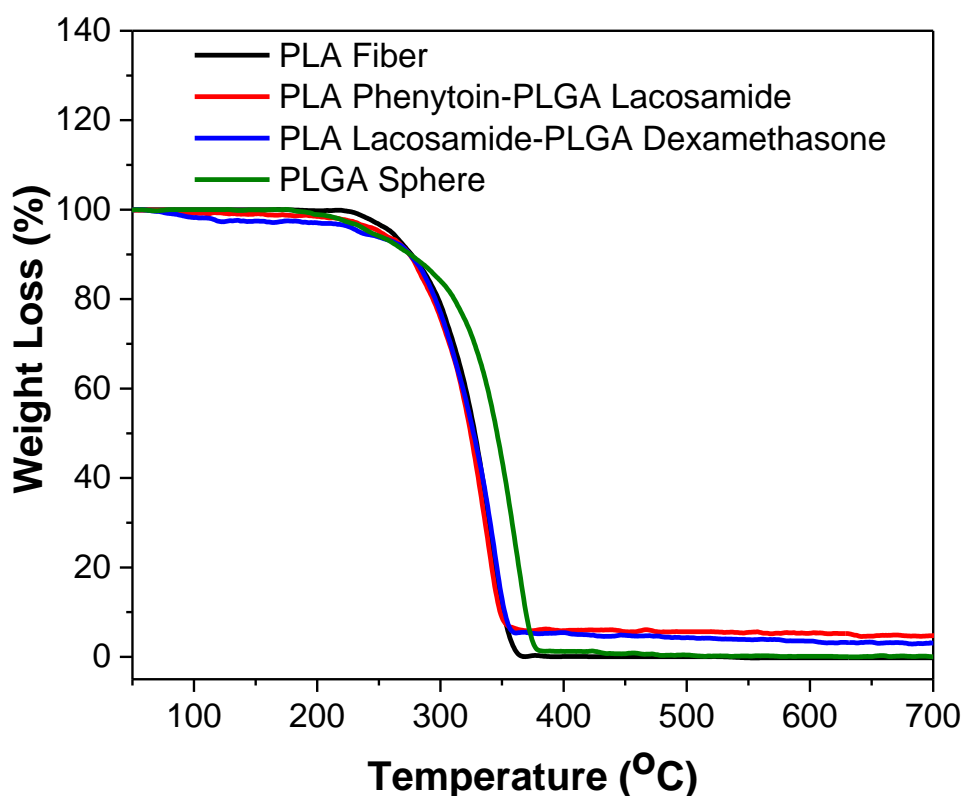


Figure 5.8 Thermogravimetric analyses (TGA) results of the as-fabricated PLGA microspheres, PLA microfibrils matrices and composite matrices which contain drugs.

The initial weight loss found up to 120 °C is probably attributable to the physical loss of moisture. It indicates that the weight loss at this stage is not related to polymer thermal

decomposition. [24]. All samples demonstrated sharp mass loss between ~240 °C to ~380°C, and this is attributed to the decomposition of the polymer chains [25]. Without the drug, both PLA microfibrils and PLGA microspheres showed nearly zero residues. However, the composite matrices demonstrated higher carbon residues. This may be ascribed to the aromatic ring structure of the model drugs. In addition, evidence for drug encapsulation is also afforded by these TGA plots which are shown above.

5.3.4 Mechanical properties of the composite matrices

For drug delivery systems, mechanical properties are important since deformation or fracture in the implanted device will significantly affect the drug release kinetics [26].

Table 5.3 Mechanical properties of electrospun PLA microfibre and the composite matrices.

Sample	Tensile strength (MPa)	Tensile modulus (MPa)	Strain at break (%)
PLA fibres	4.6±0.81	97±7.6	98±1.4
PLA phenytoin /PLGA lacosamide	6.0±0.46	172±42	62.3±8.1
PLA lacosamide /PLGA dexamethasone	2.8±0.21	66±13	76±5.7

The typical stress-strain curves acquired from PLA microfibrils matrices, PLA phenytoin microfibrils/PLGA lacosamide microspheres composite matrices, and PLA lacosamide microfibrils/PLGA dexamethasone microspheres composite matrices are shown in **Figure 5.9** and summarized in **Table 5.3**.

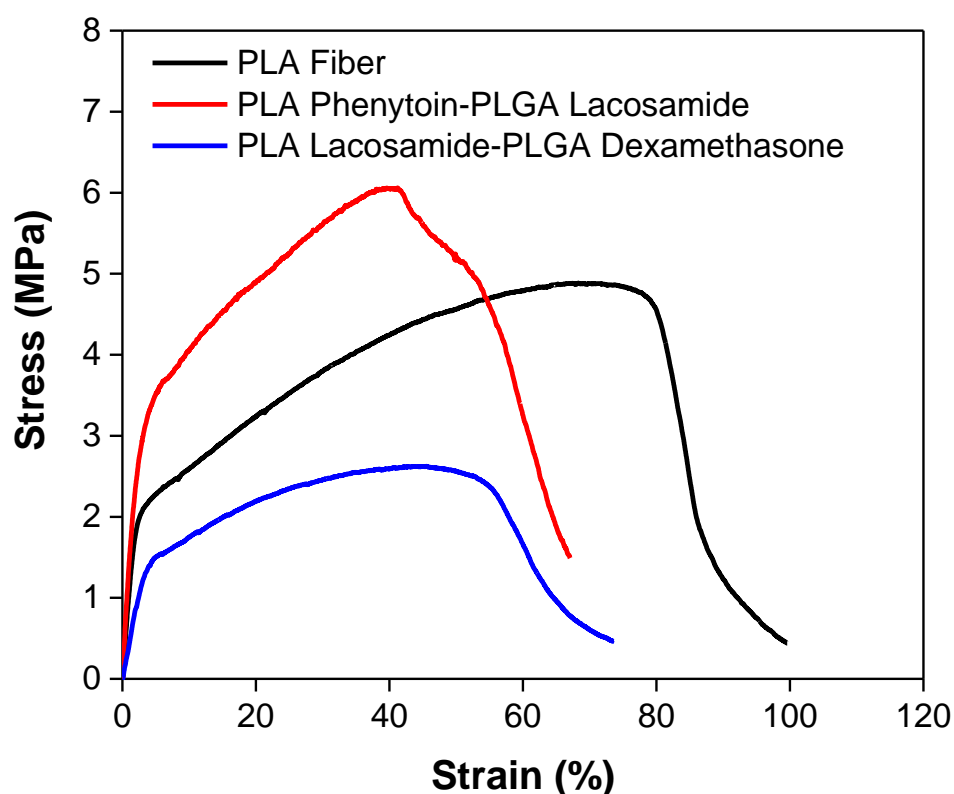


Figure 5.9 Typical tensile stress-strain results of as-fabricated PLA microfibrils matrices and composite matrices which contain drugs.

All PLA microfibrils matrices and composite matrices demonstrated high tensile strength, as well as high tensile modulus. The favourable mechanical properties can be ascribed to the high molecular orientation along the PLA microfibrils axes [27]. During the formation of microfibrils, the liquid jet undergoes a whipping or bending motion process, which is very fast and leads to the rapid drawing of the molecular chain among the microfibrils. The tensile

strength of the PLA fibres matrices is 4.6 ± 0.81 MPa, slightly increased to 6.0 ± 0.46 MPa for PLA phenytoin/PLGA lacosamide composite matrices (fibres with fewer spheres), then slightly decreased to 2.8 ± 0.21 MPa for PLA lacosamide/PLGA dexamethasone composite matrices (fibres with more spheres). While, the modulus initially increased from 97 ± 7.6 MPa to 172 ± 42 MPa, and then decreased to 66 ± 13 MPa. With increasing numbers, microspheres cannot be distributed uniformly. Instead, they formed small partial spherical accumulations, and these accumulations became structural defects in the composite matrices. When the composite matrices are under tensile testing, the defects made them fracture easily [28, 29].

5.3.5 In vitro drug release study and mathematical simulation

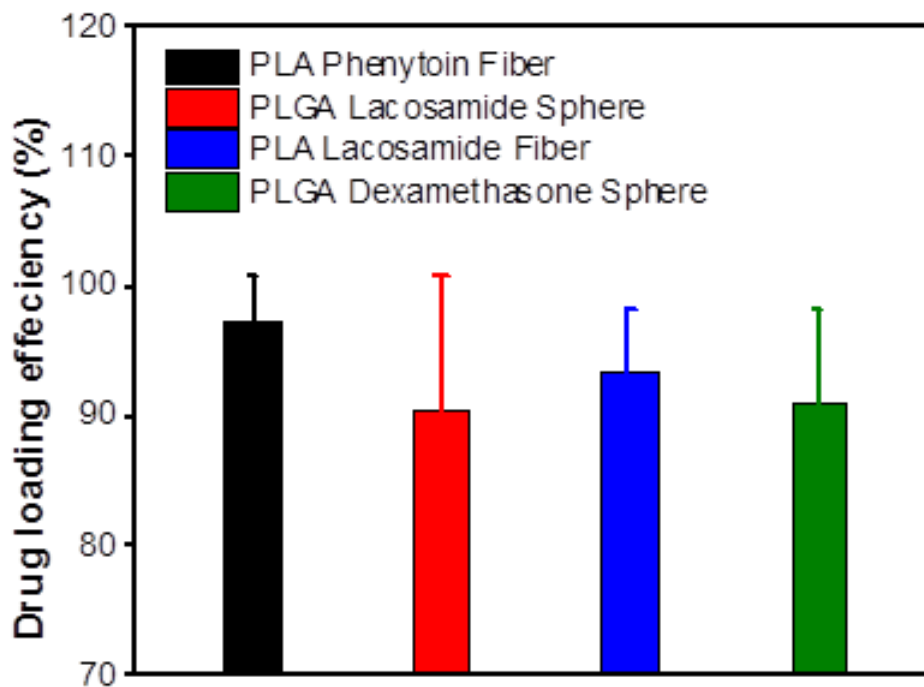


Figure 5.10 Drug encapsulation efficiency testing results of PLA fibres and PLGA spheres in composite matrices.

5.3.5 In vitro drug release study and mathematical simulation

Drug encapsulation efficiency is an important index for drug delivery systems, especially for rare and expensive drugs. A suitable microencapsulation technique should result in high encapsulation efficiency[30]. Drug encapsulation efficiency testing was conducted by using an extraction method. As shown in **Figure 5.10**, all microfibrils and microspheres demonstrated high drug encapsulation efficiency. They were $97.2\pm 3.7\%$ for PLA phenytoin microfibrils, $90.6\pm 10.3\%$ for PLGA lacosamide microspheres, $93.5\pm 4.6\%$ for PLA lacosamide microfibrils, $91.0\pm 7.2\%$ for PLGA dexamethasone microspheres. The total encapsulation content of two kinds of drugs in each microsphere was also detected by the extraction method. Composite matrices with more microspheres contained fivefold higher molar ratio of drug than those with fewer microspheres; of relative composite matrices.

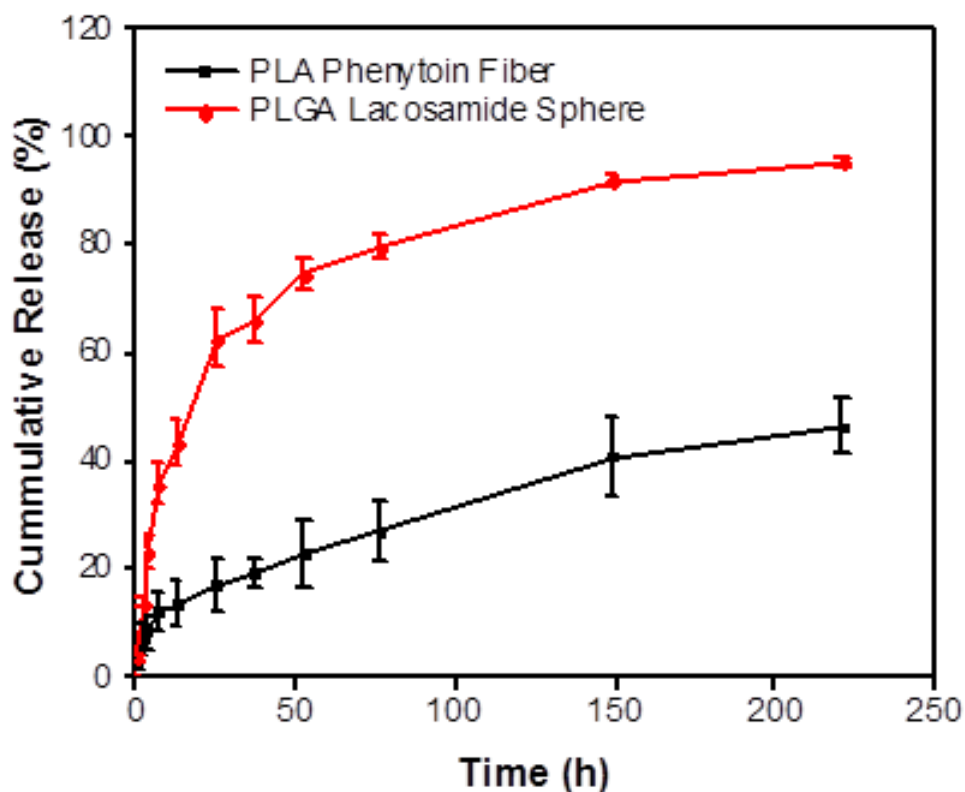


Figure 5.11 Cumulative release of each drug from PLA phenytoin microfibres-PLGA lacosamide microspheres composite matrices.

In general, drugs which were encapsulated in microspheres were released faster than those encapsulated in microfibres. PLGA lacosamide microspheres exhibited rapid release, ~62% of total lacosamide within 24 hours, and ~96% within 220 hours. While PLA phenytoin microfibres just released ~16% of total phenytoin within 24 hours, followed by a slower release of up to 45% within 220 hours. The release rates of PLA lacosamide microfibres and PLGA dexamethasone microspheres were not so obviously different, but it still exhibited independent release characteristics. The entire release rates were with an initial burst, then with a long slower period. As the composite matrices were placed in aCSF medium, water

rapidly penetrated into the exposed surface of microspheres and microfibres, and the drugs trapped within a thin surface layer were quickly released. Subsequently, it took a longer time for water to diffuse in and the drugs to diffuse out, thus limiting the later drug release rates [31].

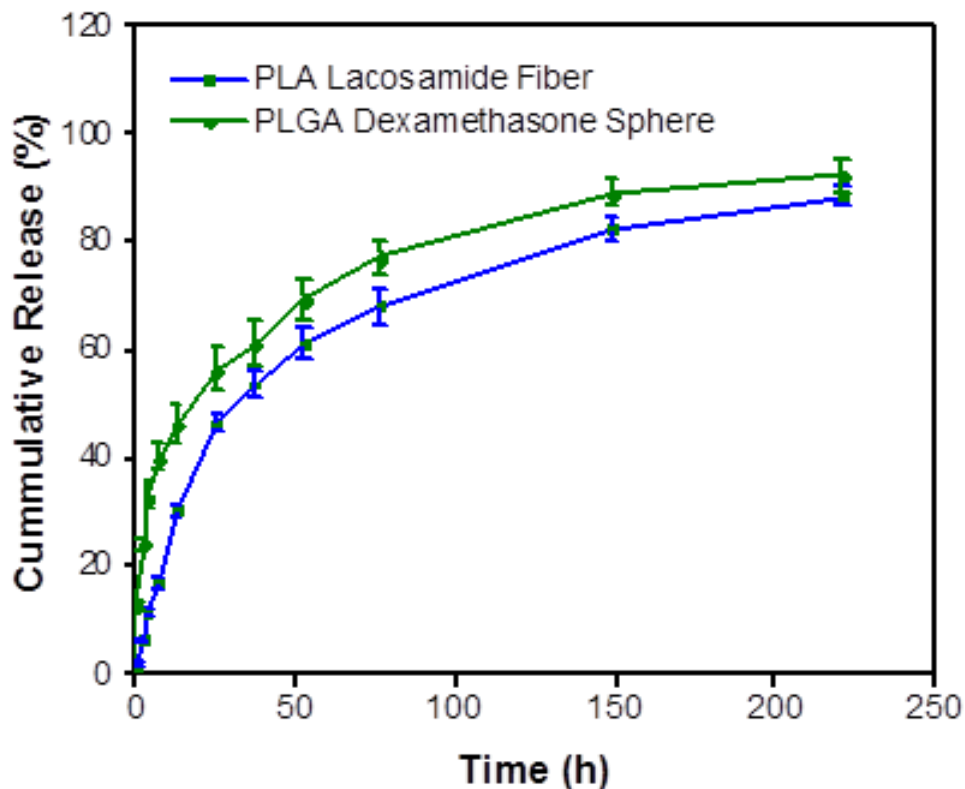


Figure 5.12 Cumulative release of each drug from PLA lacosamide microfibre/PLGA dexamethasone microspheres composite matrices.

As shown in *in vitro* drug release testing, the release profiles of the drugs vary with the morphology and shape dimension of the microfibres and microspheres. In order to evaluate the effects of morphology, shape dimension, and develop a capability for predicting the kinetics of drugs release of the microfibres and microspheres, a theoretical analysis of time-

dependent diffusion with an initially uniform drug concentration was performed. For mathematical simulation of microspheres and microfibres, a drug release profile is obtained by solving Fick's second law as described in chapter 3. The fraction of the initial drug loading released from the microcapsules (M_t/M_∞) at any time (t) can be expressed by equation 3.1 given in chapter 3 as follows:

$$\frac{M_t}{M_\infty} = 1 - \sum_{n=0}^{\infty} \frac{2i}{\lambda_n^2} e^{-\frac{4\lambda_n^2 D_e t}{d^2}} \quad (3.1)$$

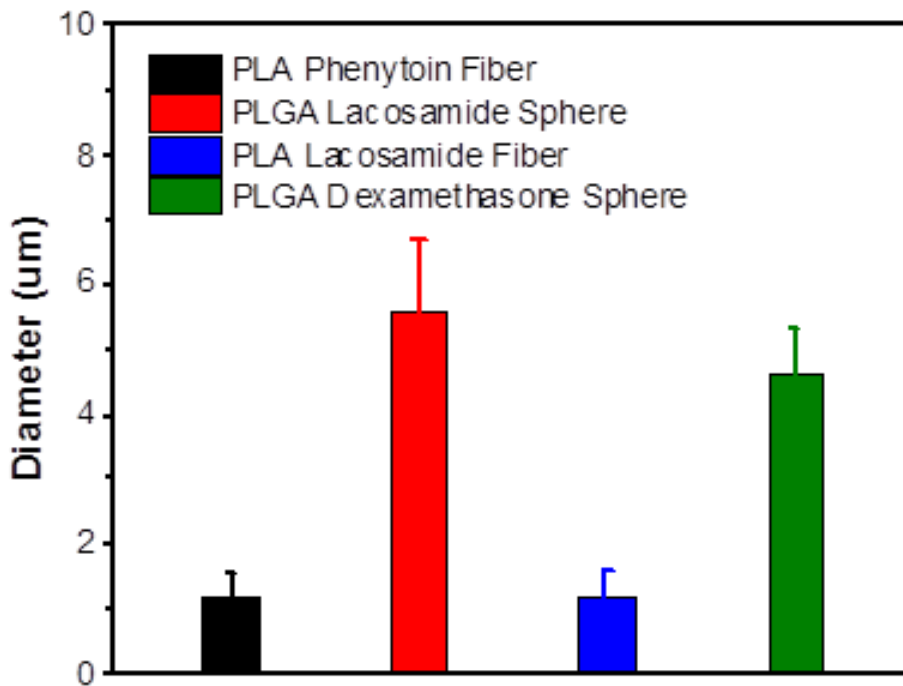


Figure 5.13 Dimensional statistical analysis results of diameters including PLA phenytoin fibres, PLGA lacosamide spheres, PLA lacosamide fibres, PLGA dexamethasone spheres.

The diameters of the microfibres and microspheres are assessed by analyzing the SEM images, and the results are shown in **Figure 5.13**. The diameters are $1.19 \pm 0.34 \mu\text{m}$ for PLA phenytoin microfibres, $5.57 \pm 1.15 \mu\text{m}$ for PLGA lacosamide microspheres, $1.22 \pm 0.37 \mu\text{m}$ for PLA lacosamide microfibres, and $4.63 \pm 0.68 \mu\text{m}$ for PLGA dexamethasone microspheres.

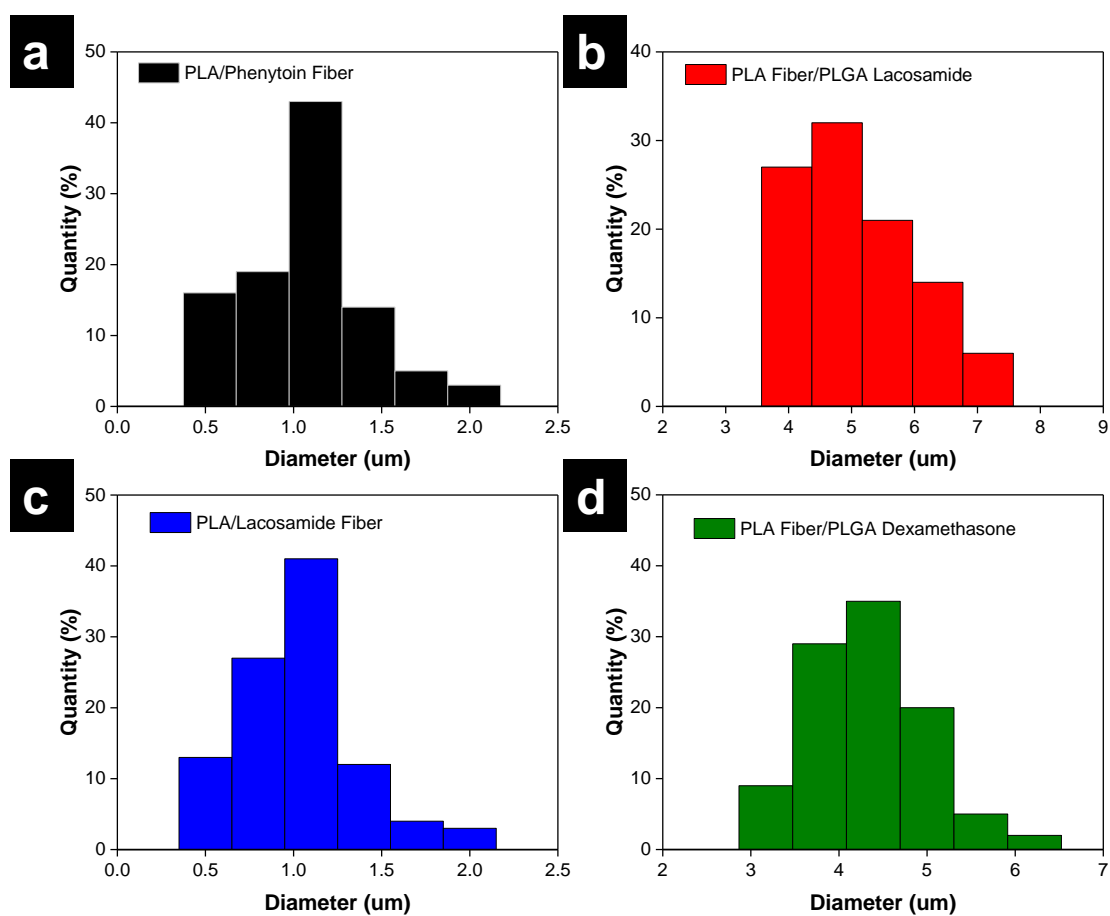


Figure 5.14 Diameters distribution of PLA phenytoin microfibres, PLGA lacosamide microspheres, PLA lacosamide microfibre, and PLGA dexamethasone microspheres.

Moreover, as shown in **Figure 5.14**, all the microfibrils and microspheres of the composite matrices exhibit narrow size distribution and uniform morphology. The mathematical modelling study is based on the equation (3.1) and using MATLAB Curve Fitting Toolbox.

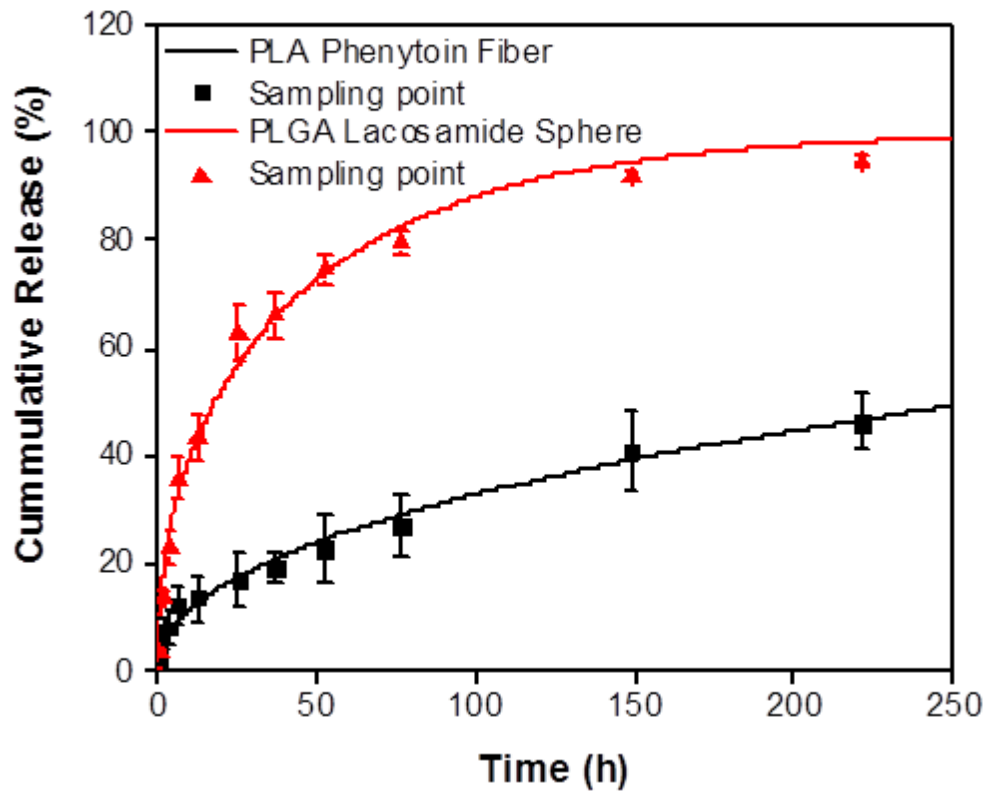


Figure 5.15 Mathematical modelling of drug release of PLA phenytoin fibres and PLGA lacosamide spheres (solid curves: theory fitting results, symbols and standard deviations: experimental sampling points).

The effective diffusivities of drugs are used as a least-squares fitting parameter, as shown in **Figure 5.15** and **Figure 5.16**, the theoretical predictions from the mathematical modelling are in agreement with the experimental cumulative release data. It indicates that drug release

from the microfibrils and microspheres of these composite matrices can be satisfactorily described as a time-dependent diffusion process [31]. The computed effective diffusivities are $1.49 \times 10^{-14} \text{ cm}^2/\text{min}$ for PLA phenytoin microfibrils, $1.48 \times 10^{-12} \text{ cm}^2/\text{min}$ for PLGA lacosamide microspheres, $9.62 \times 10^{-14} \text{ cm}^2/\text{min}$ for PLA lacosamide microfibrils, and $2.03 \times 10^{-12} \text{ cm}^2/\text{min}$ for PLGA dexamethasone microspheres. This is the reason why microspheres exhibit significantly faster release kinetics than those of microfibrils.

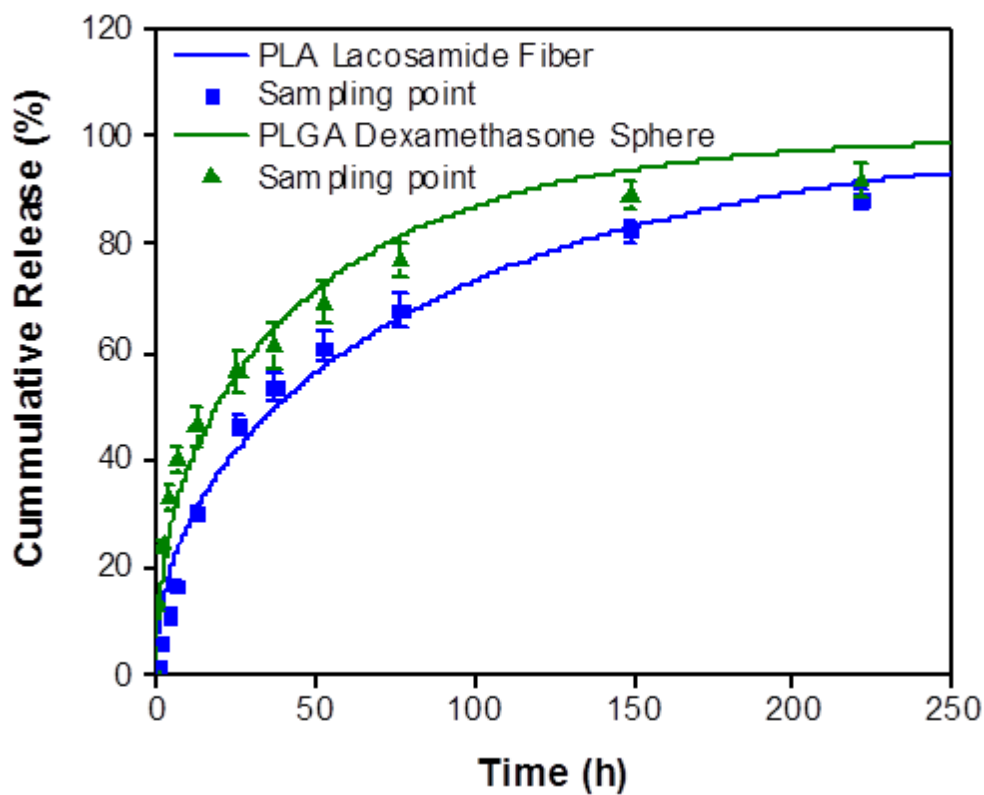


Figure 5.16 Mathematical modelling of drug release of PLA lacosamide fibres and PLGA dexamethasone spheres.

5.4 Conclusions

Overall, this study considered the use of a combinatorial electrospinning and electro spraying system to fabricate PLA microfibres/ PLGA microspheres composite matrices for dual drug delivery. The as-fabricated composite matrices showed favorable thermal and mechanical properties. And the microfibres and microspheres of the composite matrices demonstrated narrow size distribution, uniform morphology, and high efficiency of drug encapsulation. Independently controlled release behaviours are achieved in these dual drug delivery composite matrices. And the dosage ratio of different drugs in composite matrices could be tailored by simply varying the electrospinning and electro spraying time. The release profiles are fit well with the mathematical simulation model. This result indicates that the release kinetics is predictable. A similar strategy could be introduced to other dual drug release systems to provide a wide range of biomedical applications such as growth factor for cell culture or tissue engineering.

5.5 References

- [1] Pamies P, Stoddart A. Materials for drug delivery. *Nat Mater* 2013;12:957-957.
- [2] Cui W, Li J, Decher G. Self-assembled smart nanocarriers for targeted drug delivery. *Advanced Materials* 2016; 28:1302-1311 .
- [3] Mitragotri S, Lahann J. Materials for drug delivery: Innovative solutions to address complex biological hurdles. *Advanced Materials* 2012;24:3717-23.
- [4] Liu H, Webster TJ. Nanomedicine for implants: A review of studies and necessary experimental tools. *Biomaterials* 2007;28:354-69.
- [5] Anselmo AC, Mitragotri S. An overview of clinical and commercial impact of drug delivery systems. *Journal of Controlled Release* 2014;190:15-28.
- [6] Wei L, Cai C, Lin J, Chen T. Dual-drug delivery system based on hydrogel/micelle composites. *Biomaterials* 2009;30:2606-13.
- [7] Walsh C. Molecular mechanisms that confer antibacterial drug resistance. *Nature* 2000;406:775-81.
- [8] Aryal S, Hu C-MJ, Zhang L. Combinatorial drug conjugation enables nanoparticle dual-drug delivery. *Small* 2010;6:1442-8.
- [9] Lehar J, Krueger AS, Avery W, Heilbut AM, Johansen LM, Price ER, Rickles RJ, Short III GF, Staunton JE, Jin X, Lee MS, Zimmermann GR, Borisy AA. Synergistic drug combinations tend to improve therapeutically relevant selectivity. *Nat Biotech* 2009;27:659-66.
- [10] McDaid HM, Johnston PG. Synergistic interaction between paclitaxel and 8-chloro-adenosine 3', 5'-monophosphate in human ovarian carcinoma cell lines. *Clinical cancer research* 1999;5:215-20.

- [11] Calabrò F, Lorusso V, Rosati G, Manzione L, Frassinetti L, Sava T, Di Paula ED, Alonso S, Sternberg CN. Gemcitabine and paclitaxel every 2 weeks in patients with previously untreated urothelial carcinoma. *Cancer* 2009;115:2652-9.
- [12] Wang Y, Gao S, Ye W-H, Yoon HS, Yang Y-Y. Co-delivery of drugs and DNA from cationic core-shell nanoparticles self-assembled from a biodegradable copolymer. *Nat Mater* 2006;5:791-6.
- [13] Ahmed F, Pakunlu RI, Brannan A, Bates F, Minko T, Discher DE. Biodegradable polymersomes loaded with both paclitaxel and doxorubicin permeate and shrink tumors, inducing apoptosis in proportion to accumulated drug. *Journal of Controlled Release* 2006;116:150-8.
- [14] Sengupta S, Eavarone D, Capila I, Zhao G, Watson N, Kiziltepe T, Sasisekharan R. Temporal targeting of tumour cells and neovasculature with a nanoscale delivery system. *Nature* 2005;436:568-72.
- [15] Zhang L, Radovic-Moreno AF, Alexis F, Gu FX, Basto PA, Bagalkot V, Jon S, Langer RS, Farokhzad OC. Co-delivery of hydrophobic and hydrophilic drugs from nanoparticle–aptamer bioconjugates. *ChemMedChem* 2007;2:1268-71.
- [16] Hubbell JA, Langer R. Translating materials design to the clinic. *Nat Mater* 2013;12:963-6.
- [17] Chen Y, Yue Z, Moulton SE, Hayes P, Cook MJ, Wallace GG. A simple and versatile method for microencapsulation of anti-epileptic drugs for focal therapy of epilepsy. *Journal of Materials Chemistry B* 2015;3:7255-61.
- [18] Lavielle N, Hébraud A, Schlatter G, Thöny-Meyer L, Rossi RM, Popa A-M. Simultaneous Electrospinning and Electrospraying: A straightforward approach for fabricating hierarchically structured composite membranes. *ACS Applied Materials & Interfaces* 2013;5:10090-7.

- [19] Chen Y, Han D, Ouyang W, Chen S, Hou H, Zhao Y, Fong H. Fabrication and evaluation of polyamide 6 composites with electrospun polyimide nanofibers as skeletal framework. *Composites Part B: Engineering* 2012;43:2382-8.
- [20] Martinez SE, Bowen KA, Remsberg CM, Takemoto JK, Wright HM, Chen-Allen AV, Davies NM. High-performance liquid chromatographic analysis of lacosamide in canine serum using ultraviolet detection: application to pre-clinical pharmacokinetics in dogs. *Biomedical Chromatography* 2012;26:606-9.
- [21] Lin P-C, Hsieh Y-H, Liao F-F, Chen S-H. Determination of free and total levels of phenytoin in human plasma from patients with epilepsy by MEKC: An adequate alternative to HPLC. *Electrophoresis* 2010;31:1572-82.
- [22] Raval A, Parikh J, Engineer C. Dexamethasone eluting biodegradable polymeric matrix coated stent for intravascular drug delivery. *Chemical Engineering Research and Design* 2010;88:1479-84.
- [23] Almería B, Deng W, Fahmy TM, Gomez A. Controlling the morphology of electrospray-generated PLGA microparticles for drug delivery. *Journal of Colloid and Interface Science* 2010;343:125-33.
- [24] Soppirnath KS, Aminabhavi TM. Water transport and drug release study from cross-linked polyacrylamide grafted guar gum hydrogel microspheres for the controlled release application. *European Journal of Pharmaceutics and Biopharmaceutics* 2002;53:87-98.
- [25] D'Antone S, Bignotti F, Sartore L, D'Amore A, Spagnoli G, Penco M. Thermogravimetric investigation of two classes of block copolymers based on poly(lactic-glycolic acid) and poly(ϵ -caprolactone) or poly(ethylene glycol). *Polymer Degradation and Stability* 2001;74:119-24.

- [26] Cypes SH, Saltzman WM, Giannelis EP. Organosilicate-polymer drug delivery systems: controlled release and enhanced mechanical properties. *Journal of Controlled Release* 2003;90:163-9.
- [27] Huang C, Chen S, Reneker DH, Lai C, Hou H. High-strength mats from electrospun poly(p-phenylene biphenyltetracarboximide) nanofibers. *Advanced Materials* 2006;18:668-71.
- [28] Molnár S, Pukánszky B, Hammer CO, Maurer FHJ. Impact fracture study of multicomponent polypropylene composites. *Polymer* 2000;41:1529-39.
- [29] Lau K-t, Shi S-Q, Cheng H-m. Micro-mechanical properties and morphological observation on fracture surfaces of carbon nanotube composites pre-treated at different temperatures. *Composites Science and Technology* 2003;63:1161-4.
- [30] Freytag T, Dashevsky A, Tillman L, Hardee GE, Bodmeier R. Improvement of the encapsulation efficiency of oligonucleotide-containing biodegradable microspheres. *Journal of Controlled Release* 2000;69:197-207.
- [31] Fattahi P, Borhan A, Abidian MR. Microencapsulation of chemotherapeutics into monodisperse and tunable biodegradable polymers via electrified liquid jets: Control of size, shape, and drug release. *Advanced Materials* 2013;25:4555-60.

**CHAPTER 6: CONDUCTING AND
BIODEGRADABLE POLYMERS
COMBINED 3-DIMENSIONAL
ELECTRODES DELIVERY SYSTEMS**

6.1 Introduction

Conducting polymers (CPs) have received considerable interest in recent decades for their unique and tunable physical and chemical properties [1-5]. Their attractive electrical, optical, mechanical, and interfacial properties are derived from their conjugated π -electron system. CPs have been investigated for numerous biomedical applications, including electrically controlled release [6-9], tissue engineering [10, 11] [12], neural prosthesis [13, 14], bio-sensors [15], and bio-actuators [16, 17] et al. . In these applications, polypyrrole (PPy) and poly(3,4-ethylenedioxythiophene) (PEDOT) are popular candidates because of their chemical stability, superior conductivity, and biocompatibility. Moreover, they can be readily prepared by chemical or electrochemical means [4]. During the course of preparation, appropriately sized biomolecules and drugs can be incorporated into the polymer matrices. In addition, these polymers exhibit low electrochemical impedance, and this facilitates controlled release of the entrapped bioactive molecules via electrical stimulation [6].

To date, most of the CPs based electrical stimuli drug delivery systems have been limited to 2D configurations [7, 18]. However, many clinical applications in drug delivery require more sophisticated structures in three dimensions, in addition to biocompatibility and excellent mechanical properties[19]. It is a huge challenge to progress towards 3D electroactive delivery systems with well-controlled internal structures, because of their poor processability (poor solubility in solvents and inability to directly melt process) of CPs. What's more, free standing films of CPs tend to be brittle, inflexible and have poor conductivity. To overcome these drawbacks, attention has been given to developing CP coatings on prefabricated 3D electrode systems[7].

Recently, additive manufacturing, also known as 3D printing, has shown great promise as a novel technology for fabrication of 3D constructs with sophisticated internal structures. 3D printing involves layer-by-layer deposition of materials, which is controlled digitally, and thus can deliver complex, personalized and on-demand products. More recently, 3D printing has attracted increasing interest in pharmaceutical manufacturing. Progress has resulted in the Food and Drug Administration (FDA) approval of 3D printed drug products from August 2015 [20, 21].

Selective laser melting (SLM) is a popular 3D printing process to fabricate metal products [22]. During the SLM process, the laser beam selectively melts successive layers of metallic powder. Upon irradiation, the powder melts and forms a liquid pool. Then, it solidifies quickly to form 3D structures according to a 3D Computer-aided design (CAD) volume model. Being able to design and create geometrically complex metallic objects, it could be interesting for the application of SLM products in CPs drug delivery systems.

In previous chapters, a set of biodegradable microcapsules including microspheres and microfibrils have been developed. Moreover, composite membranes composed of these microcapsules also have been fabricated as dual drug delivery systems that can be used for combination therapy. In this chapter, an attempt at the application of these biodegradable microcapsules in 3D printed electrodes is considered. The attempt also aims to explore the way to continue development of dual drug delivery systems for combination therapy. Fortunately, the 3D printed electrodes based on the interdigitated structures offer the possibility of combining these biodegradable microcapsules with CPs in the third dimension [23].

This chapter aims to demonstrate a new 3D system for the controlled release of antiepileptic drugs by electrical stimulation. 3D printed (selective laser melting) interdigitated Ti₆Al₄V electrodes serve as the structural support for the electropolymerized outer layer of polypyrrole (PPy). Fosphenytoin is an anti-epilepsy prodrug (AED) and is used as the dopant for the preparation of the 3D PPy coating. The release of fosphenytoin in artificial cerebrospinal fluid (aCSF) from the 3D drug delivery system is controlled by switching the redox state of PPy. Moreover, combined with biodegradable microspheres which contain dexamethasone (independently coated on the electrode), two interdigitated electrodes can serve as a multi-functional drug delivery system. The electrical conductivity, biocompatibility and tuneable release properties of the 3D printed drug delivery system can also lead to promising localized treatment of other central nervous system diseases.

6.2 Experimental

6.2.1 Materials

Ti-6Al-4V powder was from TLS Technik Spezialpulver. Pyrrole monomer was from Merck and was freshly distilled before use. Poly(D,L lactic-co-glycolic acid) (PLGA) ($M_w \sim 60,000$ Da, molar ratio of lactide to glycolide, 75 to 25) was purchased from Purac, Singapore. Fosphenytoin and dexamethasone were purchased from Sigma-Aldrich, and used as received. All the others chemicals and reagents were purchased from Sigma-Aldrich and used as received without further purification.

6.2.2 3D printing of interdigitated electrodes

The 3D interdigitated electrodes were designed using SolidWorks modelling software. After that, the electrodes were printed by using a Realizer SLM50 metal printer (Germany). The printer is based on the additive manufacturing technology which is called Selective Laser Melting (SLM). Before printing, the printer's chamber is evacuated and then filled with an inert argon atmosphere. The high-powered laser beam of the printer focused on a bed of fine Ti-6Al-4V powder. The laser selectively fuses the particles in a layer-by-layer fashion. All untouched powder remains as it is and becomes a support structure for the electrode.

6.2.3 3D coating of fosphenytoin loaded conducting film

Milli-Q water and ethanol were used to clean the 3D printed Ti alloy electrodes. A solution containing 0.2 M pyrrole monomer and 0.02 M fosphenytoin was prepared in Milli-Q water. Electrochemical polymerization was carried out using a CHI 600 (CH Instruments) at a constant potential of 0.8 V for 20 mins at room temperature. The applied reference electrode was silver/silver chloride reference electrode, and the counter electrode was stainless steel mesh. The electrodes were rinsed with a Milli-Q water/ethanol mixture in order to remove any residual fos-phenytoin, pyrrole, and oligomers on the surface. Then, the electrodes were dried in a vacuum oven at room temperature for 24 hours.

6.2.4 Electrospray coating of PLGA dexamethasone microspheres on the 3D electrodes

PLGA was dissolved in chloroform at 4 wt.%; subsequently, dexamethasone was added into the PLGA solution to obtain the electrospraying solution (PLGA:dexamethasone, 10:1). After encapsulation efficiency testing, a drug loading of 9.35 % was achieved. The solution was

held in a syringe with a stainless steel needle having an orifice of 0.34 mm. The needle was electrically connected to a positive high voltage power supply of NANON-01A electrojetting systems (MECC Co. Ltd, Japan). Electro spraying was carried out in the electrojetting systems' chamber at room temperature. During the electro spraying process, a positive high voltage of 10 kV was applied to the needle, and the solution flow rate of 0.5 mL/h was maintained by using a syringe pump. Electro sprayed PLGA/dexamethasone microspheres were collected on the surface of the 3D printed electrodes. After that, the electrodes were held at room temperature for 48 hours in a fume hood to allow completion of the residual solvent evaporation.

6.2.5 Scanning electron microscope

The morphology characterization was performed by JEOL JSM-7500FA scanning electron microscope (SEM) with field emission gun (FEG). For conductive Ti alloy electrodes and polypyrrole, SEM testing was conducted directly without sputter-coating. Non-conductive PLGA microspheres were sputter-coated with 20 nm gold before SEM testing.

6.2.6 Electrochemical measurements

Electrochemical impedance spectroscopy (EIS) was measured using a Gamry EIS 3000 TM system with Gamry framework software using a three-electrode system. The frequency range was from 0.1 Hz to 100 kHz, and the AC perturbation was 5 mV at open circuit potential. Cyclic voltammetry (CV) was carried out in a three-electrode system with a Pt counter electrode and Ag/AgCl reference electrode by using a CHI 600 (CH Instruments) apparatus.

A scan rate of 100 mV/s was used, and the potential applied was swept between -1.0 and 0.5 V.

6.2.7 In vitro electrically controlled drug release

Electrically controlled drug release experiments were carried out in a three-electrode electrochemical cell using artificial cerebrospinal fluid (aCSF) as the release medium. A square wave, biphasic voltage stimulation was used for electrically stimulating drug release. The applied negative potentials were -1 V, -0.5 V, and -0.25 V, respectively, and the positive potential was 0.5 V. Each square wave (cycle) of the electrical stimulation was a 50% duty cycle; 5 seconds of negative potential and 5 seconds of positive potential. Every 30 cycles (or more) of square wave electrical stimulation, the release medium was collected and replenished with fresh aCSF. For comparison, passive drug release study was also conducted without electrical stimulation.

6.2.8 PLGA microsphere diametric statistics and drug release study

Diametric statistics was conducted by analysis of the high magnification SEM micrographs using the imaging software, Leica Application Suite. Drug release study was conducted in aCSF. The electrodes with PLGA microsphere were directly immersed in a certain amount of aCSF. All the samples were incubated in a shaking water bath at a constant temperature of 37 °C. The release media was replaced with the same amount of fresh aCSF periodically. An extraction method was used to evaluate the drug encapsulation efficiency of the microsphere as described in our previous work [24]. In order to predict the release profile of

dexamethasone from the electrosprayed coating, the mathematical analysis was conducted based on a time-dependent diffusion model and using MATLAB Curve Fitting Toolbox.

6.2.9 Determination of the amount of released fosphenytoin and dexamethasone

Both the amounts of fosphenytoin and dexamethasone were determined by HPLC, using an Agilent 1260 Infinity HPLC system. The analytical column was Atlantis[®] T3 C18 column (5 μ m, 250 mm \times 4.60 mm). For fos-phenytoin testing, the mobile phase consisted of 35% (v/v) methanol and 65% (v/v) of Milli-Q water. The pH was adjusted to \sim 3.8 with orthophosphoric acid; the flow rate was 1 mL/min; the wavelength of UV was 210 nm. For dexamethasone testing, the mobile phase consisted of Milli-Q water and acetonitrile (35:65, v/v) with 0.1 % trifluoroacetic acid (v/v); the flow rate was 1.0 mL/min; UV detection wavelength was set at 242 nm. The amounts of the released drug were calculated according to a pre-established calibration curve.

6.3 Results and Discussion

6.3.1 Fabrication and assembly of the interdigitated 3D electrodes

The 3D interdigitated electrodes were designed and printed by using selective laser melting (SLM). As shown in **Figure 6.1a**, electropolymerization was used to deposit a film of PPy and fosphenytoin on the surface of the 3D electrodes. In the solution containing dopant, the pyrrole monomers became electrically oxidized and underwent polymerization. During polymerization, the polymer backbone was positively charged, and the anionic dopant

molecule was incorporated to maintain charge neutrality [25]. In this study, the dopant was fosphenytoin, which is a water-soluble phenytoin prodrug and can be converted into the active form, namely phenytoin. It is often used in the acute treatment of epilepsy [26].

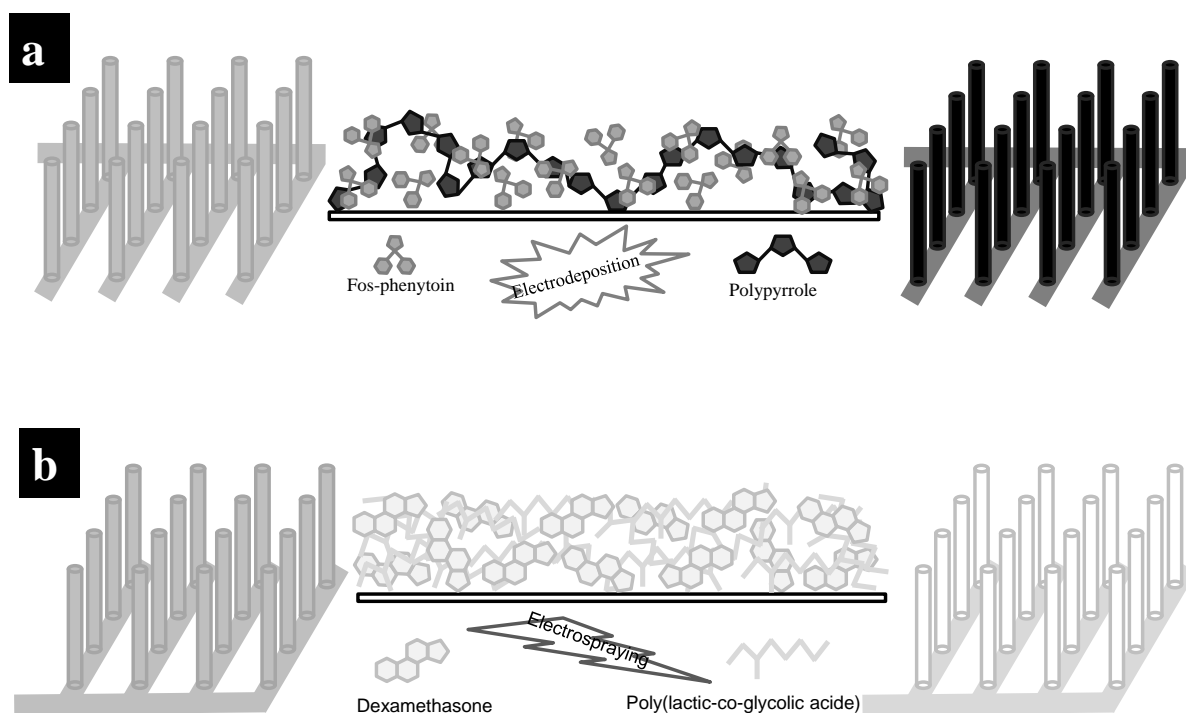


Figure 6.1 Schematic illustration of the fabrication procedures of a) electropolymerization of PPy fos-phenytoin on the 3D printed electrodes; b) electrospayed PLGA microspheres coating on 3D electrodes.

In order to incorporate the non-anionic drug into the printed 3D electrodes drug delivery system, PLGA microspheres were fabricated by electrospay as drug carrier and coated on the surface of the electrodes (**Figure 6.1b**). Dexamethasone was used as a model drug because of its wide application in anti-inflammatory uses and is an immunosuppressant [27]. Our electrodes drug delivery system is aimed at local implantation for treatment of epilepsy, therefore, inflammation and immune response may be inevitable [28]. Dexamethasone loaded PLGA microspheres coated 3D electrodes were prepared using electrospaying of PLGA-

dexamethasone chloroform solution and coating on the surface of the posts of the 3D electrode. Several parameters including the concentration of PLGA, solution feed rate, and applied voltage were tested in order to obtain appropriate microspheres. It was observed that the as-fabricated microspheres could attach firmly, not just with each other, but also on the surface of the electrodes. This is probably due to incomplete solvent evaporation when the PLGA microspheres were reaching onto the electrode collector [29].

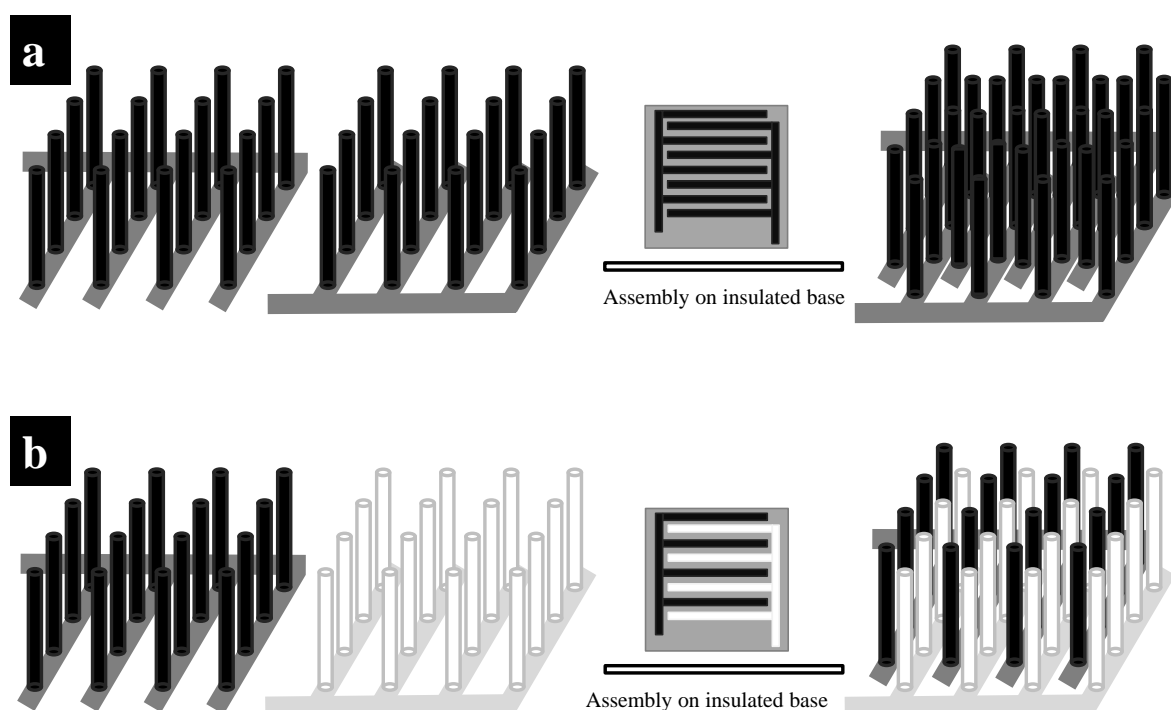


Figure 6.2 Schematic of fabrication procedures of a) assembly process of two interdigitated PPy fos-phenytoin coated electrodes; b) assembly process of interdigitated PPy fos-phenytoin coated electrode and electrospray PLGA microspheres coated 3D electrode on insulated base.

Figure 6.2 shows the interdigitated electrodes device assembly process. After electropolymerization or electro spraying, two halves of the interdigitated electrodes were

assembled on their insulated bases and served as alternating working and counter electrodes when subject to biphasic square wave electrical stimulation. This interdigitated structure combined them together and afforded more materials loading within the same dimension [30]. Furthermore, the size of the posts in these electrodes could be reduced to further increase the total materials loading. What's more, the size of the 3D electrode drug release device could be adjusted, depending on the particular application.

6.3.2 Scanning Electron Microscopy

The electrodes used in this study were 1 cm by 1cm by 1 cm and contain 54 posts. Each post had a ~500 μm diameter and 8 mm height. The High magnification SEM image shows that there are many partially welded metal particles distributed on the surface of the post (**Figure 6.3a,b**).

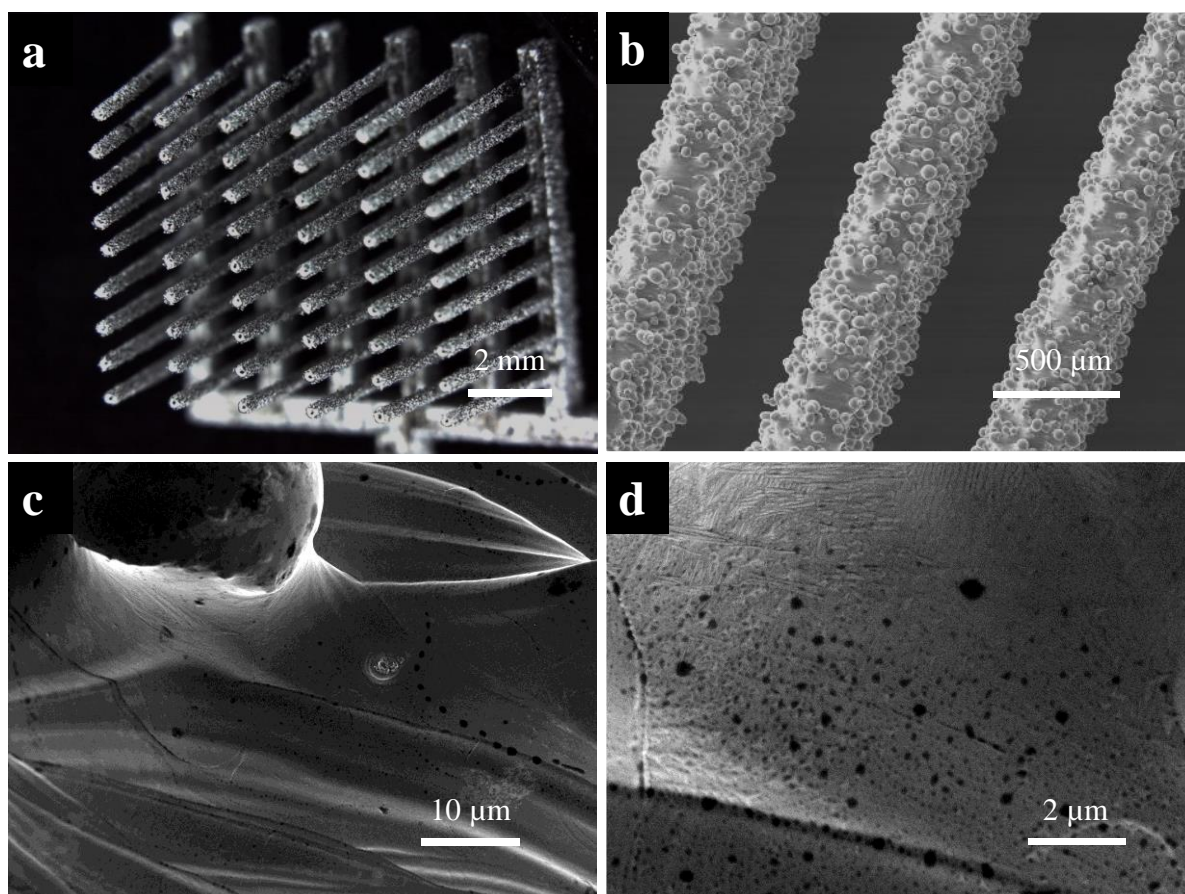


Figure 6.3 Scanning Electron Microscopy images of a,b) a whole 3D electrode and individual post; c,d) high magnification of the bare 3D electrode.

This provides an enhanced surface area for the electropolymerization. After electropolymerization, the smooth metal surface (**Figure 6.3c,d**) is covered by a layer of PPy fos-phenytoin film with cauliflower morphology (higher magnification of **Figure 6.4b**).

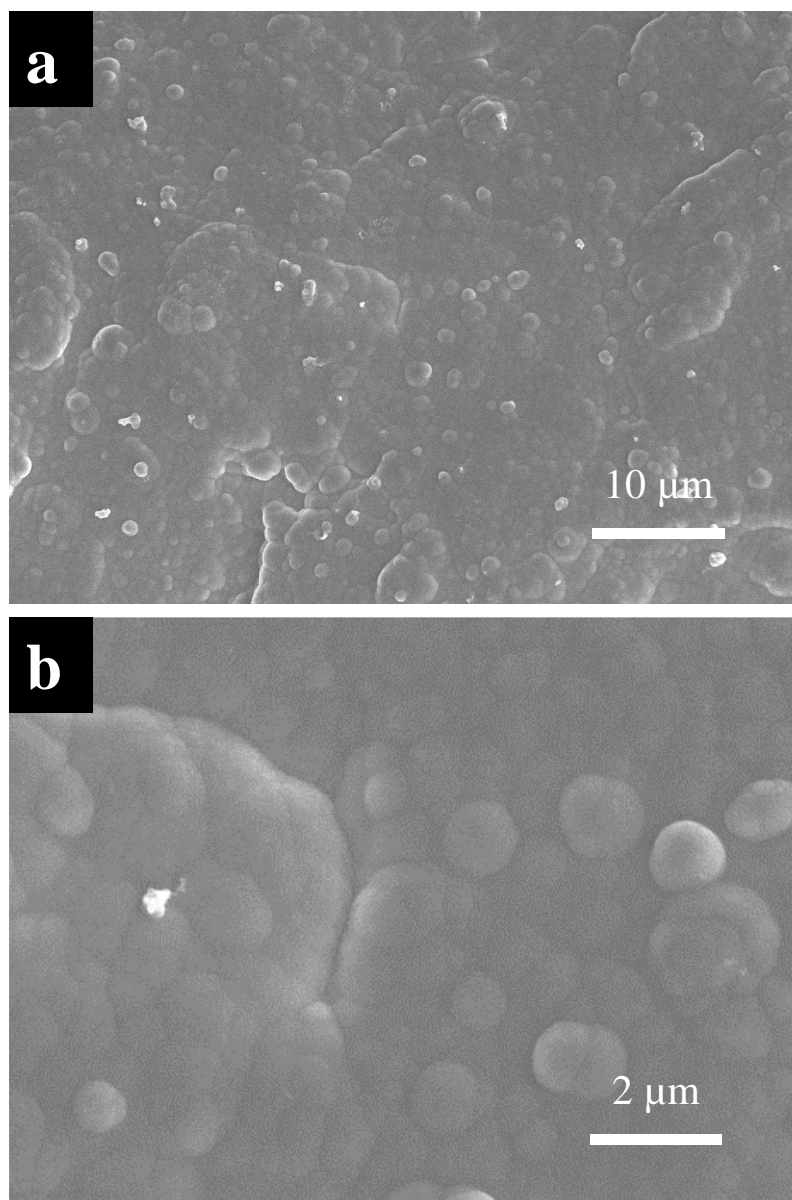


Figure 6.4 Scanning Electron Microscopy images of the PPy-fosphenytoin coating.

The dexamethasone loaded PLGA microspheres are coated on another electrode rather than on the same electrode with PPy-fosphenytoin. This aims to minimise the interaction of the drug release. As shown in **Figure 6.5**, it is noted that there are many gaps between the microspheres, which enhances the PLGA microsphere coated 3D electrode's contact with the

release media. The release media penetrates into the microsphere coating then contacts the surface of the electrode.

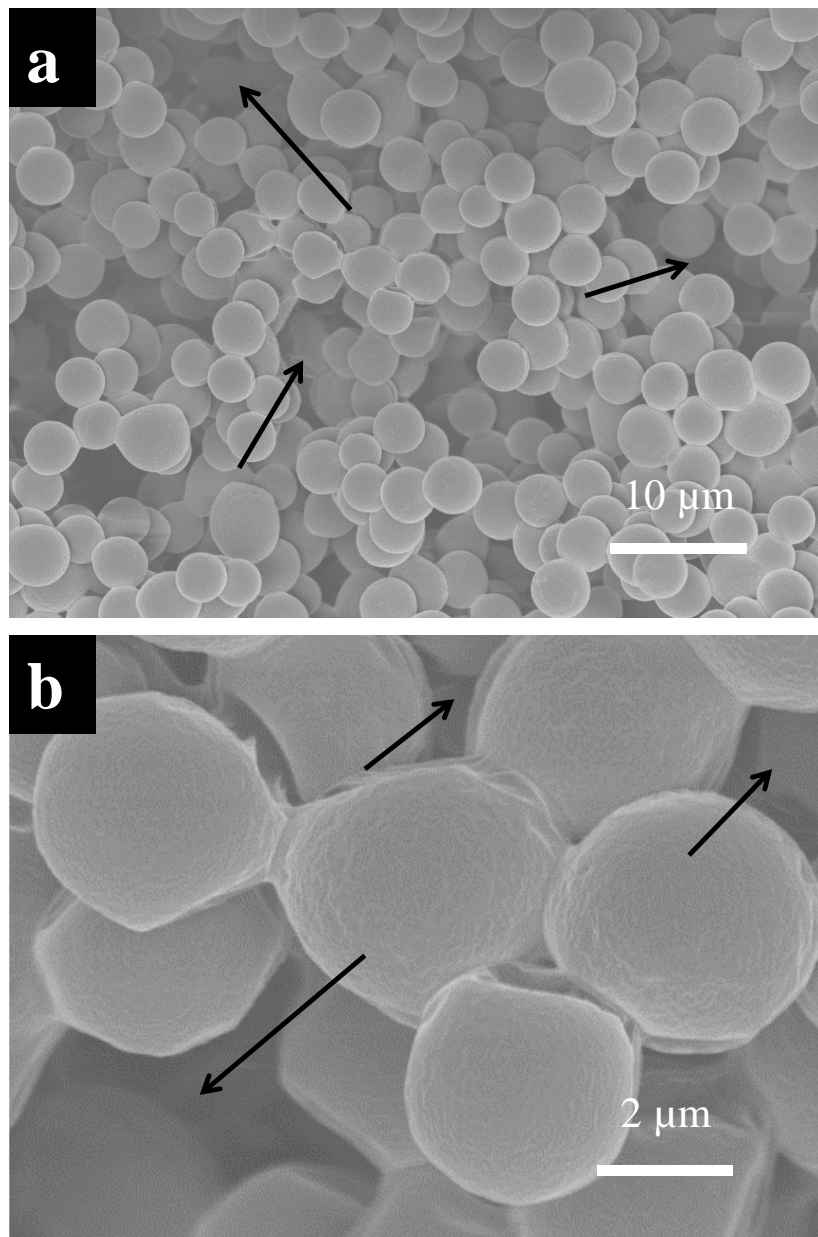


Figure 6.5 Scanning Electron Microscopy images of electrospayed PLGA dexamethasone coated 3D electrode. The arrows are pointing to the gaps between the microspheres.

6.3.3 Electrochemical impedance spectroscopy

The electrical properties of the 3D electrodes were tested using electrochemical impedance spectroscopy (EIS) and cyclic voltammetry. EIS was used to assess the conductivity of the bare electrode, PPy coated electrode and PLGA microsphere-coated electrode over the frequency from 1 Hz to 100 kHz (Figure 6.6).

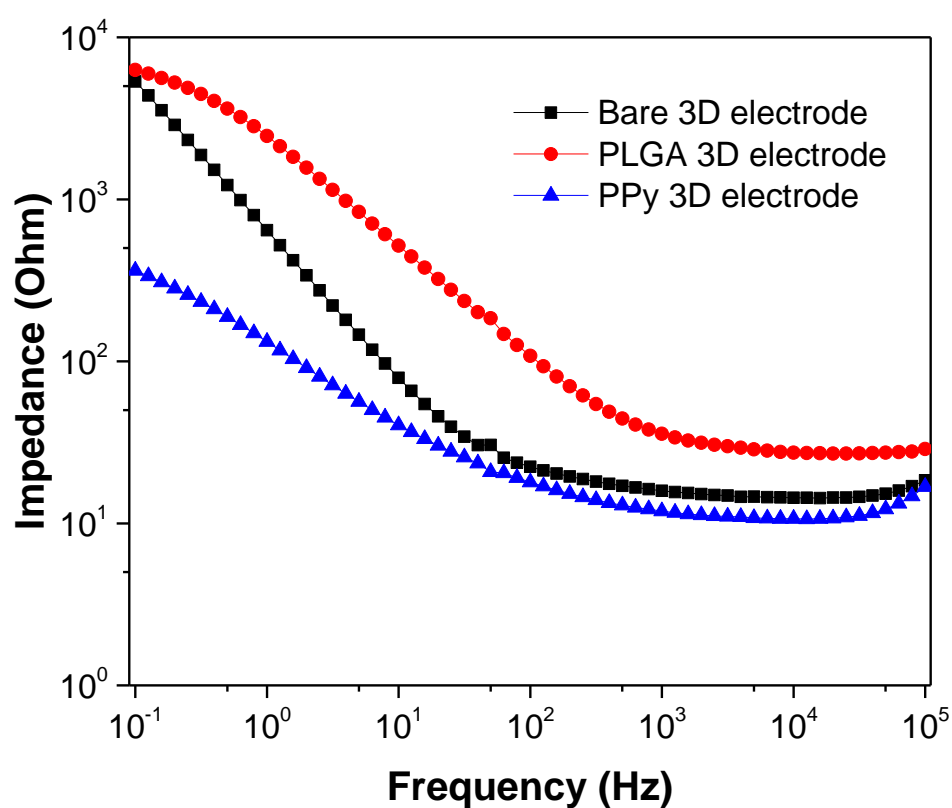


Figure 6.6 The electrochemical testing results of Impedance spectra for bare 3D electrode, PLGA dexamethasone microspheres coated 3D electrode, and PPy fos-phenytoin modified 3D electrode.

The impedance of the bare electrode was from $\sim 5.34 \text{ k}\Omega$ to $\sim 18 \Omega$. After PLGA microspheres were coated on the surface, the impedance across all frequencies was increased, from $\sim 6.28 \text{ k}\Omega$ to $\sim 29 \Omega$. However, the impedance initially significantly decreased and then slowly decreased after deposition of the PPy, from $\sim 360 \Omega$ to 16Ω . In the study here, the impedance at 1 kHz is particularly important. Since it corresponds to the characteristic frequency of neuronal action potentials [6, 31]. For the bare electrode, the impedance at 1 kHz was $\sim 16 \Omega$; it was increased to $\sim 36 \Omega$ for the PLGA microsphere-coated electrode but was decreased to $\sim 12 \Omega$ for the PPy-coated electrode. These indicate that the PLGA microspheres diminish the capacitance, while PPy coating improves the capacitance of the electrode interface. However, the modifications are not dramatic at this frequency.

6.3.4 Cyclic Voltammetry

Cyclic Voltammetry (CV) provides information about the intrinsic redox behaviour of the electrode materials (**Figure 6.7**). CV analysis results showed that both the bare electrode and PLGA microsphere-coated electrode demonstrated negligible charge-storage capacity compared with the PPy-coated electrode. The charge-storage capacity was calculated from the integrated area of the CV curves. The CV curve of the PPy-coated electrode exhibits a reduction peak at -0.71 V and an oxidation peak at -0.06 V . The reduction peak due to the anionic fos-phenytoin molecules leave the PPy film as a consequence of the negative potential sweeping. And the oxidation peak is related to re-doping of small ions in the testing media [7]. The huge reduction peak of the PPy coated electrode indicates a large amount of drug leaving the PPy film [32]. Also, with a lower impedance of the PPy coated electrode, more current will pass through the PPy film under a particular voltage pulse. It also shows that more efficient drug release would be obtained.

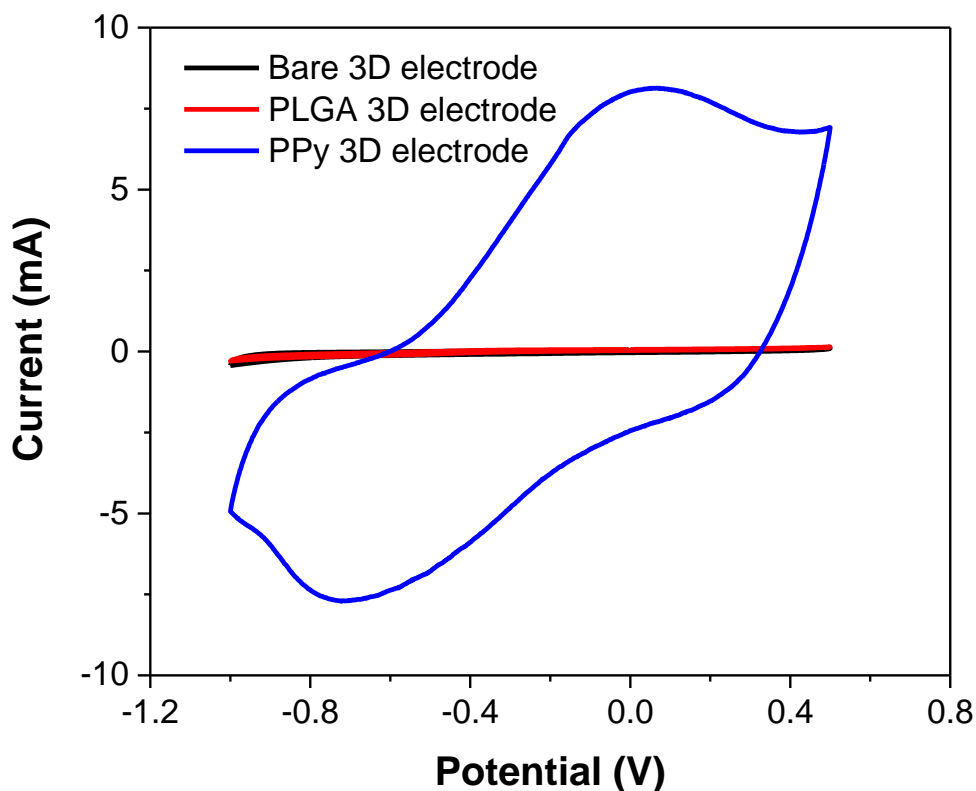


Figure 6.7 Cyclic voltammograms of the bare 3D electrode, PLGA dexamethasone microspheres coated 3D electrode, and PPy fos-phenytoin modified 3D electrode.

6.3.5 Electrically controlled release of fosphenytoin

The electrically controlled release performance of the PPy coated 3D electrodes was studied in aCSF solution by applying voltage pulses. The amount of released fosphenytoin was determined by HPLC. The electrically triggered release possibly involves a synergistic process of electrochemical reduction/oxidation and electrically driven movement of charged molecules. In this study, anionic fos-phenytoin molecules were incorporated into the PPy coating [6, 32, 33]. When the PPy coating is electrochemically reduced, the fosphenytoin molecules will be released. The release of the drug is associated with the change of the

overall net charge along the PPy backbone in the oxidized form. The drug released during the reduction process [33].

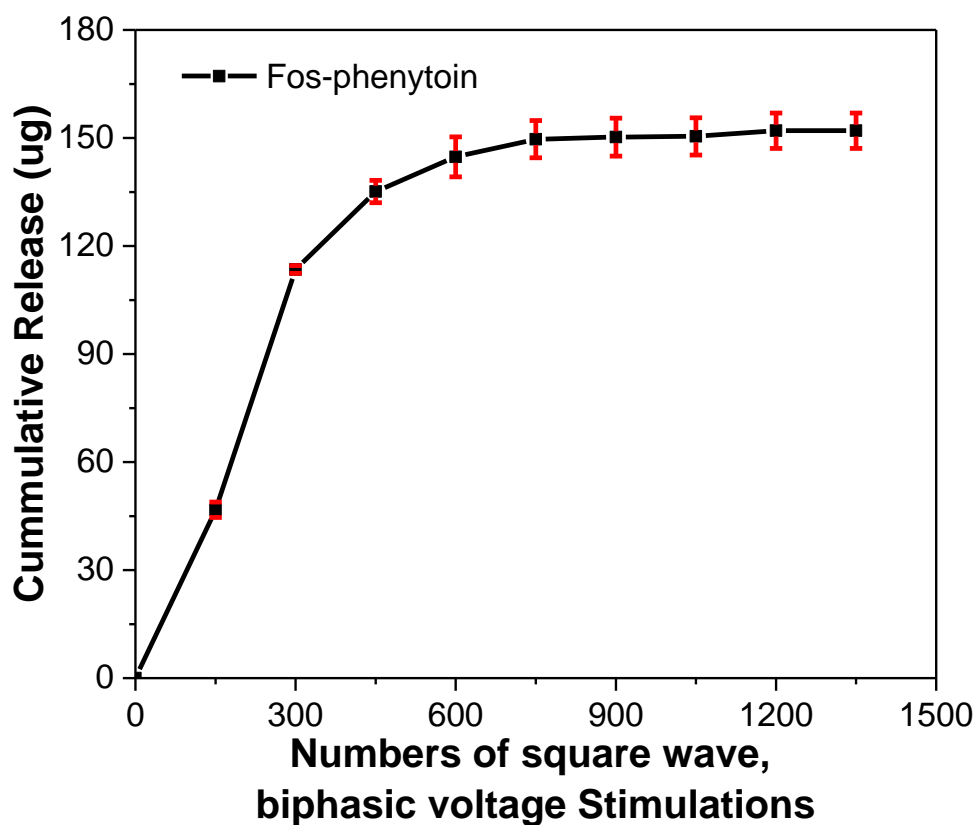


Figure 6.8 Electrically controlled fos-phenytoin release: a) cumulative release profile using repeated square wave, biphasic voltage stimulation (-1 V for 5s, followed by 0 V for 5s) to determine the total available drug.

To evaluate the maximum amount of fosphenytoin released from the PPy coating, an aggressive, biphasic voltage pulse (-1 V for 5s, followed by 0 V for 5s) was used as

stimulation until no obvious drug release could be detected (~1400 stimulations). The drug release curve in **Figure 6.8** shows a plateau after ~750 stimulations, after which no significant amount of drug release was detected.

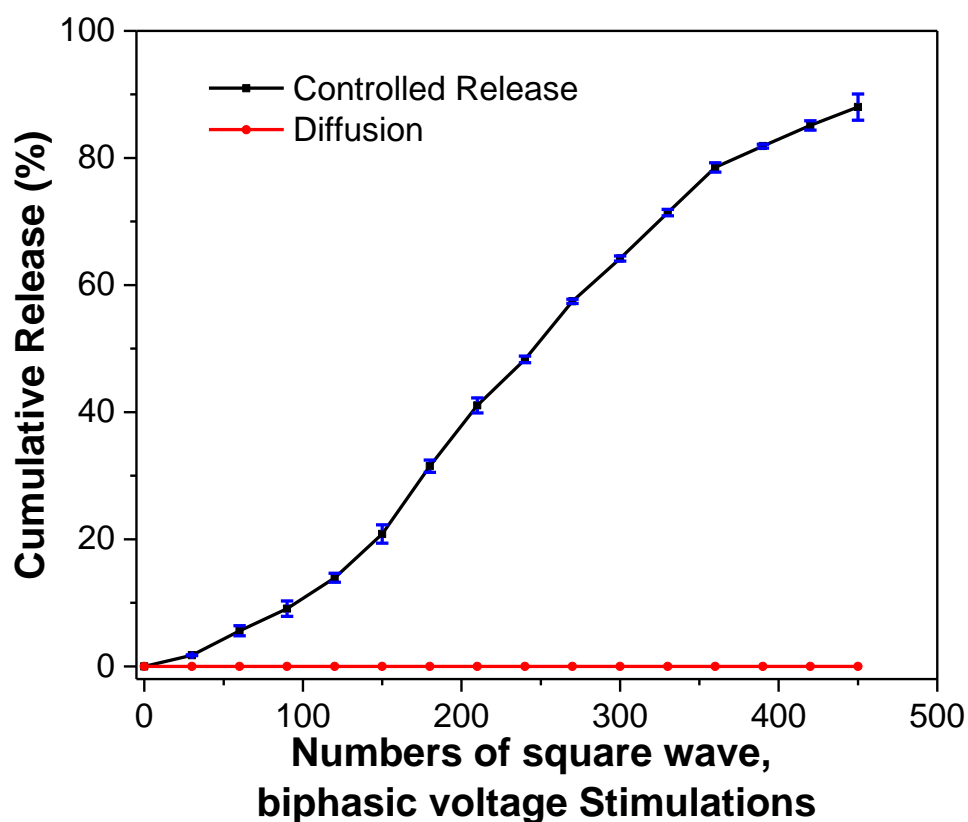


Figure 6.9 Cumulative release profiles in response to milder electrical square wave, biphasic voltage stimulation (-0.5 V for 5s, followed by 0.5 V for 5s), and without electrical stimulation.

Upon milder electrical stimulation (-0.5 V for 5s, followed by 0.5 V for 5s), a near-linear drug release profile is obtained (**Figure 6.9**). Without stimulation, there was no detection of any significant amounts of drug eluted from the 3D electrode. This is consistent with others’

observation, which suggests that this system under consideration is capable of true electrically controlled release property [32]. In order to demonstrate the flexibility in dosage control, further drug release studies under different voltage (x) biphasic stimulations (x V for 5s, followed by 0.5 V for 5s) up to 120, where the negative phase (x) was varied from -0.25 to -1 V, the positive phase was 0.5 V were performed. The released amount of drug increased with increasing negative voltage, from $13.1 \pm 5.2 \mu\text{g}$ to $54.9 \pm 5.8 \mu\text{g}$ (**Figure 6.10**).

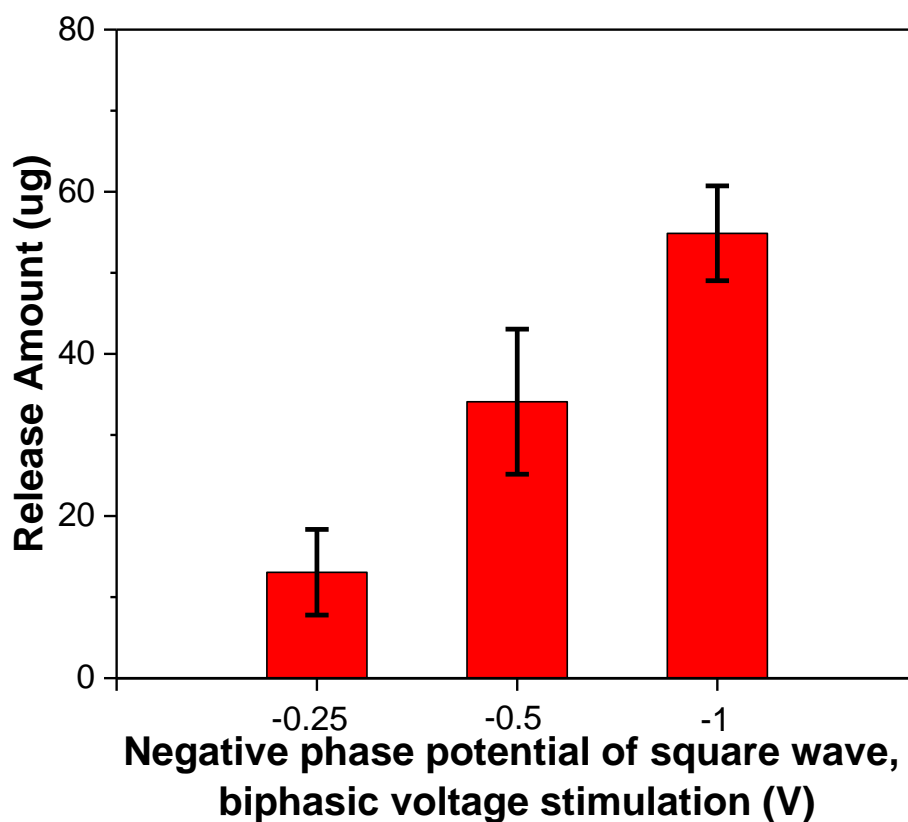


Figure 6.10 Release amount under 120 cycles of different square wave, biphasic voltage stimulation, where the negative phase is -0.25, -0.5, -1 V, positive phase is 0.5 V.

Compared with the single half-electrode, the cumulative amount of released drug from two interdigitated electrodes was $276 \pm 25.3 \mu\text{g}$, an increase of 82 % (after 1200 cycles, **Figure 6.11**). This highlights the advantage of interdigitated electrodes in the application of electrically controlled drug delivery. [7].

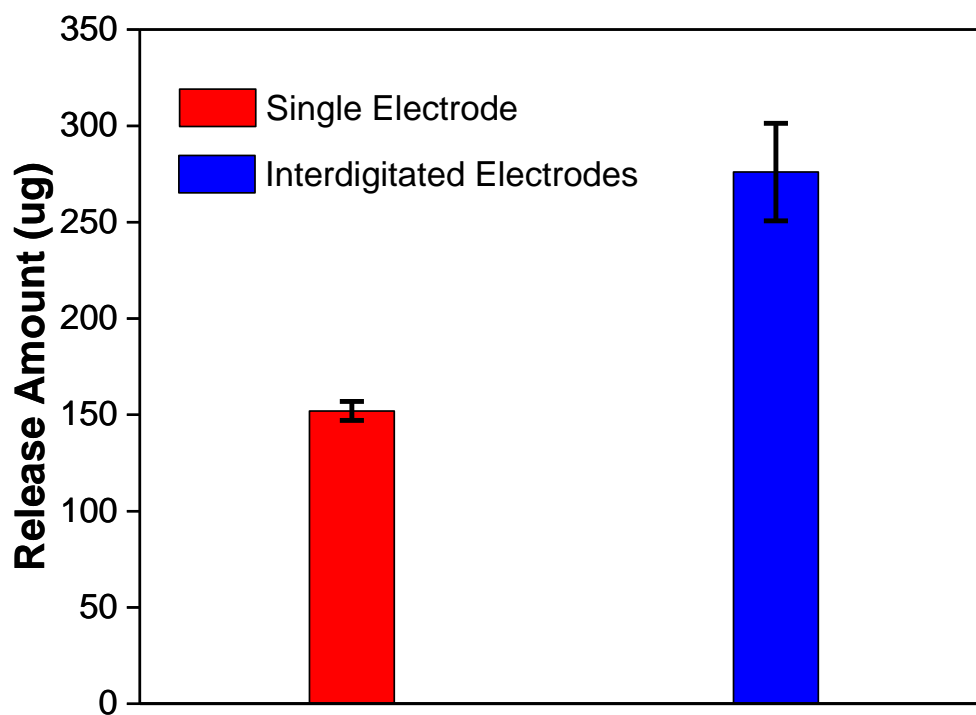


Figure 6.11 Comparison of the release amount from a single 3D electrode with that from two interdigitated 3D electrodes.

As shown in **Figure 6.12**, after 1200 cycles of electrical stimulations (pulsed waveform; -0.5 V for 5s, followed by 0.5 V for 5s), no obvious delamination or breakdown was observed on the surface of the PPy coating, indicating good stability.

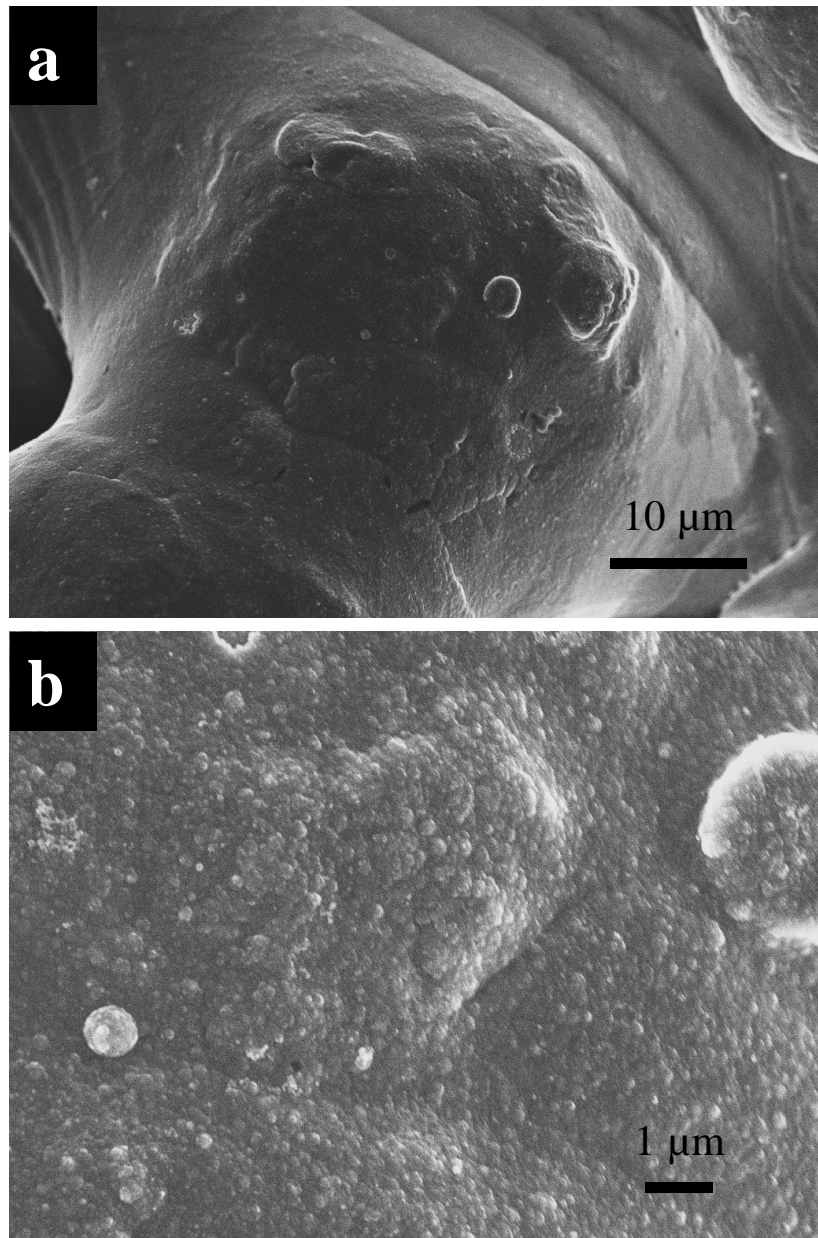


Figure 6.12 SEM images of the PPy fos-phenytoin coating after 1200 cycles of electrical square wave, biphasic voltage stimulation (-0.5 V for 5s, followed by 0.5 V for 5s), no obvious delamination or breakdown was observed on the surface of the PPy coating.

6.3.6 Drug release study of 3D electrode coated with PLGA/dexamethasone microspheres coating

The drug encapsulation efficiency and drug release were first investigated by using an extraction method as previously reported [34]. For effective drug action, improving the drug encapsulation efficiency is critical in drug carrier research [35].

The PLGA microspheres coating exhibit excellent drug encapsulation efficiency as high as $93.5 \pm 5.1\%$. The ultra-high drug encapsulation efficiency can be attributed to fast solidification rate and minimum drug loss during the PLGA microspheres coating fabrication process. Since the dexamethasone is directly encapsulated in PLGA by electro spraying, the drug loss through diffusion into other continuous liquid phase is eliminated [37].

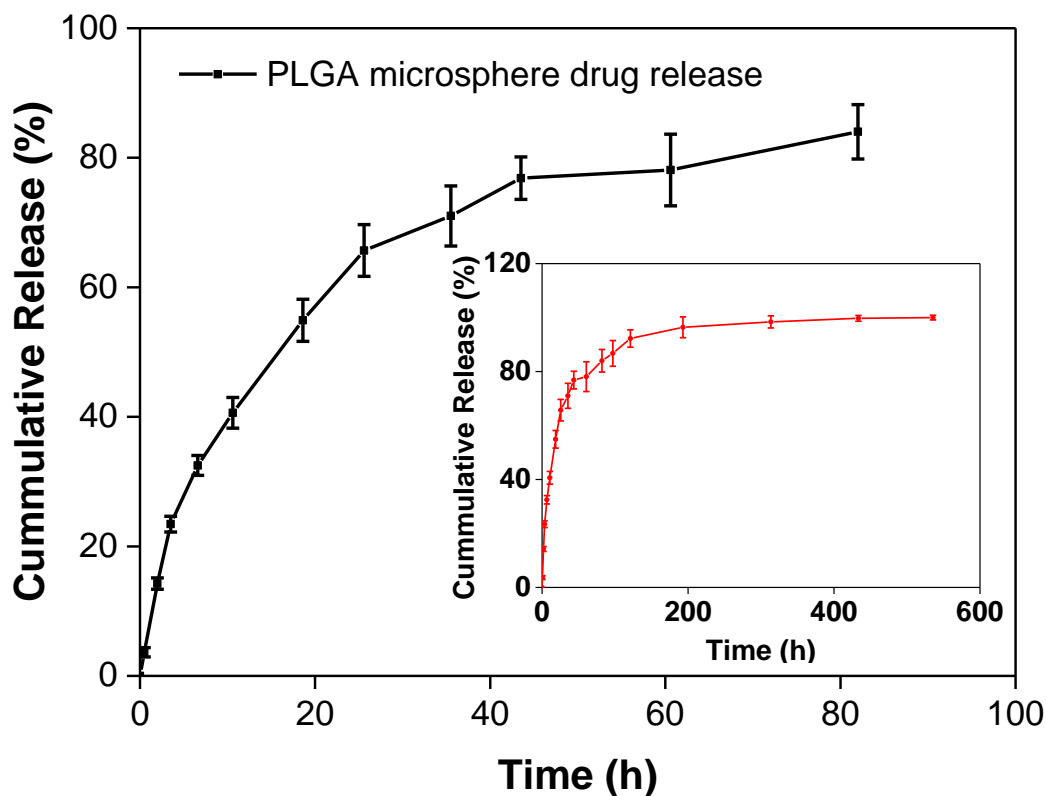


Figure 6.13 Cumulative release of PLGA dexamethasone microspheres coating in aCSF (pH 7.4) at 37 °C.

The in vitro release profile of dexamethasone from the electrospray PLGA microspheres coating is shown in **Figure 6.13**. It shows an initial burst, followed by a long period of gradual slowing release over nearly two weeks for the PLGA microspheres coating. Besides by diffusion through the polymer barrier, the dexamethasone release from the PLGA microspheres coating also occurs by erosion of the microspheres, due to the hydrolytic degradation of the ester linkages. This degradation leads to formation of interconnecting pores and channels within the microspheres in the coating which would increase diffusion of the dexamethasone into the aCSF solution. The rapid initial release was probably due to the drug aggregation close to the surface of the PLGA microspheres in the coating [36]. Due to the hydrophobic characteristics of dexamethasone, there is a tendency for it to migrate to the surface during electrospraying. Whereas the latter gradual slow release maybe ascribed to diffusion of the drug within the core of the PLGA microspheres coating.

For PPy, drug release can be switched on/off and accurately controlled by electrical stimulation, while for PLGA microspheres coating, the release of dexamethasone is passive and Fickian diffusion related. Previous studies have elucidated the complex phenomena that are involved in the control of drug release from PLGA microspheres [24, 38, 39]. It has been identified that the crucial drug release rate was controlled by a diffusion mechanism. For the PLGA microspheres coating, the diffusion controlled release rate decreases with increasing size of the microspheres coating. Size increase leads to slower drug release since the drug has a further distance to diffuse to the surface of the microsphere. It's important to apply a mathematical model which takes into consideration the size and shape matters of the PLGA microspheres [38].

The mathematical model assumes uniform initial drug distribution in the microspheres and constant drug diffusion coefficients. Based on this assumption and Fick's second law, the resulting drug release rate can be described by the following equation:

$$\frac{M_t}{M_\infty} = 1 - \sum_{n=0}^{\infty} \left(\frac{6}{(n\pi)^2} \right) e^{-\frac{4(n\pi)^2 D_e t}{d^2}} \quad (6.1)$$

Where M_t is the amount of drug release at time t , M_∞ is the total amount drug release, d is the diameters of the microspheres in coating, D_e is the effective diffusivity of the drug (International system of units).

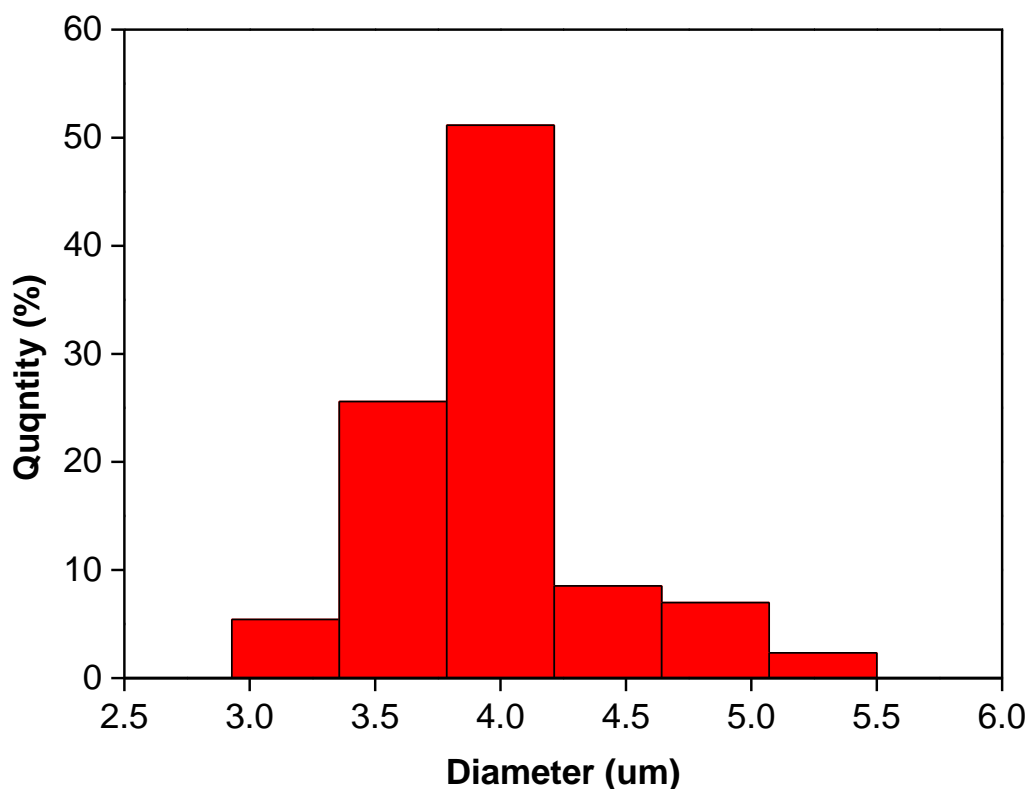


Figure 6.14 Diameters distribution of the dexamethasone PLGA microspheres.

The diameters (d) were obtained by analysis of the SEM images of the PLGA microspheres coating. The diameters are $3.97 \pm 0.44 \mu\text{m}$, and the diameters distribution is shown in **Figure 6.14**. It shows that the as-fabricated microspheres coating have uniform morphology with a narrow size distribution.

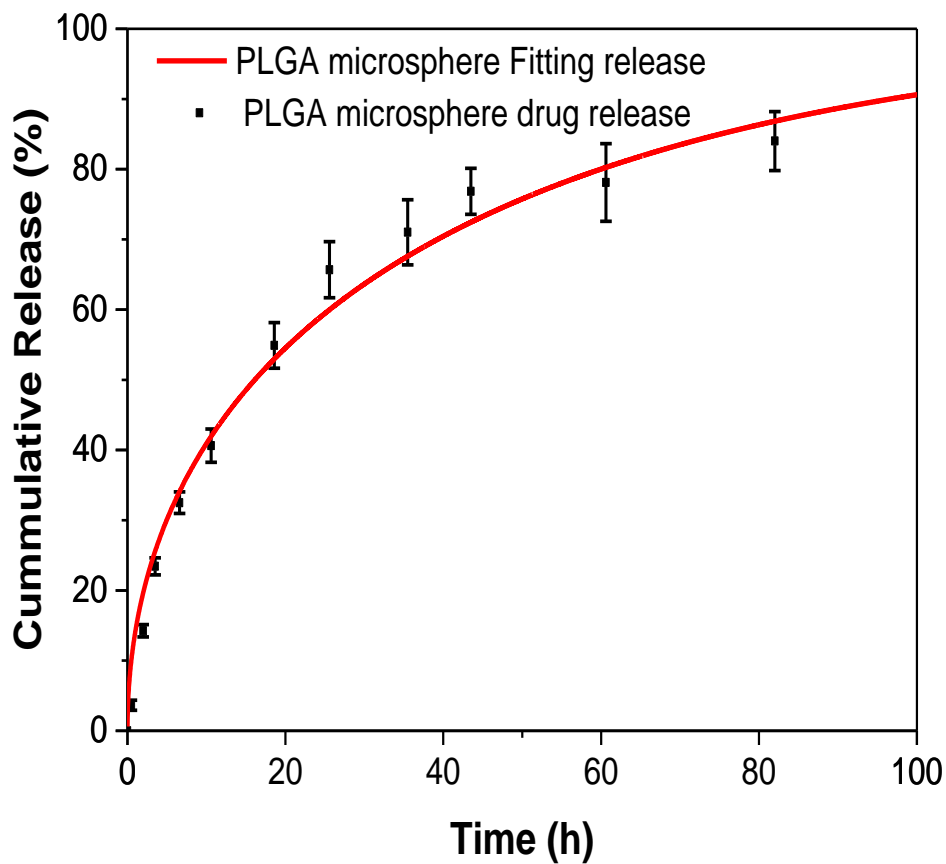


Figure 6.15 Comparison of the mathematical modelling results with the experimental drug release profiles of electrospay PLGA dexamethasone microspheres coating.

The fitting method was based on the minimization of the differences between experimental and theoretical results (least squares fitting method). The fitted results agree well with the

experimental drug release rate (**Figure 6.15**). It's consistent with previous studies, and the drug release mechanism of the PLGA microspheres can be described as a time-dependent diffusion controlled release [24, 38, 39]. The calculated effective diffusivity (D_e) is 1.2×10^{-12} cm^2/min , which is within the values range of hydrophobic drugs in a PLGA matrix [40].

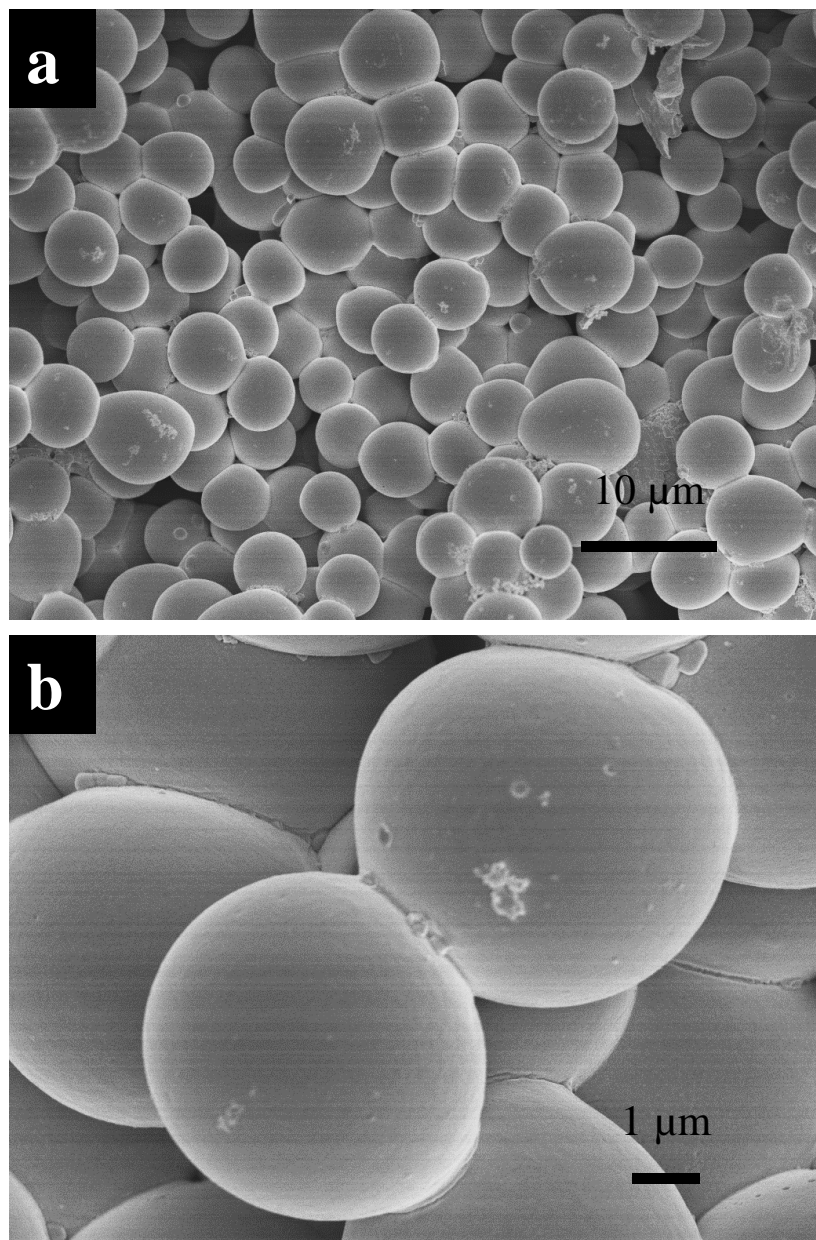


Figure 6.16 SEM images of PLGA dexamethasone microspheres coating after more than three months release incubation. It shows that the PLGA retained its spherical structure.

We also conducted SEM observations on the PLGA microspheres coating after more than three months of release. **Figure 6.16** shows that the PLGA retained its spherical structure. This confirms that the breakdown of the polymeric network does not occur during the whole drug release period. Thus, it does not contribute to the control of the release process.

6.4 Conclusion

In summary, this work developed 3D drug delivery systems based on 3D printed electrodes. After electropolymerization of a layer of PPy fos-phenytoin coating, the 3D electrodes showed electrically controlled property, sustained near-linear release, flexible dosage control, and super stability. The electrospayed PLGA dexamethasone microspheres coated on the 3D electrodes demonstrated uniform morphology and theoretically predictable release properties. The combination of conducting and biodegradable polymers by these two interdigitated electrodes can serve as multi-functional drug delivery systems. The electrical conductivity, biocompatibility and controllable release of this 3D printed drug delivery system can lead to promising localized treatment of central nervous system diseases such as epilepsy.

6.5 References

- [1] Wallace GG, Teasdale PR, Spinks GM, Kane-Maguire LA. Conductive electroactive polymers: intelligent polymer systems: CRC press; 2008.
- [2] Sariciftci N, Smilowitz L, Heeger AJ, Wudl F. Photoinduced electron transfer from a conducting polymer to buckminsterfullerene. *Science* 1992;258:1474-6.
- [3] Gao M, Huang S, Dai L, Wallace G, Gao R, Wang Z. Aligned coaxial nanowires of carbon nanotubes sheathed with conducting polymers. *Angewandte Chemie* 2000;39:3664-7.
- [4] Heeger AJ. Semiconducting and Metallic Polymers: The fourth generation of polymeric materials (Nobel lecture). *Angewandte Chemie International Edition* 2001;40:2591-611.
- [5] Kang K, Watanabe S, Broch K, Sepe A, Brown A, Nasrallah I, Nikolka M, Fei Z, Heeney M, Matsumoto D, Marumoto K, Tanaka H, Kuroda S-i, Sirringhaus H. 2D coherent charge transport in highly ordered conducting polymers doped by solid state diffusion. *Nat Mater* 2016; 15: 896-902.
- [6] Abidian MR, Kim DH, Martin DC. Conducting-polymer nanotubes for controlled drug release. *Advanced Materials* 2006;18:405-9.
- [7] Svirskis D, Travas-Sejdic J, Rodgers A, Garg S. Electrochemically controlled drug delivery based on intrinsically conducting polymers. *Journal of Controlled Release* 2010;146:6-15.
- [8] Weaver CL, LaRosa JM, Luo X, Cui XT. Electrically controlled drug delivery from graphene oxide nanocomposite films. *ACS Nano* 2014;8:1834-43.
- [9] Zhang B, Molino PJ, Harris AR, Yue Z, Moulton SE, Wallace GG. Conductive and protein resistant polypyrrole films for dexamethasone delivery. *Journal of Materials Chemistry B* 2016;4:2570-7.
- [10] Langer R. Biomaterials in drug delivery and tissue engineering: One laboratory's experience. *Accounts of Chemical Research* 2000;33:94-101.

- [11] Mawad D, Stewart E, Officer DL, Romeo T, Wagner P, Wagner K, Wallace GG. A single component conducting polymer hydrogel as a scaffold for tissue engineering. *Advanced Functional Materials* 2012;22:2692-9.
- [12] Zhang H, Molino PJ, Wallace GG, Higgins MJ. Quantifying molecular-level cell adhesion on electroactive conducting polymers using electrochemical-single cell force spectroscopy. *Sci Rep-Uk* 2015;5.
- [13] Cui X, Wiler J, Dzaman M, Altschuler RA, Martin DC. In vivo studies of polypyrrole/peptide coated neural probes. *Biomaterials* 2003;24:777-87.
- [14] Green RA, Lovell NH, Wallace GG, Poole-Warren LA. Conducting polymers for neural interfaces: Challenges in developing an effective long-term implant. *Biomaterials* 2008;29:3393-9.
- [15] Wei F, Liao W, Xu Z, Yang Y, Wong DT, Ho CM. Bio/abiotic interface constructed from nanoscale DNA dendrimer and conducting polymer for ultrasensitive biomolecular diagnosis. *Small* 2009;5:1784-90.
- [16] Spinks GM, Mottaghitalab V, Bahrami-Samani M, Whitten PG, Wallace GG. Carbon-nanotube-reinforced polyaniline fibers for high-strength artificial muscles. *Adv Mater* 2006;18:637-40.
- [17] Ma M, Guo L, Anderson DG, Langer R. Bio-inspired polymer composite actuator and generator driven by water gradients. *Science* 2013;339:186-9.
- [18] Johnston JH, Moraes J, Borrmann T. Conducting polymers on paper fibres. *Synthetic Metals* 2005;153:65-8.
- [19] Hubbell JA, Langer R. Translating materials design to the clinic. *Nat Mater* 2013;12:963-6.

- [20] United states food and drug administration, highlights of prescribing information—spritam, http://www.accessdata.fda.gov/drugsatfda_docs/label/2015/207958s000lbl.pdf. 2015.
- [21] Norman J, Madurawe RD, Moore CMV, Khan MA, Khairuzzaman A. A new chapter in pharmaceutical manufacturing: 3D-printed drug products. *Advanced Drug Delivery Reviews* 2017; 108: 39-50.
- [22] Levy GN, Schindel R, Kruth J-P. Rapid manufacturing and rapid tooling with layer manufacturing (LM) technologies, state of the art and future perspectives. *CIRP Annals-Manufacturing Technology* 2003;52:589-609.
- [23] Zhao C, Wang C, Gorkin Iii R, Beirne S, Shu K, Wallace GG. Three dimensional (3D) printed electrodes for interdigitated supercapacitors. *Electrochemistry Communications* 2014;41:20-3.
- [24] Chen Y, Yue Z, Moulton SE, Hayes P, Cook MJ, Wallace GG. A simple and versatile method for microencapsulation of anti-epileptic drugs for focal therapy of epilepsy. *Journal of Materials Chemistry B* 2015;3:7255-61.
- [25] Luo X, Matranga C, Tan S, Alba N, Cui XT. Carbon nanotube nanoreservoir for controlled release of anti-inflammatory dexamethasone. *Biomaterials* 2011;32:6316-23.
- [26] Browne TR, Kugler AR, Eldon MA. Pharmacology and pharmacokinetics of fosphenytoin. *Neurology* 1996;46:3S-7S.
- [27] Norris D, Weston W, Sams Jr W. The effect of immunosuppressive and anti-inflammatory drugs on monocyte function in vitro. *The Journal of laboratory and clinical medicine* 1977;90:569-80.
- [28] Franz S, Rammelt S, Scharnweber D, Simon JC. Immune responses to implants – A review of the implications for the design of immunomodulatory biomaterials. *Biomaterials* 2011;32:6692-709.

- [29] Almería B, Deng W, Fahmy TM, Gomez A. Controlling the morphology of electrospray-generated PLGA microparticles for drug delivery. *Journal of Colloid and Interface Science* 2010;343:125-33.
- [30] El-Kady MF, Kaner RB. Scalable fabrication of high-power graphene micro-supercapacitors for flexible and on-chip energy storage. *Nat Commun* 2013;4:1475.
- [31] Kandel ER, Schwartz JH, Jessell TM. *Principles of neural science*: McGraw-hill New York; 2000.
- [32] Wadhwa R, Lagenaur CF, Cui XT. Electrochemically controlled release of dexamethasone from conducting polymer polypyrrole coated electrode. *Journal of Controlled Release* 2006;110:531-41.
- [33] Jeon G, Yang SY, Byun J, Kim JK. Electrically actuatable smart nanoporous membrane for pulsatile drug release. *Nano Letters* 2011;11:1284-8.
- [34] Salonen J, Laitinen L, Kaukonen AM, Tuura J, Björkqvist M, Heikkilä T, Vähä-Heikkilä K, Hirvonen J, Lehto VP. Mesoporous silicon microparticles for oral drug delivery: Loading and release of five model drugs. *J Control Release* 2005;108:362-74.
- [35] Yang X, Zhang X, Liu Z, Ma Y, Huang Y, Chen Y. High-efficiency loading and controlled release of doxorubicin hydrochloride on graphene oxide. *The Journal of Physical Chemistry C* 2008;112:17554-8.
- [36] Govender T, Stolnik S, Garnett MC, Illum L, Davis SS. PLGA nanoparticles prepared by nanoprecipitation: drug loading and release studies of a water soluble drug. *Journal of Controlled Release* 1999;57:171-85.
- [37] Anderson JM, Shive MS. Biodegradation and biocompatibility of PLA and PLGA microspheres. *Advanced Drug Delivery Reviews* 2012;64, Supplement:72-82.

- [38] Fattahi P, Borhan A, Abidian MR. Microencapsulation of chemotherapeutics into monodisperse and tunable biodegradable polymers via electrified liquid jets: Control of size, shape, and drug release. *Advanced Materials* 2013;25:4555-60.
- [39] Faisant N, Siepmann J, Benoit JP. PLGA-based microparticles: elucidation of mechanisms and a new, simple mathematical model quantifying drug release. *European Journal of Pharmaceutical Sciences* 2002;15:355-66.
- [40] Arifin DY, Lee LY, Wang C-H. Mathematical modeling and simulation of drug release from microspheres: Implications to drug delivery systems. *Advanced Drug Delivery Reviews* 2006;58:1274-325.

CHAPTER 7: CONCLUSIONS AND FUTURE WORK

7.1 General Conclusion

The main aim of this study was to develop biocompatible controlled drug delivery systems for treatment of central nervous system disorders such as epilepsy. Biodegradable polymer and conducting polymer were used as carriers. The US Food and Drug Administration (FDA) approved lacosamide, phenytoin and dexamethasone are used as model drugs. Electrojetting and electropolymerization are used as fabrication methods.

The preparation and characterization of microcapsules including flattened microspheres, microspheres, and microfibrils are described in chapter 3. Electrojetting technology (electrospraying and electrospinning) were used to fabricate these microcapsules containing the anti-epilepsy drug, lacosamide. The SEM images and their statistical analysis results showed uniform morphology and a narrow size distribution of the microcapsules. The drug release study demonstrated high drug encapsulation efficiency, and that their drug release profiles are dependent on the shape and size of the microcapsules. The mathematical modelling studies demonstrated that all drug release profiles could be predicted, with a good agreement between the modelling and experimental results. Human neural stem cell culture results indicated the neuro-cytocompatibility of the microcapsules. It was confirmed by the cell attachment and viability during extended cell culture with the microcapsules. These findings broadly support the utility and efficacy of the local drug delivery systems for treating human brain disorders such as epilepsy.

After successful fabrication of the neuro-compatible microcapsules, the development of core-shell structural microcapsules using the same biodegradable polymer was investigated in chapter 4. A series of core-shell microcapsules were prepared via novel core-shell electrojetting, where a more hydrophobic polymer shell acts as a barrier component to control the rate of drug release from the polymeric core. By adjusting the applied voltage and the core and shell solution compositions, different kinds of microcapsules were successfully obtained, including core/-shell microflakes, flattened microspheres and microspheres, microspheres/fibres, microbeads/fibres, and microfibres. The release profile varies with the morphologies and shape of the core-shell microcapsules and thus can be readily controlled over long periods of time.

Many central nervous system disorders in clinical situations require more than mono drug release. For example, combination therapy with drugs of different therapeutic effects provides an effective strategy in the treatment of epilepsy. Electrospun microfibres and electrospayed microspheres composite membranes were prepared as dual drug delivery systems in chapter 5. These composite membranes were loaded with two drugs, one in the biodegradable microspheres and the other in the microfibres. The microspheres and microfibres could form stable composite structures. Thermogravimetric analysis and tensile testing results indicated favourable thermal and mechanical properties. Independently controlled release behaviours are achieved in these dual drug delivery composite membranes.

In chapter 6, 3D printed interdigitated electrodes were used as drug delivery systems by a combination of conducting polymer film and biodegradable polymer microspheres. The interdigitated structure provided flexible drug delivery combination both for mono drug

delivery and dual drug delivery systems. The electrochemical impedance spectroscopy (EIS) and cyclic voltammetry (CV) results showed the excellent electrochemical properties of the 3D electrodes. Conducting polymer coated electrodes demonstrated sustained near-linear release. The release amount of drug could be controlled by altering the stimuli potential. Assembling of two conducting polymer coated interdigitated electrodes significantly increased the capacity of drug loading. The biodegradable polymer microspheres coated 3D electrodes were also fabricated. By the assembling of microspheres coated electrode with the conducting polymer coated electrode, interdigitated dual drug delivery systems were developed.

In summary, a series of biodegradable microcapsules and 3D conducting polymer drug delivery systems have been successfully developed in this thesis. All delivery systems showed biocompatibility, controllable shape, size, and drug release properties. These novel drug delivery systems demonstrate great potential application in the local treatment of central nervous system (CNS) disorders such as epilepsy.

7.2 Future work

7.2.1 Electrojetting biodegradable microcapsules

Electrojetting has been a facile and simple technique for fabricating many kinds of microcapsules including micro-particles and microfibres [1-3]. These microcapsules demonstrated varied drug release profiles depending on their shape and size. The release periods are from several days to several months. However, further increasing the release time is still a huge challenge [4-6].

The drug release time already has been extended to several months by using the core-shell electrojetting technique. From the perspective of clinical applications, the longer release with even kinetics over the duration of the implant would be best. In order to further prolong the drug release duration, one promising method is to increase the shell/core ratio of the microcapsules [5]. For the microcapsules, the drug release rate decreases with increasing size of the microcapsules, as a result of increased diffusion distance.

Another approach is to add a more hydrophobic component as drug carrier [7]. The hydrophobic component would prevent water penetration into the microcapsules. It will also decrease the degradation of the polymer carrier leading to reduction of drug diffusion.

Two administrations would be applied to the delivery of electrojetting microparticles and microfibrils to a patient. Because the granular polymeric delivery systems could be distributed in an injection solution, the microcapsules including microflakes, flattened microspheres, and microspheres are suitable for injected administration. However, for the fibrous polymeric delivery systems, which are gathered as fibre matrix, administration by implanting should be considered.

For the electrospun microfibrils and electrosprayed microspheres combined structure, it would be worth undertaking more detailed investigations incorporating modelling based on this new structure using a single drug.

Apart from drug delivery applications, electrojetting microparticles and microfibrils could be used in other biological areas such as cell culture and tissue engineering [6, 8]. Some

biomacromolecules e.g. protein, DNA, and growth factor could be incorporated into the biodegradable microcapsules for these related biomedical applications.

7.2.2 Electropolymerization of conducting polymer

3D printing is a novel technology for fabrication of complex, personalized products from digital designs [9-11]. Since a 3D printed drug had been approved by the FDA recently, 3D printing has attracted increasing interest in pharmaceutical fabrication [12]. In this study, 3D printed interdigitated electrodes were used as drug delivery systems. This technique also can be used to fabricate many other micro-structures. These structures can be designed to fulfil clinical requirements. Furthermore, the surface of the printed electrodes also can be modified by using conducting polymers and biodegradable polymers.

Carbon nanomaterials, such as carbon nanotube, graphene, and graphene oxide have received tremendous attention in controlled drug delivery applications recently due to their large surface area and sp^2 carbon lattice [13-18]. Graphene oxide is composed of a honeycomb carbon lattice structure with hydroxyl, carboxyl, and epoxide functional groups. The aromatic drug compounds enable π - π interactions with graphene oxide by localized π -electrons [19]. Targeted drug delivery can be achieved by covalently modifying drug loaded graphene oxide.

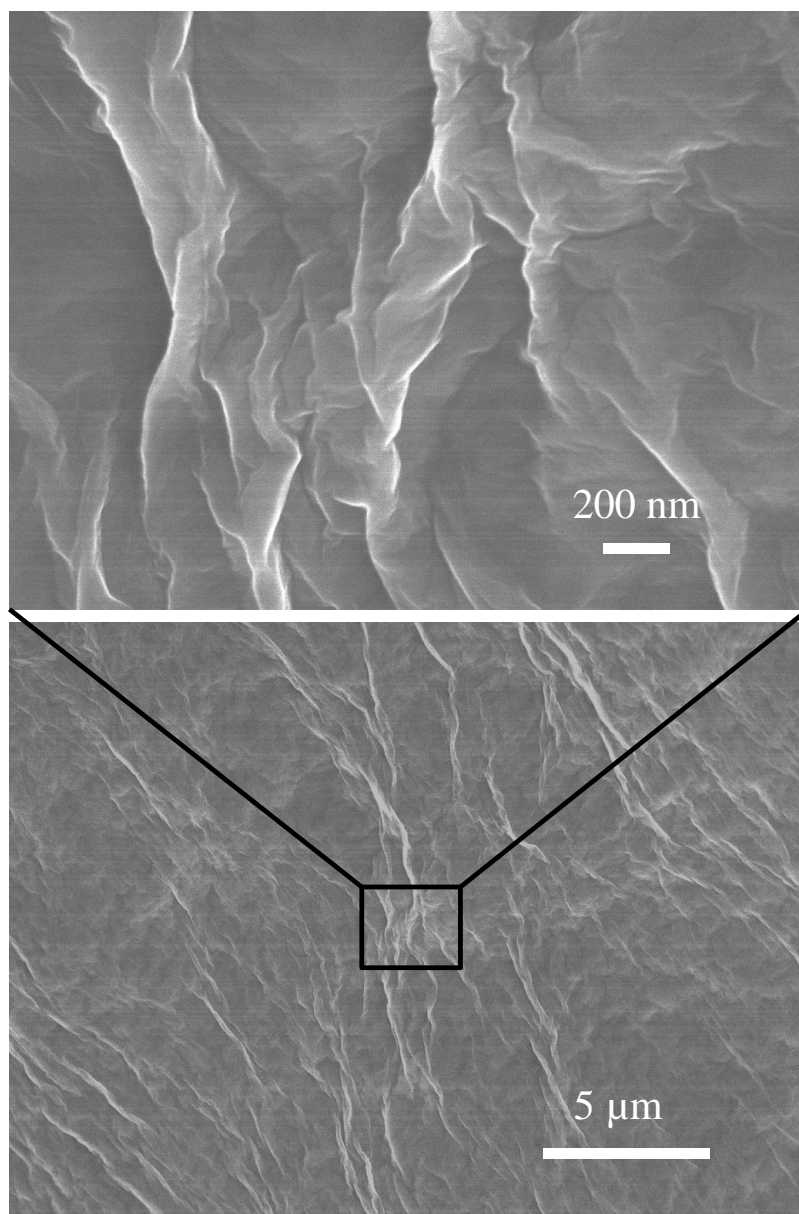


Figure 7.1 SEM images of PPy/graphene oxide/fosphenytoin coated on the surface of 3D printed electrode.

Preliminary studies showed that the graphene oxide sheets could be incorporated into conducting polymer (PPy) film (**Figure 7.1**). The conducting polymer and graphene oxide could be co-deposited on the surface of the 3D printed microstructures. The as-fabricated composite film shows promising possibilities for electrically controlled drug release application.

7.3 References

- [1] Zheng J, He A, Li J, Xu J, Han CC. Studies on the controlled morphology and wettability of polystyrene surfaces by electrospinning or electrospraying. *Polymer* 2006;47:7095-102.
- [2] Fattahi P, Borhan A, Abidian MR. Microencapsulation of chemotherapeutics into monodisperse and tunable biodegradable polymers via electrified liquid jets: Control of size, shape, and drug release. *Advanced Materials* 2013;25:4555-60.
- [3] Huang Z-M, Zhang YZ, Kotaki M, Ramakrishna S. A review on polymer nanofibers by electrospinning and their applications in nanocomposites. *Composites Science and Technology* 2003;63:2223-53.
- [4] Pillay V, Dott C, Choonara YE, Tyagi C, Tomar L, Kumar P, du Toit LC, Ndesendo VMK. A review of the effect of processing variables on the fabrication of electrospun nanofibers for drug delivery applications. *Journal of Nanomaterials* 2013;2013:22.
- [5] Yu D-G, Li X-Y, Wang X, Yang J-H, Bligh SWA, Williams GR. Nanofibers fabricated using triaxial electrospinning as zero order drug delivery systems. *ACS Applied Materials & Interfaces* 2015;7:18891-7.
- [6] Hu X, Liu S, Zhou G, Huang Y, Xie Z, Jing X. Electrospinning of polymeric nanofibers for drug delivery applications. *Journal of Controlled Release* 2014;185:12-21.
- [7] Yohe ST, Colson YL, Grinstaff MW. Superhydrophobic materials for tunable drug release: Using displacement of air to control delivery rates. *Journal of the American Chemical Society* 2012;134:2016-9.
- [8] Xie J, Liu W, MacEwan MR, Bridgman PC, Xia Y. Neurite outgrowth on electrospun nanofibers with uniaxial alignment: The effects of fiber density, surface coating, and supporting substrate. *ACS Nano* 2014;8:1878-85.

- [9] Gross BC, Erkal JL, Lockwood SY, Chen C, Spence DM. Evaluation of 3D printing and its potential impact on biotechnology and the chemical sciences. *Analytical Chemistry* 2014;86:3240-53.
- [10] Ambrosi A, Pumera M. 3D-printing technologies for electrochemical applications. *Chemical Society Reviews* 2016;45:2740-55.
- [11] Xing J-F, Zheng M-L, Duan X-M. Two-photon polymerization microfabrication of hydrogels: an advanced 3D printing technology for tissue engineering and drug delivery. *Chemical Society Reviews* 2015;44:5031-9.
- [12] Norman J, Madurawe RD, Moore CMV, Khan MA, Khairuzzaman A. A new chapter in pharmaceutical manufacturing: 3D-printed drug products. *Advanced Drug Delivery Reviews* 2017; 108: 39-50.
- [13] Bianco A, Kostarelos K, Prato M. Applications of carbon nanotubes in drug delivery. *Current Opinion in Chemical Biology* 2005;9:674-9.
- [14] Chen D, Dougherty CA, Zhu K, Hong H. Theranostic applications of carbon nanomaterials in cancer: Focus on imaging and cargo delivery. *Journal of Controlled Release* 2015;210:230-45.
- [15] Siu KS, Chen D, Zheng X, Zhang X, Johnston N, Liu Y, Yuan K, Koropatnick J, Gillies ER, Min W-P. Non-covalently functionalized single-walled carbon nanotube for topical siRNA delivery into melanoma. *Biomaterials* 2014;35:3435-42.
- [16] Jiang T, Sun W, Zhu Q, Burns NA, Khan SA, Mo R, Gu Z. Furin-mediated sequential delivery of anticancer cytokine and small-molecule drug shuttled by graphene. *Advanced Materials* 2015;27:1021-8.
- [17] Feng T, Ai X, An G, Yang P, Zhao Y. Charge-convertible carbon dots for imaging-guided drug delivery with enhanced in vivo cancer therapeutic efficiency. *ACS Nano* 2016;10:4410-20.

[18] Weaver CL, LaRosa JM, Luo X, Cui XT. Electrically controlled drug delivery from graphene oxide nanocomposite films. *ACS Nano* 2014;8:1834-43.

[19] He Q, Kieseewetter DO, Qu Y, Fu X, Fan J, Huang P, Liu Y, Zhu G, Liu Y, Qian Z, Chen X. NIR-Responsive On-demand release of CO from metal carbonyl-caged graphene oxide nanomedicine. *Advanced Materials* 2015;27:6741-6.